

THE HYDRODYNAMIC AND CAPTURE/RETENTION PERFORMANCE OF A GROSS POLLUTANT TRAP

Jehangir T. Madhani

Master of Science (Marine Technology), Strathclyde University, Glasgow, UK

A thesis by publication submitted in fulfilment of the requirements for the degree of
Doctor of Philosophy (PhD)

School of Engineering Systems
Faculty for Built Environment and Engineering
Queensland University of Technology

June 2010

Keywords

Acoustic Doppler Velocimeter

ADV

Anthropogenic litter

Organic matter

Computational fluid dynamics

CFD

D rain

Dye

Flow visualisations

Fluent

Gross pollutants

Gross pollutant trap

GPT

Komori probe

Litter

Line integral convolution

LIC

Residence time distribution

RTD

Stormwater

Abstract

This research shows that gross pollutant traps (GPTs) continue to play an important role in preventing visible street waste—gross pollutants—from contaminating the environment. The demand for these GPTs calls for stringent quality control and this research provides a foundation to rigorously examine the devices.

A novel and comprehensive testing approach to examine a dry sump GPT was developed. The GPT is designed with internal screens to capture gross pollutants—organic matter and anthropogenic litter. This device has not been previously investigated.

Apart from the review of GPTs and gross pollutant data, the testing approach includes four additional aspects to this research, which are: field work and an historical overview of street waste/stormwater pollution, calibration of equipment, hydrodynamic studies and gross pollutant capture/retention investigations.

This work is the first comprehensive investigation of its kind and provides valuable practical information for the current research and any future work pertaining to the operations of GPTs and management of street waste in the urban environment.

Gross pollutant traps—including patented and registered designs developed by industry—have specific internal configurations and hydrodynamic separation characteristics which demand individual testing and performance assessments. Stormwater devices are usually evaluated by environmental protection agencies (EPAs), professional bodies and water research centres. In the USA, the American Society of Civil Engineers (ASCE) and the Environmental Water Resource Institute (EWRI) are examples of professional and research organisations actively involved in these evaluation/verification programs. These programs largely rely on field evaluations alone that are limited in scope, mainly for cost and logistical reasons. In Australia, evaluation/verification programs of new devices in the stormwater industry are not well established.

The current limitations in the evaluation methodologies of GPTs have been addressed in this research by establishing a new testing approach. This approach uses

a combination of physical and theoretical models to examine in detail the hydrodynamic and capture/retention characteristics of the GPT.

The physical model consisted of a 50% scale model GPT rig with screen blockages varying from 0 to 100%. This rig was placed in a 20 m flume and various inlet and outflow operating conditions were modelled on observations made during the field monitoring of GPTs. Due to infrequent cleaning, the retaining screens inside the GPTs were often observed to be blocked with organic matter. Blocked screens can radically change the hydrodynamic and gross pollutant capture/retention characteristics of a GPT as shown from this research.

This research involved the use of equipment, such as acoustic Doppler velocimeters (ADV) and dye concentration (Komori) probes, which were deployed for the first time in a dry sump GPT. Hence, it was necessary to rigorously evaluate the capability and performance of these devices, particularly in the case of the custom made Komori probes, about which little was known.

The evaluation revealed that the Komori probes have a frequency response of up to 100 Hz—which is dependent upon fluid velocities—and this was adequate to measure the relevant fluctuations of dye introduced into the GPT flow domain. The outcome of this evaluation resulted in establishing methodologies for the hydrodynamic measurements and gross pollutant capture/retention experiments.

The hydrodynamic measurements consisted of point-based acoustic Doppler velocimeter (ADV) measurements, flow field particle image velocimetry (PIV) capture, head loss experiments and computational fluid dynamics (CFD) simulation.

The gross pollutant capture/retention experiments included the use of anthropogenic litter components, tracer dye and custom modified artificial gross pollutants. Anthropogenic litter was limited to tin cans, bottle caps and plastic bags, while the artificial pollutants consisted of 40 mm spheres with a range of four buoyancies.

The hydrodynamic results led to the definition of global and local flow features. The gross pollutant capture/retention results showed that when the internal retaining screens are fully blocked, the capture/retention performance of the GPT rapidly deteriorates.

The overall results showed that the GPT will operate efficiently until at least 70% of the screens are blocked, particularly at high flow rates. This important finding indicates that cleaning operations could be more effectively planned when the GPT capture/retention performance deteriorates. At lower flow rates, the capture/retention performance trends were reversed. There is little difference in the poor capture/retention performance between a fully blocked GPT and a partially filled or empty GPT with 100% screen blockages.

The results also revealed that the GPT is designed with an efficient high flow bypass system to avoid upstream blockages. The capture/retention performance of the GPT at medium to high inlet flow rates is close to maximum efficiency (100%).

With regard to the design appraisal of the GPT, a raised inlet offers a better capture/retention performance, particularly at lower flow rates. Further design appraisals of the GPT are recommended.

Table of Contents

CHAPTER 1: INTRODUCTION	1
1.1 MOTIVATION AND OVERVIEW OF WORK	2
1.2 RESEARCH AIMS AND OBJECTIVES.....	9
1.3 SCOPE OF THIS STUDY	9
1.4 LINKING THE RESEARCH OBJECTIVES AND THE SCIENTIFIC PAPERS.....	11
1.5 RESEARCH CONTRIBUTIONS.....	17
CHAPTER 2: LITERATURE REVIEW	19
2.1 GROSS STORMWATER POLLUTANTS AND THE NEED FOR GPTS.....	19
2.2 GROSS POLLUTANT DATA	22
2.3 GROSS POLLUTANT TRAPS (GPTs).....	23
2.4 CURRENT PERFORMANCE EVALUATION OF GPTS	29
2.5 HYDRODYNAMICS	30
2.6 GROSS POLLUTANT CAPTURE/RETENTION EXPERIMENTS	31
2.7 TRACER DYE	32
2.8 BLOCKAGES	33
2.9 CONCLUSION.....	34
CHAPTER 3: A HISTORICAL PERSPECTIVE ON AUSTRALIAN ATTITUDES TO LITTERING AND THEIR ENVIRONMENTAL IMPACT	69
3.1 INTRODUCTION	71
3.2 HISTORY OF LITTERING	72
3.3 DATA ON THE PRACTICE OF LITTERING.....	76
3.4 IMPACT OF LITTERING.....	79
3.5 SOLUTIONS	81
3.6 CURRENT POLLUTANT TRENDS: A CASE STUDY.....	83
3.7 SUMMARY	86
CHAPTER 4: THE FIELD/CASE STUDY	95
4.1 INTRODUCTION	95
4.2 METHOD OF ANALYSIS.....	99
4.3 RESULTS AND DISCUSSION	103
4.4 STORMWATER DRAINS AND GROSS POLLUTANTS ON STREETS	104
4.5 PHOTOGRAPHIC RESULTS	105
4.6 MOBILISATION OF GROSS POLLUTANTS ON STREETS DURING WET WEATHER	123
4.7 CONCLUSION.....	129
CHAPTER 5: A SCALAR CONCENTRATION (KOMORI) PROBE FOR MEASURING FLUCTUATING DYE CONCENTRATION IN WATER.....	143
5.1 INTRODUCTION	145
5.2 EXPERIMENTAL METHOD	147

5.3	FREQUENCY RESPONSE METHOD AND ANALYSIS	149
5.4	RESULTS AND DISCUSSION	153
5.5	CASE STUDIES	157
5.6	CONCLUSION.....	162
	CHAPTER 6: AN EXPERIMENTAL AND THEORETICAL INVESTIGATION OF FLOW IN A GROSS POLLUTANT TRAP.....	167
6.1	INTRODUCTION	169
6.2	EXPERIMENTAL METHOD.....	172
6.3	COMPUTATIONAL FLUID DYNAMICS (CFD) STUDY.....	174
6.4	RESULTS AND DISCUSSION	179
6.5	CONCLUSION.....	185
	ACKNOWLEDGEMENTS	186
	REFERENCES	186
	CHAPTER 7: THE HYDRODYNAMIC INVESTIGATION OF A GROSS POLLUTANT TRAP WITH FULLY BLOCKED SCREENS.....	191
7.1	INTRODUCTION	193
7.2	EXPERIMENTAL METHOD.....	196
7.3	DATA ANALYSIS.....	202
7.4	COMPUTATIONAL FLUID DYNAMICs (CFD) STUDY	204
7.5	RESULTS AND DISCUSSION	206
7.6	CONCLUSION.....	213
	CHAPTER 8: A NOVEL METHOD TO CAPTURE AND ANALYZE FLOW IN A GROSS POLLUTANT TRAP USING IMAGE-BASED VECTOR VISUALIZATION.....	219
8.1	INTRODUCTION	221
8.2	FIELD STUDY	224
8.3	PHYSICAL MODELLING	226
8.4	EXPERIMENTAL METHOD.....	228
8.5	THE LINE INTEGRAL CONVOLUTION (LIC).....	230
8.6	RESULTS AND DISCUSSION	235
8.7	CONCLUSION.....	241
	CHAPTER 9: AN INVESTIGATION OF THE CAPTURE AND RETENTION CHARACTERISTICS OF A GROSS POLLUTANT TRAP.....	247
9.1	INTRODUCTION	249
9.2	EXPERIMENTAL METHOD.....	252
9.3	COMPUTATIONAL FLUID DYNAMIC (CFD) STUDY	258
9.4	DATA ANALYSIS.....	260
9.5	RESULTS AND DISCUSSION	263
9.6	CONCLUSION.....	270
	CHAPTER 10: GENERAL DISCUSSION	275
10.1	MODELLING CONSIDERATIONS OF THE GPT	275
10.2	FIELD STUDIES AND THE EXTENDED LITERATURE REVIEW	277

10.3	CALIBRATION OF EQUIPMENT	280
10.4	HYDRODYNAMIC STUDIES	283
10.5	GROSS POLLUTANT CAPTURE/RETENTION INVESTIGATION	289
10.6	SUMMARY	291
	CHAPTER 11: CONCLUSION	295
11.1	RESEARCH OUTCOMES	296
11.2	FUTURE WORK	298
	APPENDICES	301
	APPENDIX A: RAINFALL DATA	303
	APPENDIX B: WIRING DIAGRAM	307
	APPENDIX C: ADV DATA ANALYSIS	311
	APPENDIX D: FLUME/PHYSICAL MODELLING OF THE GPT	327
	APPENDIX E: SIGNAL PROCESSING PROGRAMS FOR THE DYE DATA	333
	APPENDIX F: VECTOR PLOTS FROM PIV SOFTWARE AND OPENDX	337
	APPENDIX G: GROSS POLLUTANT CAPTURE/RETENTION EXPERIMENTAL RESULTS	345

List of Figures

Figure 1.1 Overview of the research as outlined by the titles of the thesis chapters and papers.....	5
Figure 1.2 Flowchart showing an overview of the research and the work as presented in the chapters of the thesis.	7
Figure 2.1 Anthropogenic waste—a Pelican strangled by a plastic bag (Healthy Waterways & Brisbane City Council, 2008).....	21
Figure 2.2 Fish kill caused by ingress of cigarette butts (Healthy Waterways & Brisbane City Council, 2008).....	21
Figure 2.3 A block diagram representing the interaction of the public with the environment, where A and B are the pollution preventive point and diffusive sources respectively. These sources can be treated using stormwater quality improvement devices such as GPTs.	24
Figure 2.4 An open GPT consisting of a basin, a trashrack with vertical bars atop a weir located at Bedivere Street, Carindale on the outskirts of Brisbane (November, 2008).	26
Figure 3.1 A litter bin on Mary Street, Brisbane, 2008 surrounded by discarded cigarettes butts.	77
Figure 3.2 (a) Sydney Street, Sydney, 1934, (Image courtesy of The City of Sydney Archives) and (b) Stephens Road, South Brisbane, 2009	78
Figure 3.3 (a) A stormwater channel at Kingsgrove, 1954, (Image courtesy of The State Library of NSW) and (b) View of a stormwater drain fully blocked with organic matter at Graham Street in South Brisbane, 2008.	80
Figure 3.4 Graph showing the results of the litter field survey taken in 2006 to 2008. Comparison of gross pollutant (organic and litter) data are made with data collected from Sydney (Van Drie, 2002), Melbourne (Lewis, 2002) and Los Angeles (Lippner and Moeller, 2000; Quasebarth et al., 2001).	86
Figure 4.1 The overall terrain map of surveyed stormwater drains, hotspot littering areas and GPTs in Brisbane (Queensland) and its suburbs as defined in Google maps (author developed database available at: http://maps.google.com/maps/ms?ie=UTF&msa=0&msid=102965336134023288187.-00047b6e955a7b89a666d for further details, such as scale and orientation).....	96
Figure 4.2 A detailed terrain view of the mapped stormwater drains, GPT, catchment outlet and littering areas in Brisbane and the inner suburbs for the field study as defined in Google maps (author developed database available at: http://maps.google.com/maps/ms?ie=UTF&msa=0&msid=-102965336134023288187.00047c2cd8a137d829c19 for further details, such as scale and orientation). The shaded areas represent the perimeters of the surveys conducted.	97
Figure 4.3 A field survey map of inspected stormwater drains and littering areas in Burleigh Heads, a suburb of the Gold Coast as defined in Google maps (author developed database available at: http://maps.google.com/maps/ms?ie=UTF&msa=0&msid=102965336134023288187.-00047c4ca557459ca0e62 for further details, such as scale and orientation).	98
Figure 4.4 Storm water inlet drain in a residential area (West Street, Highgate Hill) of an inner suburb of Brisbane City clogged mainly with organic matter (small amounts of litter—plastic bottles and paper) just after a wet weather flow. Lower left is a view inside the drain (empty) and the top right shows the view of street and the drain location (June 2008). Lower right, the shaded area is used to map and estimate the gross pollutant contents (see SWD No. 75 in Tables 4.1 and 4.2).	99
Figure 4.5 Inspection of road-side stormwater drains SWD 8 and 9 (See Tables 4.1 and 4.2) on Crown St T junction to Annerley Road. Both storm water drains include a grate and	

kerb inlet and are partially clogged, mainly with organic matter and fine sediments. Sumps A and B are relatively empty and mainly consist of organic matter, paper, packaging material, plastic bags, cigarettes butts etc.	102
Figure 4.6 Using Google maps to locate the surveyed stormwater drains, GPTs and littering areas.	103
Figure 4.7 The field investigation results (Tables 4.1 and 4.2) expressed as average percentage of gross pollutants (organics & litter) found inside and on top of stormwater drains and on streets located in inner southern suburbs of Brisbane and Burleigh Heads.	104
Figure 4.8 A fully blocked stormwater drain (SWD No. 22, See Tables 4.1 and 4.2), mainly with leaves and fine sediments (at T junction between Graham Street and Vulture Street, South Bank) located in partly residential and partly commercial area (South Bank) of Brisbane. The upper right shows a tree-lined street with the drain situated on the right, and lower left is the overall view of the drainage system. The stormwater drain on the opposite side of the road (not shown) was also blocked (June 2008).	107
Figure 4.9 A view of the stormwater inlet drain (SWD No. 74 (See Tables 4.1 and 4.2) at the corner of Laura Street and Prospect Terrace, Highgate Hill) blocked with organic matter in a residential suburb of Brisbane. Inside the drain is shown on upper left and upper right is the top view.	108
Figure 4.10 An unblocked stormwater drain during rainfall event. Water entering into the inlet (right) and existing (left) as shown by the arrows.	108
Figure 4.11 A storm water inlet drain (SWD No. 19, See Tables 4.1 and 4.2) on a busy route under a railway bridge is covered with organic waste (at the T junction between Park Road and Annerley Road, South Brisbane). Lower left is inside the drain which is blocked with stagnant water contaminated with traffic dust. The upper left is the front view of the drain located at the junction (May 2008).	109
Figure 4.12 In the vicinity of stormwater drain (Figure 4.11) in fine sediment residue is an accumulation of traffic dust and organic material after a wet weather period (T junction between Park Road and Annerley Road, South Brisbane). This creates hazardous conditions for cyclists (May 2008).	110
Figure 4.13 A collection of litter (plastic bottles, cigarette butts polystyrene and organic matter) in a stormwater drain (SWD No. 10, See Tables 4.1 and 4.2) during wet weather.	111
Figure 4.14 Inside the landscaped garden in front of the hotel Diana shopping complex (Annerley Road, South Brisbane). Patrons from a nearby public drinking house contribute to the discarded waste. Overall view of the front garden is shown on the upper right (October 2007).	112
Figure 4.15 Passive dumping (litter discarded at public seating places) of food/drink and cigarette butts at a bus stop in front of a sport shop on a busy road (June 2008).	113
Figure 4.16 Cigarette butts litter the pavement and gutter next to a public drinking house - Clarence Hotel (situated on the corner of Stanley Street and Annerley Road, South Brisbane, June 2008).	114
Figure 4.17 The South Bank railway station in Brisbane has a no smoking policy ban on the platform and on trains. Hence, the approaching park area to the station is used as a dumping ground by smoking passengers prior to entering the platform. Upper right is a part view of the park area next to the station.	115
Figure 4.18 The no smoking policy at a local private hospital (Mater, South Brisbane) encourages smokers to use the area outside the buildings for disposing of their cigarette butts, for example, in the garden bed as shown. The garden bed (upper left) is situated next to the car park and busway which is opposite the entrance to the hospital (upper right).	116
Figure 4.19 This drain is located on a pedestrian crossing at a busy intersection along the Brisbane River. The roadside gutters at the pedestrian crossing are commonly used	

to dispose of cigarette butts. Lower right shows the drain at the road intersection (October 2007).	117
Figure 4.20 The traffic island (see map in Figure 4.19) which is on a popular pedestrian route from the Mater bus station to local universities, South Bank entertainment precinct and the city.	118
Figure 4.21 Broken beer bottles found on a busy pedestrian route (South Bank) next to a community centre and the railway station.	119
Figure 4.22 Lower right is a gross pollutant trap for the nearby housing estate (Sinnamon Park an outer suburb of Brisbane) catchment. Gross pollutants captured mainly consist of organic matter such as leaves and grass clippings which clog the internal retaining screens.	121
Figure 4.23 Field monitoring of the <i>LitterBank</i> GPT at a residential catchment area in an outer suburb of Brisbane (Marsden Park). The surrounding area is similar to the view shown in map of Figure 4.22. The capture of mainly fine sediments was due to a nearby construction site of new houses.	122
Figure 4.24 The view of the pipe inlet attached to the GPT in Figure 4.23. Fine sediments deposited are a result of a low incoming stormwater flow rate.	122
Figure 4.25 Definition of variables for the gutter/pavement flow relationship of roadway channels. See Figure 2.26 (Clarke et al., 1981).	124
Figure 4.26 Theoretical gutter/pavement flow relationship for roadway channels (Clarke et al., 1981) with (a) smooth gutter and smooth pavement and (b) smooth gutter and moderately rough pavement. For definition of variable see Figure 2.25.	126
Figure 4.27 An accumulation of organic matter (mainly grass clippings) obstructing the water flow course at the stormwater drain.	127
Figure 4.28 Flow characteristics of various organics during light rainfall: (a) accumulation of smaller matter into a mulch formation; (b) mainly litter with some organics; (c) twigs and small litter items and (d) leaves and twigs.	128
Figure 5.1 The Komori probe frequency response experimental setup in the flume.	148
Figure 5.2 The Komori (scalar dye concentration) controller (voltage supply unit) (a), the dye probe (b), the essential measurement features and the dimensions (c).	149
Figure 5.3 The frequency response methods shown in graphical form, used on data sampled by the Komori probe.	151
Figure 5.4 Theoretical frequency response curves for effective measurement width $D_{\text{eff}} = 0.5, 1, 2 \text{ \& } 6 \text{ mm}$.	151
Figure 5.5 A typical data plot showing a sharply defined rise peak.	152
Figure 5.6 Typical experimental data plots showing false peaks caused by the partial detection of dye.	152
Figure 5.7 Comparison of experimental rise data (FrmA, FrmB, FrmC, FrmD, FrmE) with theoretical frequency response (FrmTs, $D_{\text{eff}} = 0.5 \text{ \& } 1.0 \text{ mm}$).	154
Figure 5.8 Comparison of the experimental fall data (FrmA, FrmB, FrmC, FrmD, FrmE) with theoretical frequency response (FrmTs, $D_{\text{eff}} = 0.5, 2 \text{ \& } 6 \text{ mm}$).	154
Figure 5.9 Experimental and theoretical frequency response curves (FrmA-B & FrmT $D_{\text{eff}} = 0.5, 1, 2 \text{ \& } 6 \text{ mm}$) with 95% confidence prediction limits.	155
Figure 5.10 A histogram of the rise and fall response time ratio and the corresponding frequency response methods.	156
Figure 5.11 Average experimental rise and fall response times.	156
Figure 5.12 (a) Measuring the dispersion of blue dye from an outboard motor (b) A closer view of the Komori probes and the boat stern with the outboard motor (Honda).	157

Figure 5.13 An example of a time series graph with peak concentration dye measurement from one of probes shown in Figure 12 (b).....	158
Figure 5.14 Maximum concentration in each successive 10 second window corresponding to the data in Figure 5.13.....	159
Figure 5.15 SQID (GPT)— <i>LitterBank</i> insitu.	159
Figure 5.16 Plan view of <i>LitterBank</i> Scale Model with the Komori probes at inlet and outlet.....	160
Figure 5.17 Time series of peak concentration measurements obtained by introducing dye (a) instantaneously (pulse input) and (b) continuously (step input).....	161
Figure 6.1 GPT— <i>LitterBank</i> in situ.	169
Figure 6.2 Plan view of the <i>LitterBank</i> with the measurement stations St.1 (x = 137.5), St.2 (x = 182.5) and St.3 (x = 450).	170
Figure 6.3 Front view of upstream inlet structure showing the measured plane.	173
Figure 6.4 The computational domain: uniform 40 mm grid and, detail of near-wall mesh refinement adjoining 6 mm grid.....	177
Figure 6.5 Axial velocity profiles at station 2.	178
Figure 6.6 (a) Key diagram (see Figure 6.8) (b) experimental and CFD lengths (mm) for the smaller (near wall) flow feature.	179
Figure 6.7 Experimental vector plots at 27 mm from the GPT bed for (a) experiment and (b) CFD (SKE).....	181
Figure 6.8 Streamlines illustrating global flow structure for (a) SKE (standard two-equation k- ϵ) or (b) EWT (enhanced wall treatment).....	181
Figure 6.9 Axial velocity profiles at station 1, 27 mm from GPT bed, CFD (SKE: standard two-equation k- ϵ ; EWT: enhanced wall treatment) versus experiment (Expt).....	182
Figure 6.10 Axial velocity profiles at station 1, 27 mm from GPT bed, CFD (SKE: standard two-equation k- ϵ ; EWT: enhanced wall treatment) versus experiment (Expt).....	182
Figure 6.11. Axial velocity profiles at station 3, 27 mm from GPT bed, CFD (SKE: standard two-equation k- ϵ ; EWT: enhanced wall treatment ;) versus experiment (Expt).....	183
Figure 6.12 (a) near-wall region ($Re_y = 0$ to 200) and (b) mean axial velocity profiles at station 3 for SKE (standard two-equation k- ϵ) and EWT (enhanced wall treatment) models computed on bl-grid06 grid.....	184
Figure 7.1 Plan view of the <i>LitterBank</i> with the measurement stations St.1 (x = 137.5), St. 2 (x =182.5) and St. 3 (x=450).	193
Figure 7.2 Front view of upstream inlet structure showing the measured planes.....	197
Figure 7.3 Local coordinate systems for the ADV probes, (a) down-looking and (b) side-looking.....	199
Figure 7.4 (a) Key diagram and (b) global and local coordinate Cartesian system for the GPT and the ADV probes, respectively.....	200
Figure 7.5 Axial velocities (V_x) measured at the trap entry (See 2, in Figure 7.1) using 3 ADV operations. Measurements with the side-looking probe are taken—left facing the inner wall and, right towards the baffle for Run 4 (Table 7.1).	200
Figure 7.6 Analytically calculating the exact area under a typical spline interpolated velocity profile $[P(x)]$ of a dataset using the definite integral.	204
Figure 7.7 (a) Experimental and computed axial velocity profiles (Run 1, Table 7.1) at St. 1 (b). Measurements taken with 3D side (SL) and down-looking (DL) ADV probes. Comparisons are made with the previous dataset (pipe, DL, 27) for the pipe-inlet-configured GPT taken at 27 mm from floor, and with the 2D CFD simulation (Madhani et al., 2009b).	207

Figure 7.8 (a) Experimental and computed axial velocity profiles (Run 1, Table 7.1) at St. 2 (b). Measurement taken with 3D side and down-looking ADV probes Comparisons are made with the previous dataset (pipe, DL, 27) for the pipe-inlet-configured GPT taken at 27 mm from floor, and with the 2D CFD simulation (Madhani et al., 2009b).....	208
Figure 7.9 (a) Experimental and computed axial velocity profiles (Run 1, Table 7.1) at St. 3 (b). Measurement taken with 3D side and down-looking ADV probes. Comparisons are made with the previous dataset (pipe, DL, 27) for the pipe-inlet-configured GPT taken at 27 mm from floor, and with the 2D CFD simulation (Madhani et al., 2009b).....	208
Figure 7.10 (a) Experimental axial velocity profiles (Run 4, Table 7.1) at St. 1 (b). Measurement taken with 3D side and down-looking ADV probes.....	209
Figure 7.11 (a) Experimental axial velocity profiles (Run 4, Table 7.1) at St. 2 (b). Measurement planes taken with 3D side and down-looking ADV probes.....	211
Figure 7.12 Measurement comparison at the trap entry (St. 2) between the side-looking (SL) and the down-looking (DL) ADV probes at 40 mm distance from the floor for Run 1(Table 7.1).....	211
Figure 7.13 (a) Percentage of net flow at the three cross sections of the GPT (St. 1, St. 2 and, St. 3) and, (b) key diagram.....	212
Figure 7.14 Head loss experiments with various screen blockages (100%, 68% and 38%) and no screens.....	212
Figure 8.1 GPT—LitterBank <i>in situ</i>	221
Figure 8.2 Clippings from grass verge collected at a stormwater drain at Park Road, South Brisbane (2008).....	224
Figure 8.3 Results of the litter field survey taken from 2006 to 2008. Comparison of gross pollutant (organic & litter) data are made with data collected from Sydney (Van Drie, 2002), Melbourne (Lewis, 2002) and Los Angeles (Lippner and Moeller, 2000; Quasebarth et al., 2001).	226
Figure 8.4 Field surveys showing the GPT LitterBank with (a) high, and (b) low water tidal levels, partially and (c) fully blocked screens.	227
Figure 8.5 Overall view of the steps for producing the LIC image.....	231
Figure 8.6 A single frame capture of the experimental flow for R3 (Table 8.2) with (a) particle seeding, (b) the vector plot from the data processed by the PIV software and (c) the improved vector plot using Matlab (version 2008b) for R3 dataset.	236
Figure 8.7 Image based vector fields (a) R1, 100% blocked, water depth 0.1m; (b) R2, 100% blocked, water depth 0.3m; (c) R3, 68% blocked water depth 0.1m; (d) R4, 68% blocked water depth 0.3m; (e) R5, 33% blocked water depth 0.1m; (f) R6, 33% blocked water depth 0.3m; (See Table 8.2for R1 to R6). Color map: red, yellow, green, blue and violet denotes high to low velocities respectively.....	238
Figure 8.8 Image based vector fields (a) R7, 100% blocked, water depth 0.1m; (b) R8, 100% blocked, water depth 0.3m; (c) R9, 68% blocked water depth 0.1m; (d) R10, 68% blocked water depth 0.3m; (e) R11, 33% blocked water depth 0.1m; (f) R12, 33% blocked water depth 0.3m; (See Table 2 for R8 to R12). Color map: red, yellow, green, blue and violet denotes high to low velocities respectively.....	239
Figure 8.9 CFD global flow structures for run R1 in Table 2, in form of (a) streamlines and (b) vector plots. Source (Madhani et al. 2009).	240
Figure 9.1 GPT—LitterBank <i>in situ</i>	249
Figure 9.2 Plan view of the gross pollutant trap (LitterBank) with labelled sections.	250
Figure 9.3 Deposits of gross pollutants modelled with polystyrene blocks (1-5) to represent partial and a fully blocked GPT. Only the retention area is considered (See also Table 9.4).	256

Figure 9.4 Left, a snapshot of the preliminary litter deposit experiments with tin cans. The partially blocked GPT is modelled with three polystyrene blocks (see blocks 1, 2 and 3, Figure 9.3).	257
Figure 9.5 Left, A snapshot of a fully blocked GPT taken from litter deposit experiments with tin cans. The partially blocked GPT is modelled with all five polystyrene blocks (see blocks 1-5, Figure 9.3).	257
Figure 9.6 A typical residence time distribution (RTD) normalised F curve.	261
Figure 9.7 Left, experiments with fully blocked screen show the neutrally buoyant spheres (RD =1.0) escaping the GPT via the bypass (See data point A in Figure 9.8 at 1.3 L/s on the abscissa). B (See left of figure) denotes the existence of large negative horizontal velocities (right to left).	266
Figure 9.8 Normalised capture/retention profiles (R') for continuously fed variable density spheres (RD) = 0.1, 0.9, 1.0 and 1.1. The channel-inlet-configured GPT experiment is with fully blocked screens tested under varying flow rates (See Figure 9.7 for B).	266
Figure 9.9 Deposition pattern for the GPT with 68% blocked screen shows total (100%) capture/ retention of the lightest pollutants (RD = 0.1) at a high (35 L/s) flow rate (See C, Figure 9.10).	266
Figure 9.10 Normalised capture/retention profiles (R') for continuously fed variable density spheres (RD) = 0.1, 0.9, 1.0 and 1.1. The channel-inlet-configured GPT experiment is with 68% blocked screens tested under varying flow rates. See Figures 9.9 and 9.11 for C and D, respectively.	267
Figure 9.11 Single layer deposition pattern for the GPT with 68% blocked screen capture/retention of the lightest pollutants (RD = 0.9) at a low (3.9 L/s) flow rate (See D, Figure 9.10).	267
Figure 9.12 A snapshot of a field investigated GPT showing deposits of sediments which are similar to the pattern from the gross pollutant capture/retention experiments with partially buoyant spheres (See Figure 9.11). Note the blocked inlets in both cases.	267
Figure 9.13 Normalised escaped artificial pollutants (spheres, RD = 0.9), and experimental dye concentration residence time profiles C1 (Run 1, Table 9.1), C2 (Run 2, Table 9.1) and CFD for 100% blocked screen.	270
Figure 9.14 Comparisons of residence times obtained with GPT blockages using polystyrene shapes and plug flow theory.	270
Figure 10.1 An overview of the current research with main subdivisional headings is shown in the flowchart. The experimental setup parameters are grouped under R1–R12 in Table 10.1.	276
Figure 10.2 An overview of the field work and associated areas of investigations, namely: littering habits in urban areas and street waste which enters stormwater systems and is eventually captured by GPTs. The illustrated removable cover and internal view of the GPT <i>LitterBank</i> are shown at the top and bottom of this figure. The figure on the upper right is the view of the stormwater outlet from the South Bank urban catchment discharging into the Brisbane River.	279
Figure 10.3 A flowchart to show the signal processing methodology used on data collected from dye experiments. In addition to addressing the spikes, the integrity of data was checked using the mass balance routine (see last box in the above flowchart).	282
Figure 10.4 The signal processing routine in Figure 10.3 provides (a) an option menu to compare the raw with filtered data as shown in (b) in the form of a comparative plot.	283
Figure 10.5. A 3D overview of the visualised flow in the GPT with fully blocked screens, obtained from initial hydrodynamic investigations. The sparsely spatial resolution of the velocity points (50 mm) does not capture the local flow features.	284
Figure 10.6. Velocity profiles from ADV and 2D PIV measurements in the retention area of the GPT are shown for a high (a) and (b) low flow inlet rates. The CFD profile for the lower flow rate is also included.	287

Figure 10.7 Head loss for (a) the rectangular and (b) the circular-pipe-inlet-configured-GPT
measured under various screen blockages and no screens.288

List of Tables

Table 1.1 Comparative published data on GPTs and other SQIDs	4
Table 2.1 Tabulation of published gross pollutant data.....	35
Table 2.2 Comparative published data on GPTs and other SQIDs	41
Table 4.1 Gross pollutants in stormwater drains in South Brisbane (monitored from 2006 to 2008)	131
Table 4.2 Gross pollutants on stormwater drains in inner southern Brisbane suburbs (monitored from 2006 to 2008).....	137
Table 4.3 Gross pollutants on streets in inner southern Brisbane suburbs (monitored from 2006 to 2008)	138
Table 5.1 Summary of frequency response tests performed, Expt-A (tests 1-5) and Expt-B (tests 6-9).....	153
Table 5.2 Rise and fall time constants using the five methods (see equation 5.2), and E is the measurement uncertainty (equation 5.3).	154
Table 7.1 A matrix of flow regimes used in the experimental setup for litter capture.	197
Table 7.2 Material used in place of normal screens in the GPT to represent percentage of blocked screens.	201
Table 7.3 Integrated data (Q_I) across station St. 1, see key diagram in Figure 12 (b) and the measured flow rate (Q_i) at the collection tank	210
Table 7.4 Error between positive and negative integrals at St. 1 and 2 (See Figure 7.13).	210
Table 8.1 Material used in placed of normal screens in the GPT to represent percentage of blocked screens	228
Table 8.2 Experimental setup of flow regimes through a GPT with designated blocked screen runs.....	228
Table 9.1 Matrix of flow regimes used in the experimental setup for litter capture.....	252
Table 9.2 Material used in placed of normal screens in the GPT to represent percentage of blocked screens	252
Table 9.3 Generic spherical particles used in the litter capture experiments.....	254
Table 9.4 Shaped polystyrene blocks and the corresponding percentage of GPT volume reduction.....	255
Table 9.5 The average capture/retention efficiencies for the four spheres with different densities using the step input function (continuous feed).....	265
Table 9.6 The average capture/retention efficiencies for the three blockage conditions and both the continuous and intermittent methods of input	265
Table 9.7 Residence times t obtained from capture/ retention experiments using spheres, dye measurements and CFD simulation. Key: Water depth (WD), relative density (RD), inlet flow rate (Q_{in}), variance σ^2 , skewness (s^3) and kurtosis (k^4).	268
Table 10.1 Experimental setup parameters for the GPT rig.....	276
Table 10.2 A comparison of the capture/retention results for the channel and the pipe-inlet configured GPT	290
Table 10.3 Summary of data collected for the current scientific research of a GPT	292

List of Abbreviations

Abbreviations

ADV	Acoustic Doppler Velocimeter
API	Application Programming Interface
ASCE	American Society of Civil Engineers
AUSMEPA	Australian Marine Environment Protection Association
BMP	Best Management Practice
CC	Convergence Criteria
CDS	Circular Deflective Separation
CFD	Computational Fluid Dynamics
CLA	Chemiluminescent
CW	Cold Wire
COR	Correlation
CRC	Cooperative Research Centre
DAF	Dissolved Air Flootation
EWRI	Environmental and Water Resource Institute
Expt	Experiment
EWT	Enhanced Wall Treatment
GIS	Geographic Information System
GPT	Gross Pollutant Trap
IV	Intravenous
KAB	Keep Australia Beautiful
KABCQLD	Keep Australia Beautiful Council Queensland (KABC Qld)
KESAB	Keep South Australia Beautiful
MASTEP	The Massachusetts Stormwater Technology Evaluation Project

NET	In Line Netting Systems
NJCAT	The New Jersey Corporation for Advanced Technology
PC	Personal Computer
PIV	Particle Image Velocimeter
RANS	Reynolds Averaged Navier Stokes
Re	Reynolds Number
RD	Relative Density
SEPT	Side Entry Pit Trap
SKE	Standard Two-Equation k- ϵ Turbulence Model
SQID	Stormwater Quality Improvement Device
SNR	Signal Noise Ratio
SWD	Stormwater drain
RTD	Residence Time Distribution
TAPE	Technology Assessment Protocol – Ecology
TARP	Technology Acceptance and Reciprocity Partnership
u-gridXX	Uniform Grid XX
WSUD	Water Sensitive Urban Design

Statement of Original Authorship

The work contained in this thesis has not been previously submitted to meet requirements for an award at this or any other higher education institution. To the best of my knowledge and belief, the thesis contains no material previously published or written by another person except where due reference is made.

Signature: *J. Madhani*

Date: 8/6/2010

Acknowledgments

The completion of this PhD thesis is attributed to support and guidance from numerous QUT members. I would like to express my sincere thanks to my principal supervisor A/Professor Richard Brown and associate supervisors Dr Neil Kelson, A/Professor Les Dawes and Dr Joe Young for their interest, continuing support and encouragement.

I wish to thank the Faculty of Built in Environment and Engineering (BEE) and the QUT High Performance Computing & Research staff for their ongoing research support during my candidature.

I acknowledge QUT and in particular Phil Thomas: for the ARC linkage grant support.

To Professors Alex Fonarev and Mehmet Atlar, my friends and previous work colleagues I express my sincere thanks for their friendship and encouragement in pursuing this journey.

I graciously thank my parents for giving me opportunities to undertake my earthly lessons of which this journey is one of many. To my mother and father, I say: I share the joy in completing this journey with you.

Finally, I dedicate this work to the most important person in my life. To Sarita, I say: Without your love, understanding and support in more ways than one I would not have succeeded on this journey.

List of Publications

PEER REVIEWED CONFERENCES

Madhani, J. T., Kwek, L. M. K., Brown, R. J., Kelson, N. A. and Frost, R. L. (2005).

Investigating the flow field of a stormwater quality improvement device. Paper presented at the Environmental Engineering & Sustainability (EES). Power House, Sydney: Institution of Engineers Australia.

Madhani, J. T., Pendrey, D. C., Situ, R. and Brown, R. J. (2007). Assessment of a

Scalar Concentration (Komori) Probe for Measuring Fluctuating Dye Concentration in Water. Paper presented at the *16th Australasian Fluid Mechanics Conference (AFMC)*. Crown Plaza, Gold Coast, Australia: School of Engineering, University of Queensland.

Madhani, J. T. and Brown, R. J. (2010). A summary of an investigation of the

capture and retention characteristics of a gross pollutant. Paper to be presented at the *17th Australasian Fluid Mechanics Conference (AFMC)*. Auckland, New Zealand: Faculty of Engineering, University of Auckland.

Madhani, J. T., Young, J. and Brown, R. J. (2010). A summary of the hydrodynamic

investigation of a gross pollutant trap. Paper to be presented at the *17th Australasian Fluid Mechanics Conference (AFMC)*. Auckland, New Zealand: Faculty of Engineering, University of Auckland.

Madhani, J. T. and Brown, R. J. (2011). A Comprehensive investigation into the

hydrodynamic and capture/retention performance of a gross pollutant trap. Paper to be presented at the *34th World Congress of the International Association for Hydro-Environmental Engineering and Research (IAHR)*. Brisbane Convention & Exhibition Centre, Brisbane, Australia: IAHR and Engineers Australia.

PEER REVIEWED JOURNALS

Madhani, J. T. and Brown, R. J. (2008). A Scalar Concentration (Komori) Probe for Measuring Fluctuating Dye Concentration in Water. *WSEAS Transactions on Fluid Mechanics*, 3(3), 224-233.

Madhani, J. T., Kelson, N. A. and Brown, R. J. (2009). An experimental and theoretical investigation of flow in a gross pollutant trap. *Water Science and Technology*, 59(6), 1117-1127.

Madhani, J. T., Young, J., Kelson, N. A. and Brown, R. J. (2009). A novel method to capture and analyze flow in a gross pollutant trap using image-based vector visualization. *Water, Air, & Soil Pollution : Focus*, 9(5-6), 357-369

Madhani, J. T., Dawes, L. A. and Brown, R. J. (2009). A perspective on littering attitudes in Australia. *The Environmental Engineer: Journal of the Society for Sustainability and Environmental Engineering*, The institution of Engineers, Australia, 9(4), 13-20.

An historical perspective on Australian littering attitudes and their environmental impact. *Journal of Australian Studies* (Revised draft pending submission).

Madhani, J. T. and Brown, R. J. (2010). An investigation of the capture and retention characteristics of a gross pollutant. (To be submitted).

Madhani, J. T., Young, J. and Brown, R. J. (2010). The hydrodynamic investigation of a gross pollutant trap. (To be submitted).

Madhani, J. T., Young, J. and Brown, R. J. (2010). Visualisation experimental flows through a gross pollutant trap. *Water Research* (Under review).

[This page has been left blank intentionally.]

Chapter 1: Introduction

This thesis is presented through a series of peer-reviewed scientific publications. The thesis details the development of a novel and comprehensive testing approach to examine a recently manufactured dry sump gross pollutant trap (GPT). The design of the GPT is based on linear fluid motion characteristics with internal screens to capture gross pollutants—organic matter and anthropogenic litter.

The testing approach uses a combination of physical and theoretical models to examine in detail the hydrodynamic and capture/retention characteristics of the GPT. The experimental and theoretical modelling was based on the likely operations of the GPT under real conditions which included fully and partially blocked screens as observed during field work.

In addition to the field work, a review on the testing of GPTs and gross pollutant data was extended to include an historical overview of street waste and stormwater pollution. These above mentioned studies are the most comprehensive available to date and provide valuable information for the current research, and for any future work pertaining to the operations of GPTs and management of street waste in the urban environment.

In the current research, further contributions were also made by establishing measurement methodologies for deploying acoustic Doppler velocimeters (ADV) and custom made scalar dye concentration probes in a GPT for the first time. Here, a methodology has been developed using the dye concentration probes for effective operations under a range of flow conditions in the GPT.

In this chapter, the motivation and overview of work are presented in Section 1.1 and the research aims and objectives are given in Section 1.2. In Section 1.3 the scope of the work is outlined. The narrated accounts linking the research objectives and the scientific publications (Chapters 4-9) are provided in Section 1.4. Finally, Section 1.5 summarises the key contributions arising from this study.

1.1 MOTIVATION AND OVERVIEW OF WORK

During a rainfall event, stormwater—surface water runoff from urban areas—transports pollutants accumulated on streets and roadside gutters into receiving waterways. Stormwater pollutants are harmful to the aquatic and terrestrial ecosystem when transported into the environment. This has led to the development of stormwater quality improvement devices (SQIDs) to capture and prevent the various pollutants from contaminating the environment. Gross pollutant traps are a class of SQIDs and are designed to capture visible waste such as anthropogenic litter and organic matter. Gross pollutants on streets are usually the first stormwater pollutants targeted for removal in urban catchment management, and GPTs are deployed as stand-alone devices or as part of a treatment process that also includes ponds and wetlands. This deployment is necessary, since street sweeping mechanisms and practices alone appear to be inadequate in tackling street waste.

To investigate the management of street waste, the comprehensive literature review in Chapter 2 has been complemented with an evaluation of the past and current Australian littering culture and its potential impact on the environment (as documented in Chapter 3). The nature of this evaluation involved collecting historic material from the websites of local city councils, the National Library of Australia and educational institutions. The outcome of this chapter established the need to address the long term management of street waste and GPTs play an important role in this process.

Despite the influx of new and varied GPT designs due to stormwater pollution concerns in the past decade, scientific literature on the topic is surprisingly limited, as shown in Chapter 2. The applied nature of this research encompasses activities involving professional and research organisations together with government agencies and industries—often in partnership with one or more of these bodies. In view of this, a comprehensive literature review was compiled including unpublished manuscripts from these bodies along with peer-reviewed scientific publications.

Gross pollutant traps—including patented and registered designs developed by industry—have some specific internal configurations and hydrodynamic separation characteristics which demand individual testing and performance assessments. Newly developed stormwater devices are usually evaluated by environmental

protection agencies (EPAs), professional bodies and water research centres. In the USA, the American Society of Civil Engineers (ASCE) and the Environmental Water Resource Institute (EWRI) are examples of professional and research organisations actively involved in these evaluation/verification programs. These programs largely rely on field evaluations that alone are limited in scope, mainly for cost and logistical reasons. In Australia, evaluation/verification programs of new devices in the stormwater industry are not well established.

To address these limitations, this research extends beyond conventional field evaluation methods to investigate a recently developed *LitterBank* GPT by C-M Concrete Products Pty. Limited. Unlike most other devices, this type of GPT is designed with a dry sump to avoid waste decomposition in water. The design also has a separate bypass channel to minimise flooding due to blockages. The prefabricated unit can be installed on ground level, thereby reducing installation costs. Currently, there are approximately 20 *LitterBanks* operating at strategic stormwater locations throughout Queensland, Australia. However, despite the increasing use of this type of GPT, research database on the *LitterBank* GPT—or on a GPT of similar design—is scant.

A summary of the extensive research database on GPTs and other SQIDs from Chapter 2 is shown in Table 1.1. This table presents an overview of the research relative to the classification of the ‘Linear’ and ‘Radial’ type GPTs, ‘Storage detention tanks’, ‘Vortex separators’ and ‘Conventional GPTs/trashraks’ (as described in Chapter 2). In Table 1.1, the cited literature was organised into nine possible research areas—methods which have been used to investigate the capture/retention characteristics of these devices. Further details of these investigations are provided later. In Table 1.1, a ‘YES’ or a ‘NO’ signifies whether the device has been investigated under the relevant given ‘Research Areas’.

The *LitterBank* GPT device has been classified as a ‘Linear GPT’, see Column 2, in Table 1.1. To expand the database in Table 1.1 under ‘Linear GPT’, and meet the growing need for evaluating GPTs and other SQIDs more efficiently and systematically, this work represents, to the author’s knowledge, the first attempt to develop and apply more comprehensive testing methodologies. These methodologies provide tools for rigorously examining the performance of GPTs under a range of in-field operating conditions.

The GPT examination followed a systematic order in which each testing methodology was executed as described later in this chapter. The outcome of each test either informed or expanded on the previous work. Subsequently, the work resulted in several chapters and peer-reviewed papers as shown in Figure 1.1.

In this figure, the work commences with the previously mentioned complementary investigation of the past and current generation of street waste (as documented in Chapter 3). This was followed by field studies as presented in Chapter 4.

Table 1.1 Comparative published data on GPTs and other SQIDs

<i>Research Areas</i>	<i>Linear GPT</i>	<i>Radial GPT Continuous Deflective Separation (CDS)</i>	<i>Storage/ Detention Tanks</i>	<i>Vortex/ hydrodynamic Separators</i>	<i>Conventional GPTs/ (trashracks)</i>
1. Design/optimisation & overview studies	*YES	YES	YES	YES	YES
2. Field monitoring/testing	NO	YES	YES	YES	YES
3. Flow field	NO	YES	YES	YES	YES
4. Dye experiments	NO	NO	YES	YES	NO
5. Laboratory capture/retention experiments (real/artificial pollutants)	NO	YES	YES	YES	YES
6. Hydraulic head loss	* YES	YES	NO	YES	YES
7. Screen blockages	NO	NO	NO	NO	YES
8. Flow visualisation	NO	NO	NO	YES	NO
9. CFD	NO	NO	YES	YES	NO

* Water retaining (wet sump) devices only

In the remaining chapters (See Chapters 5-9, Figure 1.1), the testing methodologies comprise experimental and theoretical modelling techniques. These techniques were informed by findings from field work in specific urban areas of Queensland, covering an interval of approximately 2 years (as reported in Chapter 4).

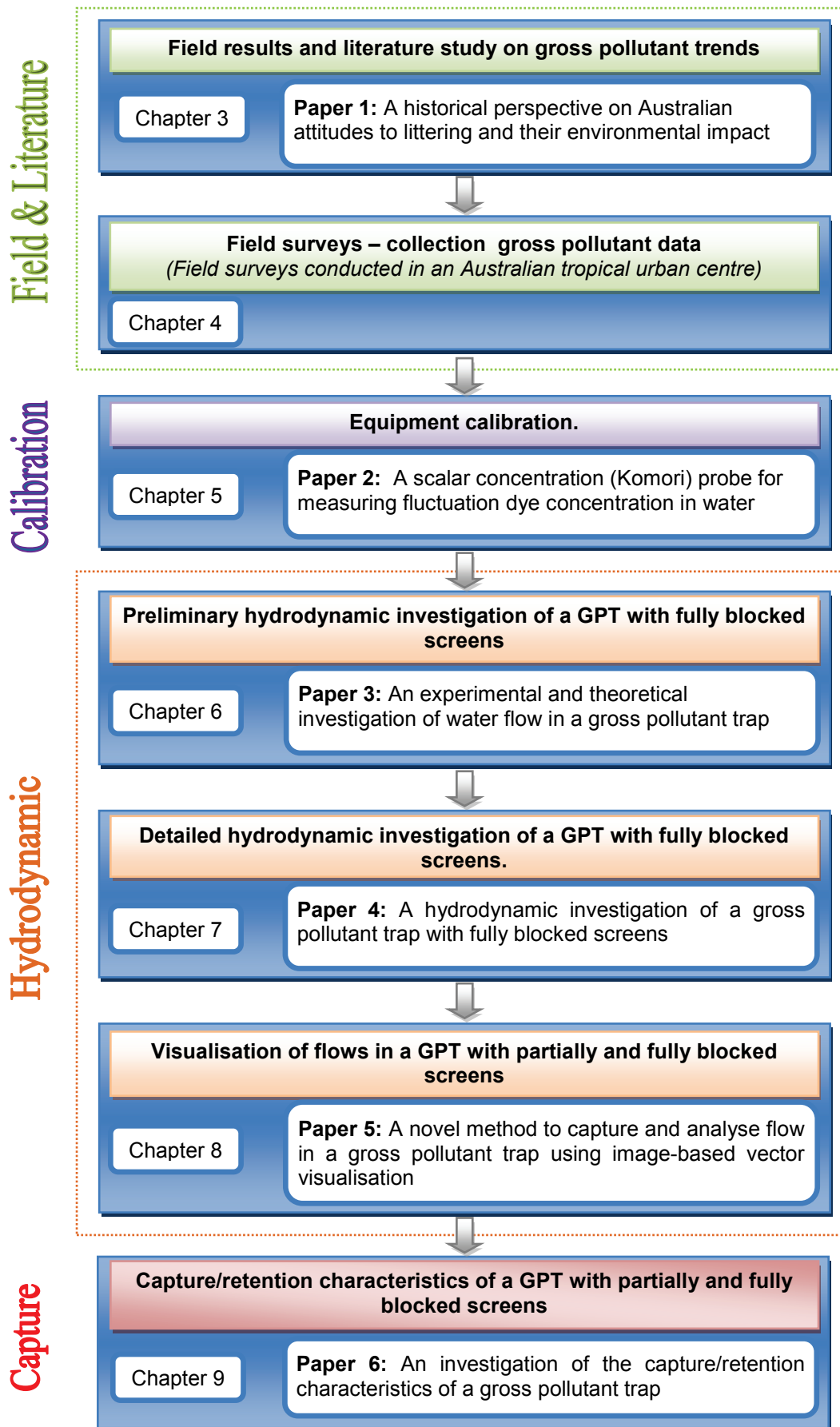


Figure 1.1 Overview of the research as outlined by the titles of the thesis chapters and papers.

An important observation noted from the field studies was that internal retaining screens of GPTs are often clogged with organic matter due to infrequent cleaning. Partially or fully blocked screens can radically change the hydrodynamic and pollutant capture/retention characteristics of a GPT. In contrast, the literature review later presented in Chapter 2—and summarised in Table 1.1, revealed that there is little data pertaining to GPTs operating with screen blockage conditions. The general consensus amongst researchers and the stormwater industry is that SQIDs should be tested under adverse operating conditions such as blockages. In view of this, testing of the hydrodynamic and pollutant capture/retention performance of the GPT undertaken in this research included blocked and unblocked retaining screens under a range of flow regimes.

Observations made during the course of this research indicate that the possible flow regimes inside the GPT can range from turbulent time dependent free surface to steady state, depending on the operating conditions. This presents significant challenges for either experimental or theoretical studies. Particularly when conducting experiments in GPTs with dry sumps, since some measuring devices with intrusive probes require a minimum water depth for proper operations.

To overcome these challenges, an experimental approach was developed which also included calibration and performance assessment of equipment such as scalar dye concentration probes (as documented in Chapter 5 and discussed in Chapter 10).

The experimental approach used a weir arrangement to physically model the possible flows in the GPT. This facilitated a sequence of hydrodynamic and gross pollutant capture/retention experiments as shown in Figure 1.1. Figure 1.2 provides a more detailed view of the work outlined above, including field and equipment calibration, in addition to the hydrodynamic and gross pollutant capture/retention experiments.

Initial hydrodynamic experiments focused on establishing and analysing flow regimes within the *LitterBank* GPT with fully blocked retaining screens. Hydrodynamic data was collected using point-based velocity measurements (See ADV, Figure 1.2). Theoretical studies using CFD simulations were performed for the assumed steady state flow and comparisons were made with the measurements (as reported in Chapter 6).

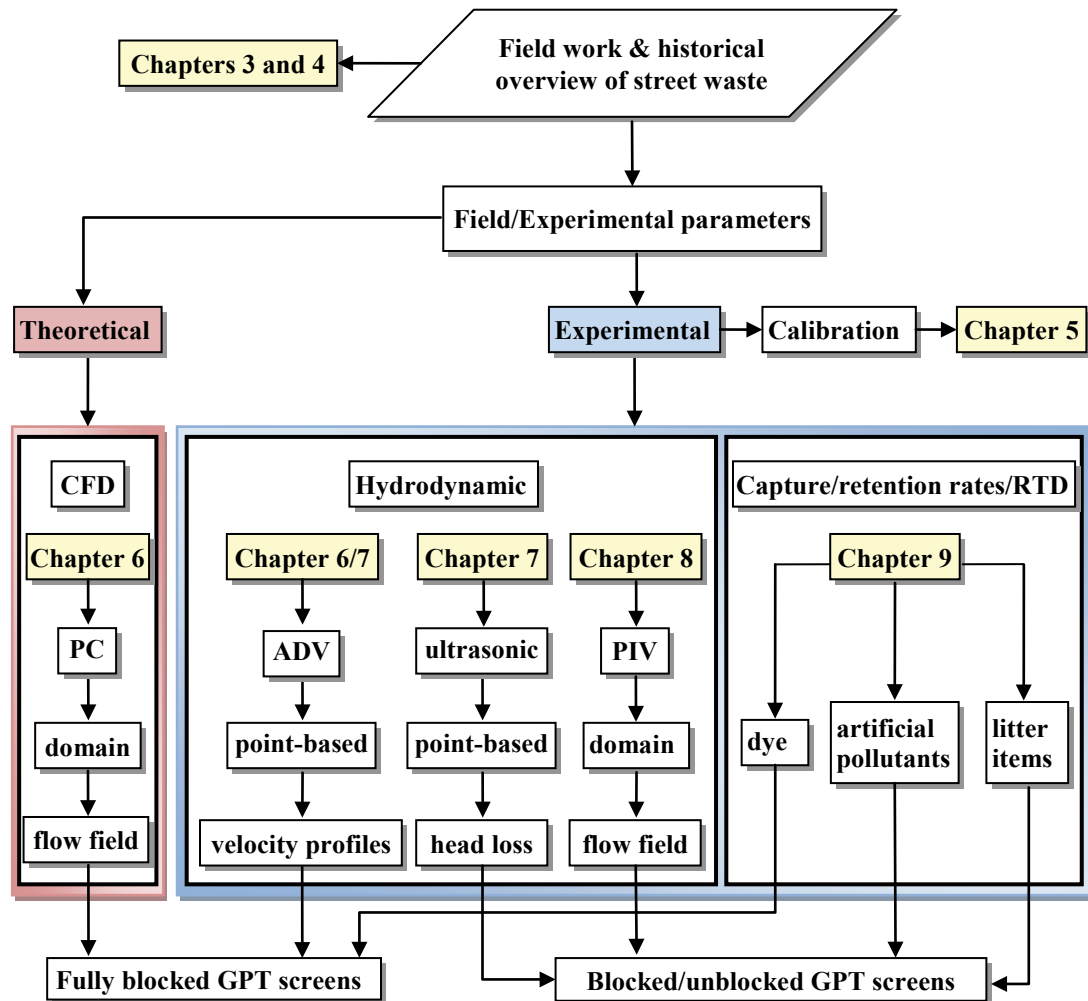


Figure 1.2 Flowchart showing an overview of the research and the work as presented in the chapters of the thesis.

A key outcome of this initial investigation was the identification of global and local flow structures, important for understanding gross pollutant capture/retention experiments.

Subsequently, further investigations of flow structures in the GPT were undertaken using a more refined point-based measurement technique and this enabled a more comprehensive collection of experimental dataset (See ADV, Figure 1.2). Results of this work are presented in detail in Chapter 7. However, the hydrodynamic dataset was limited to the GPT *LitterBank* with fully blocked retaining screens due to the labour-intensive nature of point-based measurements.

To overcome the limitations of point-based measurements, another approach was used to capture a more detailed GPT flow data. The particle image velocimetry

(PIV) technique was used to investigate the GPT with partially and fully blocked screens, for a range of flow regimes (See PIV, Figure 1.2).

An issue arose while displaying the PIV data, since conventional methods of visualisation—for example, vector plots—lacked clarity; the larger the dataset the more cluttered the plots. This issue was addressed by using dense texture-based vector field visualisation as shown in Chapter 8. This is the first time that texture-based vector field techniques have been used to visualise experimentally collected vector data. The outcome of this technique resulted in a number of images which were used to compare the hydrodynamic data of various flow regimes and screen blockages.

In addition to experiments using point-based velocity and PIV methods, head loss measurements were also conducted under similar flow screen blockage conditions (See head loss, Figure 1.2). Head loss experiments pertaining to the GPT with different inlet configurations and no internal screens were also undertaken. The additional head loss experiments were taken to supplement hydrodynamic data where flow field data was not possible, mainly due to time constraints.

A clear distinction in the hydraulic head loss performance between the GPT with fully and partially blocked screens was observed. This distinction was also noted in the gross pollutant capture/retention experiments for similar configurations and operating conditions.

Finally, in addition to the hydrodynamic studies outlined above, gross pollutant capture/retention experiments were also undertaken (Figure 1.2). Here, tracer dye or customised variable density pollutants were introduced into the GPT flow for a range of operating conditions. Key measures for the gross pollutant capture/retention such as removal/trapping efficiencies and residence time distributions (RTDs) were obtained and analysed.

This facilitated the gross pollutant capture/retention performance to be quantified in terms of maximum (100%) and minimum performance (0%) under normal and adverse operating conditions.

Furthermore, comparisons between the RTDs of dye and variable density pollutants were also made and reported (See dye and artificial pollutants, Figure 1.2). Such comparisons are scarcely reported.

1.2 RESEARCH AIMS AND OBJECTIVES

The threat of storm water pollution to the aquatic and terrestrial ecosystems has prompted scientific efforts to investigate environmental protection devices and inform the community of their findings. The aim of this thesis is to address the shortcomings and need, as summarised in Table 1.1 under ‘Linear GPT’ (See item 2 to 9 under ‘Research Areas’, highlighted in red) which are:

1. To develop a comprehensive approach using field survey, experimental and theoretical techniques for evaluating GPTs
2. To apply this approach to a recently developed GPT and thus create a comprehensive database accessible to the research community
3. To collect data pertaining to the past and current generation of gross pollutants for evaluating the long term management of street waste.

1.3 SCOPE OF THIS STUDY

As mentioned above, the scope of this research includes a detailed field investigation which indicated the need for scientific investigations of a GPT with blocked screens (as documented in Chapter 4). The scope of this research covers: field work and an extended literature review, equipment calibration, hydrodynamic studies and gross pollutant capture/retention investigations (Figure 1.2).

Field work was confined to the monitoring of gross pollutants in Brisbane City, South Brisbane, Highgate Hill, South Bank and Burleigh Heads, a growing seaside suburb. These areas were chosen for their residential, business and commercial urban activities and their proximity to the city. Here, gross pollutant data was collected over a period of two years from streets, public places and urban drainage systems. The installation sites of the GPT *LitterBanks* were also monitored to inform hydrodynamic and gross pollutant capture/retention experiments in the laboratory.

All experiments conducted as part of this research were performed on a 50% scale model GPT rig with screen blockages varying from 0 to 100%. This rig was placed in the 19 m flume located in the hydraulic laboratory at Queensland University of Technology as shown in Appendix D. Also shown in this appendix are the various GPT configurations used in the experimental investigations.

The gross pollutant capture/retention experiments were conducted mainly with customised variable density artificial pollutants and tracer dye. A restricted number of experiments were conducted with anthropogenic litter items.

Apart from gross pollutant capture/retention experiments, the hydrodynamic investigation consisted of experimental and CFD modelling. Experimental data consisted of acoustic Doppler velocimetry (ADV) measurements and flow field capture—using a high speed camera and PIV software (Figure 1.2). Experimental head loss data was collected using ultrasonic sensors and vernier height gauges. These depth measuring devices were also used to constantly monitor the flow conditions in the flume. This enabled the quantification of experimental errors and also to inform CFD modelling. The CFD modelling was restricted to 2D and such predictions appeared to be adequate for the purpose of this research.

Prior to these experiments, calibrations and independent checks on laboratory equipment were conducted to ensure the authenticity of data collected. For the hydrodynamic investigation, a routine calibration of the ADVs was undertaken as a result of commissioning difficulties. Generally, the ADVs and most other instrumentation used in the current research, are well documented and require little calibration or preparation. However, for the custom made scalar dye concentration instrumentation, a lack of characterisation data warranted a detailed performance and suitability feasible investigation for the residence time measurements planned in this research.

The detailed investigation included the development of calibration procedures and the methodology for deploying the scalar dye (Komori) probes. The Komori dye probes were used to measure the residence times of gross pollutants entering the GPT in the capture/retention experiments.

The gross pollutant capture/retention investigations were limited to specific types of anthropogenic litter and artificial pollutants (as documented in Chapter 9). Anthropogenic litter was limited to tin cans, bottle caps and plastic bags, while the artificial pollutants consisted of 40 mm spheres with a range of four buoyancies.

The scaling of data obtained from the experiments was not an issue since full scale comparisons were not required at this stage. The focus was solely on the

different testing methods for collecting hydrodynamic and capture/retention performance data for the GPT under investigation.

1.4 LINKING THE RESEARCH OBJECTIVES AND THE SCIENTIFIC PAPERS

The research outcome is presented through a series of peer reviewed scientific publications and chapters centred on the key aspects of this research as shown in Figure 1.1. The main body of this thesis consists of a field investigation (Chapter 4) and six research papers (Chapters 3 and 5 to 9) which systematically and sequentially address the research objectives broadly outlined in Section 1.2. The following discussion of the more specific objectives and their corresponding papers, therefore, provides the research narrative and overview.

1. To collect and examine the characteristics of historical and current gross pollutant trends in Australia and their effect on the environment

[Ref. Chapter 3 (Paper 1): Madhani, J. T., Dawes, L. A. and Brown, R. J. (2009). *A historical perspective on Australian attitudes to littering and their environmental impact*. Journal of Australian Studies (Revised draft pending submission). See also a related paper (not included in this thesis): Madhani, J. T., Dawes, L. A. and Brown, R. J. (2009). *A perspective on littering attitudes in Australia*. The Environmental Engineer: Journal of the Society for Sustainability and Environmental Engineering, The Institution of Engineers, Australia, 9/10(4/1), 13-20.]

The research objective of Chapter 3 (Paper1) is to examine the past and current urban activities that promote street waste which is likely to harm the environment. Little data is available on the history of street waste. Hence, information was collected from old photographs, municipal records, published literature and private individuals. The information gathered, together with the results of the field/case study (as documented in Chapter 4), reveals both the increasing volume of anthropogenic litter and the high amount of organic matter found on streets and in stormwater systems. This chapter provides valuable information for current and future street waste management practices and serves to better inform architects and planners who are designing environmentally friendly green urban centres.

2. To collect field data of a recently developed GPT for the conduct of experimental and theoretical investigations. To investigate (for this purpose) waste/gross pollutants found on streets and stormwater systems in a typical Australian sub-tropical urban environment

[Ref. Chapter 4: *The field/case study.*]

The field/case study (as documented in Chapter 4) consisted of collecting and analysing gross pollutant data from streets, stormwater systems and GPTs. Such data provides important insights for the subsequent physical and theoretical modelling performed in this study. The data was also used to identify public littering attitudes and typical street waste which are important factors in the design, testing and placement of GPTs in urban environments. For example, during the surveys it was found that GPTs were placed in residential areas where the main source of stormwater pollution was sediments rather than gross pollutants.

The outcome of this chapter shows that a high percentage of organic matter is generally found on the streets and in the stormwater systems of mixed activity urban areas. This matter blocks or clogs the retaining screens of strategically placed GPTs, and inspections of their internal retaining screens often found that they were clogged due to infrequent cleaning. In commercial/business areas, larger amounts of anthropogenic litter were found compared to mainly residential areas. Also, low flow rates as a result of intermittent rainfall are common in GPTs and the motion behaviour of gross pollutants in stormwater was found to have varying characteristics of buoyancy.

3. To develop relevant experimental methodologies, including calibration techniques for flow field, residence time and gross pollutant experiments

[Ref. Chapter 4 (Paper 2): Madhani, J. T. and Brown, R. J. (2008). *A Scalar Concentration (Komori) Probe for Measuring Fluctuating Dye Concentration in Water*. WSEAS Transactions on Fluid Mechanics, 3(3), 224-233.]

Under the research objective of Chapter 4 (Paper 2), methodologies for conducting flow field, head losses, residence time and gross pollutant experiments were developed. The techniques for calibrating instruments were also incorporated in these methodologies where applicable. Flow field experiments were conducted with ADVs which required little or no testing prior to deployment (Chapters 5 and 6). The widely used ADVs rely on the speed of sound in water for their calibration.

However, in this case, some difficulties were experienced with the new ADVs and a troubleshooting strategy was developed to ensure the quality of data collected was maintained throughout the measurements. Further information on these ADV measurement issues are reported in the ‘Results and Discussion’ section of Chapter 9 and in Appendix C.

The ultrasonic probes for the water depth measurements required minimal calibration. However, satisfactory checks of these probes were made with the vernier height gauge.

The Komori tracer (dye) instrumentation for performing residence time measurements in conjunction with gross pollutant experiments (described in Chapter 9) was custom built. For this research, the custom built dye concentration (Komori) probe was used for its multi-channel high frequency sampling performance and its compact, slender geometrical configuration—the diameter of the probe casing is 6mm—was best suited for measurements in the GPT.

Initial appraisals revealed problems with noise and drift when sampling data. Since no history of measurements of the Komori probe is reported, a comprehensive performance assessment was conducted. Therefore, Chapter 4 (Paper 2) meets this research objective by undertaking this assessment and using case studies to establish a standard testing methodology. The dye experimental results for the GPT are elaborated in Chapter 8 (Paper 6) and in the General Discussion section.

4. To carry out a preliminary experimental and theoretical investigation of water flow in a GPT with fully blocked screens and to refine the measurement methodologies

[Ref. Chapter 6 (Paper 3): Madhani, J. T., Kelson, N. A. and Brown, R. J. (2009). *An experimental and theoretical investigation of flow in a gross pollutant trap*. *Water Science and Technology*, 59(6), 1117-1127.]

Field observations in Chapter 3 showed that internal retaining screens are commonly blocked with organic matter due to infrequent cleaning. Low flow rates and elevated outflow water levels into the receiving waters were also commonly observed onsite.

In Chapter 5 (Paper 3), the fourth set of research objectives are achieved by collecting hydrodynamic data for such flow conditions in a GPT with fully blocked

screens. Flow field data for GPTs with fully blocked screens is rarely reported. The data was experimentally and theoretically obtained using computational fluid dynamics (CFD) where the flow is assumed to be approximately two-dimensional. Seven distinct flow features are identified as important in describing the gross pollutant capture characteristics of the trap. The outcome of this chapter warranted a more detailed hydrodynamic investigation.

5. To comprehensively experimentally investigate a range of flow regimes in a GPT with fully blocked screens using extensive point velocity measurements, and to examine the head losses

[Ref. Chapter 6 (Paper 4): Madhani, J. T., Young, J. and Brown, R. J. (2010). *The hydrodynamic investigation of a gross pollutant trap with fully blocked screens*. Water Research (Under review).]

Chapter 6 (Paper 5) extends the two-dimensional study and meets the above objective with a comprehensive set of velocity measurements taken within a channel inlet configured GPT under a wider range of flow conditions, various depths and measurements near walls. This was achieved by using a combination of new ADV probes to overcome the measurement limitations from the previous experiments (Chapter 5). However, the use of these semi-intrusive probes within the restricted space of the GPT required the development of a specific technique to perform these measurements. Between vertical walls, a series of measurements were taken with a combination of geometrically configured—down and side-looking—ADV probes. The side-looking probe was aligned to face each of the walls and measurements were taken in both directions. This technique resulted in a comprehensive collection of point-based velocities and the precise alignment of the ADV probe ensured the continuity of the dataset from each of measurement direction when combined.

The results of the ADV measurements facilitated greater comparison with the previous 2D CFD data (Chapter 5), and similarities were noted. The ADV, CFD and the measured head loss data showed that the GPT with fully blocked screens radically change the hydrodynamic operations within the GPT for all inlet cases. For example, a large recirculating flow pattern occurred within the retention area of the GPT, and was accompanied by hydraulic short circuiting where the preferred outflow path was via a bypass. This data provided a detailed map of the amount of fluid entering and leaving the GPT at various points.

It was shown that 20% of the incoming flow enters and leaves the capture/retention area of the GPT. This is based on the assumption that the fluid does not recirculate at the point of entry into the capture/retention area. Thus, the majority of the incoming gross pollutants are more likely to escape via the bypass channel. Regions where the velocity profiles varied across the depth, potentially showed that pollutants with varying densities will behave differently in the fluid path motion. Head loss experiments further showed that the hydrodynamic performance of the GPT will remain unaffected if the blockages of the internal screens are below 70%.

6. To experimentally investigate a range of flow regimes in a GPT with fully and partially blocked screens using image based techniques

[Ref. Chapter 7 (Paper 5): Madhani, J. T., Young, J., Kelson, N. A. and Brown, R. J. (2009). *A novel method to capture and analyze flow in a gross pollutant trap using image-based vector visualization*. *Water, Air, & Soil Pollution: Focus*, 9(5-6), 357-369.]

Point-based velocity measurements with the ADV are more suited to collecting flow data in localised areas. Such measurements are labour intensive and spatially limited in terms of flow domain coverage. Previous chapters have mainly focused on a GPT with fully blocked screens. The research objectives of Chapter 7 (Paper 5) were met by developing a method to spatially capture and analyse several experimental flow regimes through a GPT with both fully and partially blocked screens.

While acknowledging some uncertainties in the two-dimensional depth coverage method, the simplified approach permitted the added benefit of a range of flow regimes and screen blockage conditions. A high speed camera above the GPT and PIV software were used to track neutrally buoyant particles. Subsequently, a set of flow patterns was obtained and visualised through an image-based line integral convolution (LIC) algorithm producing a dense representation of streamlines. Due to the finely spaced dataset—which are rarely possible with experimental results—image-base visualisations were widely used in CFD to highlight both global and local flow features. An interpolation technique was used on the experimental dataset to deploy such visualisations which are superior to conventional hedgehog or arrow plots. For example, there are distinct differences between the shallow and deeper

water depth flow patterns in the retention area of the GPT. The visualised flow patterns clearly showed superior flow domain coverage than the previous ADV measurements. Similarities were observed for all inlet cases, with distinct variations in the length and size of the flow features. These flow features indicated that the hydrodynamic performance of the GPT with partially blocked screens of at least 70% will remain unaffected, as indicated by the previous head loss data (Chapter 7).

7. To develop and use the relevant methodology to investigate the gross pollutant capture/retention characteristics of a GPT with variable relative density objects; to relate these characteristics to the hydrodynamic data from the research objectives above (See item 6)

[Ref. Chapter 8 (Paper 6): Madhani, J. T. and Brown, R. J. (2010). *An investigation of the capture and retention characteristics of a gross pollutant*. Water Research (Under review).]

Previous chapters discussed the hydrodynamic performance of a GPT with fully and partially blocked screens. Here, flow features important to the capture/retention characteristics of gross pollutants were also identified through experimental and theoretical studies. These studies were conducted in a pollutant-free testing environment. The investigation did not include factors such as the concentration and remobilisation of pollutants; the hydrodynamic forces due to pressure, inertia and drag; or the interaction with neighbouring pollutants and the boundary walls. For larger pollutants, the process of accumulation rapidly transforms the free space in the GPT to solid boundaries. This changes the fluid path motion. These factors and modelling issues are a relatively new concept in CFD predictions using particle/coupling mechanism simulation. Consequently, capture/retention experiments are still necessary despite their lengthy preparation. Tracer dye experiments are often used in place of real or artificial pollutants but are limited in their density representation, as demonstrated in this chapter.

The final above mentioned research objective is met in Chapter 8 (Paper 6) by using dye and customised variable density spherical objects—artificial pollutants—filled with liquid to investigate the capture/retention characteristics of a GPT. Since the GPT is designed to treat a range of gross pollutants, these objects were classified into floatables—partially submerged, neutrally buoyant and sinkable objects—for the capture/retention experiments. Experiments were conducted for both the pipe and

channel inlet configured GPT. The hydrodynamic findings from previous studies, along with the results from these experiments, provided a comprehensive dataset. The dataset was used to describe the positive and negative attributes of both the capture/retention characteristics and design of the GPT.

1.5 RESEARCH CONTRIBUTIONS

There are numerous direct and indirect benefits emanating from this research and these are highlighted below.

Firstly, the literature review on GPTs and gross pollutant data undertaken in this work (as documented in Chapter 2) is, to the author's knowledge, the most comprehensive to date. Similarly, the published historical overview of the street waste for this thesis paper (See Chapter 3) is also the first of its kind to be compiled.

Secondly, the observations made from the field study (Chapter 4) provide for the first time, valuable information for this research and for future work pertaining to the operations of GPTs and management of street waste in the urban environment.

Thirdly, a detailed investigation of a recently manufactured dry sump GPT based on linear fluid motion characteristics is conducted. The outcome of the investigation adds to the GPT database and addresses the research gaps identified by the literature review (as summarised in Table 1.1 under 'Linear GPT' (See item 2 to 9 under 'Research Areas', highlighted in red).

Fourthly, this is the first and most detailed investigation on a GPT conducted to date using a combination of hydrodynamic and capture/retention assessment techniques. The hydrodynamic study includes point-based measurements, flow field capture, head loss experiments and CFD simulation. The gross pollutant capture/retention work included the use of anthropogenic litter components, tracer dye and custom modified artificial gross pollutants.

Fifthly, the findings from this research are of practical significance and form a basis for operations, management and maintenance of GPTs including any future design improvement studies undertaken.

In addition to the above outlining research contributions, this research also provides for the first time a detailed performance assessment and a methodology—

including calibration procedures—for using the Komori scalar dye concentration probes.

Lastly, one of the indirect benefits associated with this research, is related to the use of ADV probes for velocity measurements in a GPT for the first time. This approach involved developing a specific technique for performing measurements in limited spaces due to the intrusive nature of the ADV probes.

Chapter 2: Literature Review

This chapter contains the scientific review of work pertaining to gross pollutants and GPTs. As previously mentioned in Chapter 1, the applied nature of this work involves professional societies, research organisations, local city councils, government agencies and the stormwater industry—often in partnership with one or more of these bodies. In view of this, the comprehensive literature review included unpublished manuscripts from these bodies along with scientific peer reviewed conferences and journal publications. In this thesis, these references are defined herein as primary, secondary and tertiary literature sources for journals, conferences and unpublished/non-peer reviewed manuscripts, respectively.

The review presented in this chapter pertains to the collection of gross pollutant data Australia-wide and the testing of GPTs. The chapter commences with a discussion of gross stormwater pollutants from urban areas and the need for GPTs (See Section 2.1). The review of literature relating to gross pollutant data is given in Section 2.2. Scientific works relating to GPTs, SQIDs and similar devices are reviewed in Section 2.3. Section 2.4 elaborates on the current approaches for the testing of newly developed GPTs. Other possible approaches are also discussed, such as hydrodynamic studies (See Section 2.5), gross pollutant capture/retention experiments (See Section 2.6) and residence time measurements using a tracer scalar dye (See Section 2.7). Work involving blockages in GPTs is presented in Section 2.8. Finally, in Section 2.9 a summary of the research gap identified in this literature review is given.

2.1 GROSS STORMWATER POLLUTANTS AND THE NEED FOR GPTS

In urban areas, natural vegetation is replaced by artificial surfaces and the soil beneath is compacted. Such impervious surfaces prevent the natural absorption of rain thereby increasing the amount and the rate of runoff discharge (Goonetilleke et al., 2005; Livingston and McCarron, 1991). During a storm, pollutants are collected

by stormwater on the urban runoff path and discharged into receiving waterways (Bochis-Micu and Pitt, 2005).

Unmanaged, stormwater pollution can result in considerable damage to the aquatic and terrestrial ecosystem. Stormwater pollutants can inflict physical, chemical and/or biological damage. The detrimental impact of stormwater pollutants are well documented (Borchardt and Sperling, 1997; Grapentine et al., 2008; Pitt and Burton, 2001). The visible impact of gross accumulated pollutants in waterways is generally perceived to indicate poor water quality. However, some researchers argue that the finer pollutants such as toxicants and nutrients are more harmful. The toxicity of traffic-generated dust and nutrients from decomposed organic matter are some examples (Sansalone et al., 1998; Strynchuk et al., 2000a). Investigations also show that suspended solids—small solid particles such as sediments which remain suspended in moving waters—are carriers for these finer harmful pollutants (Field and Sullivan, 2003).

Findings from field work conducted as part of this study (documented in Chapter 3) show that gross pollutants are also potential carriers for these finer and more harmful pollutants. During field observations, it was noted that gross pollutants with water absorbing surfaces such as leaves and paper appeared to be more efficient carriers. Further investigations are necessary to quantify these gross pollutant findings.

The generation and composition of gross stormwater pollutants in a specific urban area in Victoria, Australia have been investigated (Allison et al., 1994; Allison et al., 1997; Allison et al., 1998; Chiew et al., 1997). The results were translated as mass per hectare per year. This indicates that a city the size of Melbourne in Victoria, generates approximately 60,000 tonnes/230,000 cubic metres of gross pollutants—120 Olympic sized swimming pools—and 2 billion items of litter annually (Allison et al., 1997).

Gross pollutants are visible waste such as anthropogenic litter and organic matter dimensionally greater than 5 mm (Wong et al., 2006). On waterways, gross waste is not only unsightly; it emit strong odours and can attract vermin; it may cause a major health risk due to the putrefying contents of fast food and beverage containers and pathogenic organisms attached to discarded hypodermic needles; it can serve as a breeding ground for mosquitoes; threaten aquatic fauna with

entanglement or suffocation (Figures 2.1 and 2.2) through ingestion (Allison et al., 1998; Marais and Armitage, 2004; Russell, 1999); or can cause landscape erosion and blockages in urban drainage systems. More importantly, a large proportion (60% to 80%) of non-biodegradable waste entering the waterways via stormwater drains on streets eventually becomes a source of marine pollution, and this is also of public concern.



Figure 2.1 Anthropogenic waste—a Pelican strangled by a plastic bag (Healthy Waterways & Brisbane City Council, 2008).



Figure 2.2 Fish kill caused by ingestion of cigarette butts (Healthy Waterways & Brisbane City Council, 2008).

Non-biodegradable waste has increased dramatically over the past four decades due to the growth of the manufacturing industries and the changing lifestyle (Chapter 3). Chapter 3 includes an extended literature review which elaborates on the historical perspective of Australian littering attitudes and street waste during this period.

As highlighted in the historical review, in urban catchments, significant amount of street waste enters stormwater/urban drainage systems during bursts of rain and wind (Walker and Wong, 1999). Walker and Wong (1999) also reported that the current Australian street sweeping practises are generally ineffective against this growing street waste problem.

Similar findings were reached elsewhere; in the USA, the constant flow and concentration of litter discharged made street sweeping ineffective (Lippner and Moeller, 2000).

It was concluded from these studies, that there is little correlation between the frequency of sweeping and the actual transportation of gross pollutants into the stormwater system and urban waterways.

This led to the development of SQIDs such as GPTs in order to protect the urban waterways from street borne pollution. The investigation of gross pollutants found on streets and in stormwater systems are a prerequisite for the design and placement of GPTs within the urban environment. Subsequently, the collection of gross pollutant data becomes an important factor as demonstrated in this research.

A compilation of literature on urban wet weather flow has been comprehensively conducted by a group of researchers and the Environmental protection Agency (EPA) in the USA (Clark et al., 2007) . The EPA is essentially the governing body that provide policies and regulations relating to urban waste and stormwater management to protect the environment from discharged pollutants. The compilation consists of over 6,000 articles from conferences and journal publications spanning over a period of 11 years (1996-2006) concerning stormwater and sewage treatment. However, within this body of work, there is little information pertaining to gross pollutant data and GPTS.

2.2 GROSS POLLUTANT DATA

A detailed list of factors contributing to the generation and composition of gross pollutants has been compiled (Marais et al., 2001). This list mainly comprises human activities, land use, climatic conditions, traffic volume, population density and community awareness in urban catchments. These factors were based on studies conducted in an inner Melbourne city suburb (Allison and Chiew, 1995; Allison et al., 1998). A decade ago, these authors concluded that more gross pollutant data was needed Australia wide; since then, little progress has been made (Allison et al., 1998). The most recent Australian gross pollutant data was collected in 2002 and reported in 2004 (Chrispijn, 2004).

Table 2.1 (Page 35) shows a comprehensive tabulation of gross pollutant data from streets and GPTs. This table includes data collected from the previously mentioned—primary, secondary and tertiary—sources such as the local city councils

and the stormwater industry to compensate for the little progress made. The table extends over several pages which is located at the end of this chapter.

In this table, details of the cited literature including the names of authors were tabulated under the relevant headings. Details of the citation included: the collection period, the location and the type of devices used to monitor/collect the gross pollutants. The method of analysis used to quantify the percentages of dried gross pollutant components—that is ‘Volume/Mass’—is tabulated in the last column of Table 2.1. The percentages of the gross pollutant components were tabulated under ‘Organic’ and ‘Litter’ in column 5 and 6 of Table 2.1. The percentages of sediment collected were also included in the table if given by the authors.

With regard to the method reported by the author for collecting the gross pollutants, some variations were noted. In Table 2.1, some authors have monitored street borne gross pollutants at the beginning of the stormwater systems (Allison et al., 2000; Chrispijn, 2004; Lewis, 2002; Lippner et al., 2000). Other authors have mainly reported captured gross pollutant loads in GPTs downstream prior to discharging into receiving waterways (Brisbane City Council, 2004). For example, on the outskirts of Brisbane, only these latter loads have been reported.

The above outlined review of gross pollutant data—as tabulated in Table 2.1—mainly relates to urban cities in Australia. Similar gross pollutant studies have been conducted in South Africa and in the USA which are also included in this table. However, the most recent gross pollutant data studies were conducted in 2001 (Marais et al., 2004) and 2002 (Kim et al., 2006) in South Africa and the USA, respectively. In both these cases, the results of the gross pollutant collection were reported much later than the actual date of collection. Despite this, the data was useful for making comparisons with the field/case study results documented in Chapter 4.

2.3 GROSS POLLUTANT TRAPS (GPTS)

The block diagram in Figure 2.3 was specifically drawn to illustrate the placement of GPTs in tackling street waste. In this figure, the ‘Stormwater System’ block diagram is the intermediary between the ‘Public’ and the ‘Environment’. Waste discarded by the public enters the stormwater systems and discharges into the

environment. The placement of GPTs within urban environments depends on factors such as public littering attitudes and street waste (see A and B in Figure 2.3). For example, in Figure 2.3, A refers to the treatment at *point source* in public places; B represents any drainage catchments prior to entering receiving waters where pollution is treated as *non-point* or *diffuse source*. Here, GPTs can also be deployed with other SQIDs such as ponds and wetlands to capture both the gross and fine stormwater pollutants, respectively.

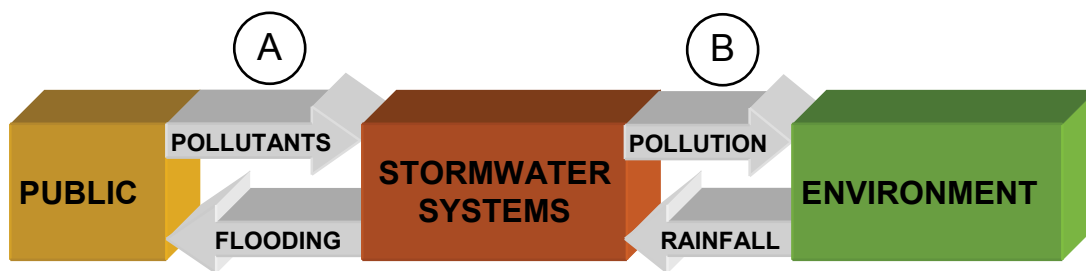


Figure 2.3 A block diagram representing the interaction of the public with the environment, where A and B are the pollution preventive point and diffusive sources respectively. These sources can be treated using stormwater quality improvement devices such as GPTs.

Gross pollutants are usually the first target for removal in urban catchments. Subsequently, in water sensitive urban design (WSUD), GPTs are essentially used as a pre-treatment process prior to using ponds and wetlands.

The treatment of fine stormwater pollutants with sedimentation in ponds and wetlands has been well documented in recent years. However, ponds and wetlands suffer complex and costly maintenance issues when they are blocked with pollutants. An informal report indicated that a local council in Queensland, Australia is faced with just such a problem which has arisen a few years earlier than the treatment device's anticipated design life expectancy. However, such issues with ponds and wetlands are not within the scope of this study since the focus of this research relates mainly to GPTs.

Despite the introduction of new GPT designs over the past decade due to stormwater pollution concerns, scientific literature is surprisingly limited. It is not clear whether this lack of GPT data is due to cost factors, insufficient resources and government standards, or to the reluctance of manufacturers in sharing their GPT

data. For example, a local city council in Australia listed over 15 types of GPTs available for purchase. However, despite the availability of the GPTs, evaluation data pertaining to their gross pollutant capture/retention performance is scant (Hunter, 1998; Victoria Stormwater Committee, 1999).

As with the previous literature review of gross pollutant data, the scientific works pertaining to GPTs were also obtained from the primary, secondary and tertiary sources. The outcome of the GPT review was tabulated in Table 2.2 (Page 41) located at the end of this chapter.

This table presents an overview of the research relative to the classification of ‘Linear’ and ‘Radial’ type GPTs, ‘Storage detention tanks’, ‘Vortex separators’ and ‘Conventional GPTs/trashracks’. In Table 2.2, the cited literature, is organised into nine possible research areas for investigating the performance characteristics of these devices. These research areas are elaborated later in this chapter under their respective headings.

A brief introduction of the GPT devices listed in Table 2.2 are given below commencing with ‘Conventional GPTs/trashracks’ under Column 2, Table 2.2. This is followed by the description of the more recent GPTs.

Conventional GPTS/trashracks

Conventional and non-proprietary GPTs/trashracks—the forerunners of SQIDs, were designed to trap larger gross pollutants and sediments in open stormwater detention areas. This GPT was first commissioned in Canberra, Australia in 1979 (Phillips et al., 1989).

A similar but smaller non-proprietary GPT—located in a Brisbane suburb—shown in Figure 2.4 was primarily constructed to treat urban drainage catchments or large areas commonly termed ‘non-point’ or ‘diffuse source’.

A conventional open GPT structure shown in Figure 2.4 typically consists of a large concrete wet basin, weir and trashrack to screen gross pollutants. The sedimentation basin is designed to reduce the velocity of the incoming stormwater flow by its large dimensional width. Within the basin, the reduced velocities encourage the deposition of sediments. Downstream, across the basin, atop a weir,

the vertical or horizontal bars of the trashrack capture the larger pollutants. Bars are typically spaced between 40 to 100 mm.

Conventional GPTs, like most SQIDs that use trashracks, require frequent cleaning, especially after a storm event. Trashrack devices are associated with frequent maintenance and the cleaning is labour-intensive. These devices are susceptible to hydraulic head losses and blockages which often lead to upstream flooding (Beecham and Sablatnig, 1994). Moreover, when the trashrack screens are blocked, without a separate bypass channel, the captured pollutants are often scoured from within the retention area and transported downstream during major storm events.



Figure 2.4 An open GPT consisting of a basin, a trashrack with vertical bars atop a weir located at Bedivere Street, Carindale on the outskirts of Brisbane (November, 2008).

The demand for more compact and efficient GPTs produced an influx of mostly proprietary devices (Brown and Clarke, 2007). The newer and more recent devices were designed to only remove gross pollutants. Hence, the velocities of the incoming stormwater flow were not considered to be an important design consideration as with the sediment basins. The installation of modern smaller-footprint GPTs was not restricted to large open spaces, since a sedimentation basin was no longer required.

Also, unlike the exposed trashracks, these more recent GPT designs had finer screens and the trapped contents were concealed, thus preventing odour problems during dry periods (Zaman and Kandasamy, 1996).

More recent GPTS

The more recent and newer GPTs are classified as either radial or linear fluid motion devices used to capture gross pollutants from stormwater.

In contrast to the linear GPT designs, ‘Continuous Deflective Separation (CDS)’ GPTs and ‘Vortex/hydrodynamic Separators’—under Columns 2 and 3 in Table 2.2—use radial fluid motion for capturing/retaining pollutants.

The use of vortex/hydrodynamic separators for treating combined sewer overflow (CSO) effluent in urban drainage was first documented in the early 1960s (Andoh and Saul, 2003). These separators were the modified original hydro-cyclones which were used in the coal, food, paper and petroleum industries (Bergström and Vomhoff, 2007). Here, the hydro-cyclones were deployed to separate solids, liquids or gases of different densities by gravity.

The tapered body of the hydro-cyclone was modified to incorporate a wider constant cross section insert to treat sewer and stormwater effluent. Depending on the design, either baffle/deflection plates or screens were fitted to capture the incoming pollutants.

The vortex/hydrodynamic has been further modified for the stormwater industry. For example, the continuous deflective separation (CDS) uses circular internal retaining screens to capture/retain stormwater pollutants (Allison, 1999; Wong, 1997). The Australian designed CDS has received considerable scientific interest in comparison to ‘Linear GPTs’ (Allison et al., 1998; Walker et al., 1999).

Although several design variants of ‘Linear GPTs’ (See Column 2, Table 2.2) exist, data is scant for these linear fluid motion devices (Hunter, 1998). Furthermore, the current data shown in Table 2.2 relates to water retaining GPTs, which is similar to the other devices listed in this table. Data for GPTs which do not retain water—dry sump—is not available. It is unclear, whether the modelling complexities of the GPT with dry sump are a deterrent for scientific investigations.

As regards to wet sump GPTs, there are issues due to waste biodegradation in water. Wet GPT systems generally require frequent cleaning as waste biodegradation in water releases toxic substances downstream through a biological and chemical decomposition process. Biodegradation of organics in a GPT is also capable of producing strong odours during cleanouts, prompting nearby residents to complain (Ho, 2001). Brisbane City Council (2004) also reports similar anaerobic conditions for their devices in which ammonium nitrogen is produced.

Wet sump GPTs also require costly maintenance schedules due to the procedure in draining and removing the captured pollutants. Additionally, during cleanouts, informal reports by local residents indicate many of the aquatic inhabitants are killed. Both issues would be a cause for public concern. Overall, data on the issues of wet sump GPTs are lacking in scientific literature.

Floating booms are also GPTs which operate in water and have received little interest. They comprise a string of partly submerged booms located across waterways and were originally designed as oil slick retention devices suitable in slow moving waters. Consequently, these devices are highly suited for the retention of buoyant articles such as plastic bottles and polystyrene. However, they were omitted from Table 2.2, due to the lack of available scientific data.

To compensate for the general lack of GPT data, literature on similar devices that have common investigating methodologies have been included in Table 2.2. Such devices include storage/detention tanks and vortex/hydrodynamic separators which have been deployed in sewer networks (Andoh and Saul, 2003; Stovin et al., 1999; Stovin and Saul, 1994).

Sedimentation and settling basin/detention tanks have received considerable interest since 1904 (Hazen, 1904). Here, the velocities of the incoming effluent are reduced and the settling of pollutants is achieved through gravity. More recent investigations of the storage/detention tanks which separate both gross and fine sewer solids are included in Table 2.2.

2.4 CURRENT PERFORMANCE EVALUATION OF GPTS

Gross pollutant traps—including patented and registered designs—have some specific internal configurations and hydrodynamic separation characteristics which demand individual testing and performance assessments.

There are currently no recognised standard procedures for either field or laboratory testing of GPTs in Australia. Design guidelines for GPTs in Australia have recently been documented (Wong et al., 2006), but these guidelines do not take into account recent field and laboratory findings such as typical performance data (Osei et al., 2008).

In Australia, evaluation/verification programs of new devices in the stormwater industry are not well established. Overall, these programs largely rely on field evaluations. In this regard, field monitoring and comparative investigation of proprietary GPTs have been previously reported—no specific testing procedures were followed (Greenway et al., 2002; Nnadi et al., 2005; Rushton, 2006; Walker and Wong, 1999; Wells and Schwarz, 1999; Younis, 2005). These authors concluded that comparative investigations are only possible if the testing procedures are standardised, regardless of their unique stormwater treatment application.

To regulate the performances of newly developed stormwater treatment devices, field testing verification programs have been established in the USA (Frederick and Stevens, 2007; MASTEP, 2004; NJCAT, 2001; TAPE, 2008; TARP, 2003). The verification programs are usually carried out by the environmental protection agencies (EPAs), professional bodies and water research centres. The American Society of Civil Engineers (ASCE) and the Environmental Water Resource Institute (EWRI) are examples of professional and research organisations actively involved in these evaluation/verification programs.

Recently, the American Society of Civil Engineers (ASCE)/Environmental and Water Resource Institute (EWRI) went a step further by forming a task committee to review the current regulations and to propose new guidelines for the certification of manufactured stormwater best management practices (BMPs).

The new guidelines shifted the earlier focus of field monitoring assessments to evaluation methodologies such as laboratory testing (Bannerman et al., 2009; Guo et al., 2008). This shift is understandable because the collection of field data is site

specific and dependent on weather conditions, with a single test taking years to complete (Hansen, 2001; Rushton et al., 2007).

Most field results also lack meaningful performance assessments of GPTs, since it is only the captured pollutant data that is recorded and not the removal efficiencies (Fletcher et al., 2004; Wong et al., 2000; Wong et al., 2006). To determine the removal efficiency of the GPT, the escaped pollutants should also be monitored. Consequently, laboratory testing is considered to be more effective, rapid and less costly than the conducting of numerous field trials (Allen, 2005; Armitage and Rooseboom, 2000; Luyckx and Berlamont, 2004; Nnadi et al., 2005; Phillips, 1999; Younis, 2005).

The inclusion of laboratory testing in the evaluation/verification of the performance on newly developed GPTs is supported by researchers and those related to the stormwater industry. The advantage of laboratory testing usually outweighs field monitoring assessments of GPTs for a number of reasons such as: logistics, resources, non-site specifics, non-weather dependence, and cost (as demonstrated by this research).

The scientific review of authors evaluating GPTs, SQIDs and other devices using experimental and theoretical methodologies are discussed under the following section: Hydrodynamic, Capture/retention experiments, Tracer dye and Blockages.

2.5 HYDRODYNAMICS

Hydrodynamic investigations of SQIDs have been undertaken to understand their removal capture/retention characteristics. For example, flow field data obtained by CFD simulations have been used to complement measurements and provide detailed flow insights (Hilgenstock and Ernst, 1996; Stovin et al., 1999). Best practise guidelines for CFD studies are well documented (Casey and Wintergerste, 2000) . Such guidelines have been used in this research for performing theoretical hydrodynamic studies using CFD.

Examples of insights gained from hydrodynamic studies include the identification of areas relating to high and low velocity, and regions of flow re-circulation. These flow features can cause erosion, containment and/or mobilisation of pollutants respectively (Harwood, 2002). The deposition pattern of particles have

been shown to be directly related to the flow patterns observed on the surface of the water (Stovin et al., 1999).

In vortex separators, the presence of low velocity regions encourage the formation and settling of large particles, thereby improving the separation efficiency (Tyack and Fenner, 1999). Flow patterns are used to determine characteristics conducive to the removal or retention of particles in stormwater treatment chambers (Faram and Harwood, 2002).

Velocity measurements and CFD have also been used to study flow patterns with a view to identifying important features such as short-circuiting in vortex stormwater separators, sewer structures, sedimentation basins, dissolved air floatation (DAF) tanks and aquaculture raceways (Bochis-Micu and Pitt, 2005; Faram and Harwood, 2002; Huggins et al., 2005; Kwon et al., 2006; Lundh et al., 2002; Oca et al., 2004; Park et al., 2006; Stovin et al., 1999; Tyack and Fenner, 1999). Short-circuiting in GPTs plays an important role when the device is blocked. In other devices, short-circuiting denotes a lack of mixing such as in ponds and wetlands.

The analyses of flow features with a view to understanding the capture/retention characteristics of GPTs—particularly ones with blocked screens—have received limited scientific interest to date. More specifically, experiments using velocity measurements, flow visualisation techniques and CFD data (Table 2.2) are scarcely reported.

Image based flow visualisation techniques using experimental hydrodynamic dataset have also not been previously reported. Such techniques were used to overcome the lack of clarity and the cluttering of information when displaying large datasets with conventional vector plot routines. Further details on the image based visualisation technique used in this research to better understand the pollutant capture/retention characteristics of the GPT is provided in Chapter 8

2.6 GROSS POLLUTANT CAPTURE/RETENTION EXPERIMENTS

Capture/retention experiments (See item 5 in Column 1, Table 2.2) of GPTs have been conducted using mostly real floating litter items (Phillips, 1999) and artificial pollutants (Armitage and Rooseboom, 2000). In those experiments, artificial

pollutants were chosen for their settling velocities; often, a single type was used for simulating sediments. The use of plastic pollutants with different densities has been reported elsewhere but no details were given (Armitage and Rooseboom, 2000).

Custom made pollutants with different densities require lengthy preparation. Thus, tracer dye has also been used to study the removal efficiency of SQIDs such as hydrodynamic separators, ponds and wetlands (Persson and Wittgren, 2003; Phipps et al., 2008). However, dye is limited in its representation of pollutants of varying densities.

The above mentioned dye investigations did not include factors such as the concentration and remobilisation of pollutants; the hydrodynamic forces due to pressure, inertia and drag; or the interaction with neighbouring pollutants and the boundary walls. For larger pollutants, the process of accumulation rapidly transforms the free space in the GPT to solid boundaries, which in turn changes the fluid path motion. The particle/coupling mechanism in CFD simulation to address these factors and modelling issues is a relatively new concept.

Alternatively, the decoupling approach to CFD simulation of the separation of fine sediments and suspended gross solids is well established; nevertheless, the outcomes are not always successful (Stovin et al., 1999). Consequently, capture/retention experiments are still necessary despite their lengthy preparation. For this reason, tracer dye experiments are still used as an alternative option.

2.7 TRACER DYE

Tracer dye experiments are rarely reported for the devices shown in Table 2.2, and none for GPTs. The tracer dye studies shown in the table for vortex/hydrodynamic separators are based on CFD simulation.

Dye is often used in place of real or artificial pollutants but is limited in its density representation, as demonstrated in Chapter 9.

The dye experiments are useful to study flow characteristics in fluid systems (Lapidus, 1957). For example, fluids entering dead zones have very long residence times and a high percentage of suspended and buoyant particles are held here indefinitely (Thackston et al., 1987). The output time series data (dye concentration

versus time curves of the effluent) was used to determine the RTD and the average time the fluid takes to pass through the boundary systems (Levenspiel, 1999).

The relationship between the fluid residence time and pollutant removal in SQIDs has been investigated (Kadlec, 2000; Persson and Wittgren, 2003). The pollutant removal efficiency of vortex devices was shown to be strongly related to the residence time distributions (RTD) within wastewater and stormwater treatment processes (Alkhaddar et al., 2001).

Existing methods of tracer dye experiments tend to rely on non-continuous grab samples or sampling at low frequencies. Probes used to detect dye concentrations in open waterways (rivers, ponds, wetlands etc.) tend to be bulky, and the sampling frequencies are much lower as discussed in one of the author's publications—see Chapter 5 (Madhani and Brown, 2008).

Furthermore, most authors only report results of the outlet tracer concentrations; hence, the mass balance error with the inlet is unquantifiable. The mass balance error is an important confidence level indicator of the data sampled. The inlet data also indicates the homogeneity of the dye and water mixture in order to achieve consistency in the measured concentrations.

The Komori tracer dye instrumentation for performing residence time measurements in conjunction with gross pollutant experiments (described in Chapter 9) was custom built. These experiments have not been previously reported, particularly in the investigation of a GPT with screen blockage characteristics.

2.8 BLOCKAGES

Field observations undertaken in this research and reported in Chapter 3 showed that internal retaining screens are commonly blocked with organic matter due to infrequent cleaning. Blocked GPTs can cause upstream flooding, resulting in the stormwater system to become inoperable.

A bypass is a necessary design feature of the GPT, to allow the incoming pollutants to escape—short-circuiting—when the device is blocked (Wong et al., 2000). Subsequently, the study of devices operating under adverse conditions becomes even more important.

Blockages in a GPT/trashrack impacted by flooding have been previously studied (Abt et al., 1992). Experimental and CFD flow field were used to investigate blocked hydrodynamic separators used for CSO systems (Tyack and Fenner, 1999). The capture/retention performance of a GPT vortex separator with blocked screens have also been documented (Ismail and Nikraz, 2007, 2009).

However, screen blockages for dry linear devices, considered a part of this research, have not been previously reported to the author's knowledge.

2.9 CONCLUSION

Specific aspects of this research are now addressed in the context of a review of the scientific works. The review shows that field and laboratory testing methodologies generally follow no standard procedures or guidelines. The assessments of newly developed GPTs are limited to field evaluations. Testing methodologies of GPTs are not well established abroad and in Australia.

Proprietary GPTs have unique internal configurations and hydrodynamic separation characteristics which demand specific testing. Despite an influx of GPT designs, scientific data on these devices is limited. There is also little information pertaining to GPTs operating under adverse conditions such as screen blockages.

Research data on the *LitterBank* GPT—or on a GPT of similar rectangular/linear straight flow through design—is scant, despite the increasing need for this type of device.

It is also concluded from this review that there is a lack of gross pollutant data in Australia to support the current and future management of street waste. This includes street waste generated by merging green planning concepts as discussed later in Chapter 3.

Chapter 3 is an extended literature review comprising an historical overview of street waste, stormwater pollution and SQIDs. This is supported by a field case study documented in Chapter 4 which also includes preparatory work for the remaining chapters. The remaining chapters (Chapters 5-9) report the equipment calibration, hydrodynamic and gross pollutant capture/retention testing results of the GPT under in-field settings.

Table 2.1 Tabulation of published gross pollutant data

Author/notes	Period	Location	Device	Organic (%)	Litter (%)	Sediments (%)	Method
Nielsen & Carleton (1989)	1986-7	Sydney (Cooks River), NSW					
		1. Muddy Creek	} Floating booms Trashracks	50	50	-	volume
		2. Cup and Saucer Creek		41	59	-	volume
		3. Marrickville-Mackay Park		22	78	-	volume
Sim & Webster (1992)	1990	Sydney (Cooks River), NSW Floating booms					
		1. Cup & Saucer Creek		60	40	-	volume
Gamtron (1992)	1992?	Sydney region, NSW					
		(Hawthorne Canal, Dobroyd Canal, Rushcutters Bay & Blackwattle Bay)	} Floating booms				
		Average		71	29	-	volume
O'Brien (1995)	1993	Sydney, NSW					
		1. Lamrock Avenue, Bondi	GPT	61	31	8	mass
		2. Roscoe Street, Bondi	GPT	60	36	4	mass

Table 2.1(cont.) Tabulation of published gross pollutant data

Author/notes	Period	Location	Device	Organic (%)	Litter (%)	Sediments (%)	Method
Ignacio (2000)	1999/	Sydney					
Circular Deflective Separator (CDS)	2000	1. Drummoyne	CDS	85	15	-	volume
Van Drie (2002)	2001	Sydney region, NSW					volume
		1. Roscoe Street, Bondi	GPT	72	28	-	volume
No given details on GPTs.		2. Lamrock Avenue, Bondi	GPT	72	28	-	volume
The author acts as a consultant to		3. Botany	GPT	79	21	-	volume
Sydney Water where the GPT database		4. Orissa Street, Canterbury	GPT	76	24	-	volume
was obtained.		5. Roslyn Gardens	GPT	75	25	-	volume
		5. Wollli Creek	GPT	77	23	-	volume
		6. Cup & Saucer Creek		76	24	-	volume
		7. Marrickville - Mackay Park	Trashracks	73	27	-	volume
		8. DPS 2 – Marrickville		70	30	-	volume
Manly Hydraulic Laboratory (2002)	2002	New South Wales					
(Mossman City Council)		Little Sirius Cove, Sydney	CDS	86	6	8	volume
Circular Deflective Separator (CDS)							

Table 2.1(cont.) Tabulation of published gross pollutant data

Author/notes	Period	Location	Device	Organic (%)	Litter (%)	Sediments (%)	Method	
		Victoria						
Jago (1997)	1996	Melbourne Airport	CDS	53	1	46	mass	
		Coburg	CDS	39	26	35	mass	
Lewis (2002)	2001	Melbourne, Victoria						
In line netting system (NET)			Average	NET	58	42	-	volume
Side entry pits traps (SEPT)			Average	SEPT	73	27	-	volume
Residential area		St Kilda		SEPT	79	21	-	volume
Commercial/ shopping precinct		Frankston (SEPT)		SEPT	48	52	-	volume
Lewis (2002)	2001	Victoria						
In line netting system (NET)		Melbourne City	Average	NET	83	17	-	mass
Side entry pits trap (SEPT)		Melbourne City	Average	SEPT	91	9	-	mass
Residential area		St Kilda		SEPT	94	6	-	mass
Commercial/ shopping precinct		Frankston		SEPT	76	24	-	mass
Chrispijn (2004)	2002	Hobart, Tasmania						
Commercial area (city)		63 traps in Sullivans Cove		n/a	n/a	n/a		
Mixed retail centre		Gully pits entrance		Gullies	n/a	n/a	n/a	
Light industrial areas				GPT	n/a	n/a	n/a	
Outside bars				SEPT	n/a	n/a	n/a	
Average values given by the author			Average		96	4	-	mass

Table 2.1(cont.) Tabulation of published gross pollutant data

Author/notes	Period	Location	Device	Organic (%)	Litter (%)	Sediments (%)	Method
Greenway et al. (2002)	1999-	Brisbane (prior to 2002)					mass
Circular Deflective Separator (CDS)	2003	1. Golden Avenue, Calamvale	CDS	90	3	7	mass
70% impervious		2. Golden Avenue, Calamvale	vortex	91	1	8	mass
84% residential							
10% urban rural							
6% commercial							
Only average values quoted for GPT manufacturer – Escol (vortex)							
		Data from Brisbane City Council					
Brisbane City Council (2004)		(The latest data – August 2004)					
78% residential	1999	Ellison Road, Aspley	Trashrack	39	1	60	mass
Opposite a commercial site							
97% residential		Kalinga Park, Eagle Junction	CDS	59	5	36	mass
84% residential	1999-	Golden Avenue, Calamvale (see below)	CDS				
Residential development – cleanout 1	2000	cleanout 1		16	4	78	mass
Residential development – cleanout 2		cleanout 2		10	5	85	mass
		cleanout 3		55	15	30	mass
		cleanout 4		91	2	7	mass
Car park, hydrocarbons		Bicentennial Road, Boondall	CDS			62 to 97	
92% Manly boat harbour, commercial		Cambridge Road, Manly	vortex	72	20	8	mass
70% residential and next to industrial		Elliot Road, Nudgee	vortex	17	8	75	mass
98% residential		Tuberose Place, Calamvale	vortex	83	7	10	mass
		Average		42	9	49	mass
		Ex sediments		93	7	-	mass

Table 2.1(cont.) Tabulation of published gross pollutant data

Author	Period	Location	Device	Organic (%)	Litter (%)	Sediments (%)	Method
Kim et al. (2006)	2000-2	Southern California					
Mean values of wet gross pollutants reported from 17 storm events		UCLA2	drain	74	26	-	volume
Drain outfalls monitored on highway		UCLA3	drain	85	15	-	volume
		URS6-20F	drain	90	10	-	volume
		URS8-23C	drain	72	28	-	volume
		URS23	drain	86	14	-	volume
Lippner et al. (2000)	2000	Los Angeles, USA					
Caltrans Highway California Transport Dept. stormwater drains		Street sweeping/ drain inlet	drains	75	25	-	mass
Quasebarth et al. (2001)	1998-9	Los Angeles, USA					
Caltrans District 7		72 Highway drains inlet	drains	55	20	25	mass
Greater Metropolitan area		2. Residential site	drains	85	15	-	mass
		3. Light industrial	drains	36	64	-	mass
		4. Combined site	drains	78	22	-	mass
Allison et al. (2000)	1997-1999	Los Angeles, USA					
Caltrans Highway		(Paired freeway catchment)		n/a	n/a	n/a	
Average values given by the authors		Street sweeping		n/a	n/a	n/a	
		Litter pickup – streets		n/a	n/a	n/a	
		Inlet grate		n/a	n/a	n/a	
		Freeway surface		n/a	n/a	n/a	
		Litter inlet deflector					
		Average		70	30	-	mass

Table 2.1(cont.) Tabulation of published gross pollutant data

Author/notes	Year	Location	Device	Organic (%)	Litter (%)	Sediments (%)	Method
Marais et al. (2004)		South Africa					
Low income		1. Imizamo Yethu					
High-density residential area	2000/1	6 SEP and 15 GP	GPT	10	79	11	mass
Side inlet catchpits (SEP)		(see left for abbreviations)					
Grid catchpits (GP)							
Low income	2000/1	2. Ocean View					
High-density residential area		29 SEP and 5 GP	GPT	50	40	10	mass
Low income		3. Summer Greens					
Medium-density residential area		8 SEP and 15 GP	GPT	20	36	44	mass
High income	2000/1	4. Fresnaye					
Medium-density residential area		20 GP	GPT	99	0	1	mass
High income	2000/1	5. Welgemoed					
Low-density residential area		35 GP	GPT	99	0	1	mass
Central business district (CBD)	2000/1	6. Cape Town CBD					
		9 SEP and 43 GP	GPT	62	35	3	mass
Light industrial park	2000/1	7. Montague Gardens					
		16 SEP and 14 GP	GPT	5	62	33	mass

Table 2.2 Comparative published data on GPTs and other SQIDs

<i>Research Areas</i>	<i>Linear GPT</i>	<i>Radial GPT Continuous Deflective Separation (CDS)</i>	<i>Storage/ Detention Tanks</i>	<i>Vortex/hydrodynamic Separators</i>	<i>Conventional GPTs/(trashracks)</i>
1. Design, optimisation & overview studies (includes qualitative experiments for design evaluations)	*Phillips (1992) *Phillips (1999) Victoria Stormwater Committee, (1999) *Armitage & *Rooseboom (2000) Wong et al. (2000) *Davis & Birch (2009) *Wong et al. (2006)	Wong et al. (1996) Wong (1997) Jago (1997) Walker (1999) USAEPA (1999) Davis & Birch (2009)	Ellis (1992) Stovin & Saul (1994) Ali & Otman (1997) Adamsson (2004)	Maslen et al. (1989) Huebner and Geiger (1995) Andoh & Smission (1996) Field & Connor (1996) Fenner & Tyack (1997) WeiB (1997) USAEPA (1999) Strecker et al. (2001) Andoh & Saul (2003) Veerapen et al. (2005) Mietzel et al. (2007)	Goyen et al. (1985) Goven et al. (1989) Willing & Partners (1988) Phillips et al. (1989) Phillips (1992) Nguyen and Naudascher (1991) Boulton et al. (1993) Beecham & Sablatnig (1994) Allred-Coonrod (1994) Brownlee (1995) Southcott (1995) Zaman & Kandasamy (1996) Victoria Stormwater Committee (1999) Favely & Weldon (2002) Britton et al. (2003) Wong et al. (2006) Kuroiwa & Zubiaur (2007) Romali (2008) Yu & Wong (2008)

Table 2.2 (cont.) Comparative published data on GPTs and other SQIDs

Research Areas	Linear GPT	Radial GPT Continuous Deflective Separation (CDS)	Storage/ Detention Tanks	Vortex/hydrodynamic Separators	Conventional GPTs/(trashracks)
2. Field monitoring/testing	*Endicott et al. (2002) *Younis (2005) *Brisbane C. C. (2004)	Wong et al. (1996) Allison et al. (1996) Allison et al. (1998) Walker (1999) Strynchuk et al. (2000b) Greenway et al. (2002) Manly Hall Lab (2002) Ball (2004) Lippner et al. (2004) Cordery (2005) Brisbane C. C. (2004) Rushton (2006)	Stovin & Saul (1999) Brisbane C. C. (2004)	Hedges et al. (1992) Andoh & Smission (1996) Konieek et al. (1996) Waschbusch (1999) Andoh & Saul (2003) Guo (2005) Roseen et al. (2005) Wilson et al. (2007)	Molinari & Carleton (1987) Nielsen & Carleton (1989) Sim & Webster (1992) McKay & Marshall (1993) Brownlee (1995) Southcott (1995) Harrison et al. (2000) Rawson et al. (2002) Brisbane C. C. (2004) Romali (2008)
3. Velocity flow field measurements	no	Wong & Wootton (1995) Schwarz & Wells (1999)	Stovin & Saul (1994) Adamsson (2004) Duffresne et al. (2009)	Tyack & Fenner (1999) Bergström & Vomhoff (2007)	Vermeyen (2002) Tsikata et al. (2009)
4. Scalar dye experiments	no	no	Ali & Otman (1997) Adamsson (2004)	Alkhaddar et al. (2002) Lim et al. (2002) Phipps et al. (2004a) Phipps et al. (2004b) Phipps et al. (2008)	no

Table 2.2 (cont.) Comparative published data on GPTs and other SQIDs

<i>Research Areas</i>	<i>Linear GPT</i>	<i>Radial GPT Continuous Deflective Separation (CDS)</i>	<i>Storage/ Detention Tanks</i>	<i>Vortex/hydrodynamic Separators</i>	<i>Conventional GPTs/(trashracks)</i>
5. Laboratory experiments (capture/retention)	no	Wong & Wootton (1995) Nnadi et al. (2005)	Stovin & Saul (1994) Adamsson (2004) Dufresne et al. (2009)	Fenner & Tyack (1997) Fenner & Tyack (1998) Lim et al. (2002) Andoh & Saul (2003) Lee et al. (2003) Luyckx & Berlamont (2004) Phipps et al. (2004a) Phipps et al. (2004b) Phipps et al. (2005) Nnadi et al. (2005) Dierkes et al. (2006) Lee et al. (2006) Phipps et al. (2008) Egarr et al. (2009) Ismail and Nikraz (2009)	Nielsen & Carleton (1989) Carleton & Nielsen (1990) Beecham & Sablatnig (1994)
6. Hydraulic head loss	Younis (2005)	Wong & Wootton (1995)	no	Fenner & Tyack (1997)	Beecham & Sablatnig (1994)

Table 2.2 (cont.) Comparative published data on GPTs and other SQIDs

<i>Research Areas</i>	<i>Linear GPT</i>	<i>Radial GPT Continuous Deflective Separation (CDS)</i>	<i>Storage/ Detention Tanks</i>	<i>Vortex/hydrodynamic Separators</i>	<i>Conventional GPTs/(trashracks)</i>
7. Screen blockages	no	no	no	no	Abt et al. (1992)
8. Flow visualisations	no	no	no	Phipps et al. (2004b)	no
9. CFD	no	no	Stovin & Saul (1996) Ali & Otman (1997) Stovin & Saul (1998) Stovin et al. (1999) Stovin & Saul (2000) Stovin et al. (2002a) Stovin et al. (2002b) Adamsson (2004) Dufresne et al. (2009)	Saul & Svejksky (1994) Tyack & Fenner (1999) Alkhaddar et al. (2001) Alkhaddar et al. (2002) Lim et al. (2002) Faram & Harwood (2002) Faram et al. (2002) Faram & Harwood (2003) Slack et al. (2004) Egarr et al. (2005) Ismail and Nikraz (2009)	no

* water retaining GPTs

REFERENCE

- Abt, S. R., Brisbane, T. E., Frick, D. M. and McKnight, C. A. (1992). Trash rack blockage in supercritical flow. *Journal of Hydraulic Engineering*, 118(12), 1692-1696.
- Adamsson, A. (2004). *Three-dimensional simulation and physical modelling of flows in detention tanks – studies of flow pattern, residence time and sedimentation*. Unpublished PhD, Chalmers University of Technology, Goteborg.
- Ali, K. H. M. and Othman, K. (1997). Investigation of jet-forced water circulation in reservoir. *ICE Proceedings, Water Maritime and Energy*, 124(1), 44-62.
- Alkhaddar, R. M., Higgins, P. R., Phipps, D. A. and Andoh, R. Y. G. (2001). Residence time distribution of a model hydrodynamic vortex separator. *Urban Water*, 3(1-2), 17-24.
- Alkhaddar, R. M., Higgins, P. R., Phipps, D. A. and Andoh, R. Y. G. (2002). The experimental and residence time distribution estimation of the decomposition of hydrogen peroxide within a hydrodynamic vortex separator. In E. W. Strecker and Wayne C. Huber (Eds.), *Proceedings of 9th International Conference on Urban Drainage (9ICUD)* (pp. 301-318). Portland, Oregon, USA: American Society of Civil Engineers (ASCE).
- Allen, V. (2005). A comprehensive approach to performance verification for stormwater treatment systems. *Whitepapers/research/conference papers*. Retrieved 14 January 2010, from <http://www.stormwaterauthority.org/assets/A%20COMPREHENSIVE%20APPROACH%20TO%20PERFORMANCE%20VERIFICATION%20FOR%20STORMWATER%20TREATMENT%20SYSTEMS.pdf>
- Allison, R. (1999). Innovative technology reduces stormwater trash. *Public Works*, 130(2)

- Allison, R., Essery, C. I. and McMahon, T. A. (1994). How gross is pollution?: Its occurrence and measurement in stormwater channels within Australian cities. *Water Down Under 94: Surface Hydrology and Water Resources: Preprints of Papers NCP No. 94/15* (pp. 281-286). Adelaide, South Australia: Institution of Engineers, Australia.
- Allison, R. A. and Chiew, F. H. S. (1995). Monitoring of stormwater pollution from various land uses in an urban catchment. *Integrated Management of Urban Environments: Proceedings of the Second International Symposium on Urban Stormwater Management: Preprints of Papers NCP 95/03* (pp. 511-516). Melbourne, Victoria: Institute of Engineers, Australia.
- Allison, R. A., Chiew, F. H. S., McMahon, T. A. and Cooperative Research Centre for Catchment Hydrology (1997). *Stormwater gross pollutants*. Clayton, Victoria: CRC for Catchment Hydrology. Retrieved 14 January 2010, from <http://www.catchment.crc.org.au/pdfs/industry199711.pdf>
- Allison, R. A., Walker, T. A., Chiew, F. H. S., O' Neill, I. C. and Mc Mahon, T. A. (1998). *From roads to rivers: gross pollutant removal from urban waterways*. Clayton, Victoria: CRC for Catchment Hydrology. Retrieved 14 January 2010, from <http://www.catchment.crc.org.au/pdfs/technical199806pt1.pdf>
<http://www.catchment.crc.org.au/pdfs/technical199806pt2.pdf>
<http://www.catchment.crc.org.au/pdfs/technical199806pt3.pdf>
<http://www.catchment.crc.org.au/pdfs/technical199806pt4.pdf>
- Allison, R. A., Walter, K. A., Marx, D., Lippner, G. and Churchwell, R. (2000). A method for monitoring and analyzing litter in freeway runoff as part of the Caltrans litter management pilot study. In R. H. Hotchkiss and M. Glade (Eds.), *Building Partnerships: Proceedings of Joint Conference on Water Resource Engineering and Water Resources Planning and Management 2000* (pp. 81-91). Minneapolis, Minnesota, USA: American Society of Civil Engineers (ASCE).

- Allison, R. A., Wong, T. H. F. and Mc Mahon, T. A. (1996). Field trials of the pollutec stormwater pollution trap. *Water*, 23(5), 29-33.
- Allred-Coonrod, J. E. (1994). Safety grates in supercritical channels. *Journal of Irrigation and Drainage Engineering*, 120(1), 218-224.
- Andoh, R. Y. and Saul, A. J. (2003). The use of hydrodynamic vortex separators and screening systems to improve water quality. *Water Science And Technology*, 47(4), 175-183.
- Andoh, R. Y. G. and Smisson, R. P. M. (1996). The practical use of wastewater characterisation in design. *Water Science and Technology*, 33(9), 127-134.
- Armitage, N. and Rooseboom, A. (2000). The removal of urban litter from stormwater conduits and streams: paper 1- the quantities involved and catchment litter management options. *Water SA (South Africa)*, 26(2), 181-188.
- Ball, J. E. (2004). Monitoring of a gross pollutant trap in Centennial Park, Sydney, Australia, *Research Report 221*. Sydney: Water Research Laboratory Univesity of New South Wales (UNSW).
- Bannerman, R., de Bruijn, H., Karimipour, S., Kayhanian, M., Mailloux, J., McDonald, J., Miller, M., Mohseni, O., Osei, K. and Perry, S. (2009). Laboratory testing guidelines for certification of manufactured stormwater BMPs. In S. Starrett (Ed.), *World Environmental and Water Resources Congress 2009: Great Rivers Proceedings of World Environmental and Water Resources Congress 2009* (pp. 1309-1313). Kansas City, Missouri: ASCE.
- Beecham, S. C. and Sablatnig, S., J. (1994). Hydraulic modelling of stormwater trashracks. *Hydraulics Working with the Environment: 5th International Conference on Hydraulics in Civil Engineering Preprints of Papers* (pp. 97-

- 104). University of Queensland, Brisbane, Australia: Institution of Engineers, Australia.
- Bergström, J. and Vomhoff, H. (2007). Experimental hydrocyclone flow field studies. *Separation and Purification Technology*, 53(1), 8-20.
- Bochis-Micu, C. and Pitt, R. E. (2005). Impervious surfaces in urban watersheds. Paper presented at the *78th Annual Water Environment Federation Technical Exposition and Conference*. Washington, DC, USA: Water Environment Federation. Retrieved 14 January 2010, from <http://unix.eng.ua.edu/~rpitt/Publications/Pollutant%20Sources/WEFTEC05%20impervious%20surfaces%20Bochis%20and%20Pitt.pdf>
- Bouton, C. W., Lawson, C. H. and Phillips, B. C. (1993). Design and construction aspects of gross pollutant traps at Forest Lake, *Presented at the water panel meeting: Technical Paper No. 8*: Institution of Engineers, Australia. Queensland Division.
- Brisbane City Council (2004). Stormwater quality improvement devices (SQIDs) monitoring program summary, *Draft report prepared by Water and Environment City Design for Waterways program*. Brisbane, Queensland: Brisbane City Council.
- Britton, S. L., Hanson, G. J. and Temple, D. M. (2003). A Historic look at the USDA-ARS Hydraulic Engineering Research Unit. In Glenn O. Brown, Jürgen D. Garbrecht and Willi H. Hager (Eds.), *Henry P.G. Darcy and Other Pioneers in Hydraulics* (pp. 263-276). Philadelphia, Pennsylvania, USA: ASCE.
- Brown, R. R. and Clarke, J. M. (2007). *Transition to water sensitive urban design: the story of Melbourne, Australia*. Melbourne, Victoria: Monash University.
- Brownlee, P. (1995). Evaluation of effectiveness and efficiency of North Sydney Council litter control device program. Paper presented at the *the 2nd*

International Symposium on Urban Stormwater Management Melbourne: Institution of Engineers, Australia.

- Carleton, M. G. and Nielsen, J. S. (1990). Study of trash and trash interception devices. *Water Science & Technology*, 22(10), 287-290.
- Casey, M. and Wintergerste, T. (2000). *Special interest group on quality and trust in Industrial CFD: best practice guidelines*. Switzerland: European Research Community on Flow Turbulence and Combustion (ERCOFTAC).
- Chiew, F., H. S., Mudgway, L. B., Duncan, H. P. and Mc Mahon, T., A. (1997). *Urban stormwater pollution*. Clayton, Victoria: CRC for Catchment Hydrology. Retrieved 14 January 2010, from <http://www.catchment.crc.org.au/pdfs/industry199705.pdf>
- Chrispijn, J. A. (2004). Assessing different at-source stormwater treatment devices in Hobart: Sullivans Cove and Brooker Highway performance trials. *Stormwater Industry Association (SIA) bulletin* (117), 6. Retrieved 14 January 2010, from <http://www.stormwater.asn.au/tas/Enviro04Paper-Chrispijn.pdf>
- Clark, S., Middleton, P. A., Pitt, R., Tuscaloosa, A. L., Burian, S., City, S. L., Field, U. T. R., Fan, E., Edison, N. J. and Heaney, J. (2007). *Annotated Bibliography of Urban Wet Weather Flow Literature from 1996 through 2006*. Retrieved 1 June 2010, from <http://rpitt.eng.ua.edu/Publications/Publications.shtml>
- Cordery, I. (2005). Field performance of a vortex type gross pollutant trap. *Australian Journal of Water Resources*, 9(1), 49-54.
- Davis, B. S. and Birch, G. F. (2009). Catchment-wide assessment of the cost-effectiveness of stormwater remediation measures in urban areas. *Environmental Science and Policy*, 12(1), 84-91.

- Dierkes, C., Gobel, P., Lohmann, M. and Coldewey, W. G. (2006). Development and investigation of a pollution control pit for treatment of stormwater from metal roofs and traffic areas. *Water Science and Technology*, 54(6-7), 291-298.
- Dufresne, M., Vazquez, J., Terfous, A., Ghenaim, A. and Poulet, J. B. (2009). CFD modeling of solid separation in three combined sewer overflow chambers. *Journal of Environmental Engineering*, 135(9), 776-787.
- Egarr, D. A., Faram, M. G., O'Doherty, T., Phipps, D. A. and Syred, N. (2005). Computational fluid dynamic prediction of the residence time distribution of a prototype hydrodynamic vortex separator operating with a base flow component. *Proceedings of the Institution of Mechanical Engineers, Part E: Journal of Process Mechanical Engineering*, 219(1), 53-67.
- Egarr, D. A., Faram, M. G., O'Doherty, T. and Syred, N. (2009). Experimental study of a hydrodynamic vortex separator. *Proceedings of the Institution of Mechanical Engineers, Part E: Journal of Process Mechanical Engineering*, 223(1), 1-10.
- Ellis, J. B. (1992). Design criteria for managing detention basin quality. *International Symposium on Urban Stormwater Management Preprints of Papers* (pp. 23-29). Sydney, NSW, Australia: Institution of Engineers, Australia.
- Endicott, J., D., Berger, B., J. and Stone, S., J. (2002). Design and performance of non-proprietary devices for highway runoff litter removal. Paper presented at the *9th International Conference on Urban Drainage*. Portland, Oregon, USA: American Society of Civil Engineers (ASCE). Retrieved 15 January 2010, from <http://www.owp.csus.edu/research/papers/papers/PP031.pdf>
- Falvey, H. T. and Weldon, J. H. (2002). Case study: Dillon dam trashrack damage. *Journal of Hydraulic Engineering*, 128(2), 144-150.
- Faram, M., G. and Harwood, R. (2002). Assessment of the effectiveness of stormwater treatment chambers using computational fluid dynamics. In Eric

W. Strecker and Wayne C. Huber (Eds.), *Urban Drainage 2002: Proceedings of 9th International Conference on Urban Drainage - 9ICUD* (pp. 7-13). Portland, Oregon, USA: American Society of Civil Engineers (ASCE).

Faram, M. G., Harwood, R., Bertrand-Krajewski, J. L. and Chebbo, G. (2002). A method for the numerical assessment of sediment interceptors. *Water Science and Technology*, 47(4), 167-174. Retrieved 14 January 2010, from <http://lequia.udg.es/lequianet/WatSciTech/04704/0167/047040167.pdf>

Faram, M. G., Harwood, R. and Deahl, P. J. (2003). Investigation into the sediment removal and retention capabilities of stormwater treatment chambers. Paper presented at the *North American Surface Water Quality Conference: StormCon 2003*. San Antonio, Texas, USA.

Fenner, R. A. and Tyack, J. N. (1997). Scaling laws for hydrodynamic separators. *Journal of Environmental Engineering*, 123(10), 1019-1026.

Fenner, R. A. and Tyack, J. N. (1998). Physical modelling of hydrodynamic separators operating with underflow. *Journal of Environmental Engineering*, 124(9), 881-886.

Field, R. and O'Connor, T. P. (1996). Swirl technology: enhancement of design, evaluation, and application. *Journal of Environmental Engineering*, 122(8), 741-748.

Field, R. and Sullivan, D. (2003). *Wet-weather flow in the urban watershed: technology and management*. Boca Raton, Florida: Lewis Publishers.

Fletcher, T., Duncan, H., Poelsma, P. and Lloyd, S. (2004). *Stormwater flow and quality, and the effectiveness of non-proprietary stormwater treatment measures-a review and gap analysis: Report 04/08*. Clayton, Victoria: CRC for Catchment Hydrology. Retrieved 14 January 2010, from <http://www.catchment.crc.org.au/pdfs/technical200408.pdf>

- Frederick, R. M. and Stevens, T. G. (2007). Performance verification of stormwater treatment devices under EPA's environmental technology verification program. In K. C. Kabbes (Ed.), *Restoring our natural habitat: Proceedings of the World Environmental and Water Resources Congress 2007* (pp. 57-72). Tampa, Florida, USA: American Society of Civil Engineers (ASCE).
- Gamtron, P. (1992). Performance assessment of four rubbish interception booms., *Report for the Water Board Southern Region Stormwater Management* (pp. 68). Rockdale, New South Wales, Australia.
- Goonetilleke, A., Thomas, E., Ginn, S. and Gilbert, D. (2005). Understanding the role of land use in urban stormwater quality management. *Journal of Environmental Management*, 74(1), 31-42.
- Goyen, A. G., Moodie, A. R. and Nuttall, P. M. (1985). Enhancement of urban runoff quality. *16th Hydrology and Water Resources Symposium: Preprints of Papers NCP No. 85/2* (pp. 202-208). Sydney, NSW: Institution of Engineers, Australia.
- Goyen, A. G. and Phillips, B. C. (1989). Stormwater planning and management. Paper presented at the *13th Australian Water and Wastewater Association. Federal Convention Preprints of Papers NCP No. 89/2*. Barton, ACT: Institution of Engineers, Australia.
- Greenway, M., Muth, N. L. and Jenkins, G. (2002). Monitoring spatial and temporal changes in stormwater quality through a series of treatment trains: a case study -Golden Pond, Brisbane, Australia. In Eric W. Strecker and Wayne C. Huber (Eds.), *Urban Drainage 2002: Proceedings of 9th International Conference on Urban Drainage -9ICUD* (pp. 52-68). Portland, Oregon, USA: American Society of Civil Engineers (ASCE).
- Guo, Q. (2005). Development of adjustment and scaling factors for measured suspended solids removal performance of stormwater hydrodynamic treatment devices. In Raymond Walton (Ed.), *World Water and*

Environmental Resources Congress: Impacts of Global Climate Change (pp. 175-175). Anchorage, Alaska, USA: American Society of Civil Engineers (ASCE).

Guo, Q., England, G. and Johnston, C. E. (2008). Development of certification guidelines for manufactured stormwater BMPs. In J. Roger W. Babcock and Raymond Walton (Eds.), *Ahupua'a: Proceedings of the World Environment and Water Resources Congress 2008* (pp. 17-25). Honolulu, Hawaii: American Society of Civil Engineers (ASCE).

Hansen, P. (2001). EPA's environmental technology verification program: an evaluation of a public-private process. *Environmental Quality Management*, 11(2), 15-28.

Harrison, L. L., MacArthur, R. C. and Sanford, R. A. (2000). Lake Solano sediment management study. In Marshall Flug, Donald Frevert and J. David W. Watkins (Eds.), *Watershed Management & Operations Management 2000* (pp. 167-167). Fort Collins, Colorado, USA: American Society of Civil Engineers (ASCE).

Harwood, R. (2002). CSO modelling strategies using computational fluid dynamics. In Eric W. Strecker and Wayne C. Huber (Eds.), *Urban Drainage 2002: Proceedings of 9th International Conference on Urban Drainage -9ICUD* (pp. 8-17). Portland, Oregon, USA: American Society of Civil Engineers (ASCE).

Hazen, A. (1904). On sedimentation. *American Society of Civil Engineers Transactions*, 3, 45–88.

Hedges, P. D., Lockley, P. E. and Martin, J. R. (1992). A field study of an hydrodynamic separator combined sewer overflow. *Re-discover water, a priority: International Conference on Innovative Technologies in the Domain of Urban Storm Water Drainage* (pp. 349-358). Lyon, France.

- Hilgenstock, A. and Ernst, R. (1996). Analysis of installation effects by means of computational fluid dynamics--CFD vs experiments? *Flow Measurement and Instrumentation*, 7(3-4), 161-171.
- Ho, E. (2001). *The Balmoral stormwater management project report: monitoring the biodegradation of organics retained in a CDS device*. Mosman, NSW: Mosman City Council. Retrieved 13 February 2010, from <http://www.mosman.nsw.gov.au/environment/water/documents>
- Huebner, M. and Geiger, W., F. (1995). Review of hydrodynamic separator-regulator efficiencies for practical application. *Water Science and Technology*, 32(1), 109-117.
- Huggins, D. L., Piedrahita, R. H. and Rumsey, T. (2005). Use of computational fluid dynamics (CFD) for aquaculture raceway design to increase settling effectiveness. *Aquacultural Engineering*, 33(3), 167-180.
- Hunter, G. J. (1998). Evaluation of some readily available stormwater quality control technologies. *Waterfall Journal of the Stormwater Industry Association*, 1(17), 16-23.
- Ignacio, I. (2000). The Drummoyne City Council: three ways to improve the bays gross pollutant monitoring program, *Unpublished post graduate project, University of Technology (UTS)*. Sydney, Australia.
- Ismail, M. and Nikraz, H. (2007). Numerical modelling of Rocla Versa trap type G. Paper presented at the *International Conference on Natural Resources and Environmental Management and Environmental Safety and Health*. Sarawak, Malaysia.
- Ismail, M. and Nikraz, H. (2009). Experimental and numerical modelling of Versa trap type W. *Agricultural Engineering International: The Commission Internationale du Genie Rural (CIGR) EJournal*. Retrieved 14 February 2010, from <http://www.cigrjournal.org/index.php/Ejournal/issue/view/34>

- Jago, R. A. (1997). CDS -a new screening technology for the environment. *Water-Melbourne* (24), 47-50.
- Kadlec, R. H. (2000). The inadequacy of first-order treatment wetland models. *Ecological Engineering*, 15(1-2), 105-119.
- Kim, L. H., Kang, J., Kayhanian, M., Gil, K. I., Stenstrom, M. K. and Zoh, K. D. (2006). Characteristics of litter waste in highway storm runoff. *Water Science And Technology*, 53(2), 225.
- Konieek, Z., Pryl, K. and Suchanek, M. (1996). Practical applications of vortex flow separators in the Czech Republic. *Water Science and Technology*, 33(9), 253-260.
- Kuroiwa, J. M. and Zubiaur, M. A. (2007). Use of trashracks as anti vortex structures at submerged intakes. In K. C. Kabbes (Ed.), *World Environmental and Water Resources Congress 2007* (pp. 248-248). Tampa, Florida, USA: American Society of Civil Engineers (ASCE).
- Kwon, S. B., Park, N. S., Lee, S. J., Ahn, H. W. and Wang, C. K. (2006). Examining the effect of length/width ratio on the hydro-dynamic behaviour in a DAF system using CFD and ADV techniques. *Water Science and Technology*, 53(7), 141-149.
- Lee, J., Bang, K., Choi, J., L. H. Ketchum, J. and Cho, Y. (2003). The vortex concentrator for suspended solids treatment. *Water Science and Technology*, 47(7), 335-341.
- Lee, J. H., Bang, K. W., Cho, Y. J. and Joh, S. J. (2006). The hydrodynamic filter separator for removal of urban storm runoff. *Water Science and Technology*, 53(7), 243-252.
- Levenspiel, O. (1999). *Chemical reaction engineering* (3rd ed.). New York: Wiley.

- Lewis, J. (2002). *Effectiveness of stormwater litter traps for syringe and litter removal report for Melbourne Water Corporation*. Melbourne, Victoria: Cooperative Reserach Center (CRC) for Catchment Hydrology. Retrieved 14 January 2010, from http://www.clearwater.asn.au/resources/325_1.pdf
- Lim, M. T. N., Lam, S. W., Amal, R., Cathers, B. and Pinson, D. (2002). Computational and experimental studies of floc behaviour in a vortex separator. In E. W. Strecker and W. C. Huber (Eds.), *Global Solutions for Urban Drainage: Proceeding of 9th International Conference on Urban Drainage* (pp. 303-317). Portland, Oregon, USA: American Society of Civil Engineers (ASCE).
- Lippner, G., Churchwell, R., Allison, R., Moeller, G. and Johnston, J. (2000). A scientific approach to evaluating stormwater best management practices for litter. Paper presented at the *California Water Environment Association (CWEA), 72nd Annual Conference*. Sacramento, California. Retrieved 14 JJanuary 2010, from <http://www.owp.csus.edu/research/papers/papers/PP014.pdf>
- Lippner, G. and Moeller, G. (2000). Study quantifies broom sweeper litter pickup ability. *American Sweeper Magazine*, 8(1). Retrieved 14 February 2010, from www.owp.csus.edu/research/papers/papers/PP012.pdf
- Lippner, G., Singh, A. and James, R. (2004). Evaluation of monitoring and analysis methods yielding significant differences in BMP efficiency. In Gerald Sehlke, Donald F. Hayes and David K. Stevens (Eds.), *Critical Transitions in Water and Environmental Resources Management* (pp. 60-69). Salt Lake City, Utah, USA: ASCE.
- Livingston, E. H. and McCarron, E. (1991). *Stormwater management: a guide for Floridians*. Retrieved 15 January 2010, from www.floridadep.net/water/nonpoint/docs/nonpoint/Stormwater_Guide.pdf

- Lundh, M., Joensson, L. and Dahlquist, J. (2002). Flow structures in a dissolved air flotation pilot tank and the influence on the separation of MBBR floc. *Water Science and Technology: Water Supply*, 2(2), 69-76.
- Luyckx, G. and Berlamont, J. (2004). Removal efficiency of swirl/vortex separators. *Urban Water Journal*, 1(3), 251 - 260.
- Madhani, J. T. and Brown, R. J. (2008). A scalar concentration (Komori) probe for measuring fluctuating dye concentration in water. *WSEAS Transactions on Fluid Mechanics*, 3(3), 224-233. Retrieved 15 February 2010, from <http://www.worldses.org/journals/fluid/fluid-2008.htm>
- Manly Hydraulics Laboratory (2002). Little Sirius Cove stormwater quality improvement device monitoring and analysis, *Report No. MHL 1190*. Manly, NSW: Manly Hydraulics Laboratory, The New South Wales Department of Public Works and Services.
- Marais, M., Armitage, N. and Pithey, S. (2001). A study of the litter loadings in urban drainage systems--methodology and objectives. *Water Science and Technology*, 44(6), 99.
- Marais, M., Armitage, N. and Wise, C. (2004). The measurement and reduction of urban litter entering stormwater drainage systems: Paper 1-Quantifying the problem using the City of Cape Town as a case study. *Water South Africa (SA)*, 30(4), 469-482.
- Marais, M. J. and Armitage, N. (2004). Problems encountered with the measurement of urban litter entering the stormwater systems of Cape Town. In William James (Ed.), *Innovative modelling of urban water systems* (pp. 475-504). Guelph, Ontario CHI Publications.
- Maslen, P. G., Bell, J. A. and Weis, F. G. (1989). Efficient grit collection by modern Pista grit chamber. Paper presented at the *Investing in Water Futures, the Australian Water Industry in the 1990's:13th Australian Water and*

Wastewater Association Federal Convention, preprints of papers. Barton, ACT: Institution of Engineers, Australia.

MASTEP (2004). *The Massachusetts stormwater technology evaluation project (MASTEP) -Stormwater technologies clearinghouse*. Retrieved 14 January, from <http://www.mastep.net/index.cfm>.

McKay, P. and Marshall, M. (1993). *Backyard to bay: tagged litter report*. Melbourne, Victoria: Melbourne Water and Melbourne Parks and Waterways.

Mietzel, T., Klepiszewski, K. and Weiss, G. (2007). Development and verification of a general approach to describe the efficiency of vortex separators in combined sewer systems. *Water Science And Technology: A Journal Of The International Association On Water Pollution Research*, 55(4), 165-173.

Molinari, S. and Carleton, S. (1987). Interception and collection of litter in urban waterways. Paper presented at the *Proceedings of Urban Runoff Water Quality*. Milsons Point, New South Wales: Institution of Engineers, Australia.

Nguyen, T. D. and Naudascher, E. (1991). Vibration of beams and trashracks in parallel and inclined flows. *Journal of Hydraulic Engineering*, 117(8), 1056-1076.

Nielsen, J. S. and Carleton, M. G. (1989). A study of trash and trash interception devices on the cooks river catchment, Sydney. *Investing in Water Futures, the Australian Water Industry in the 1990's:13th Australian Water and Wastewater Association Federal Convention Preprints of Papers NCP No. 89/2* (pp. 23-29). Barton, Canberra, Australia: Institution of Engineers, Australia.

- NJCAT (2001). *A comprehensive treatment approach to performance verification for stormwater treatment*. Retrieved 14 January 2010, from <http://www.njcat.org/education/glossary.cfm>
- Nnadi, F., N., Al-Hamdan, A., Z. and Romah, M., S. (2005). Side-by-side evaluation of stormwater proprietary BMPs. In Raymond Walton (Ed.), *Impacts of Global Climate Change: Proceedings of World Water and Environmental Resources Congress 2005* (pp. 147-159). Anchorage, Alaska, USA: American Society of Civil Engineers (ASCE).
- O' Brien, E. J. (1995). Water quality changes associated with the Installation of the Bondi gross pollutant traps. *16th Federal Convention proceedings* (pp. 807-812). Darling Harbour, Sydney, Australia: Australian Water and Wastewater Association (AWA).
- Oca, J., Masaló, I. and Reig, L. (2004). Comparative analysis of flow patterns in aquaculture rectangular tanks with different water inlet characteristics. *Aquacultural Engineering*, 31(3-4), 221-236.
- Osei, K., Andoh, R. Y. G., MacKinnon, J. and Faram, M. G. (2008). Assessment of laboratory test protocols for determining the pollutant removal capabilities of stormwater separators. Paper presented at the *11th International Conference on Urban Drainage*. Edinburgh, Scotland, UK. Retrieved 2 May 2010, from http://plc.hydro-intl.com/index2.php?option=com_docman&task=doc_view&gid=12&Itemid=88
- Park, N. S., Lim, J. L., Lee, S. J., Lee, K. H. and Kwon, S. B. (2006). Examining the effect of transverse troughs on hydrodynamic behavior in a sedimentation basin with CFD simulation and ADV technique. *Journal of Water Supply: Research and Technology-Aqua*, 55(4), 247-256.
- Persson, J. and Wittgren, H. B. (2003). How hydrological and hydraulic conditions affect performance of ponds. *Ecological Engineering*, 21(4-5), 259-269.

- Phillips, B. C. (1992). Revised guidelines for gross pollutant traps. *The Global Environment-Australian Implications: National Conference on Environmental Engineering* (pp. 155-160). Gold Coast, Queensland: Institution of Engineers, Australila.
- Phillips, B. C., Lawrence, A. I. and Szlapinski, P. M. (1989). Recent developments in gross pollutant traps. *Australian Water and Wastewater Association 13th Federal Convention Preprints of Papers NCP No. 89/2* (pp. 143-147). Canberra, ACT, Australia: Institution of Engineers, Australia.
- Phillips, D. I. (1999). A new litter trap for urban drainage systems. *Water Science and Technology*, 39(2), 85-92.
- Phipps, D. A., Alkhaddar, R. M., Dodd, J., Faram, M. G. and Deahl, P. J. (2004a). Evaluation of different configurations of stormwater treatment chamber. Paper presented at the *North American Surface Water Quality Conference and Exposition: StormCon'03*. Palm Desert, California, USA. Retrieved 14 January 2010, from <http://www.hydro-international.biz/library/stormwater/Phipps-et-al-2004-StormCon.pdf>
- Phipps, D. A., Alkhaddar, R. M., Dodd, M. J., Faram, M. G., Andoh, R. Y. G. and Roberts, M. C. (2004b). Experimental investigation into solids re-entrainment in hydrodynamic vortex separators. *Novatech: 5th International Conference on Sustainable Techniques and Strategies in Urban Water Management* (pp. 69-76). Lyon, France.
- Phipps, D. A., Alkhaddar, R. M. and Faram, M. G. (2005). Pollutants retention in stormwater treatment chambers. *10th International Conference on Urban Drainage* (pp. 21-26). Copenhagen, Denmark.
- Phipps, D. A., Alkhaddar, R. M., Loffill, E., Andoh, R. Y. G. and Faram, M. G. (2008). Efficiency testing of a hydrodynamic vortex separator. *11th International Conference on Urban Drainage* Edinburgh, Scotland, UK.

Retrieved 14 January 2010, from http://plc.hydro-intl.com/index2.php?option=com_docman&task=doc_view&gid=16&Itemid=88

- Quasebarth, T., Schroeder, D., Chappell, R., Churchwell, R. and Lippner, G. (2001). An investigation of factors influencing solids transport and deposition into highway drain inlets. *Bridging the Gap: Meeting the World's Water and Environmental Resources Challenges: Proceedings of World Water and Environmental Resources Congress 2001* (pp. 184-194). Orlando, Florida, USA: American Society of Civil Engineers (ASCE).
- Rawson, C. A., Sheehan, R. A. and Skelton, S. (2002). The effect of the gross pollutant trap on water quality in Brookvale Creek. In R. Lim (Ed.), *Univeristy of Technology Sydney (UTS) Freshwater Ecology Report 2002* Departmental of Environmental Science: University of Technology, Sydney.
- Romali, N. S. (2008). *Evaluation and performance of gross pollutant traps (GPTs) for open channel flow*. Unpublished Master of Engineering, Universiti Teknologi Malaysia, Johor Bahru.
- Roseen, R. M., Ballestero, T. P., Houle, J. J. and Avelleneda, P. (2005). Normalized technology verification of structural BMPs, low impact development (LID) fesigns, and manufactured BMPs. In Glenn E. Moglen (Ed.), *Managing Watersheds for Human and Natural Impacts: Engineering, Ecological, and Economic Challenges* (pp. 135-147). Williamsburg, Virginia, USA: American Society of Civil Engineers (ASCE).
- Rushton, B. (2006). Removal of pollutants by a CDS unit at a major storm outfall in Florida. In Randall Graham (Ed.), *Examining the Confluence of Environmental and Water Concerns: Proceedings of the World Environmental and Water Resources Congress 2006* (pp. 391-401). Omaha, Nebraska, USA: American Society of Civil Engineers (ASCE).

- Rushton, B., England, G. and Smith, D. (2007). Proposed guidelines for monitoring stormwater gross solids. In K. C. Kabbles (Ed.), *Restoring our natural habitat: World Environmental and Water Resources Congress 2007* (pp. 58-58). Tampa, Florida, USA: American Society of Civil Engineers (ASCE).
- Russell, R., C. (1999). Constructed wetlands and mosquitoes: health hazards and management options--an Australian perspective. *Ecological Engineering*, 12(1-2), 107-124.
- Sansalone, J. J., Koran, J., Buchberger, S. G. and Smithson, J. (1998). Physical characteristics of highway solids transported during rainfall. *Journal of Environmental Engineering*, 124(5), 427-440.
- Saul, A. J. and Svejksky, K. (1994). Computational modelling of a vortex CSO structure. *Water Science & Technology*, 30(1), 97-106.
- Sim, R. L. and Webster, J. L. (1992). Performance of trash rack on Cup and Saucer Creek stormwater channel. . *International Symposium on Urban Stormwater Management Preprints of Papers NCP No. 95/03* (pp. 143-145). Sydney, NSW, Australia: Institution of Engineers, Australia.
- Slack, M. D., Del Porte, S. and Engelman, M. S. (2004). Designing automated computational fluid dynamics modelling tools for hydrocyclone design. *Minerals Engineering*, 17(5), 705-711.
- Southcott, P. (1995). A case study of minor gross pollutant trap. Paper presented at the *The Second International Symposium on Urban Stormwater Management: Integrated Management of Urban Environments*. Melbourne, Victoria, Australia: institution of Engineers, Australia.
- Stovin, V., R. and Saul, A., J. (1996). Efficiency prediction for storage chambers using computational fluid dynamics. *Water Science and Technology*, 33(9), 163-170.

- Stovin, V., R. and Saul, A., J. (1998). A computational fluid dynamics (CFD) particle tracking approach to efficiency prediction. *Water Science and Technology*, 37(1), 285-293.
- Stovin, V., R., Saul, A., J., Drinkwater, A. and Clifforde, I. (1999). Field testing CFD-based predictions of storage chamber gross solids separation efficiency. *Water Science and Technology*, 39(9), 161-168.
- Stovin, V. R., Grimm, J. P., Buxton, A. P. and Tait, S. J. (2002a). Parametric studies on CFD models of sewerage structures. In Eric W. Strecker and Wayne C. Huber (Eds.), *9th International Conference on Urban Drainage : Global Solutions for Urban Drainage* (pp. 312-327). Portland, Oregon, USA: ASCE.
- Stovin, V. R., Grimm, J. P. and Saul, A. J. (2002b). Fine sediment retention in storage chambers: an assessment of time-dependent effects. *Water Science & Technology*, 45(7), 123-131.
- Stovin, V. R. and Saul, A. J. (1994). Sedimentation in storage tank structures. *Water Science & Technology* 29(1-2), 363-372.
- Stovin, V. R. and Saul, A. J. (2000). Computational fluid dynamics and the design of sewage storage chambers. *Journal of Institution Water Environmental Management*, 14(2), 103-110.
- Strecker, E. W., Quigley, M. M., Urbonas, B. R., Jones, J. E. and Clary, J. K. (2001). Determining urban storm water BMP effectiveness. *Journal of Water Resources Planning and Management*, 127(3), 144-149.
- Strynchuk, J., Royal, J. and England, G. (2000a). Grass and leaf decomposition and nutrient release study under wet conditions. In Rollin H. Hotchkiss and Michael Glade (Eds.), *Building Partnerships: Proceedings of Joint Conference on Water Resource Engineering and Water Resources Planning and Management 2000* (pp. 168-178). Minneapolis, Minnesota, USA: American Society of Civil Engineers (ASCE).

Strynchuk, J., Royal, J. and England, G. (2000b). Using a CDS unit for sediment control in Brevard County, Florida. In Rollin H. Hotchkiss and Michael Glade (Eds.), *Building Partnerships : Proceedings of Joint Conference on Water Resource Engineering and Water Resources Planning and Management 2000* (pp. 169-179). Minneapolis, Minnesota, USA: American Society of Civil Engineers (ASCE).

TAPE (2008). *Guidance for evaluating emerging stormwater treatment technologies, technology assessment protocol –ecology (TAPE) publication number 02-10-037*. Retrieved 14 January 2010, from <http://www.ecy.wa.gov/pubs/0210037.pdf>

TARP (2003). *A state tool to promote scientifically sound, effective environmental decision-making*. Retrieved 15 January 2010, from <http://www.dep.state.pa.us/dep/deputate/pollprev/techservices/tarp/>

Thackston, E. L., Shields, J. F. D. and Schroeder, P. R. (1987). Residence time distributions of shallow basins. *Journal of Environmental Engineering*, 113(6), 1319-1332.

Tsikata, J. M., Tachie, M. F. and Katopodis, C. (2009). Particle image velocimetry study of flow near trashrack models. *Journal of Hydraulic Engineering*, 135(8), 671-684.

Tyack, J. N. and Fenner, R. A. (1999). Computational fluid dynamics modelling of velocity profiles within a hydrodynamic separator. *Water Science and Technology*, 39(9), 169-176.

USAEPA (1999). *Storm water technology fact sheet: hydrodynamic separators EPA-F-99-017*. Washington, DC: United States Environmental Protection Agency. Retrieved 14 February 2010, from <http://www.epa.gov/owm/mtb/hydro.pdf>

- Van Drie, R. (2002). Development of a pollutant load algorithm (for Sydney Australia). In Eric W. Strecker and Wayne C. Huber (Eds.), *Global Solutions for Urban Drainage: Proceedings of 9th International Conference on Urban Drainage - 9ICUD* (pp. 207-221). Portland, Oregon, USA: American Society of Civil Engineers (ASCE).
- Veerapen, J. P., Lowry, B. J. and Couturier, M. F. (2005). Design methodology for the swirl separator. *Aquacultural Engineering*, 33(1), 21-45.
- Vermeyen, T. B. (2002). Measuring selective withdrawal characteristics using an Argonaut acoustic Doppler velocimeter in Folsom Lake, California. In Tony L. Wahl, Clifford A. Pugh, Kevin A. Oberg and T. B. Vermeyen (Eds.), *Proceedings of Hydraulic Measurements and Experimental Methods Conference 2002* (pp. 63-72). Estes Park, Colorado, USA: American Society of Civil Engineers (ASCE).
- Victoria Stormwater Committee (1999). *Urban stormwater best practice environmental management guidelines*. Melbourne, Australia: CSIRO publishing.
- Walker, T. and Wong, T. H. F. (1999). *Effectiveness of street sweeping for stormwater pollution control* (Vol. 3800). Clayton, Victoria: CRC for Catchment Hydrology. Retrieved 14 February 2010, from <http://www.catchment.crc.org.au/pdfs/technical199908.pdf>
- Walker, T. A., Allison, R. A., Wong, T. H. F. and Wootton, R. M. (1999). Removal of suspended solids and associated pollutants by a CDS gross pollutant trap. *Cooperative Research Centre for Catchment Hydrology. Victoria*. Retrieved 14 February 2010, from <http://www.catchment.crc.org.au/pdfs/technical199902.pdf>
- Waschbusch, R. (1999). Evaluation of the effectiveness of an urban stormwater treatment unit in Madison, Wisconsin, 1996-97, *Report 99-4195 Wisconsin*

Department of Natural Resources, Geological Survey (U.S.). Middleton, Wisconsin, USA.

- WeiB, G. J. (1997). Vortex separator: proposal of a dimensioning method. *Water Science and Technology*, 36(8-9), 201-206.
- Wells, S. and Schwarz, T. (1999). Stormwater particle removal using a cross-flow filtration and sedimentation device. *Advances in Filtration and Separation Technology*, 13(A), 219-226.
- Willing & Partners (1988). *Gross pollutant trap - conceptual guidelines brief no. E245/85*. Canberra: National Capital Development Commission.
- Wilson, M., A., Gulliver, J., S., Mohseni, O. and Hozalski, R., M. (2007). Assessing the Effectiveness of Proprietary Stormwater Treatment Devices. *World Environmental and Water Resources Congress 2007* (pp. 578-578). Tampa, Florida, USA: ASCE.
- Wong, T., Wootton, R., Argue, J. and Pezzaniti, D. (2000). Bringing order to the pollution control industry-issues in assessing the performance of gross pollutant traps. *Australian Civil Engineering Transactions*, 42, 57-62.
- Wong, T., Wootton, R. and Fabian, D. (1996). A solid separator using a continuous deflective system. In F. Sieker and H.-R. Verworn (Eds.), *7th International Conference on Urban Stormwater Drainage* (pp. 881-886). Hannover, Germany.
- Wong, T. and Wootton, R. M. (1995). An innovative gross pollutant trap for stormwater treatment. *The Second International Symposium on Urban Stormwater Management: Preprints NCP 95/03* (pp. 407-412). Melbourne, Australia: Institution of Engineers, Australia.

- Wong, T. H. F. (1997). Continuous deflective separation: its mechanism and applications. Paper presented at the *70th Water Environment Federation Annual Conference & Exposition*. Chicago, Illinois, USA.
- Wong, T. H. F., Allison, R. A., Argue, J., R., Breen, P., Brown, R., Coombes, P., Duncan, H., Evangelisti, M., Fletcher, T., Lawrence, I., McAlister, T., Mitchell, G., Mouritz, M., Pezzaniti, D., Phillips, B. and Taylor, A. (2006). *Australian runoff quality—a guide to water sensitive urban design*. Crows Nest, New South Wales: Engineers Australia.
- Younis, B. A. (2005). *Laboratory testing of gross solids removal devices*. Sacramento, California: Division of Environmental Analysis, Stormwater Unit, California Department of Transportation. Retrieved 18 April 2010, from <http://www2.dot.ca.gov/hq/env/stormwater/pdf/CTSW-RT-05-073-18-1.pdf>
- Yu, D., Lee, J. H. W. and Wong, C. K. C. (2008). Stormwater overflow in stepped channel. *Journal of Hydro-environment Research*, 2(2), 119-128.
- Zaman, S. and Kandasamy, J. (1996). Feasibility of GPT construction in established urban catchments. Paper presented at the *23rd Hydrology and Water Resources Symposium Water and the Environment Preprints of Papers*. Hobart, Tasmania: Institution of Engineers, Australia.

[This page has been left blank intentionally.]

Chapter 3: A historical perspective on Australian attitudes to littering and their environmental impact

Jehangir T. Madhani¹, Les A. Dawes² and Richard J. Brown¹

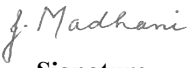
¹ School of Engineering Systems

² School of Urban Development

Queensland University of Technology


Publication: Journal of Australian studies (Revised draft pending submission).

This chapter is an exact copy of the above journal paper.

Contributor	Statement of contribution
Jehangir T. Madhani	<p style="text-align: center;">Candidate</p> <p>Field work design, conducted field work over a two year period and data analysis, performed a review of literature, wrote the manuscript and acted as the corresponding author.</p>
 Signature	
8/6/2010 Date	
Les A. Dawes	<p style="text-align: center;">Associate Supervisor</p> <p>Assisted with data analysis, reviewed and edited the manuscript.</p>
Richard J. Brown	<p style="text-align: center;">Principal Supervisor</p> <p>Assisted with organisation of material, reviewed and edited the manuscript.</p>

Principal Supervisor Confirmation

I have sighted email or other correspondence from all Co-authors confirming their certifying authorship.

A/Professor Richard J. Brown		8/6/2010
Name	Signature	Date

ABSTRACT

Street litter is a continuing problem both in residential and commercial areas despite decades of anti-litter campaigning. During urban wet weather flows, litter is transported into receiving waterways and has a devastating impact on the environment. The purpose of this paper is to investigate the past and present Australian littering culture and its potential impact on the environment. To this end, photographs from the National Library archives are analysed, together with results obtained from a field litter study conducted in Brisbane and Burleigh Heads. Study results reveal that, overall the major source of litter is organic: grass clippings, leaves, twigs and fine sediments. However, on pedestrian routes and in open spaces near public services, litter is dominated by cigarette butts. Smoking bans may have shifted the problem of cigarette butt disposal from ashtrays to outdoors. Observations also show that public spaces where greenery is cultivated to promote pleasant surroundings are used as garbage sites for human-derived material. Furthermore, while architects and planners are keen to promote the concept of green roofs and walls, these also have the potential to generate street litter.

Keywords: Litter, gross pollutant, organic matter, cigarette butts, stormwater.

3.1 INTRODUCTION

Australian society has undergone substantial changes since its colonial origins in the late eighteenth century. An important but little considered aspect of these socio-economic shifts is the relation between inhabitants and the type of litter they generate. As consumer behaviour and production styles change. It does so, because the form and the amount of litter discarded also changes. These changes relate to the movement of people having greater access to throw away items.

This article explores these trends from an historical point of view and examines current street waste typically found in Australian urban areas. The latter was achieved by conducting case studies in the streets of Brisbane city and Burleigh Heads which is a growing seaside suburb. The results were compared with case studies from other major Australian cities to explore common street littering trends. Understanding the socio-historical development of littering can help develop better means for its control now and in the future, yet little information pertaining to the history of Australian street litter is available. In order to address this deficiency and to investigate past and present Australian attitudes towards littering and its effect on the environment, evidence was collected through archive photographs posted on the National Library and City of Sydney websites (The City of Sydney, 2003). Interpreting the photographs will help to form sustainable concepts for the future and promote a low pollutant environment.

National efforts have been made through various litter campaigns by local government to reduce the amount of street pollution entering the environment. For example, case study reports from the Beverage Council Industry (Curnow et al., 1997) indicate litter reduction in some of the major cities in Australia. However, these reports do not take into account other street pollutants such as organic matter. Furthermore, cigarette butts remain the major source of street waste. In most urban centres, these pollutants are often left uncollected while local city councils struggle to maintain street sanitation that has exceeded their cleaning capacity. Subsequently, during rainfall, uncollected street pollutants are transported readily along the impervious urban surfaces into the roadside stormwater drains, which then discharge into receiving waterways. There is much evidence of the extent and deleterious effect of discharged stormwater pollutants on the environment.

The urgency of addressing stormwater pollution was recently echoed in the Senate's inquiry into Australia's urban water management (Allison et al., 2002). Many of Australia's waterways are in a critical condition because of stormwater pollution. For example, pollutants from many rivers, creeks and stormwater drains have been entering Sydney's harbour over the past two hundred years. Commercial fishing has been banned due to the thick layer of toxic silt and mud which lies on the harbour bed. It is estimated that ninety per cent of gross pollutants—human derived litter, debris and organic matter dimensionally greater than 5 millimetres—entering the harbour, sink to the bottom giving the deceptive appearance of a relatively clean water surface (Pratten, 2009). Similarly, a study of gross pollutants in Melbourne reported that twenty per cent of litter and less than ten percent of organic waste floats when transported in urban waterways (Allison et al., 1998).

3.2 HISTORY OF LITTERING

The early Aboriginal inhabitants of Australia produced little or a no human derived matter and all waste—such as bones, shells, and stone and bone tools, judging from remains discovered by archaeologists at Aboriginal campsites (middens) in coastal regions—was of organic origin (KESAB, 2008). However, in the middle of the nineteenth century early in European settlements, the first sign of mass littering commenced with the influx of gold diggers who came by the shipload from overseas. Beachfronts, for example the mouth of the Yarra River, became clogged with people and goods awaiting transportation to the goldfields. Consequently, debris and garbage from ships and new arrivals blocked the bay. Similar situations existed in the mining settlements around Australia during this period (Everingham, 2007). This clearly signalled links between littering and population, activity, transport and production. These little-considered links are further examined in this article through the socio-economic shifts in the transition from colonialism to the new Australian society.

Other means were sought to carry out to further these examinations, since insufficient published resources were currently available. From a historical perspective, examining the municipal records for this article helped bridge the gaps in information on street waste. These records, which included archive photographs,

were based on housekeeping reports of roads and urban drainage systems with notes on complaints and problems. Such problems refer to stormwater pollution, which is a direct recipient of street waste. Furthermore, although street waste and drainage are separate issues, they were initially managed under the same municipal road maintenance program during the early development of transportation.

In the early period of European settlement, transportation mainly was horse-drawn. The wheels of carriage of carts gouged deep, dangerous ruts and the unmade road surfaces became either unpleasantly dusty in dry weather or boggy after rain. Municipal records in Sydney from 1870 onwards reveal public complaints about the state of the roads (Fraser, 1989). The local council was responsible for watering, flushing and sweeping the roads to keep the dust down and employed a small army of boys known as 'block boys' to remove the offending horse manure. Road-works were frequent, causing public inconvenience and traffic chaos resulting in the rapid deterioration of road surfaces. Roads were also constantly dug open by utility companies and local city council workers, and this work was often uncoordinated and badly managed. This led to newspaper complaints that the road-works, were road-wreckers (The City of Sydney, 2003). Horses were gradually replaced by steam, cable and electric powered vehicles. With the invention of the motor car and a rapid increase in vehicle ownership, local government was compelled to address road management issues more effectively, not the least of which was drainage.

Prior to the construction of urban drainage systems, cess pits and nightsoil collection services emptied waste into natural waterways and harbours. The Brisbane River, the Yarra River and Sydney Harbour, for instance became heavily polluted. This prompted local governments to embark on an urban drainage construction program. Consequently, the stormwater and sewer systems of Australia grew alongside cities and towns, evolving from natural drainage paths and creeks to a formal network of pipes and open channels (O'Loughlin and Joliffe, 1987). Historical reviews of urban drainage systems for cities in Australia have been documented by several authors (Argue, 1991; Gibson and Evernden, 1992; O'Loughlin and Robinson, 1999; Richard, 1980; Robinson and O'Loughlin, 1999). Prior to 1890s, urban runoff was initially channelled into a combined stormwater and sewer system in some major cities. Subsequently, stormwater was viewed as a nuisance due to the flooding, poor land drainage and transportation of sediment from unsealed roads that

intensified the sanitation problems. For example, the Sewage and Health Board of NSW, raised the issue of sedimentation (O'Loughlin and Joliffe, 1987). Ironically, it was the sewer systems that contaminated the stormwater and thereby exacerbated the pollution of receiving waters. Stormwater transporting solid wastes was also viewed with concern by the 1890s (O'Loughlin and Joliffe, 1987; O'Loughlin and Robinson, 1999). These authors do not elaborate on the type or content of litter found on the streets during this period. Apart from the loose road sediment, animal manure and leaves, there was a tendency to dump household waste onto the city streets, which was flushed into receiving waterways. Litter consisted of tin cans, paper, rags, and glass bottles, (National Library of Australia, 2009) these were rarely discarded because they were in short supply and were generally recycled. Milk, beer, and soft drink bottles were refilled and newspapers were reused. Since goods had to be shipped to Australia from Europe, very little was discarded.

Initially, stormwater and discarded items on streets were not considered an issue in Australia. However, by the 1920s, the design and construction of separate stormwater and sewerage systems became standard Australian practice due to public health concerns about waterborne diseases (O'Loughlin and Robinson, 1999). Brisbane may have been the first city in Australia to focus on separate stormwater and sewerage networks to protect the city from flooding. The first stormwater drain in Brisbane was designed prior to the 1920s (Richard, 1980). Sewer networks then became more important due to the nature of pollution, and from this point onwards the roadside drain became an efficient mechanism for transporting street waste into receiving waters.

Street waste was still considered a minor problem compared to the road development that was necessary due to the increasing population. The population growth was initially due to the gold rush which resulted in a boom during the second half of the nineteenth century. Progress in the field of agriculture and manufacturing also took place within this period. Despite this progress and the increase in population, commodities were still mostly reused or were limited in supply.

The two World Wars hampered socio-economic progress in that commodities were in even shorter supply. It was not until after the Second World War that Australia began to prosper again with the rapid increase in migration from Europe. This prosperity fuelled public spending and a rise in manufacturing and economic

development. Photographs from this period show that litter from public gatherings in streets and stadiums mainly consisted of discarded paper cups, newspapers, and other paper products (National Library of Australia, 2009). However, this soon changed when cigarettes became a worldwide commodity. Ironically, in both the First and Second World Wars, the government's rationing of cigarettes encouraged habitual smoking. In 1950, cigarettes with filters were manufactured to reduce the amount of chemicals inhaled by smokers, and these became an additional source of street litter. Towards the end of 1960, with the growth in consumerism, non-biodegradable plastic or aluminium containers became more viable and versatile than conventional paper packaging, which led to the generation of greater amounts of portable waste. These developments, combined with an increasing mobile population and improper disposal habits, intensified the proliferation of litter in public places. Furthermore, the American lifestyle culture (based on popular Hollywood films) influenced Australian society to the point where consumerism and materialism became the new goals. Mass production and fast turnover in consumer products brought about radical changes in the Australian household at all levels, including complacent attitudes towards the environment. Consumer products became more accessible through self service supermarkets rather than from the comparatively understocked local corner shops. The first supermarket was established in 1960 and, by the 1970s, supermarkets were common in all Australian cities (Coles, 2009). At the same time, fast food chains rapidly expanded their franchises; this led to a greater demand for disposable items such as packaging for the fast food industry and convenience shopping. New methods of packaging products were developed and items such as plastic milk bottles became common. As a consequence of these changes, typical human derived waste now consisted of cigarette butts, plastic, glass, metal, paper and cardboard.

The availability of these mass produced items together with the proliferation of cafes, restaurants and fast food outlets changed Australian eating habits dramatically. An increase in disposable income and the greater consumption of convenience foods led to a complacent and indifferent attitude to recycling. Consumers and smokers then became a significant source of litter in the urban environment. The industrial expansion required to feed these business and commercial activities generated a new form of chemically harmful pollutants, with heavy metals and hydrocarbons now

adding to human derived waste and organic material. The new motor car culture and the subsequent increase in vehicle ownership became a means for the dissemination of litter on Australian highways (Stokes, 2007). Most states in the USA showed a similar pattern of litter composition and a correlation between average daily traffic and total litter volume (Beck, 2007).

3.3 DATA ON THE PRACTICE OF LITTERING

Since the 1970s, the scientific community has viewed littering as a social behavioural and educational problem (Andre, 1983). For example, a correlation was found between heavy littering and crime and disorder in neighbourhoods (Dunstan et al., 2005; Perkins et al., 1992). In England, a government Minister viewed the litter crisis and the decline in standards of cleanliness and tidiness as a symptom of moral and spiritual decline (Jack, 2005). Although, this opinion may seem extreme and was made about a particular society, recent surveys in the occupied West Bank found that religious groups were less likely to litter (Al-Khatib et al., 2009). Whether these findings can be applied to multicultural Australian society requires further investigation. It was not until research funding became available in the 1990s, that data on littering attitudes and behaviour was seriously researched in order to improve educational campaigns (Taylor, 2004).

The most comprehensive litter behaviour database, created in 1997, was funded by the Beverage Industry Environment Council (BIC). The database currently consists of 94,000 observations and 18,900 interviews conducted in all major Australian cities. The database is a way of measuring the impact of anti-littering campaigns and the littering attitudes of Australians. The outcome showed that the process of disposing unwanted items was more complex than had been previously recognised. No clear distinction is made in the littering habits of people from different socio-economic backgrounds since they were all observed to litter. However, scientific studies from the Middle East and South America showed a more definitive trend in littering practises based on socio-economic characteristics such as gender, income, marital status and religious conviction (Al-Khatib et al., 2009).



Figure 3.1 A litter bin on Mary Street, Brisbane, 2008 surrounded by discarded cigarettes butts.

Other outcomes from the Australian littering database and scientific studies reveal that less than one third of older persons who were observed littering admitted to their behaviour when questioned; students are more likely to litter than other people; men litter more than women and women use bins more than men. In addition, the most common reasons for littering are: “too lazy”, “no ashtray” and “no bin.” Bin use was most common between 11.00 am and 2.00 pm. Litter generation was shown to be highest towards the weekend and daily litter accumulation peaked at about 4 pm (Curnow and Spehr, 2005). Most littering occurred within five metres of a bin particularly in the case of cigarette butts (See Figure 3.1). Nearly three quarters of litter consisted of smoking-related products, and of these, the most common objects were cigarette butts. This outcome is consistent with findings from other litter monitoring organisations (Curnow and Spehr, 1999). An interesting comparative study was also undertaken in 1997 to determine the usage of bins and the amount of

litter that enters stormwater drains. Results showed that numerically, cigarette butts accounted for 50% of human derived street litter, 40% of drain litter and 10% of bin waste (Hall and Phillips, 1997). Street sweeping studies show similar statistics that at least 80% of street waste generated as a by-product of littering attitudes, enters stormwater drains.

To this day, public littering attitudes appear to have remained relatively unchanged, despite technological and educational transformation. This is demonstrated by comparing photographs of litter bins taken in 1934 and 2009 [Figures 3.2 (a) and (b)]. In these photographs the surrounding areas are scattered with litter, despite the presence of nearby bins. The unchanged disposal patterns indicate that the public still carelessly discard litter (Curnow and Spehr, 1999). More specifically, putting litter near the bin appears to be good enough.



Figure 3.2 (a) Sydney Street, Sydney, 1934, (Image courtesy of The City of Sydney Archives) and (b) Stephens Road, South Brisbane, 2009

3.4 IMPACT OF LITTERING

The environmental impact of large quantities of gross pollutants in urban waterways has become widely recognised through scientific and media involvement. For example in the early 1990s, considerable media coverage and community involvement in clean-up litter campaigns and the tagged litter experiment in Melbourne increased public awareness of pollution from urban runoff (Brown and Clarke, 2007). The tagged litter experiment consisted of tracing 1,307 labelled items of litter through the Melbourne urban drainage system (McKay and Marshall, 1993). It was concluded that litter from the greater Melbourne urban drainage system contributed an estimated ninety-five per cent of all human derived waste polluting Port Phillip Bay. The report recommended that litter from local waterways be removed by installing more gross pollutant traps (GPT). It has become common practice for GPTs to be installed in urban developments throughout Australia.

In the late 1990, litter data from the Cooperative Research Centre for Catchment Hydrology (CRC) revealed that in any urban area, approximately 60,000 tonnes or 230,000 cubic metres of gross pollutants were generated annually. This equates to about 120 Olympic-sized swimming pools or about two billion items of litter (Allison et al., 1998). Litter on waterways is unsightly, emits strong odours, attracts vermin and is a major health risk due to the putrefying contents of fast food and beverage containers and pathogenic organisms attached to discarded hypodermic needles. Although the public perception of accumulated litter in waterways indicates poor water quality due to its visible impact, some researchers argue that it is the finer pollutants like toxicants and nutrients that are more harmful. However, the damaging effects of litter cannot be underestimated since they are carriers for these finer pollutants. Waste is also a breeding ground for mosquitoes and threatens aquatic fauna with entanglement or suffocation through ingression (Allison et al., 1998; Marais and Armitage, 2004). More importantly, a large proportion—60% to 80%—of litter entering the waterways via stormwater drains eventually becomes a source of marine pollution (Hassan, 2006; Zann et al., 1995). There is also a longstanding problem of cumulative non-biodegradable litter in the marine environment. Floating marine debris through the accumulation of land-based non-biodegradable waste is increasing at an alarming rate causing concern to the authorities and society. The largest mass of floating debris, about double the size of Texas (USA), exists in the

central North Pacific Ocean; it contains about 3.5 million tons of rubbish (Bond, 2006; Clayton, 2006; Zann et al., 1995). It has been estimated, for example, that 4,000 tonnes of plastic enters Australian seas annually and approximately 29,000 pieces of plastic float in each square kilometre (Derraik, 2002). The significant increase in marine pollution has recently prompted the Australian Marine Environment Protection Association (AUSMEPA) to adopt educational programs and other activities relating to stormwater pollution reduction.



Figure 3.3 (a) A stormwater channel at Kingsgrove, 1954, (Image courtesy of The State Library of NSW) and (b) View of a stormwater drain fully blocked with organic matter at Graham Street in South Brisbane, 2008.

Scientific studies also show that not only is human derived litter detrimental to the ecosystem, equally important are other forms of street pollutants, such as organic matter. Ian Cordery (2005) describes the change in the constitution of gross pollutants in Australian stormwater over the last thirty years. While street litter in the 1970s consisted equally of human derived waste and organic matter, the current components of gross pollutants consist of a much larger proportion of organic waste. As organic matter in waterways decomposes, it releases oxygen-demanding nutrients thus threatening the survival of aquatic flora and fauna and wildlife. Recently, in the suburbs of Brisbane, the ever-growing population of midges has been linked to damp leaf litter, open garbage bins, compost and decomposing organic matter such as grass or garden clippings, which provide ideal breeding conditions (Seeney, 2009). A comparison of organic matter found in stormwater drains in Brisbane can be seen in photographs [Figures 3.3 (a) and (b)] taken in 1954 and 2008 respectively. Organic

matter continues to be a source of stormwater pollution with leaves, twigs, bark and needles from trees blocking stormwater drains. Street flooding can also be caused by litter blocking the drainage system.

As towns and cities developed from their colonial origins in the nineteenth century, Australian society underwent dramatic socio-economic changes up until the current day. Prosperity through rapid population and industrialisation brought changes in consumer spending habits to suit a more convenient lifestyle. Such lifestyles meant a greater turnover of manufactured products and the accompanying disposable non-recycled packaging became a perfect recipe for street litter. Whereas, initially, litter was seen as a renewable resource, it has now become an environmental issue. The turning point came in the 1960s, when street litter was part of Australia's outdoor recreational culture. Public littering habits have always been a difficult problem to overcome, despite decades of intervention efforts by both government and community organisations.

3.5 SOLUTIONS

Three decades of attempted remedial action to reduce street litter are highlighted below. Early attempts were in the form of grass-roots educational campaigns. Later, drastic action came in the form of incorporating structural measures such as trapping devices into the management of collected street waste. Although local city councils were aware of street waste pollution in stormwater since the 1880s, serious concerns began only in the late 1960s. As the volume of street waste became a problem, national and local authorities became involved in litter-reduction drives and campaigns. Brisbane City Council conducted its first litter campaign in 1966, the Keep Australia Beautiful (KAB) National Association became active in 1969, and the Litter Act was introduced in 1971 (O'Loughlin and Robinson, 1999). It became apparent that these efforts had little impact on public littering habits. However, by the end of this period, the first gross pollutant trap was commissioned in Canberra (Phillips et al., 1989). This open trap consisted of a large concrete wet basin, a weir and a trash-rack to screen gross pollutants. Trash-racks are constructed from vertical or horizontal bars inserted in the stormwater flow path.

Up to the 1980s, the general consensus was that the Australian problem was not as acute as elsewhere due to our low population density, limited industrial growth and very little stormwater harvesting (O'Loughlin and Robinson, 1999). The tide changed in 1986, when authorities officially regarded littering as part of a wider environmental issue and incorporated stormwater quality improvement devices as requirements for land developers that led to the development of stormwater pollution controls (O'Loughlin and Robinson, 1999). Consequently, the non-proprietary trash-rack styled traps were adapted to suit varied terrain. Floating booms were also introduced across waterways to collect growing street waste where buoyant materials such as plastic and polystyrene were of prime concern. Towards the late 1980s, numerous scientific reports became available on these aspects of stormwater pollution controls. An Australian environmental conservation organisation was also formed to tackle the growing street waste through the Clean Up Australia campaign (<http://www.cleanup.org.au/au/>).

Efforts by scientific researchers, environmental groups and media attention (for example, the tagged litter study, see under the impact of littering) prompted greater awareness of street waste and its damaging effect on the environment, particularly from non-biodegradable products. The ever-increasing volume of street litter became a problem for existing traps and subsequently, blockages were more frequent. Eventually, the high maintenance and labour-intensive characteristics of these open devices were seen to be a deterrent. The exposed waste was unpleasant to sight and smell. Many proprietary stormwater quality improvement devices were developed to suit specific locations such as car parks or shopping precincts where litter was collected or where stormwater pollution was treated at a point source. By the mid to late 1990s efforts were intensified, not only with trapping devices but with other source control measures such as litter bins, educational campaigns, enforcement and environmental participation programs. These efforts are continuing more so since marine pollution is of great concern.

There is recent evidence that community groups in Australia are working towards the ultimate goal of a zero waste policy (<http://www.zerowasteaustralia.org/>). Such a policy involves greater focus on recycling urban waste which includes nutrients and organic matter which can then be recultivated in rural areas. For example, the City To Soil project to recycle organic

waste from urban communities to farmland has just been successfully completed (<http://groundswellproject.blogspot.com/>). The West Australian government is also currently investigating the use of recycled organic products in road verges, median strips and wetland constructions (<http://www.zerowastewa.com.au/organics/-resources/cstudy/>). The possibility of recycling organic matter from street waste is a subject for further research.

3.6 CURRENT POLLUTANT TRENDS: A CASE STUDY

This study also contributes to the lack of published data on litter and subsequent gross pollutants for the Brisbane area (which would be generally representative of other Australian cities), and to further the understanding of such pollution, a field survey was conducted. The field survey consisted of inspecting gross pollutants on streets and stormwater drains in the Brisbane Central Business District (CBD), South Brisbane and Burleigh Heads CBD. These sites were chosen to reflect a combined range of residential and commercial urban activities, and data was collected over a two-year period (2006 to 2008). Photographs and field notes were taken for analysis. The concentrations of gross pollutants were determined by mapping the surface of the littered area on the photograph and using an area ratio method to derive a percentage value. In cases where organic matter and litter were well mixed and difficult to segregate, the waste components were visually approximated.

The results of the field litter study are consistent with the litter audits performed by other sources and confirm that, in Australia, cigarette butts are numerically the most common (Clean Up Australia Ltd, 2008; Curnow and Spehr, 2005; KABCQLD and Healthy Waterway, 2004). This is a critical problem as a cigarette filter is designed to trap toxic chemicals that include gases, metals and radioactive compounds. When dispersed in water, these can leak into the environment and be extremely harmful to wildlife (Novotny and Zhao, 1999). Cigarette filters have been found in the stomachs of fish, whales and birds and these can choke and interfere with the animal's digestive systems. In many cases, gross pollutant traps are not able to retain cigarette butts due to their coarse screens.

Since the recent smoking ban (2006) in Queensland, the problem of disposing of cigarette butts has shifted from ashtrays inside buildings to streets and open spaces. The litter study identified cigarette butt hotspots such as pedestrian routes, roadside shops, green spaces and eating and drinking places. The worst affected areas are pedestrian routes leading to local transport centres, car parks and seating areas outside the hospitals. Commuters using an inner city railway station near Brisbane City were seen smoking prior to entering the platform. While a 'No Smoking' sign is clearly visible on the platform, the area around the station entrance is literally covered with cigarette butts that have been accumulating over a long period. A similar pattern was observed at traffic light islands and pedestrian crossings. Roadside gutters outside hotels and street cafés were no exception to this littering trend. The magnitude of the problem has led to a careless attitude regarding the disposal of cigarette butts whereby the managers of eating and drinking places tend to sweep the cigarette ends into the roadside gutter. As smoking bans continue to be more stringent, it is important for businesses and state and local governments to provide better receptacles and signage to prevent cigarette butts from becoming a persistent litter component.

One of the most noticeable characteristics of littering attitudes observed in this field litter study is that cultivated green spaces around offices, car parks, hospitals, shopping precincts, hotels, cafes and pubs are a dumping ground for human derived waste which is often hidden from public view until closely inspected. Even green spaces—used to enhance the appearance of a city—have inadvertently and ironically become litter traps. Bus stops have also become passive dumping grounds for litter. [Here, 'passive' is defined as litter left behind at public seating places (Sibley and Liu, 2003)].

It is a popular misconception that gross pollutants are mostly, if not all, human derived. However, studies (Allison et al., 2000) show that, irrespective of the method used to analyse the concentration of gross pollutant components by volume or mass, the derived values are usually between 70% to 90% for organic matter and 10% to 30% for human derived litter in mixed commercial, industrial and residential urban centres. This also applies to gross pollutants found on streets and in stormwater drains, as shown by the field survey (Figure 3.3). Figure 3.4 shows the high percentage of organic matter (60% to 70%) in all areas, with the exception of the

footpaths of the Brisbane CBD where the infrequent greenery is almost invisible beside the human derived litter such as paper, fast-food packaging, plastic and beverage containers.

Trees in urban areas usually contribute a large amount of fallen litter such as leaves, twigs, bark, and needles. Clippings from grass verges on pavements are commonly left behind by council maintenance workers, and a large proportion ends up in the stormwater drains. During wet weather, the roadside gutters (scattered with organic matter especially grass clippings) prevent a continuous flow of stormwater into the drains, thereby causing blockages. The decomposing mass contributes largely to the nutrients that enter our waterways, creating oxygen-depleting substances that are detrimental to the aquatic habitat.

The amount of gross pollutants observed in areas with different urban intensities of residential, commercial and industrial activities is further related to climatic conditions such as wind, the volume of traffic, topography, population density, community awareness and, most importantly, hydrological parameters (Walker and Wong, 1999). The hydrological parameters are energy factors that govern the mechanism of mobilisation and transportation of gross pollutants from the streets or pathways into stormwater systems. These factors relate to the number of stormwater drains in a given urban or catchment area, the fraction of imperviousness, the topography and the profile of the roadside gutter. In dry conditions, wind and traffic movement are likely to convey material into the drains. During a rain event, on the other hand, it has been observed (in a Melbourne suburb) that approximately 77% of street litter entered the drains, and as little as 2.6 mm of rainfall was enough to provide the transport mechanism (Hall and Phillips, 1997). Sustainable and green cities are the focus of current urban planning, and city planners and designers are promoting the concepts of green (or 'living') walls and roofs in urban centres (Callaghan, 2008). However, as these plans are implemented, the generation of green litter will proportionally increase and buildings clad with vegetation will add to the nutrient load in our waterways. The concept is not a modern one: houses with green roofs were built in medieval times, turf roofs were used in Viking dwellings in Scandinavia, and the most impressive example was the overhanging gardens of Babylon that decorated the roofs and terraces of the royal palace. It is assumed that

the organic waste matter was allowed to decompose locally, since no known efficient stormwater system existed; hence, this matter posed little threat to the environment.

The possibility of green cities as fire hazards is unclear due to a lack of published information, and Australian guidelines for green buildings are currently unavailable. Particularly in view of the recent worst natural disaster in Australian history (the Victorian bushfires of 2009) there should be greater concern, since dead organic matter and discarded cigarette butts are volatile combustible materials.

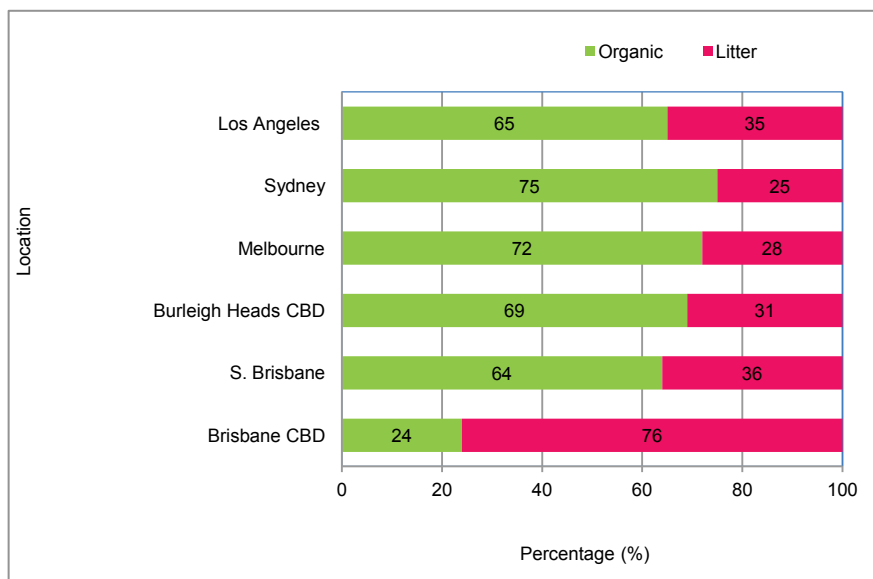


Figure 3.4 Graph showing the results of the litter field survey taken in 2006 to 2008. Comparison of gross pollutant (organic and litter) data are made with data collected from Sydney (Van Drie, 2002), Melbourne (Lewis, 2002) and Los Angeles (Lippner and Moeller, 2000; Quasebarth et al., 2001).

3.7 SUMMARY

This paper has given a historical perspective of Australian litter culture which indicates that our habits have not changed over the past fifty years or more, despite the progress in education and technology for the majority of the populace. Whereas prior to the 1960s litter was seen as a vital renewable source, it has now become an environmental issue. Climate change has received considerable attention, yet society remains unaware of the serious environmental consequences of generating street litter. Litter surveys indicate that most citizens would be far less likely to litter if the

ecological consequences of their actions were known. This not only applies to human derived litter but also to organic waste, which is also a major stormwater pollutant.

The case study shows the need to tackle street waste using a holistic approach when incorporating new design goals for greener and safer cities. This should include greater cooperation between city councils and business owners—for example, owners of outdoor cafés and restaurants—to promote street cleanliness. Furthermore—and these are largely unrecognised problems—landlords of private dwellings with overhanging greenery should take responsibility for minimising the organic waste that falls on public footpaths, and those who promote innovations in greening our cities should be aware of both the positive and negative environmental impacts of these endeavours. Organic material can be easily collected, composted and reused as mulch (Andrews, 2008). Street maintenance undertaken by local city councils that includes grass cutting, and sweeping and cleaning stormwater drains should be undertaken in an environmentally friendly manner. It has been observed from field studies and literature surveys that gross pollutant traps are often inappropriately located. Additional research is needed to ensure a more efficient system approach.

Furthermore, provisions should be made to involve local communities to implement stricter penalties and rewards, through volunteer organisations such as Clean Up Australia which have had considerable success in this regard. Finally, innovative educational methods—such as the talking closed circuit television cameras introduced in Middlesbrough, England by which staff monitors litter offenders who are instantly corrected over a loudspeaker system—should be encouraged (BBC, 2007). As Tim Flannery, the renowned Australian environmentalist warns:

‘You can’t just grow forever and hope that the environment will take care of itself.’

ACKNOWLEDGEMENTS

The authors would like to thank Ms Sarita Gupta Madhani for her editorial contributions.

REFERENCE

- Al-Khatib, I. A., Arafat, H. A., Daoud, R. and Shwahneh, H. (2009). Enhanced solid waste management by understanding the effects of gender, income, marital status, and religious convictions on attitudes and practices related to street littering in Nablus-Palestinian territory. *Waste Management*, 29(1), 449-455.
- Allison, L., Tierney, J., Lundy, K., Mackay, S., Tchen, T. and Wong, P. (2002). *The value of water: inquiry into Australia's management of urban water*. Canberra, ACT, Australia: The Parliament of the Commonwealth of Australia. Retrieved 16 March 2010, from http://www.aph.gov.au/senate/committee/ecita_ctte/completed_inquiries/2002-04/water/report/report.pdf
- Allison, R. A., Walker, T. A., Chiew, F. H. S., O' Neill, I. C. and Mc Mahon, T. A. (1998). *From roads to rivers: gross pollutant removal from urban waterways*. Clayton, Victoria: CRC for Catchment Hydrology. Retrieved 14 January 2010, from <http://www.catchment.crc.org.au/pdfs/technical199806pt1.pdf>
<http://www.catchment.crc.org.au/pdfs/technical199806pt2.pdf>
<http://www.catchment.crc.org.au/pdfs/technical199806pt3.pdf>
<http://www.catchment.crc.org.au/pdfs/technical199806pt4.pdf>
- Allison, R. A., Walter, K. A., Marx, D., Lippner, G. and Churchwell, R. (2000). A method for monitoring and analyzing litter in freeway runoff as part of the Caltrans litter management pilot study. In R. H. Hotchkiss and M. Glade (Eds.), *Building Partnerships: Proceedings of Joint Conference on Water Resource Engineering and Water Resources Planning and Management 2000* (pp. 81-91). Minneapolis, Minnesota, USA: American Society of Civil Engineers (ASCE).
- Andre, D. L. (1983). *Synthesis of highway practice 184: disposal of roadside litter mixtures*. Washington, DC, USA: Transportation Research Board.

Andrews, P. (2008). *Beyond the brink: Peter Andrews' radical vision for a sustainable Australian landscape*. Sydney: ABC Books for the Australian Broadcasting Corporation.

Argue, J. R. (1991). A short history of water and wastewater in Adelaide: 1838 to 1980. *Managing stormwater in Adelaide perspectives: problems: possibilities: putting the pieces together* (pp. 1-13). Frewville, Adelaide: Institution of Engineers (South Australian Division), Australia.

BBC (2007). 'Talking' CCTV scolds offenders. Retrieved 13 September 2010, from <http://news.bbc.co.uk/2/hi/6524495.stm>

Beck, R. W. (2007). *A review of litter studies, attitude surveys, and other litter-related literature*. Stamford, Connecticut, USA: Keep America Beautiful (KAB). Retrieved 15 May 2009, from http://www.kab.org/site/DocServer/Litter_Literature_-_Review.pdf?docID=481

Bond, S. (2006). Scale of floating rubbish dump highlighted by Greenpeace. Retrieved 6 November, from http://www.edie.net/news/news_story.asp?id=12224

Brown, R. R. and Clarke, J. M. (2007). *Transition to water sensitive urban design: the story of Melbourne, Australia*. Melbourne, Victoria: Monash University.

Callaghan, G. (2008, June 21-22). Green skins. *Weekend Australian*. Retrieved 15 March 2010, from <http://www.theaustralian.com.au/news/features/green-skins/story-e6frg8h6-1111116689357>

Clayton, M. (2006, 11 October). Congress acts to clean up the ocean. *The Christian Science Monitor*. Retrieved 15 March 2010, from <http://www.csmonitor.com/2006/1011/p02s01-usgn.html>

Clean Up Australia Ltd (2008). Rubbish report, 2008. Retrieved 15 May 2009, from <http://www.cleanup.org.au/au/NewsandMedia/rubbish-report.html>

Coles (2009). *History of Coles supermarket store*. Retrieved 15 March 2010, from <http://www.coles.com.au/about/info/history.asp>

Cordery, I. (2005). Field performance of a vortex type gross pollutant trap. *Australian Journal of Water Resources*, 9(1), 49-54.

Curnow, R. C. and Spehr, K. L. (1999). What works? Littering behaviour interventions report. Pyrmont, New South Wales, Australia: The Beverage Industry Environmental Council.

Curnow, R. C. and Spehr, K. L. (2005). *Littering behaviour studies VII: national benchmark 2004*. Pyrmont, New South Wales, Australia: The Beverage Industry Environmental Council.

Curnow, R. C., Streker, P. and Williams, E. (1997). *Understanding littering behaviour in Australia*. Pyrmont, Australia: Beverage Industry Environmental Council. Retrieved 15 March 2010, from <http://www.afgc.org.au/cmsDocuments/LBS%20I.pdf>

Derraik, J., G. B. (2002). The pollution of the marine environment by plastic debris: a review. *Marine Pollution Bulletin*, 44(9), 842-852.

Dunstan, F., Weaver, N., Araya, R., Bell, T., Lannon, S., Lewis, G., Patterson, J., Thomas, H., Jones, P. and Palmer, S. (2005). An observation tool to assist with the assessment of urban residential environments. *Journal of Environmental Psychology*, 25(3), 293-305.

Everingham, S. (2007). Wild ride: the rise and fall of Cobb & Co. In *chapter 1*. Camberwell, Victoria: Penguin Books (Australia).

Fraser, D. J. (1989). *Sydney, from settlement to city: an engineering history of Sydney*: Engineers Australia.

Gibson, T. G. and Evernden, J. A. (1992). Trapped street gullies. Paper presented at the *International Symposium on Urban Stormwater Management: Preprints of Papers, National Conference Publication (NCP) No. 92/1*. Sydney, NSW: Institution of Engineers, Australia.

Hall, M. D. and Phillips, D. I. (1997). Litter generation and distribution in commercial strip shopping catchments. Paper presented at the *Future directions for Australian Soil and Water Management Conference*. Brisbane, Queensland: Stormwater Industry Association.

Hassan, D. (2006). *Protecting the marine environment from land-based sources of pollution: towards effective international cooperation*. Aldershot, Hants, England; Burlington, Vermont, USA: Ashgate.

Jack, C. (2005). *Blowin' in the wind: a short history of litter in the twentieth century*. Stirling, UK: AHRC Research Centre for Environmental History, University of St Andrews.

KABCQLD and Healthy Waterway (2004). Litter strategy monitoring wave 2, *May 2004, Project Number 6583-2*. Brisbane: KABC Qld (Keep Australia Beautiful, Council Queensland Inc.) and Healthy Waterway.

KESAB (2008). *History of garbage*. Retrieved December 17, from <http://www.kesab.asn.au/uploads/File/Fact%20Sheets%20-%20History%20of%20Ga.htm>

Lewis, J. (2002). *Effectiveness of stormwater litter traps for syringe and litter removal report for Melbourne Water Corporation*. Melbourne, Victoria: Cooperative Reserach Center (CRC) for Catchment Hydrology. Retrieved 14 January 2010, from http://www.clearwater.asn.au/resources/325_1.pdf

- Lippner, G. and Moeller, G. (2000). Study quantifies broom sweeper litter pickup ability. *American Sweeper Magazine*, 8(1). Retrieved 14 February 2010, from www.owp.csus.edu/research/papers/papers/PP012.pdf
- Marais, M. J. and Armitage, N. (2004). Problems encountered with the measurement of urban litter entering the stormwater systems of Cape Town. In William James (Ed.), *Innovative modelling of urban water systems* (pp. 475-504). Guelph, Ontario CHI Publications.
- McKay, P. and Marshall, M. (1993). *Backyard to bay: tagged litter report*. Melbourne, Victoria: Melbourne Water and Melbourne Parks and Waterways.
- National Library of Australia (2009). *Picture Australia*. Retrieved 15 May 2009, from <http://www.pictureaustralia.org/index.html>
- Novotny, T. E. and Zhao, F. (1999). Consumption and production waste: another externality of tobacco use. *Tobacco Control*, 8(1), 75-80.
- O'Loughlin, G. G. and Joliffe, I. B. (1987). Historical overview of urban stormwater drainage hydraulics. *Conference on Hydraulics in Civil Engineering: Preprints of Papers NCP No. 87/14* (pp. 82-87). Melbourne, Victoria: Institution of Engineers, Australia.
- O'Loughlin, G. G. and Robinson, D. K. (1999). The coming quality, the recognition of urban stormwater pollution in Australia. In I. Joliffe, B. and J. Ball, E. (Eds.), *Proceedings of the 8th international conference on urban storm drainage* (pp. 1132 -1141). Sydney Hilton Hotel, Sydney, Australia: 30 August-3 September 1999.
- Perkins, D. D., Meeks, J. W. and Taylor, R. B. (1992). The physical environment of street blocks and resident perceptions of crime and disorder: implications for theory and measurement. *Journal of Environmental Psychology*, 12(1), 21-34.

- Phillips, B. C., Lawrence, A. I. and Szlapinski, P. M. (1989). Recent developments in gross pollutant traps. *Australian Water and Wastewater Association 13th Federal Convention Preprints of Papers NCP No. 89/2* (pp. 143-147). Canberra, ACT, Australia: Institution of Engineers, Australia.
- Pratten, A. (2009). The state of Sydney's waterways, *Telephone interview with the managing director of Stormwater Systems on 25 February 2009*. Sydney: J. Madhani.
- Quasebarth, T., Schroeder, D., Chappell, R., Churchwell, R. and Lippner, G. (2001). An investigation of factors influencing solids transport and deposition into highway drain inlets. *Bridging the Gap: Meeting the World's Water and Environmental Resources Challenges: Proceedings of World Water and Environmental Resources Congress 2001* (pp. 184-194). Orlando, Florida, USA: American Society of Civil Engineers (ASCE).
- Richard, E. L. (1980). Early drainage of Brisbane. *Queensland Division Technical Papers* (pp. 1-7). Institution of Engineers, Australia.
- Robinson, D. K. and O'Loughlin, G. G. (1999). A critical review of the development of stormwater management practice in New South Wales, Australia. In I. B. Joliffe and J. E. Ball (Eds.), *Proceedings of the 8th international conference on urban storm drainage* (pp. 1132 -1141). Sydney Hilton Hotel, Sydney, Australia: 30 August-3 September 1999.
- Seeney, B. (2009). Eaten alive! Midge plague bites hard. *City South News*. Retrieved 16 March 2010, from <http://city-south-news.whereilive.com.au/news/story/eaten-alive-by-moorooka-midges/>
- Sibley, C. G. and Liu, J. H. (2003). Differentiating active and passive littering: a two-stage process model of littering behavior in public spaces. *Environment and Behavior*, 35(3), 415.

Stokes, K. (2007). Litter and other roadside anomalies: an exploration of loss on Australian highways. *The international journal of environmental cultural, economic & social sustainability*, 3(1), 101-108.

Taylor, A. (2004). The bigger picture: evaluating litter programs in the context of stormwater management. Paper presented at the *Leading on Litter conference: 2004 National Conference & Expro*. Melbourne, Victoria. Retrieved 15 May 2009, from http://www.ecorecycle.sustainability.vic.gov.au/resources/documents/Andre_Taylor1.pdf

The City of Sydney (2003). *The City of Sydney archives: a history of Sydney Streets*. Retrieved 15 March 2010, from <http://www.cityofsydney.nsw.gov.au/history/sydneystreets/default.html>

Van Drie, R. (2002). Development of a pollutant load algorithm (for Sydney Australia). In Eric W. Strecker and Wayne C. Huber (Eds.), *Global Solutions for Urban Drainage: Proceedings of 9th International Conference on Urban Drainage - 9ICUD* (pp. 207-221). Portland, Oregon, USA: American Society of Civil Engineers (ASCE).

Walker, T. and Wong, T. H. F. (1999). *Effectiveness of street sweeping for stormwater pollution control* (Vol. 3800). Clayton, Victoria: CRC for Catchment Hydrology. Retrieved 14 February 2010, from <http://www.catchment.crc.org.au/pdfs/technical199908.pdf>

Zann, L. P., Great Barrier Reef Marine Park Authority and Department of the Environment Sport and Territories (1995). *Our sea, our future: major findings of the state of the marine environment report for Australia*. Townsville, Queensland: Department of the Environment, Sport and Territories. Retrieved 15 March 2010, from <http://www.ea.gov.au/coasts/publications/somer/>

Chapter 4: The field/case study

SUMMARY

This chapter documents the field/case study in which gross pollutant data was collected and analysed. The data was used to identify public littering attitudes and typical street waste which are important factors in the design and placement of GPTs in urban environment. Existing installations of GPTs were also monitored to collect field operating data necessary for performing theoretical studies and experiments in the laboratory. The outcome of this chapter shows that a high percentage of organic matter which can block or clog retaining screens of strategically placed GPTs originated from streets and stormwater systems. Furthermore, low flow rates are common in GPTs because of intermittent rainfall. The field case/study also shows that the motion of gross pollutants in stormwater during transportation was found to be complex and their buoyancy properties varied.

4.1 INTRODUCTION

In the field/case study, surveys were conducted in Brisbane central business district (CBD), inner southern Brisbane suburbs and Burleigh Heads, a seaside suburb of the Gold Coast with a population less than one tenth of Brisbane's population (Figure 4.1, Figure 4.2, and Figure 4.3). Brisbane is the capital of Queensland and is the rapidly growing third largest city in Australia with a population of just under two million. Brisbane CBD is a centre for retail and business activities in Queensland and is mainly surrounded by gardens and open spaces. The areas surveyed in the inner south of Brisbane included South Bank, South Brisbane and Highgate Hill which are used for business, commercial and residential purposes. These survey areas were selected to reflect a diverse range of urban activities. The field survey consisted of inspecting storm water drains and gross pollutants on streets, investigating operational GPTs and monitoring gross pollutants on streets

during wet weather over a two year period (2006-2008). The rainfall data for this period is attached to Appendix A.

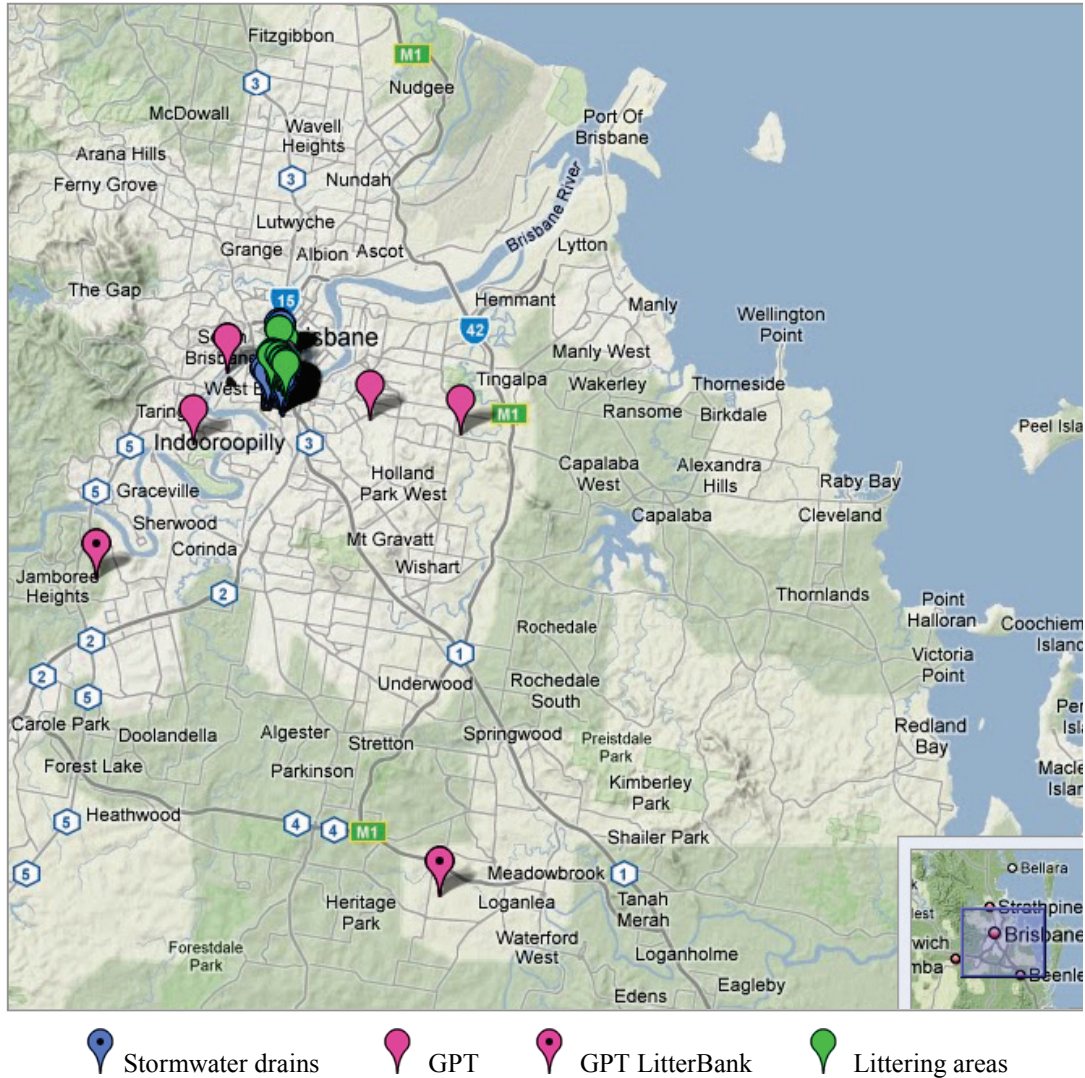


Figure 4.1 The overall terrain map of surveyed stormwater drains, hotspot littering areas and GPTs in Brisbane (Queensland) and its suburbs as defined in Google maps (author developed database available at: <http://maps.google.com/maps/ms?ie=UTF&msa=0&msid=102965336134023288187.-00047b6e955a7b89a6666d> for further details, such as scale and orientation).

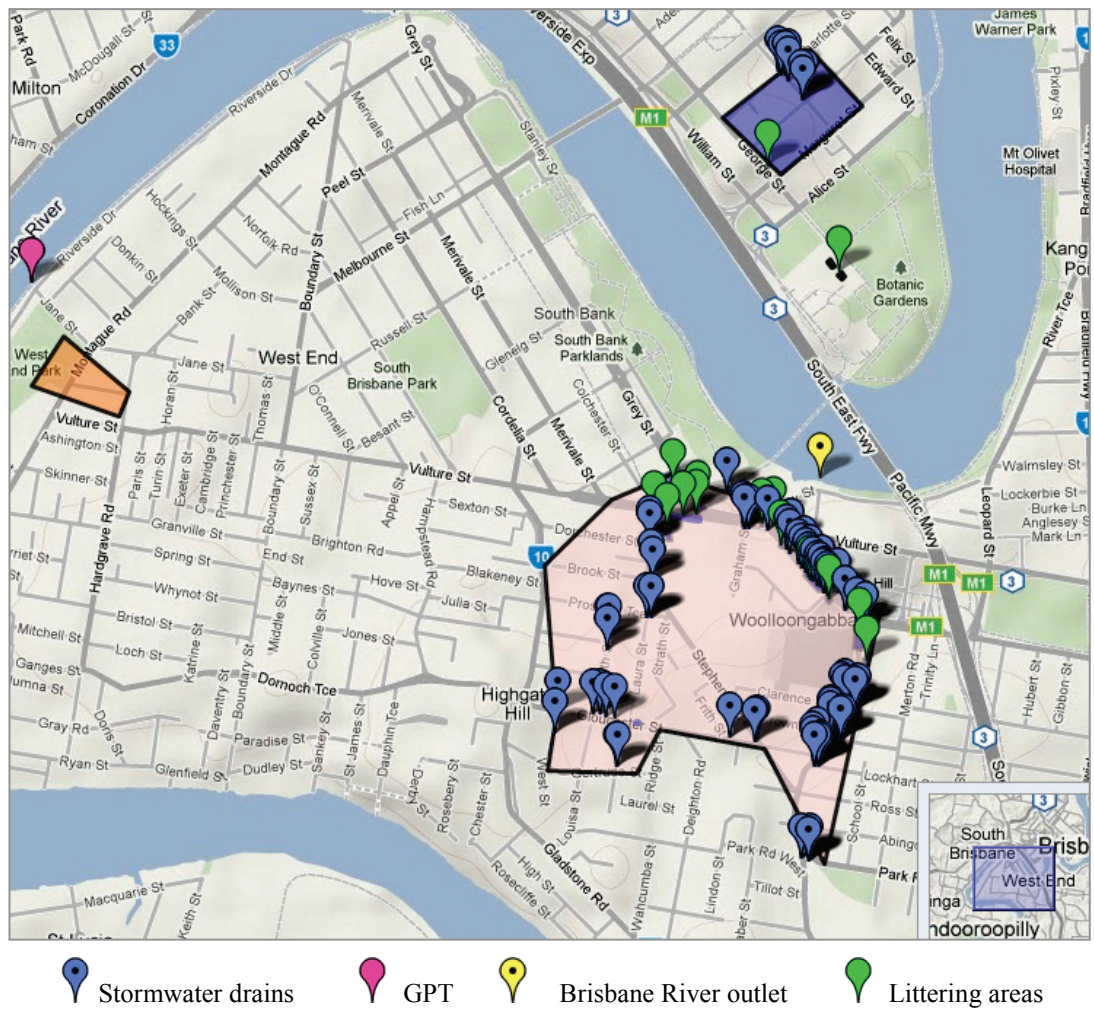


Figure 4.2 A detailed terrain view of the mapped stormwater drains, GPT, catchment outlet and littering areas in Brisbane and the inner suburbs for the field study as defined in Google maps (author developed database available at: <http://maps.google.com/maps/ms?ie=UTF&msa=0&msid=-102965336134023288187.00047c2cd8a137d829c19> for further details, such as scale and orientation). The shaded areas represent the perimeters of the surveys conducted.

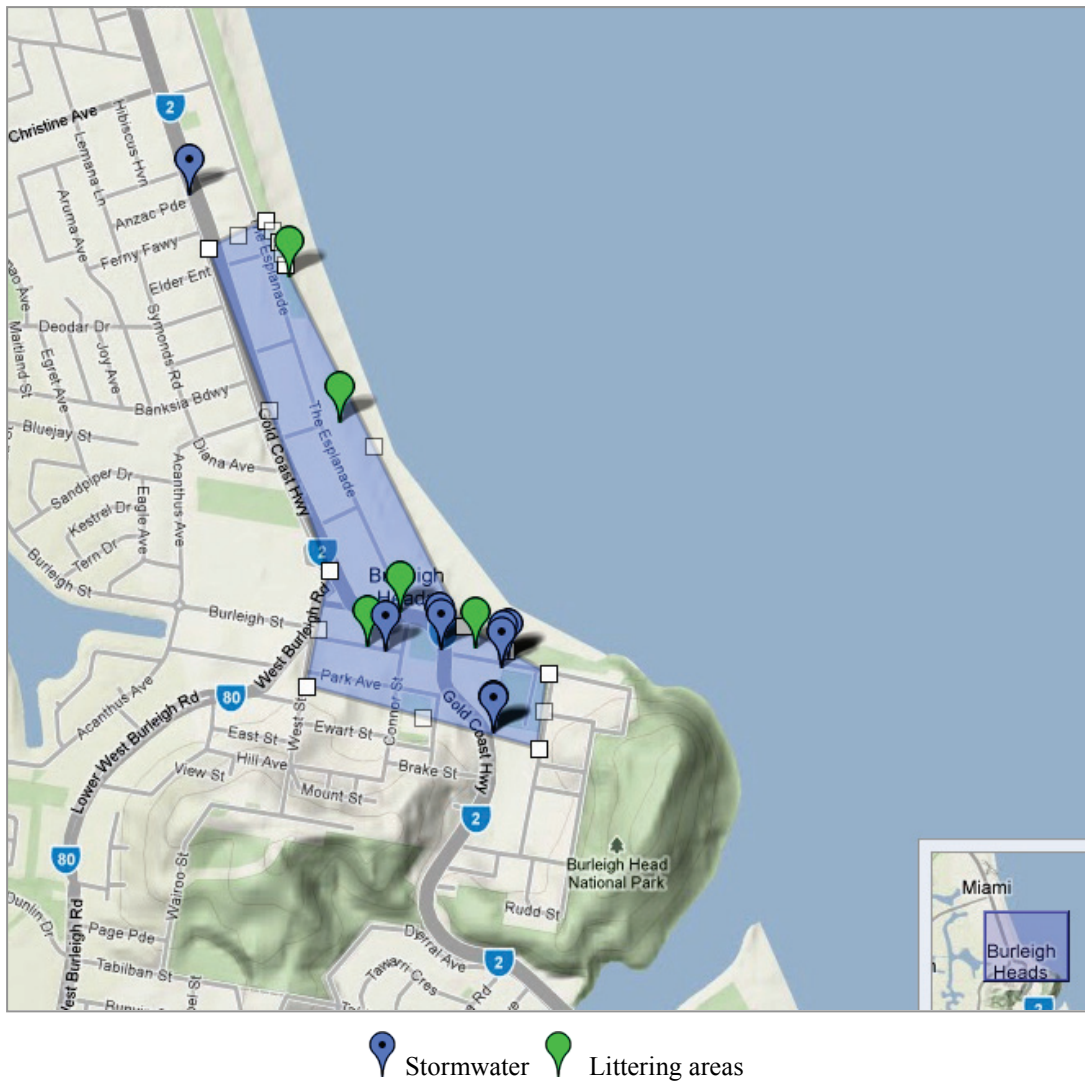


Figure 4.3 A field survey map of inspected stormwater drains and littering areas in Burleigh Heads, a suburb of the Gold Coast as defined in Google maps (author developed database available at: <http://maps.google.com/maps/ms?ie=UTF&msa=0&msid=102965336134023288187.-00047c4ca557459ca0e62> for further details, such as scale and orientation).

4.2 METHOD OF ANALYSIS

The investigation was more extensive in the inner southern suburbs of Brisbane than in the CBD because of their varied urban activities, as shown in Figure 4.2. For example, the inner southern suburbs surveyed, included schools, a sports centre, hospitals (private & public), street cafes, transport (bus and train) stations, car parks, a public house, retail shops, a shopping precinct, open areas and housing.



Figure 4.4 Storm water inlet drain in a residential area (West Street, Highgate Hill) of an inner suburb of Brisbane City clogged mainly with organic matter (small amounts of litter—plastic bottles and paper) just after a wet weather flow. Lower left is a view inside the drain (empty) and the top right shows the view of street and the drain location (June 2008). Lower right, the shaded area is used to map and estimate the gross pollutant contents (see SWD No. 75 in Tables 4.1 and 4.2).

In these areas, gross pollutants were inspected inside the stormwater drains and on top of the gratings, as shown in Figure 4.4 and these results were tabulated in Tables 4.1 and 4.2, respectively, located at the end of this chapter. For example, in Figure 4.4, the accumulation of gross pollutants on top of the stormwater drain which had blocked the grate inlet consisted of 94% organic matter and 6% litter such as

plastic bottles and paper (See SWD No. 75, Table 4.2). The gross pollutant percentages were tabulated alongside details of the catchment area and any field observation comments (See under ‘Street name’, ‘Activity’, ‘Location’ and ‘Comments’, Tables 4.1 and 4.2). In some cases, where the contents were clearly visible, a rough percentage estimate was also provided under the column ‘Sediment’ in these tables. However, the main focus of this investigation pertained to gross pollutant components—organic matter and anthropogenic litter.

Various qualitative and quantitative methods have been used by previous authors to quantify the components of gross pollutants found in the environment. For example, the volume percentage of organic matter and litter collected at a trashrack in the Cooks River catchment area was visually estimated (Sim and Webster, 1992). In Los Angeles, accumulations of organic matter on the highways were also qualitatively estimated (Allison et al., 2000; Quasebarth et al., 2001). These results have been compared with the more rigorous methods of sampling and shown to be similar in constituency (Allison et al., 1998) not only in Australia but also in the US (Lippner et al., 2000).

In this research, the components of gross pollutants were quantified by using the area ratio method. This method assumes a constant height of one unit and the gross pollutant components are visually mapped, as shown in Figure 4.4 (lower right). Inside the drain (lower left) 0% is assumed for both litter and organics since gross pollutants have not been collected (See SWD No. 75, Table 4.1).

On both sides of the road, stormwater drains were inspected and analysed, as shown in Figure 4.5. During each inspection, the contents of the drains were also visually estimated. For cases where organic matter and litter were well mixed and difficult to segregate, the breakdown of the gross pollutant contents was visually estimated. Sediments were considered part of organic matter where their origins, such as a nearby construction site, were difficult to trace.

Roadside pollutants were observed and compared with the contents inside the nearest stormwater drain to take into account the climatic conditions, dry weather flows and street sweeping. Anthropogenic litter on streets and open spaces were also surveyed for excessive amount of discarded waste and, where this occurred, these areas were classed as ‘hotspots’. These results were tabulated in Table 4.3 in the same manner as the previous tables.

In addition to field surveying notes, photographs were also taken and inspections of stormwater drains and roadside gutters were usually carried out during the weekend (early morning) to avoid traffic where possible. Most drains could be opened and inspected during these times. Some drains were periodically monitored after a period of rainfall to identify the number of blocked drains. A similar approach was taken when inspecting and monitoring GPTs.

The main aim of monitoring GPTs was to collect operating parameters necessary to physically model the flow conditions through a GPT in flume at QUT's hydraulic laboratory. Here, the data was mainly collected from GPTs located in Marsden Estate and Sinnamon Park new outer residential suburbs of Brisbane (see pink with black dot icon, right and left respectively in Figure 4.1).

The final part of the field study involved monitoring the flow motion characteristics of gross pollutants during wet weather. In sewer systems, gross solids movement in intermittent flow has been previously described using visual observations and photographic evidence (Littlewood and Butler, 2003). Littlewood and Butler (2003) modelled gross solids using plastic cylinders which do not share all the characteristics of organic solids. However, these authors state that the regularity of the solids allowed repeatable experiments to be carried out. In addition to conducting capture/retention experiments with artificial pollutants, field observation were also made in this research to examine the behaviour of the mobilisation of gross pollutants during a rainfall event using photographic evidence. Resultant data (which rarely exists in the literature) is reported in Section 4.6.

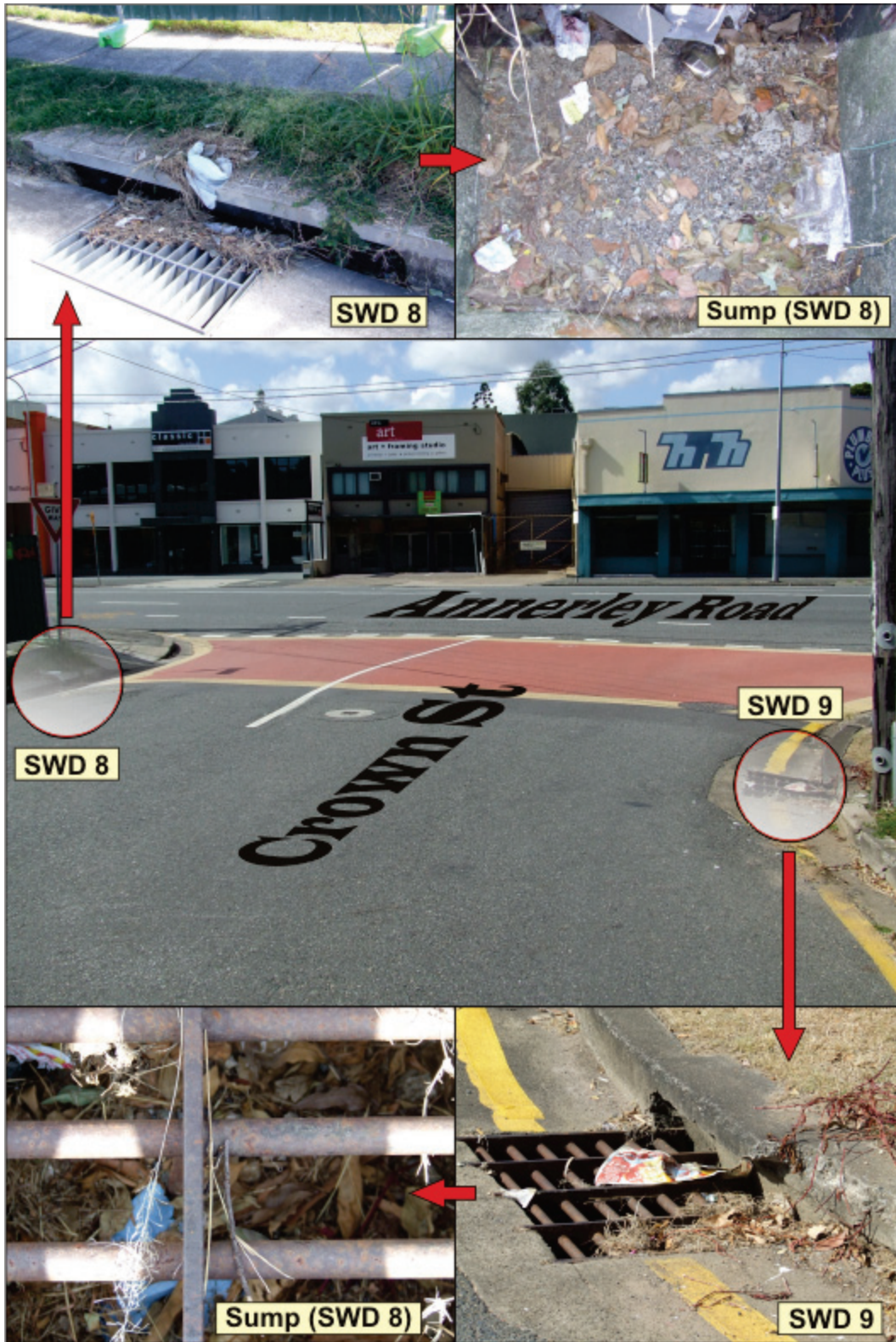


Figure 4.5 Inspection of road-side stormwater drains SWD 8 and 9 (See Tables 4.1 and 4.2) on Crown St T junction to Annerley Road. Both storm water drains include a grate and kerb inlet and are partially clogged, mainly with organic matter and fine sediments. Sumps A and B are relatively empty and mainly consist of organic matter, paper, packaging material, plastic bags, cigarettes butts etc.

4.3 RESULTS AND DISCUSSION

The results of the field investigation are tabulated in Tables 4.1, 4.2, and 4.3, together with the overall mean values for each area surveyed. Photographs and field estimates were used to derive these results pertaining to the amount of gross pollutants found in stormwater drains and on streets. Furthermore, anthropogenic litter hotspots were identified, experimental modelling parameters were collected, and the mobilisation of gross pollutants on streets was observed during wet weather.

In addition to the tabulated results shown in Tables 4.1, 4.2 and 4.3, the locations of the inspected stormwater drains, GPTs and littering areas were defined in Google maps application programming interface (API) web based program (Figure 4.6). These locations are tagged and hyperlinked in the left column of Figure 4.6. Approximately 80 stormwater drains and 22 hotspot areas were inspected. These are identified by the blue and green icons in Figure 4.2 and Figure 4.3. The shaded areas in these figures represent the perimeters of the field investigations.

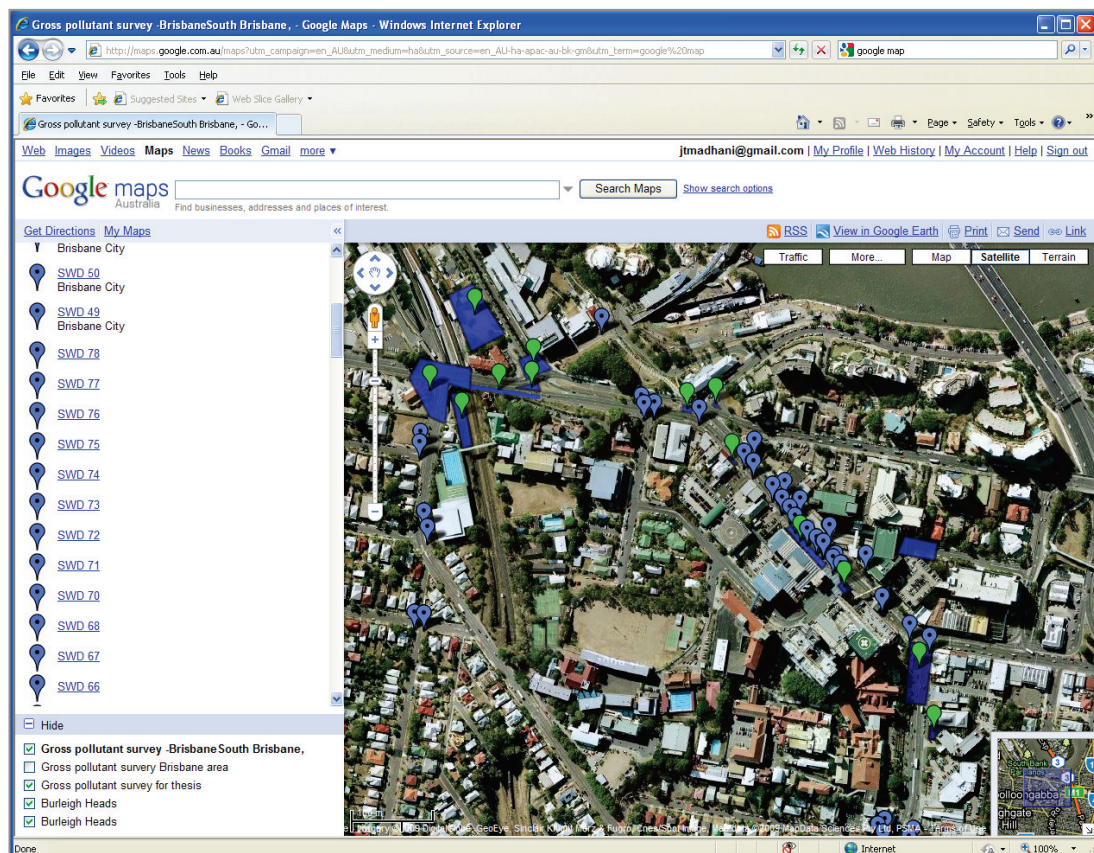


Figure 4.6 Using Google maps to locate the surveyed stormwater drains, GPTs and littering areas.

4.4 STORMWATER DRAINS AND GROSS POLLUTANTS ON STREETS

The average percentages of organic matter and litter found in stormwater drains in Brisbane CBD, the inner south of Brisbane (labelled S. Brisbane) and Burleigh Heads CBD are tabulated in Table 4.1, and plotted in

Figure 4.7.

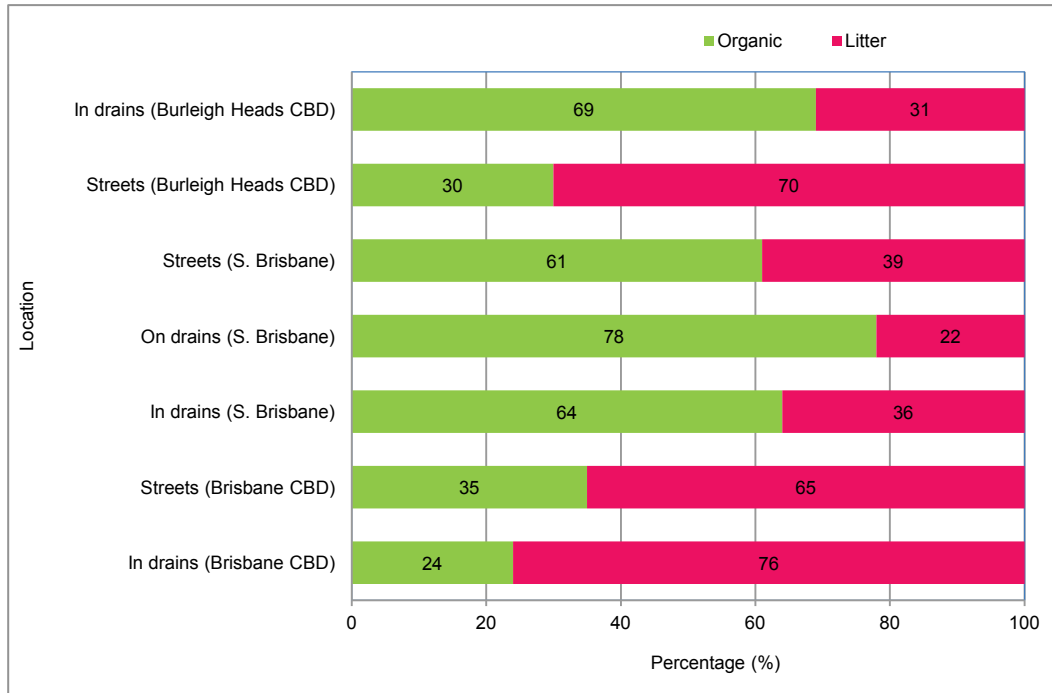


Figure 4.7 The field investigation results (Tables 4.1 and 4.2) expressed as average percentage of gross pollutants (organics & litter) found inside and on top of stormwater drains and on streets located in inner southern suburbs of Brisbane and Burleigh Heads.

During the survey of the CBDs (Brisbane and Burleigh Heads), mobilisation of gross pollutants was found to be higher in the inner suburbs where a greater amount of vegetation of vegetation exists. For example, little mobilisation of gross pollutants was found on top of the top of the stormwater drains in Brisbane and Burleigh Heads CBDs; hence, no data is shown in

shown in

Figure 4.7. In this figure, the higher litter content in the Brisbane CBD was partly due to less surrounding greenery, not taking into account any seasonal changes which could increase leaf shedding.

Figure 4.7 also shows notable differences in the organic contents on the streets and inside drains at Burleigh Heads. Here, street cleaning schedules may have influenced the data collected, or too few (8) drains were inspected due to the

restricted time schedule. Other influencing factors were climatic conditions (light material can be mobilised by wind) and dry weather flows. In addition, street cleaning was carried out more frequently than the emptying of stormwater drains.

Overall, the data trends and characteristics between the stormwater drains and the streets for the inner south of Brisbane and Brisbane CBD are comparable. The current data was also compared with results obtained from previous investigations, as shown in Table 4.3.

4.5 PHOTOGRAPHIC RESULTS

Stormwater drains and streets

In the field survey, 15% of stormwater drains were found to be blocked (Figure 4.8). Such blockages can cause upstream flooding (Figure 4.9). As seen in Figure 4.9, blockages were caused by a combination of organic matter and fine sediments which had been accumulated above the pipe outlet inside the drain sump. Figure 4.10 shows an unblocked interior of a drain sump where the incoming flow from the right is discharging through the pipe outlet, as indicated by the arrows.

On busy roads, stagnant water in blocked drains is contaminated with traffic dust (see lower left of Figure 4.11) which contains pollutants such as heavy metals from road runoff, nutrients, toxicants and hydrocarbons. Fine sediments are often contaminated with traffic dust, as shown outside the same drain in Figure 4.12. Here, the outside of the drain is covered with leaves which act as filters, thereby absorbing the fine sediments and traffic dust. Consequently, on both sides of the drains, trails of sediments were formed and these become a potential health hazard for pedestrian and cyclists.

More importantly, these leaves become carriers for the sediments and more harmful stormwater pollutants when transported into urban waterways. This observation was also noted with other form of gross pollutants, particularly with water absorbing surfaces (Figure 4.13).

Gross stormwater pollutants can also cause blockages (Figure 4.13). In Figure 4.13, a typical collection of gross pollutants is shown in a stormwater drain beside a busy road.

Since gross pollutants in stormwater drains are mobilised from streets, the surrounding areas were also inspected for excessive anthropogenic litter hotspots. A greater proportion of gross pollutant particularly anthropogenic litter was seen outside street cafés, an educational establishment, litter bins, bus stops, fast food outlets, a train station, public houses, hospitals (public and private), car parks, offices, hotels, a shopping precinct and on common walking routes. Examples of such litter hotspots are depicted in Figures 4.14-4.21.

Figure 4.14 shows that greenery spaces—in this case, besides a hotel, street café and a local shopping precinct—typically attract discarded litter. Fast food packaging, cigarette butts and beverage drink containers are also found at the bus stops (Figure 4.15). During the survey, it was common to see the management of eating and drinking places sweeping a large amount of cigarette butts onto the pavement and roadside gutter (Figure 4.16). The worst case of cigarette butt disposal was seen outside the South Bank train station (Figure 4.17). Street gardens and greenery areas are used as ashtrays in public spaces and an example is given in Figure 4.18. This photograph was taken outside a local private hospital next to a car park and a bus station. A large number of cigarette butts are also commonly found on the popular pedestrian route from the Mater bus station to the city (Figures 4.19 and 4.20). Broken glass was also another discarded item often observed during the survey (Figure 4.21). The survey also included monitoring of GPTs which is described later, under the heading Gross pollutant trap.

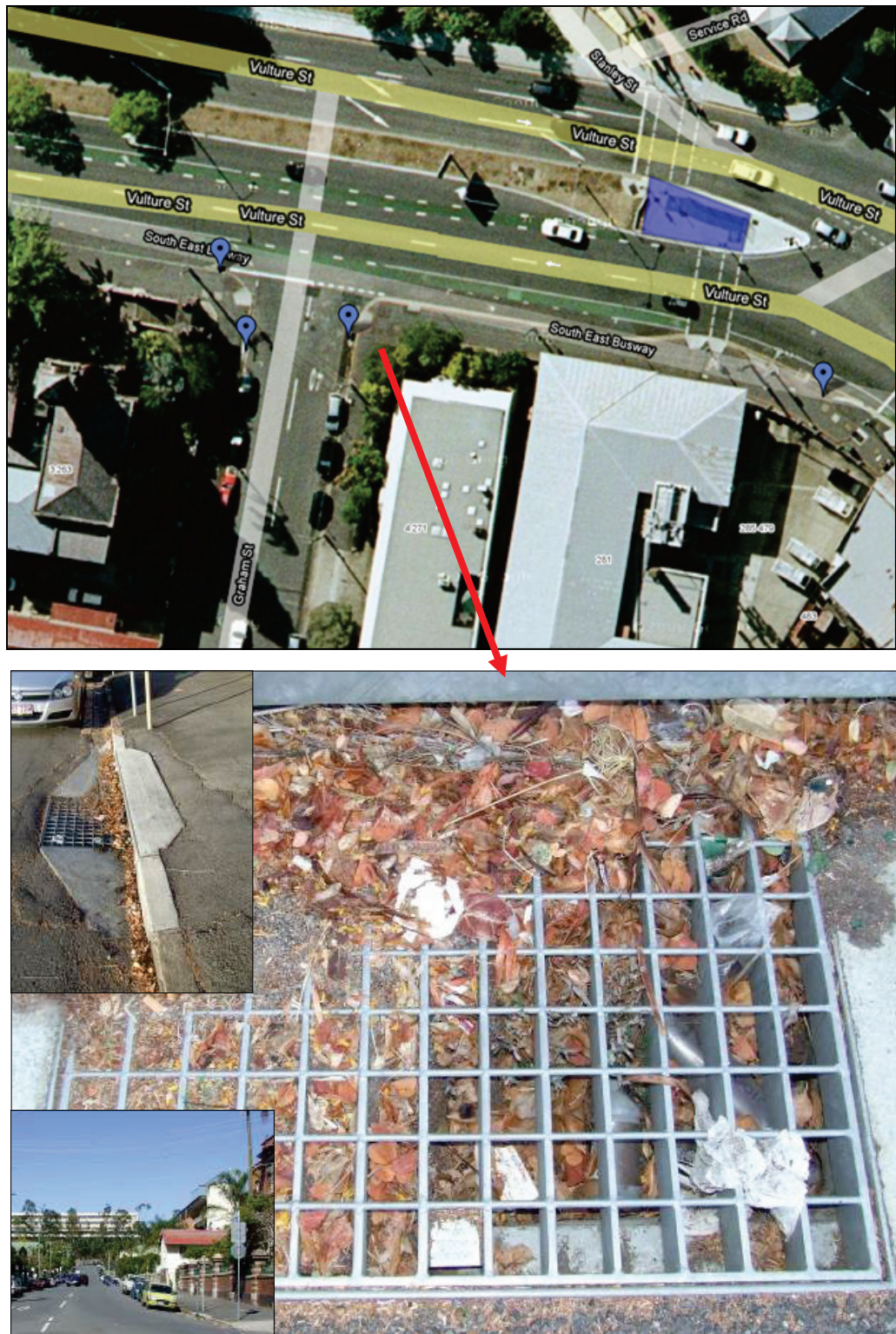


Figure 4.8 A fully blocked stormwater drain (SWD No. 22, See Tables 4.1 and 4.2), mainly with leaves and fine sediments (at T junction between Graham Street and Vulture Street, South Bank) located in partly residential and partly commercial area (South Bank) of Brisbane. The upper right shows a tree-lined street with the drain situated on the right, and lower left is the overall view of the drainage system. The stormwater drain on the opposite side of the road (not shown) was also blocked (June 2008).



Figure 4.9 A view of the stormwater inlet drain (SWD No. 74 (See Tables 4.1 and 4.2) at the corner of Laura Street and Prospect Terrace, Highgate Hill) blocked with organic matter in a residential suburb of Brisbane. Inside the drain is shown on upper left and upper right is the top view.

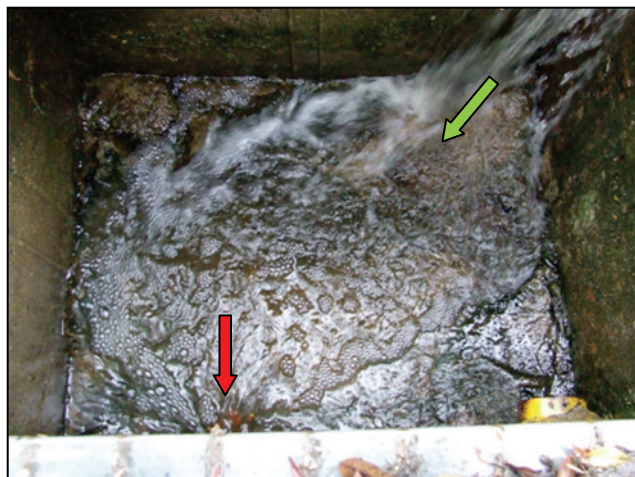


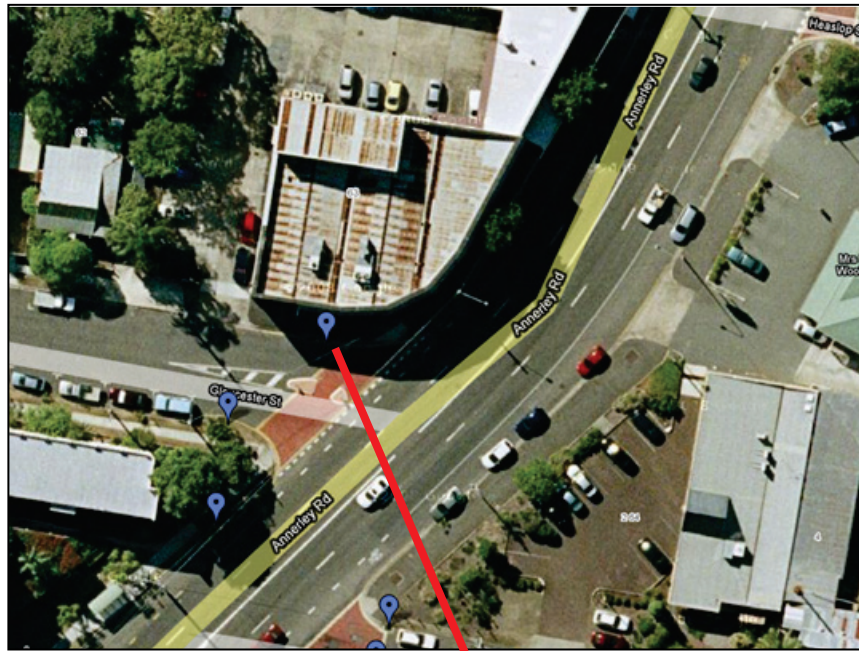
Figure 4.10 An unblocked stormwater drain during rainfall event. Water entering into the inlet (right) and existing (left) as shown by the arrows.



Figure 4.11 A storm water inlet drain (SWD No. 19, See Tables 4.1 and 4.2) on a busy route under a railway bridge is covered with organic waste (at the T junction between Park Road and Annerley Road, South Brisbane). Lower left is inside the drain which is blocked with stagnant water contaminated with traffic dust. The upper left is the front view of the drain located at the junction (May 2008).



Figure 4.12 In the vicinity of stormwater drain (Figure 4.11) in fine sediment residue is an accumulation of traffic dust and organic material after a wet weather period (T junction between Park Road and Annerley Road, South Brisbane). This creates hazardous conditions for cyclists (May 2008).



SWD 10



Figure 4.13 A collection of litter (plastic bottles, cigarette butts polystyrene and organic matter) in a stormwater drain (SWD No. 10, See Tables 4.1 and 4.2) during wet weather.



Figure 4.14 Inside the landscaped garden in front of the hotel Diana shopping complex (Annerley Road, South Brisbane). Patrons from a nearby public drinking house contribute to the discarded waste. Overall view of the front garden is shown on the upper right (October 2007).



Figure 4.15 Passive dumping (litter discarded at public seating places) of food/drink and cigarette butts at a bus stop in front of a sport shop on a busy road (June 2008).

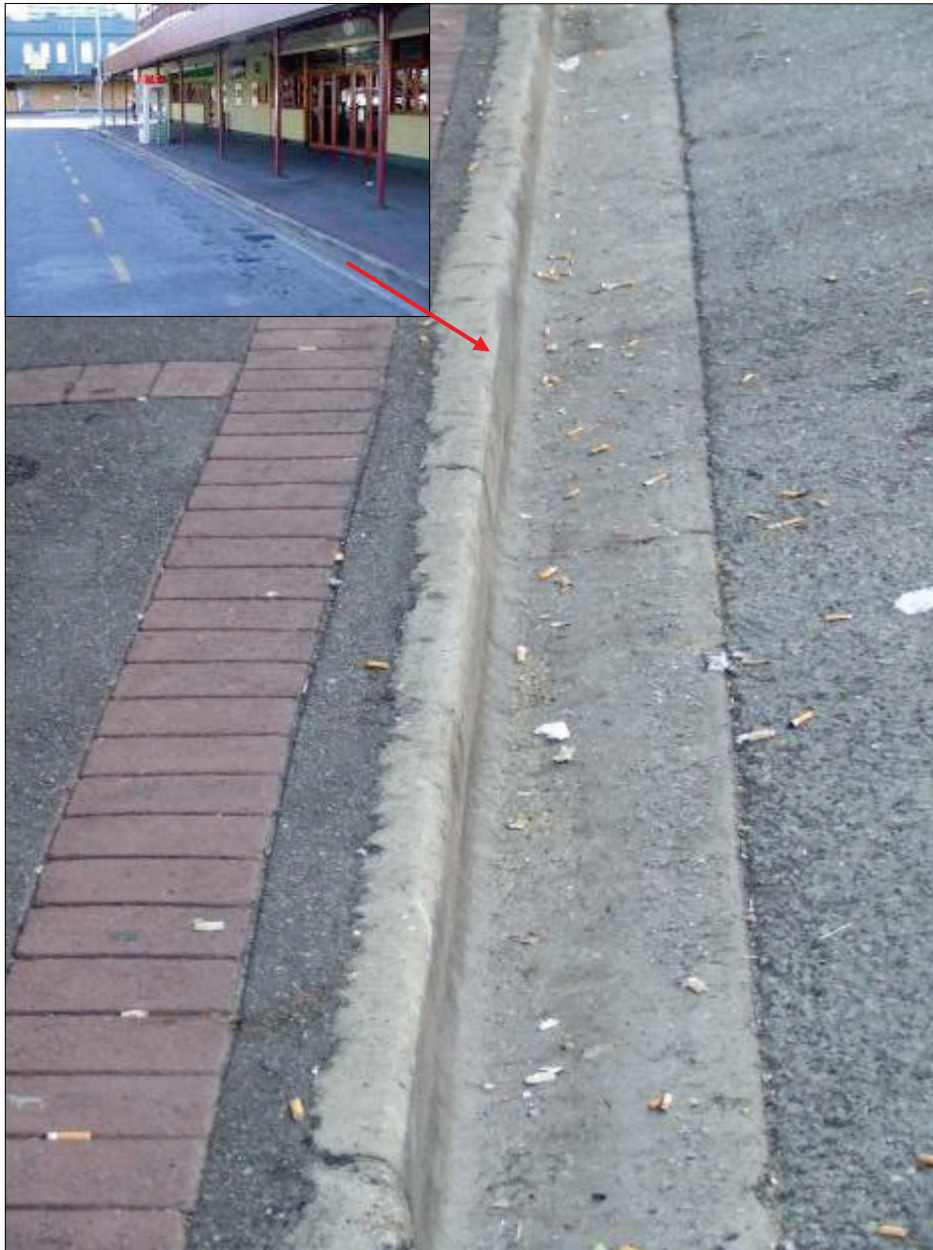


Figure 4.16 Cigarette butts litter the pavement and gutter next to a public drinking house - Clarence Hotel (situated on the corner of Stanley Street and Annerley Road, South Brisbane, June 2008).



Figure 4.17 The South Bank railway station in Brisbane has a no smoking policy ban on the platform and on trains. Hence, the approaching park area to the station is used as a dumping ground by smoking passengers prior to entering the platform. Upper right is a part view of the park area next to the station.



Figure 4.18 The no smoking policy at a local private hospital (Mater, South Brisbane) encourages smokers to use the area outside the buildings for disposing of their cigarette butts, for example, in the garden bed as shown. The garden bed (upper left) is situated next to the car park and busway which is opposite the entrance to the hospital (upper right).



Figure 4.19 This drain is located on a pedestrian crossing at a busy intersection along the Brisbane River. The roadside gutters at the pedestrian crossing are commonly used to dispose of cigarette butts. Lower right shows the drain at the road intersection (October 2007).



Figure 4.20 The traffic island (see map in Figure 4.19) which is on a popular pedestrian route from the Mater bus station to local universities, South Bank entertainment precinct and the city.



Figure 4.21 Broken beer bottles found on a busy pedestrian route (South Bank) next to a community centre and the railway station.

The Gross pollutant trap

The GPT under investigation was developed by C-M Concrete Pty. Ltd in 2004 and is based on the *LitterBank* design (See lower right in Figure 4.22). The *LitterBank* uses retaining screens to collect gross pollutants from incoming stormwater and currently there are over 20 *LitterBanks* operating at strategic stormwater locations throughout Queensland, Australia.

The densely populated outer suburbs of Brisbane (Marsden Park and Sinnamon Park) are two residential locations where the GPTs were monitored. Both these GPT sites were monitored in wet and dry conditions and, on these occasions, the following observations were made: the GPT retaining screens were blocked and tightly woven with grass clippings due to infrequent cleaning (Figure 4.22); a large amount of fine sediment in the trap was due to the fine screening effect of the grass clippings (Figure 4.23); a build-up of fine sediment was also observed along the full length of the inlet pipe due to low stormwater flow rates (Figure 4.24); a lower incidence of anthropogenic than organic litter; and the occurrence of downstream low and high tidal water depths.

The high percentages of sediment and low litter contents found in the GPTs at both residential sites, suggested that these devices were not ideally placed. It was noted that the surrounding areas of the inspected GPTs were overgrown with vegetation and used as a dumping ground by the local residents. These areas could be better utilised as fine sediment treatment zones and improve the aesthetic appearance of the surroundings.



Figure 4.22 Lower right is a gross pollutant trap for the nearby housing estate (Sinnamon Park an outer suburb of Brisbane) catchment. Gross pollutants captured mainly consist of organic matter such as leaves and grass clippings which clog the internal retaining screens.



Figure 4.23 Field monitoring of the *LitterBank* GPT at a residential catchment area in an outer suburb of Brisbane (Marsden Park). The surrounding area is similar to the view shown in map of Figure 4.22. The capture of mainly fine sediments was due to a nearby construction site of new houses.



Figure 4.24 The view of the pipe inlet attached to the GPT in Figure 4.23. Fine sediments deposited are a result of a low incoming stormwater flow rate.

4.6 MOBILISATION OF GROSS POLLUTANTS ON STREETS DURING WET WEATHER

There is little information on the mobilisation of gross pollutants in street stormwater gutters (Argue and Pezzaniti, 1996). However, the mobilisations of gross pollutant loads have been correlated with the depth of rainfall (Allison et al., 1998). This was achieved by monitoring a GPT at the outlet of a 50 hectare catchment of a Melbourne suburb. The minimum depth of rainfall in which gross pollutants were collected in this GPT was 3.7 mm. It was also found that the highest concentration of gross pollutants is generally mobilised either during the early stages of runoff or at peak discharges. Furthermore, the transportation rate of gross pollutants into the stormwater system is highly related to rainfall; that is, to the runoff rates and flow velocities (Australian runoff).

The velocity distributions of flush waves in street gutters have been investigated by Clark et al. (1981) as shown in Figures 4.25 and 4.26). Such flushes are related to shallow triangular channel flows and, in Figure 4.26, the measured and theoretical peak velocities are depicted under fully turbulent flow conditions. From the nomograph of flow in triangular channels (Clark et al., 1981), the extrapolated flow rate for the minimum rainfall depth of 3.7 mm [see D, Figure 4.25] is $Q = 0.0095 \text{ m}^3/\text{s}$. The nomograph was developed by the U. S. Bureau of Public Roads and the design charts are widely used to calculate triangular and gutter/channel flows along urban roads and highways (Clarke et al., 1981). The hydraulic behaviour of curb-opening inlets has also been investigated by Uyumaz (2002). Good correlation between experimental and theoretical data was achieved and an in-depth investigation was made with the associated flow and curb inlet variables. Further work is required to investigate the application of these variables with the current gutter/channel flow dataset from this field study.

The mechanism of gross solid movement in small and large channel sewers under various hydraulic flow regimes has also been investigated (Butler and Davies, 2004; Littlewood and Butler, 2003). It was generally observed that gross solids do not move continuously, but hop down the channel when flow and depth reaches critical values. Under low hydraulic conditions, the retarding motions of larger solids are caused by their contact with the inner channel walls. When the size of solids are large compared with the flush wave, the accumulation of water behind drives the

solids with a sliding dam mechanism. A combination of hops and sliding dam motions occurs if the flush wave is intermittent. Lastly, solids float when their sizes are small compared with the diameter of the channel and the flush wave. The governing factors of the gross solid movement and its mechanism are the flush volume, its density and its dimensions. In the sliding dam mechanism the dimensions of the solids are more important than its density, and vice versa in the case of floating.

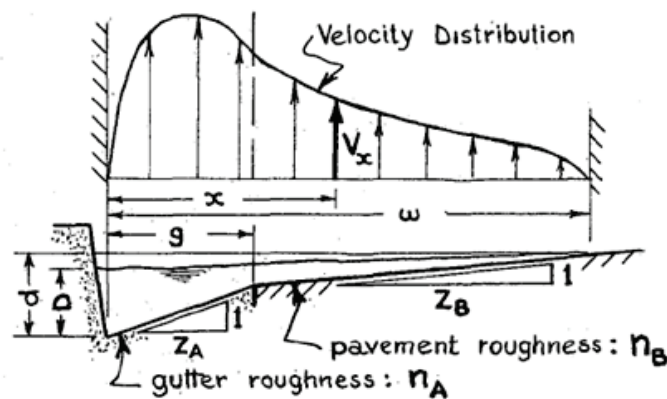


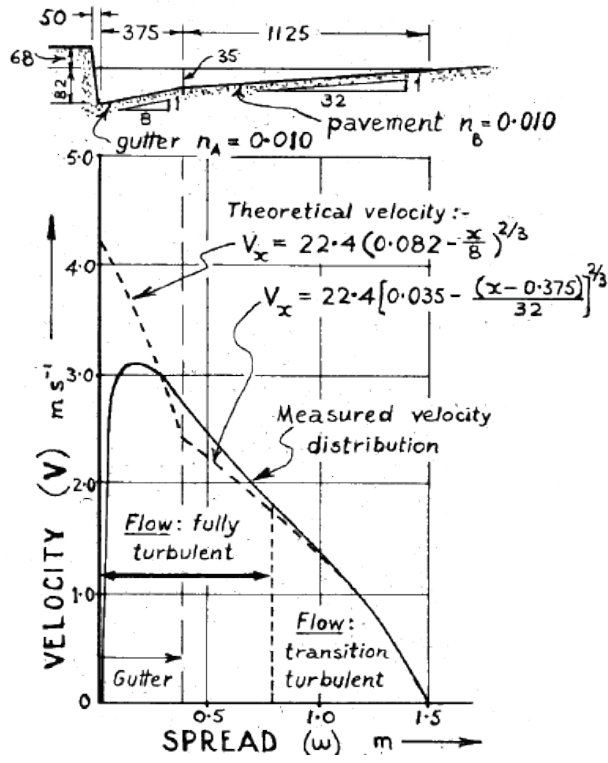
Figure 4.25 Definition of variables for the gutter/pavement flow relationship of roadway channels. See Figure 2.26 (Clarke et al., 1981).

The current research qualitatively investigated the mobilisation characteristics of gross pollutants in stormwater gutters during wet weather. Figure 4.4 is an example of gross pollutants mobilised during the first 20 minutes of heavy rainfall, where the greatest depth of flow in the gutter was approximately 15 – 20 mm [See the depth of Kerb D, on the left in Figure 4.26 (a)]. In low intensity, high frequency wet weather patterns, the mobilisation of such pollutants into the stormwater systems from streets was less effective. For example, during low flow rates the motion characteristics of gross pollutants in the gutters and on roads were similar to the floating and sliding mechanisms in combination with hops (Figures 4.26 and 4.28). These figures show a wide variety of solids and the physical conditions which influence their mechanisms of transportation. Due to their ability to deform, their physical degradation and contact with other matters, some solids in organic matter

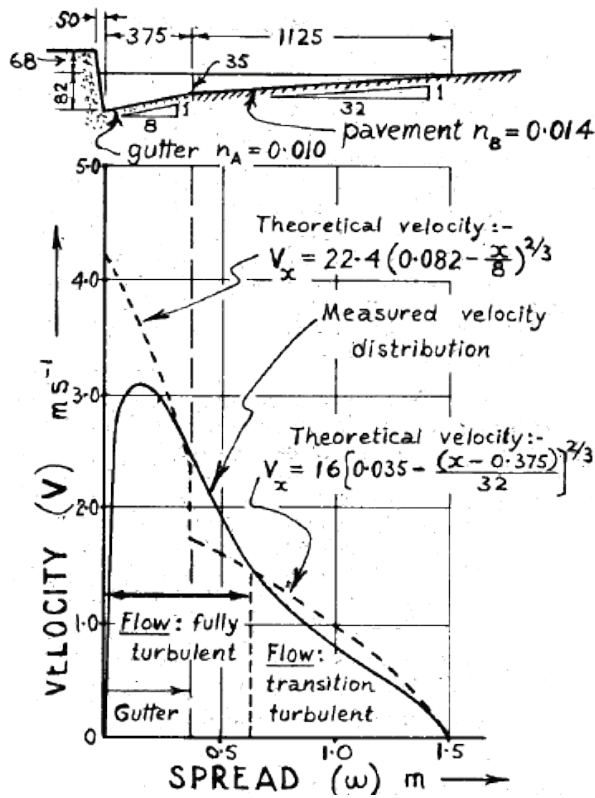
change their condition as they move along the gutters. Figure 4.27 shows such behaviour with grass clippings which accumulate on rough surfaces thus obstructing the discharging water course. In another example, fallen leaves and flowers from Jacaranda trees with overhanging branches decompose more quickly due to their small size and form clusters of mulch on streets and roads.

These islands (clusters) become an obstruction to the stormwater flow path [Figure 4.28 (a)]. Weak shearing and cohesive stresses in solid mass can precipitate into sludge, silt and sediments. The sliding and hop mechanism of litter and the heavier and larger organics [as shown in Figures 4.28 (b) and (c)] gradually form larger masses with the slower moving solids. When the stormwater flush volume in the gutter has reached critical values, the peak velocities the solids move forward. At lower velocities the solids are left standing as depicted in Figure 4.28 (d). Consequently, in some hydraulic conditions solids are carried with the flow and at lower velocities they may be deposited.

Overall, the mobilisation process of gross pollutants under low flow conditions can be extremely complex particularly due to their cohesive nature when interacting with other particles to form larger masses.



(a)



(b)

Figure 4.26 Theoretical gutter/pavement flow relationship for roadway channels (Clarke et al., 1981) with (a) smooth gutter and smooth pavement and (b) smooth gutter and moderately rough pavement. For definition of variable see Figure 2.25.



Figure 4.27 An accumulation of organic matter (mainly grass clippings) obstructing the water flow course at the stormwater drain.



Figure 4.28 Flow characteristics of various organics during light rainfall: (a) accumulation of smaller matter into a mulch formation; (b) mainly litter with some organics; (c) twigs and small litter items and (d) leaves and twigs.

4.7 CONCLUSION

Field surveys have been conducted in Brisbane and neighbouring catchment areas to collect and analyse gross pollutants from GPTs, stormwater drains and streets. Such data is important in the design, testing and placement of GPTs in urban environments.

The outcome of this chapter shows that a high percentage of organic matter was generally found in streets and stormwater systems of mixed urban activity areas. This matter can block or clog retaining screens of strategically placed GPTs. In commercial/business areas, larger amounts of anthropogenic litter were found. Generally, gross pollutants were observed to be carriers for sediment and the finer more harmful stormwater pollutants.

Also, low flow rates (because of intermittent rainfall) are common in GPTs and gross pollutants were found to have both varying characteristics of buoyancy and complex motions. For example, organic solids can deform and change their conditions as they move through the street gutters. In some hydraulic conditions, gross pollutants are carried with the flow and deposited at lower stormwater flow rates. The highest gross pollutant load occurs mostly at peak hydraulic discharge. Consequently, the GPT should be tested under these conditions to determine maximum gross pollutant capture.

Based on the results of the field survey, typically observed hydraulic flow conditions of a GPT with blocked screens, downstream high and low tidal waters, and artificial custom modified pollutants with varying densities were used as modelling parameters for experiments in the laboratory. These experiments are described in Chapters 8.

The application programming interface (API) web based program Google Maps was used as the database for identifying the field survey locations.

This work has the further potential for monitoring gross pollutants on a long term basis. Results of this monitoring could be made publicly available.

[This page is left blank intentionally]

Table 4.1 Gross pollutants in stormwater drains in South Brisbane (monitored from 2006 to 2008)

SWD No.	SWD type	Street Name	Activity	Location	Percentage of gross pollutant (%)			Total (%)	Full (%)	Comments	
					Organic	Sediments					Litter
						Coarse	Fine				
1	new	Annerley Rd	business	Clarence Corner Hotel	5	-	30	65	100	10	cigarettes butts, organic, packaging, plastic bottles, fine sediments, metal can, paper
2	old	Annerley Rd	main road	next to Mater hospital	15	-	15	70	100	20	paper, packaging, plastic bags, organic matter, cigarette butts
3	new	Annerley Rd	main road	next to shops/business	20	-	15	65	100	20	mainly paper, leaves, fine & coarse sediments
4	old	Catherine St	side street	next to pharmacy	50	5	5	40	100	5	leaves, coarse and fine sediments
5	new	Catherine St	side street	next to bus stop	90	5	5	90	100	1	cigarette butts, paper, packaging, fine sediments, polythene bag
6	new	Clarence St	side street	next to Mater hospital	45	-	5	50	100	2	organic matter
7	new	Clarence St	side street	next to medical centre	45	-	20	35	100	3	organic matter, paper, metal cans, cigarette butts
8	new	Crown St	side street	next to parade of shops	30	-	10	60	100	2	organic matter, plastic bag, paper, plastic bottles
9	old	Crown St	side street	next to business	55	-	10	35	100	10	blocked, plastic bottles, paper, stagnant water, organic
10	v. old	Gloucester St	side street	next to business	40	-	0	60	100	20	organic matter, paper, cigarette butts
11	v. old	Gloucester St	side street	next to business	80	-	0	20	100	10	organic matter, paper, cigarette butts
12	old	Annerley Rd	main road	next to business	40	-	5	55	100	10	organic matter, paper, cigarette butts, weeds
12A (74)	new	Annerley Rd	main road	81 Annerley Rd, next to apartments/ bus stop	50	-	10	40	100	10	organic matter, paper, cigarette butts
13	new	Annerley Rd	main road	next to business/bus stop opp. 81 Annerley Rd	40	-	20	40	100	8	leaves, paper, fine sediments, cigarette butts
14	new	Heaslop St (left)	side street	next to business	75	-	5	20	100	30	leaves, paper, fine sediments,
15	new	Heaslop St (right)	side street	next to business	95	-	4	1	100	30	organic matter, paper
16	new	Lockhart St (left)	side street	next to business	40	-	5	55	100	16	organic matter, paper, cigarette butts
17	new	Lockhart St (right)	side street	next to business	50	-	5	45	100	5	organic matter, polystyrene, stagnant water, packaging, fine sediments
18	new	Annerley Rd (by Park Rd)	main road	next to railway bridge	80	-	0	20	100	30	blocked, organic matter, polystyrene, stagnant water, packaging, fine sediments, cigarettes butts

Table 4.1(cont.) Gross pollutants in stormwater drains in inner southern Brisbane suburbs (monitored from 2006 to 2008)

SWD No.	SWD type	Street Name	Activity	Location	Percentage of gross pollutant (%)			Total (%)	Full (%)	Comments	
					Organic	Sediments					Litter
						Coarse	Fine				
19	new	Annerley Rd	main road	next to railway bridge	65	-	30	5	100	30	blocked, organic matter (leaves), fine sediments, plastic bottle, paper
20	new	Park Rd	main road	next to railway bridge	20	-	80	-	100	5	90% consists of organic matter, fine and coarse sediments
21	new	Graham St	side street	(next to church)	90	-	90	10	100	85	98% consists of organic matter, fine and coarse sediments
22	new	Graham St	side street	opp. the church	98	-	98	2	100	100	cigarettes butts, organic, packaging, plastic bottles, fine sediments, metal can, paper
23	new	by Goodwill Bridge	walkway	by pub & gardens	95	-	-	5	100	10	organic matter, paper
24	old	Stanley St	main road	by pedestrian crossing by Goodwill Bridge	20	-	-	80	100	40	plastic bottles, cigarettes, paper, packaging
25	new	Stanley St	main road	next to the street cafes, opp. Mater Hospital	45	-	-	55	100	< 1	cigarette butts the highest litter in count, also paper, packaging
26	new	Stanley St	main road	next to Mater Hospital	30	-	-	70	100	5	cigarette butts, paper and few leaves
27	new	Stanley St	main road	at entrance to Mater Hospital next to the smoking area	80	-	-	20	100	<1	almost empty, few leaves and paper
28	new	Stanley St	main road	at entrance to Mater Hospital next to outgoing traffic lights	1	-	-	99	100	2	polystyrene cup, plastic packaging, paper, cigarettes butts, few leaves
29	old	Stanley St	main road	at entrance to Mater Hospital by outgoing traffic lights	5	-	20	75	100	2	plastic bottle, polystyrene cup, fine sediments
30	new	Stanley St	main road	1st drain opp. shops at Mater Hospital	15	-	15	85	100	20	blocked, plastic bottles, plastic cups, plastic bags, paper, objects, metal cans, wood, cigarette butts, packaging

Table 4.1 (cont.) Gross pollutants in stormwater drains in inner southern Brisbane suburbs (monitored from 2006 to 2008)

SWD No.	SWD type	Street Name	Activity	Location	Percentage of gross pollutant (%)			Total (%)	Full (%)	Comments	
					Organic	Sediments					Litter
						Coarse	Fine				
31	new	Stanley St	main road	2nd drain opp. shops at Mater Hospital	45	-	-	55	100	1	blocked, leaves, rubber, paper, cigarette butts
32	new	Stanley St	main road	3rd drain opp. shops at Mater Hospital	60	-	-	40	100	5	organic matter, plastic, paper, cigarettes butts, packaging
33	new	Stanley St	main road	4th drain opp. shops at Mater Hospital	60	-	-	40	100	20	blocked, organic matter, polythene, paper, cigarettes butts, packaging
34	new	Stanley St	main road	5th drain opp. shops at Mater Hospital	45	-	-	55	100	<1	blocked, organic matter, paper, cigarettes butts, packaging, plastic cup
35	new	Stanley St	main road	6th drain opp. shops at Mater Hospital	15	-	50	35	100	5	organic matter, paper, cigarettes butts, packaging, plastic cup
36	new	Stanley St	main road	7th drain opp. shops at Mater Hospital	20	-	20	60	100	2	organic matter, paper, cigarettes butts, packaging, straw
37	new	Stanley St	main road	8th drain opp. shops at Mater Hospital	30			70	100	5	mainly plastic sheeting, plastic bottles, cigarette butts, paper
38	new	Stanley St	main road	9th drain opp. Mater Hospital	25		35	40	100	<0.5	mainly cigarette butts, paper, packaging, few leaves
39	new	Stanley St	main road	10th drain opp. Mater Hospital	80 *		*	20	100	?	cigarette butts on the entrance, deep cannot see the bottom
40	new	Stanley St	main road	11th drain opp. Mater Hospital	65*		*	35	100	20	cigarette butts, polythene bags, paper
41	new	Stanley St	main road	12th drain opp. Mater Hospital	20*		*	80	100	5	bottles, plastic, packaging, plastic bottles
42	new	Gloucester St	main road	near West St	100	0	0	0	100	<1	organic matter, plastic bottles, metal cans, paper, foil tray
43	new	Gloucester St	main road	near Laura St	98	0	0	2	100	10	leaves, twigs, etc
44	new	Gloucester St	main road	near Firth St	100	0	-		100	30	mainly organic matter
45	new	Gloucester St	main road	Junction of Stephens Rd	75	0	0	25	100	10	mainly organic matter

Table 4.1 (cont.) Gross pollutants in stormwater drains in inner southern Brisbane suburbs (monitored from 2006 to 2008)

SWD No.	SWD type	Street Name	Activity	Location	Percentage of gross pollutant (%)			Total (%)	Full (%)	Comments	
					Organic	Sediments					Litter
						Coarse	Fine				
46	old	Gloucester St	main road	near Ruth St	98	0	-	2	100	<1	organic matter, paper
47	new	Stephens Rd	main road	Dorchester St (right)	100		50	0	100	2	organic matter, fine sediments (visual) 50%
48	new	Stephens Rd	main road	Dorchester St (left)	0	70*	70*	30	100	2	coarse and fine sediments, packaging, plastic cup lid
66	old	Stephens Rd	main road	corner of Gloucester St						95	mainly organic matter, plastic bottle, drink carton, straws
67	old	Stephens Rd	main road	Somerville St	2	0	0	98	100	40	blocked, plastic bottles (8), paper, tennis ball, polystyrene, marker, plastic, packaging, stagnant water
68	new	Stephens Rd	main road	Somerville St	35	0	15	50	100	20	wood, packaging, plastic bottles, organic matter & fine sediments
70	new	Ruth St	side street	corner of Audenshaw St	99	0	-	1	100	30	organic matter, fine sediments, a plastic top
71	new	Ruth St	side street	corner of Audenshaw St	80	0	-	20	100	30	organic matter, fine sediments, a rubber sole
72	old	Ruth St	side street	corner of Gloucester St	100	0	-	0	100		organic matter, fine sediments, paper
73	new	Ruth St	side street	corner of Gloucester St	100	0	-	0	100		organic matter
74	new	Laura St	side street	bottom of Laura St	98	0	-	2	100		organic matter, fine sediments rubber sole, twigs, leaves
75	new	West St	side street	Drain next 7 West St	0	0	0	0	0		
				Average	55.4	1.4	7.4	35.8	100		

Table 4.1 (cont.) Gross pollutants in stormwater drains in Brisbane CBD (monitored from 2006 to 2008)

SW D No.	SWD type	Street Name	Activity	Location	Percentage of gross pollutant (%)			Total (%)	Full (%)	Comments
					Organic	Sediments Coarse	Fi ne			
49	new	Albert St	CBD	corner of Mary St/Albert St	25	-	-	75	15	organic matter (including fine sediments), cigarette butts, paper, packaging, polythene bags
50	new	Albert St	CBD	corner of Mary St/Albert St	40	-	-	60	20	metal can, leaves, cigarette butts, paper
51	new	Albert St	CBD		40	-	-	60	15	metal can, leaves, cigarette butts, paper
52	new	Albert St	CBD		60	-	-	40	20	organic matter mainly leaves (including fine sediments), cigarette butts, paper (dockets)
53	old	Albert St	CBD		15	-	-	85	20	stagnant water, plastic bottles, paper, cigarette butts, polystyrene, stick
54	old	Albert St	CBD		20			80	30	blocked, cigarette butts, paper, packaging, cigarette packets
55	new	Albert St	CBD		5	-	5	95	5	cigarette butts, paper, packaging, cigarette packets
56	new	Albert St	CBD		5	-	5	95	5	cigarette butts, paper, packaging, metal cans, stick, leaves
57	new	Albert St	CBD		5	-	5	95	5	cigarette butts, paper, packaging
				Average	24	-	-	76		

Table 4.1 (cont.) Gross pollutants in stormwater drains at Burleigh Heads (monitored from 2006 to 2008)

SWD No.	SWD type	Street Name	Activity	Location	Percentage of gross pollutant (%)			Total (%)	Full (%)	Comments	
					Organic	Sediments					Litter
						Coarse	Fine				
58		Gold Coast Hwy	main road	Burleigh Heads	50	-	-	50	100	10	trap has a bag attached to the drain
59		Gold Coast Hwy	main road	Burleigh Heads	50	-	-	50	100	30	plastic bottle, organic matter, paper, packaging, cigarette butts, plastic bucket
60		Goodwin Terrace	by beach	Burleigh Heads	30	-	69	1	100	30	mainly sand, organic matter, cigarette butts
61		Goodwin Terrace	by beach	Burleigh Heads	80	-	-	20	100	30	organic matter, cigarette butts, plastic cup, metal can
62		Gold Coast Hwy		Burleigh Heads	20	-	-	80	100	35	leaves, beer packaging, plastic and paper bags
63		James St	shops	Burleigh Heads	90	-	-	10	100	20	leaves, metal can, dockets, plastic bag
64		Gold Coast Hwy		Burleigh Heads	90	-	-	10	100	1	organic matter, cigarette butts
65		Gold Coast Hwy		Burleigh Heads	75	-	-	25	100	2	organic matter, cigarette butts, plastic, paper
				Average	61	-	9	31	100		

Table 4.2 Gross pollutants on stormwater drains in inner southern Brisbane suburbs (monitored from 2006 to 2008)

SWD No.	SWD type	Street Name	Activity	Location	Percentage of gross pollutant (%)				Total (%)	Full (%)	Comments
					Organic	Sediments		Litter			
						Coarse	Fine				
5	old	Catherine St	side street	next to bus stop	60	0	15	25	100	100	organic matter, packaging, cigarette butts, plastic, paper fine sediments
6	new	Clarence St	side street	next to Mater Hospital	90	0	10	0	100	5	organic matter, fine sediments
7	new	Clarence St	side street	next to medical centre	90	0	10	0	100	5	organic matter, fine sediments
8	new	Crown St	side street	next to building site	60	0	0	40	100	30	organic matter, plastic bag, paper
9	v. old	Crown St	side street	next to shops	97	0	0	3	100	1	organic matter
10	v. old	Gloucester St	side street	next to business	85	0	10	5	5	10	organic matter, paper, cigarette butts
11	v. old	Gloucester St	side street	next to business	80	0	0	20	20	10	organic matter, paper, cigarette butts
12	new	81 Annerley Rd	main road	next to units & bus stop	40	0	5	55	55	10	organic matter, paper, cigarette butts
12	new	81 Annerley Rd	main road	next to units & bus stop	95	0	5	0	0	2	organic matter, paper, cigarette butts
14	new	Heaslop St (left)	side street	next to business	90	0	5	5	5	25	leaves, paper, fine sediments, cigarette butts
15	new	Heaslop St (right)	side street	next to business	5	0	0	95	95	5	plastic bottles, organic matter
18	new	Annerley Rd (next to Park Rd)	main road	next to railway bridge	90	0	10	0	0	100	organic matter, fine sediments
19	new	Annerley Rd	main road	next to railway bridge	70	0	30	0	0	100	organic matter, fine sediments
20	new	Park Rd	main road	next to railway bridge	70	0	25	5	5	50	mainly fine sediments, organic matter (leaves)
21	new	Graham St	side street	next to church	95	0	0	5	5	35	
24	old	Stanley St	main road	next to pedestrian crossing by Goodwill Bridge	2	0	0	98	98	5	cigarettes butt, plastic bottle
42	new	Gloucester St	side street	near West Street	90	0	0	10	10	50	organic matter, packaging, plastic bottle, paper
46	old	Gloucester St	side street	near Ruth Street	85	0	0	15	15	100	leaves, twigs, plastic bottle
47		Stephens Rd	main road	Doncaster Street (right)	60	0	0	40	40	45	mainly organic matter, foil bag, paper
48		Stephens Rd	main road	Doncaster Street (left)	50	0	0	50	50	10	organic matter and piece of wood
74		Laura St	side street		100	0	0	0	0	0	
75	new	West St	side street	Drain next 7 West St	94	0	0	6	0	100	see Figure 4.5
				Average	72		6	22	0		
58		Gold Coast Hwy	by McDonalds		92	0	5	3	100	30	

Table 4.3 Gross pollutants on streets in inner southern Brisbane suburbs (monitored from 2006 to 2008)

No.	Street Name	Activity	Location	Percentage of gross pollutant (%)				Total	Comments
				Organic	Sediments		Litter		
					Coarse	Fine			
1	Annerley Road	business	Diana Hotel shopping precinct (in bushes and greenery space)	0	0	0	100	100	plastic bottles, glass bottles, paper, wire, fabric and organic matter, beer crate
2	Annerley Rd	main road	next to Mater Hospital, trees alongside the gutter	50	0	25	25	100	street litter (organic, cigarette butts, paper, packaging, plastic bottle, rubber, dead animal)
3	Annerley Rd	main road	next to Mater Hospital	60	0	5	35	100	organic matter, paper
4	Annerley Rd	main road	next to Mater Hospital	35	0	5	60	100	organic matter, paper
5	Annerley Rd	main road	next to Mater Hospital	50	0	5	45	100	organic matter, metal cans, paper, packaging
6	Annerley Rd	main road	Clarence Corner Hotel	0	0	30	70	100	cigarette butts, packaging, paper, traffic dust, fine sediments
7	Cnr. of Annerley Rd/ Stanley St	main road	next to Mater Hospital	30	0	10	60		cigarette butts, traffic dust, fine sediments
8	Annerley Rd	main road	next to bus stop & pharmacy shop	10	0	0	90	100	cigarettes butts, packaging, fine sediments, paper, plastic bottles, paper cups
9	Annerley Rd	main road	next to bus stop & sport shop	5	0	0	95	100	mainly cigarettes butts, packaging, fine sediments, paper, plastic
10	Annerley Rd	main road	next to businesses	30	0	40	30	100	mainly organic matter, paper, cigarette butts, packaging, metal can, fine sediments
11	Gloucester St	side street	next to drain	80	0	5	15	100	organic matter, paper, cigarette butts
12	Heaslop St	side street	next to business	95	0	0	5	100	leaves, paper, fine sediments, cigarette butts
13	Stanley St	main road	next to the street cafes, opp. Mater Hospital	45	0	0	55	100	cigarette butts the highest litter in count, also paper, packaging
14	Stanley St	main road	next to Mater Hospital	0	0	20	80	100	mainly cigarettes
15	Stanley St		business next to main road	85	0	0	15	100	Organic matter, plastic bottles, metal cans, paper, foil tray
16	Gloucester St	main road	residential/business next to main road	85	0	0	15	100	grass clippings, cigarette butts, paper
17	Gloucester St	main road	residential/business next to main road	95	0	0	5	100	mainly leaves
18	Ruth St	side Street	residential/business next to main road	80	0	0	20	100	grass clippings, paper, packaging (cigarette packet)

Table 4.3 (cont.) Gross pollutants on streets in inner southern Brisbane suburbs (monitored from 2006 to 2008)

No.	Street Name	Activity	Location	Percentage of gross pollutant (%)				Total	Comments
				Organic	Sediments		Litter		
					Coarse	Fine			
19	Stephens Rd	side street	top Clarence Street	80	0	0	20	100	plastic bottles, paper
20	Stephens Rd	main road	outside school/ sports centre	85	0	0	15	100	organic matter, paper cups, plastic, cigarette butts
21	Stephens Rd	main road	corner of Vulture St	85	0	0	15	100	organic matter, paper, cigarette butts, cigarette packet, straw
22	Stephens Rd	main road	next to St. Lawrence School & bus stop	90	0	0	10	100	Organic Matter, packaging, plastic bottles, paper
23	Stephens Rd	main road	junction of Vulture St	80	0	0	20	100	organic matter, cigarette butts, paper, packaging
24	Vulture St	main road	by the community centre	75	0	0	25	100	organic matter, cigarette butts, cigarette packet and paper
25	Vulture St	main road	at the community centre	30	0	0	70	100	organic matter, packaging, paper, metal cans, drink cartons, paper cups, cigarette butts
26	Vulture St	main road	at the community centre	20	0	0	80	100	organic matter, packaging, paper, metal cans, drink cartons, paper cups, cigarette butts
			Total	55.2	0	5.8	39	100	
27	Vulture St		South Bank train station				100		paper, cigarette butts.

[This page is left blank intentionally]

Reference

- Allison, R. A., Walker, T. A., Chiew, F. H. S., O' Neill, I. C. and Mc Mahon, T. A. (1998). *From roads to rivers: gross pollutant removal from urban waterways*. Clayton, Victoria: CRC for Catchment Hydrology. Retrieved 14 January 2010, from <http://www.catchment.crc.org.au/pdfs/technical199806pt1.pdf>
<http://www.catchment.crc.org.au/pdfs/technical199806pt2.pdf>
<http://www.catchment.crc.org.au/pdfs/technical199806pt3.pdf>
<http://www.catchment.crc.org.au/pdfs/technical199806pt4.pdf>
- Allison, R. A., Walter, K. A., Marx, D., Lippner, G. and Churchwell, R. (2000). A method for monitoring and analyzing litter in freeway runoff as part of the caltrans litter management pilot study. In Rollin H. Hotchkiss and Michael Glade (Eds.), *Building Partnerships: Proceedings of Joint Conference on Water Resource Engineering and Water Resources Planning and Management 2000* (pp. 81-91). Minneapolis, Minnesota, USA: American Society of Civil Engineers (ASCE).
- Butler, D. and Davies, J., W. (2004). *Urban drainage*. London: Spon Press.
- Clarke, W. P., Strods, P. J. and Argue, J. R. (1981). Gutter/pavement flow relationships for roadway channels of moderate or steep grade: Preprints of Papers NCP No. 81/07. *National Local Government Engineering Conference* (pp. 130-137). Adelaide, South Australia: Institution of Engineers, Australia.
- Lippner, G., Churchwell, R., Allison, R., Moeller, G. and Johnston, J. (2000). A Scientific Approach to Evaluating Stormwater Best Management Practices for Litter. *California Water Environment Association (CWEA), 72nd Annual Conference* Sacramento, California. Retrieved 14 Januray 2010, from <http://www.owp.csus.edu/research/papers/papers/PP014.pdf>
- Littlewood, K. and Butler, D. (2003). Movement mechanisms of gross solids in intermittent flow. *Water Science And Technology: A Journal Of The International Association On Water Pollution Research*, 47(4), 45.

- Quasebarth, T., Schroeder, D., Chappell, R., Churchwell, R. and Lippner, G. (2001). An investigation of factors influencing solids transport and deposition into highway drain inlets. *Bridging the Gap: Meeting the World's Water and Environmental Resources Challenges: Proceedings of World Water and Environmental Resources Congress 2001* (pp. 184-194). Orlando, Florida, USA: American Society of Civil Engineers (ASCE).
- Sim, R. L. and Webster, J. L. (1992). Performance of Trash Rack on Cup and Saucer Creek Stormwater Channel. . *International Symposium on Urban Stormwater Management Preprints of Papers NCP No. 95/03* (pp. 143-145). Sydney, NSW, Australia: Institution of Engineers, Australia.
- Uyumaz, A. (2002). Urban Drainage with Curb-Opening Inlets. *Global Solutions for Urban Drainage: Proceedings of 9th International Conference on Urban Drainage (9ICUD)* (pp. 299-299). Portland, Oregon, USA: American Society of Civil Engineers (ASCE).

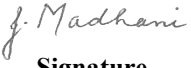
Chapter 5: A scalar concentration (Komori) probe for measuring fluctuating dye concentration in water

Jehangir T. Madhani and Richard J. Brown

School of Engineering Systems
Queensland University of Technology


Publication: WSEAS Transactions on Fluid Mechanics, 3(3), 224-233.

This chapter is an exact copy of the above journal paper.

Contributor	Statement of contribution
Jehangir T. Madhani	<p>Candidate</p> <p>Preparation/design of experiments, conducted experiments and data analysis, troubleshooting data acquisition signals with inherent noise and electrical drifts, compilation of signal processing programs, wrote the manuscript and acted as a corresponding author.</p>
 Signature	
8/6/2010 Date	
Richard J. Brown	<p>Principal Supervisor</p> <p>Conceptualisation of insitu frequency response measurements, aided in the experimental design, assisted with the manuscript.</p>

Principal Supervisor Confirmation

I have sighted email or other correspondence from all Co-authors confirming their certifying authorship.

A/Professor Richard Brown		8/6/2010
Name	Signature	Date

ABSTRACT

The scalar (dye) concentration probe of Komori has been used at QUT to measure the mixing and dispersion of pollutants in rivers from outboard motors and in a gross pollutant trap (GPT). Although usages have been documented in literature, little is known of the Komori (dye) probe's frequency response characteristics and the quality of data sampled. In this work, the frequency response characteristic of the Komori probe is determined by injecting methylene blue dye over a range of water flow velocities. Despite some noise and drift, the data collected from the probe is useful because of its high frequency response in comparison to regular commercial concentration probes. The rise and fall times are reported and the theoretical response time is also determined. It is found that the frequency response is a strong function of flow velocity and a maximum of 100 Hz is noted under typical operating conditions. Comparison between rise and fall data show that the rise time is generally shorter than half the fall time.

Keywords: Concentration probe, dye measurement, frequency response, Komori probe, tracer, rise time and fall time

5.1 INTRODUCTION

Tracer experiments are useful to study the flow characteristics in fluid systems. Examples of such systems are chemical reactors, processing equipment, stormwater quality improvement devices (ponds, wetlands, pollutant traps), biological systems, porous aquifers, groundwater flow, separators, mixing and dispersion of pollutants in open waters.

Tracer experiments are performed by injecting a tracer into the incoming fluid, and to continuously (as function of time) monitor the tracer concentrations at the system outlet. The time series data can then be used to measure the residence time distribution (RTD) and the average time it takes the fluid to pass through the system boundaries (Levenspiel, 1999). Also from the data, the average stream velocity can be estimated (Waldon, 2004). The RTD is a useful tool to analyse the flow and mixing process in a system. This information can then be used to develop and validate analytical or empirical models (Levenspiel, 1999).

A review of recent tracer methods is given (Ptak et al., 2004). Although the paper is intended for applications in unconsolidated porous media, it does provide useful experimental background information. Tracer experiments carried out in wastewater treatment plants are studied (Hart, 1994; Hart and Hom, 1996). A list of tracers used for laboratory and field experiments and implications of their usage are also given (Hart and Hom, 1996; Ptak et al., 2004). Common tracers are salts, fluorescent dyes and fluoride. For RTD studies of wastewater treatment plants (Hart, 1994) and ponds, wetlands and detention tanks (Adamsson and Bergdahl, 2006; Lin et al., 2003), the usage of fluorescent dye (rhodamine WT) with portable field analysers (a flow through fluorometer by Turner Designs) have been reported. The same tracer was used to measure the mixing transport coefficients in natural channels (Boxall and Guymer, 2003). Salt based tracers such as lithium chloride have been deployed to measure the RTD of a model hydrodynamic vortex separator (Alkhaddar et al., 2001). In the hydraulic testing of a wetland, bromide was given preference to rhodamine WT (Martinez and Wise, 2003). In both cases, the fluid samples had to be collected, stored (also termed grab sampling) and analysed. Lithium chloride was analysed with an absorption spectrophotometer and ion chromatography was used to detect bromide concentrations. In rapid changing flow conditions or where high frequency sampling is required, the grab sampling technique is not suitable. Tracer

tests carried out in water distribution networks with other salt based tracers such as sodium chloride, calcium chloride and fluoride are reported (Boccelli et al., 2004; Panguluri et al., 2005). In this case, the tracer concentrations were measured continuously with conductivity meters.

To study turbulent mixing between two species and to perform measurements of dye concentration fluctuations in reacting flows, (Komori et al., 1991) found it necessary to use custom built scalar (dye) concentration probes (manufactured by Masatoyo P/L, Japan). Unlike some tracer methods, the custom probes are capable of sampling data at high frequencies over several channels. This increases the measurement resolutions in complex flows and enables real time data comparison between the inlet and outlet probes. The geometrically slender construction of the probe provides an additional feature in that a number of probes can be deployed within confined areas causing minimum flow disturbance. Also, for ease of measurements, the custom probe has been designed to exhibit a linear voltage response to the variation of the tracer concentration such as coloured dye when immersed in a fluid. Useful results were obtained and reported (Komori et al., 1991). Herein, the custom built concentration probe is denoted as the Komori probe because of its initial use in the laboratory by Professor Satoru Komori at Kyoto University, Japan.

At QUT, the Komori probes have been used in the laboratory to study the effect of dye mixing and dispersion in a jet stream generated by a propeller (Loberto, 2007; Loberto et al., 2004), to measure the dispersion of exhaust emissions from an outboard motor in a small subtropical creek, and to measure the RTD of a blocked gross pollutant trap. The last two experiments are presented as case studies in this paper, to demonstrate the usage of the Komori probe measuring system, see Section 5.5.

From the experiments conducted at QUT, it was found that apart from the relatively low manufacturing costs [AUD\$ 10-15k for five probes in 2005] the Komori probes are easily deployable in laboratory and field studies and the tracer dye is an organic substance (methylene blue). However, issues in its usage have been reported (Loberto, 2007; Loberto et al., 2004). The probes are subject to drift and noise particularly when sampling in unclean water. Furthermore, little is documented in relation to the Komori probe's frequency response characteristics, the effect of

flow velocity on the frequency response and the quality of data sampled. It is unknown to what extent these factors will consequentially influence the data measured by the probe.

The purpose of this paper is to investigate the frequency response characteristics of the Komori probe. To this end, the time series data is collected from the probe by injecting dye over a range of typical flow velocities and analysed. Noise and frequency response are then determined. Despite noise and drift, the data collected from the probe is useful because of its high frequency response in comparison to other types of tracer measurements. The rise and fall times are reported and compared with the theoretical response time. It was found that the frequency response is a strong function of the fluid flow velocity and frequency response for rise is higher (100 Hz) than that for the fall period (60Hz) under typical operating conditions.

5.2 EXPERIMENTAL METHOD

The Komori probe frequency response experiments were performed in the 19m tilting flume at the QUT hydraulic laboratory. Water was supplied to the flume by the choice of three variable speed pumps at the set flow rate. The downstream weir arrangement (not illustrated) was used to regulate the water depth in the flume.

The experimental setup is shown in Figure 5.1. A Sontek 16 MHz Micro acoustic Doppler velocimeter (ADV) was used to measure the mean fluid velocities (Figure 5.1). The dye measuring system comprises: a voltage supply with zero adjustment [Figure 5.2 (a)], a Komori probe [Figure 5.2 (b)], an injection unit and a data acquisition system (Data Translation -DT9802, not illustrated). The injection unit consists of a volumetric infusion pump (Alaris Medical Systems—formerly IVAC Corp. Model 597), a dye outlet probe/injector tube and an intravenous (IV)/infusion bag filled with blue dye. The Komori probe is fabricated from a hollow stainless rod of 500 mm in length. The external diameter of the rod casing is 6 mm and attached to the probe end is a sampling volume of 75 mm³, coupled with a polarising lens (mirror), a light emitting diode and photodiode [Figure 5.2 (c)]. The end features of the Komori probe measure the opacity of the fluid in which dye is dissolved through the attenuation and reflection of light. The opacity of the fluid is a

measure of dye concentration. The organic methylene blue dye is considered to be the most effective tracer substance when used with the Komori measuring system due to a linear voltage response feature. For the purpose of conducting experiments, the concentration of methylene blue dye was diluted to 25,000 parts-per-million (ppm) which is sufficient to allow a maximum detection of 8 ppm when injected and mixed into a volume of water inside the flume. The 8 ppm is the maximum detection range of the Komori probe. Prior to taking measurements, the Komori probe is calibrated by measuring the output sensing voltage in clean water (0 ppm) and in a solution of known concentration i.e. 8 ppm. The corrections for both the solutions (clean water and known concentration) are performed using meters and zero adjustments [labelled as “c.min” and “c.max” as shown in Figure 5.2 (a)] on the controller (voltage supply unit). The calibration process is repeated several times.

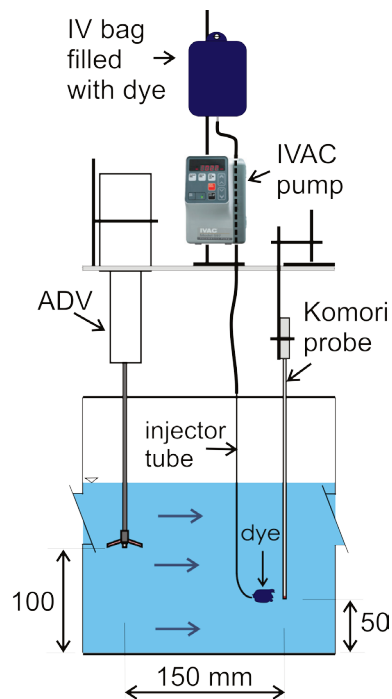


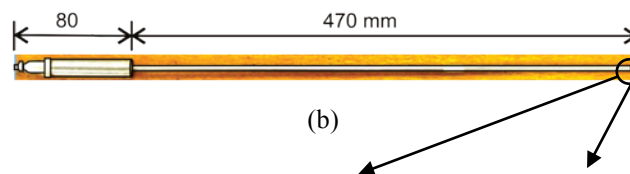
Figure 5.1 The Komori probe frequency response experimental setup in the flume.

Two sets of experiments were performed herein, denoted Expt-A (higher flow rates with the infusion pump output set to 20 mL/h) and Expt-B (lower flow rates with the infusion pump output set to 10 mL/h). Data was sampled at 20 kHz with the

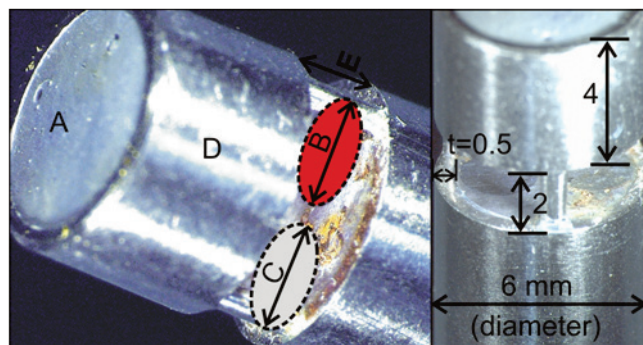
data acquisition system as previously described. The injection probe (Figure 5.1) was placed upstream of the Komori concentration probe, at a distance of 50 mm for Expt-A (high flow rates) and 100 mm for Expt-B (low flow rates).



(a)



(b)



(c)

Key features: **A**-Polarising lens/ internal mirror, **B**-Light emitting diode (2 mm diameter), **C**-Light sensor (photodiode), (2 mm diameter), **D**-Sampling volume enclosure (height = 4 mm) and **E**-aperture opening (2 mm). The thickness t is the distance between the outer casing to the inner edge of the diode/ sensor (0.5 mm).

Figure 5.2 The Komori (scalar dye concentration) controller (voltage supply unit) (a), the dye probe (b), the essential measurement features and the dimensions (c).

5.3 FREQUENCY RESPONSE METHOD AND ANALYSIS

Studies relating to the frequency response characteristics of devices are well documented. For example, a simple response time test on chemiluminescents (CLAs) revealed a typical frequency response of 1 Hz (Maffiolo et al., 1988). For the

measurement of frequency response of CLA, originally developed by (Mudford and Bilger, 1983), both time and frequency domain methods were applied (Brown, 1996). In the frequency domain analysis, the CLA is assumed to be a constant parameter linear system (Bendat and Piersol, 1971; Rabiner and Gold, 1975) where a linear relationship between concentration and voltage in steady state response exists. The signals from CLA and a reference cold wire (CW) were processed using a FFT algorithm and the corresponding energy spectra obtained. While in time domain analysis, experiments were performed by specifying a step input to the CLA and finding the time constant for the response of the CLA to rise to 63.1% $[(1-e^{-1}) \times 100\%]$ of its final value. Such methods require a known input signal which is not possible in this case. A list showing the various attributes of outputs curves are documented (Ogata, 2002) and convenient definitions are provided for these attributes to be measured with unusual shaped output curves.

The frequency response measurement of a photodiode using an optical and mechanical frequency response calibrator (1 KHz to 25 Mhz) was described (Robinson et al., 1990), and (San et al., 2007) applies laser optics for high speed photo-detectors. A similar approach on the Komori probe cannot be used as the effects of fluid interaction and dynamics with the probe are not taken into account. Furthermore, the frequencies for the given range of fluid velocities are much lower than those studied earlier (Robinson et al., 1990; San et al., 2007). It is considered appropriate to analyse the measurement response of the Komori probe as a function of fluid velocity and to simultaneously test the reliability of the real time data series sampled. With regard to the input signal, it is assumed that the injection of dye at any instant approximates a square wave. The measuring attributes (the peak detection of dye concentration) of the Komori probe is the outcome in response (rise and fall curves) to the square wave input. For example a well defined rise and fall curve (Figure 5.5) has a sharp peak. However, if the detection of dye is partial (Figure 5.6) and the true measured peak is not captured, the experimental data is rejected. The turbulent nature of the surrounding fluid interaction with the intrusive nature of the probe causes the dye to be only partially detected as shown in Figure 5.6. The orientation of the probe's measuring system [light emitter diode and photodiode, see B & C in Figure 5.2 (c)] and its alignment with the direction of flow can also

contribute to the partial detection of dye and in this case a distinct plateau in the rise portion of the curve is noted during experiments.

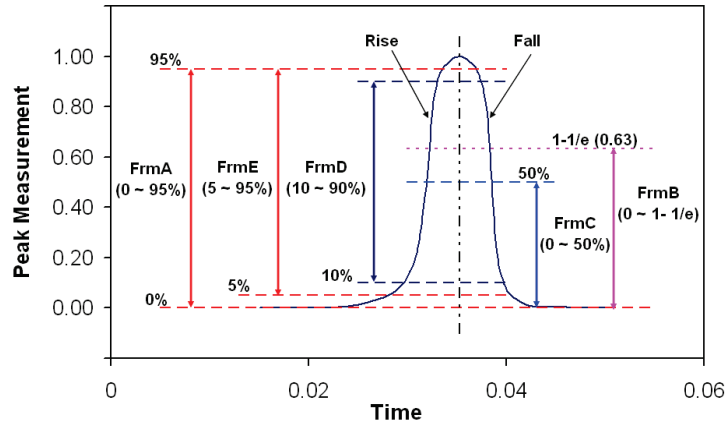


Figure 5.3 The frequency response methods shown in graphical form, used on data sampled by the Komori probe.

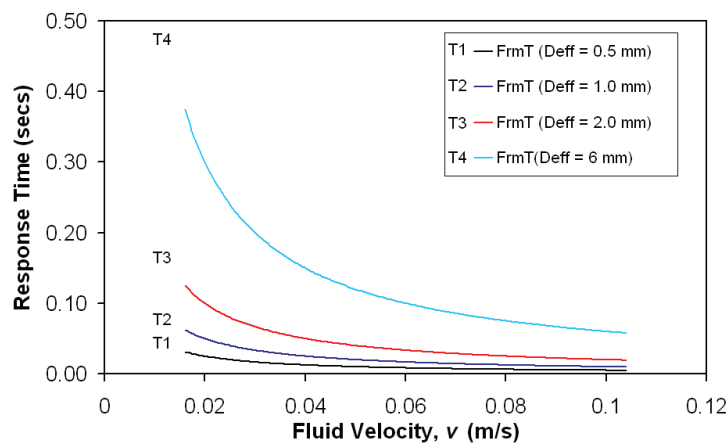


Figure 5.4 Theoretical frequency response curves for effective measurement width $D_{eff} = 0.5, 1, 2 \text{ \& } 6 \text{ mm}$.

The rise and fall response times are extrapolated from the experimental data using five different methods (Figure 5.3). The methods, described in terms of the percentage of the measured peak height (ppm), are classified as: (0 ~ 95%), (0 ~ 1-1/e), (0 ~ 50%), (10 ~ 95%) and (5 ~ 95%), denoted herein as FrmA, FrmB, FrmC, FrmD and FrmE respectively (Figure 5.3). Methods FrmB and FrmC are conservative in their approach but useful if there are measurement uncertainties in detecting peak values.

For a given flow rate, the theoretical frequency response is the effective time it takes the dye to travel across the light sensor [photodiode, see C in Figure 5.2 (c)] in the sampling volume [the aperture and the sampling volume enclosure, see D & E in Figure 5.2 (c)], ignoring the interaction between the probe and the fluid. The cross sectional width of the photodiode is 2 mm and the height of the sampling volume (SV) is 6 mm. The effective time i.e. the theoretical frequency response time [FrmT (secs)] is expressed as follows:

$$FrmT = \frac{D_{eff}}{v} \quad (5.1)$$

Where v is the fluid velocity m/s and D_{eff} (m) is the effective distance. The experimental results suggest that under varying flow rates, D_{eff} is a function of fluid velocity. To this extent four distinct values for D_{eff} (0.5, 1.0, 2.0 and 6.0 mm) are used in (1) to calculate FrmTs and are plotted in Figure 5.4.

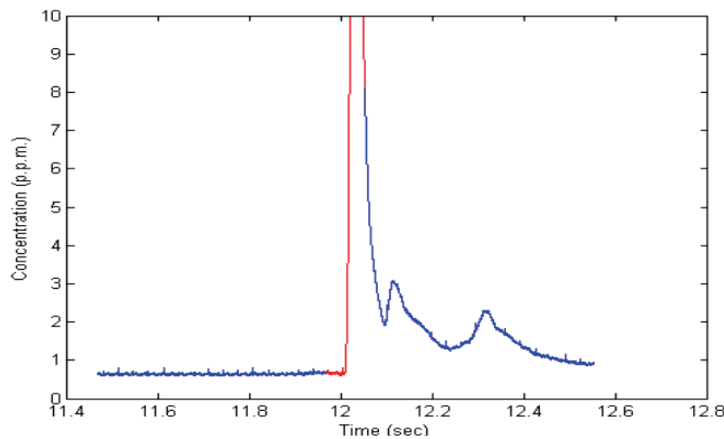


Figure 5.5 A typical data plot showing a sharply defined rise peak.

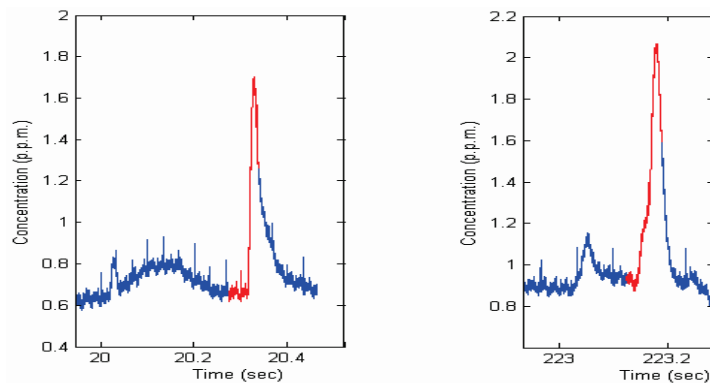


Figure 5.6 Typical experimental data plots showing false peaks caused by the partial detection of dye.

5.4 RESULTS AND DISCUSSION

Table 5.1 contains a summary of the number of rise and fall curves detected and the experimental setup conditions (water depth, fluid flow velocities and the flow rate of the dye pump).

The statistical mean response times for each batch of rise and fall curves are plotted in Figures 5.7 and 5.8 with the theoretical response times for D_{eff} (0.5, 1, 2 and 6 mm). For the purpose of graphical clarity, the rise and fall plots do not have the same frequency response axes scale.

Table 5.1 Summary of frequency response tests performed, Expt-A (tests 1-5) and Expt-B (tests 6-9).

Test	Water Depth (mm)	Water Velocity (m/s)	Dye pump flow rate (mL/h)	Rise curves (No.)	Fall curves (No.)
1	221	0.046	20	118	70
2	191	0.055	20	143	86
3	161	0.070	20	134	69
4	131	0.082	20	184	109
5	112	0.104	20	237	139
6	190	0.016	10	46	33
7	223	0.019	10	73	56
8	160	0.023	10	127	70
9	130	0.030	10	176	111

Figures 5.7 and 5.8 show that the frequency response of Komori probe characteristic is a function of the fluid velocity. In regions where the flow velocities are greater than 0.04 m/s the data appears to be almost linear and measurement is more suitable within this range. In Figure 5.7, the mean rise response curves for the methods (FrmB-C) show a maximum frequency response of 100 Hz, the lowest is 60 Hz (FrmA). Similarly for the fall curves (FrmB-C) the maximum frequency response is 60 Hz and the lowest is 10 Hz (FrmA) as indicated in Figure 5.8. It is noted from Figure 5.7 the experimental rise data falls between $D_{\text{eff}} = 0.5$ and 1 mm. The D_{eff} for the fall curves lies between 0.5 and 6 mm (Figure 5.8). It is unclear whether the slower response time is attributed to the retarded behaviour of the dye injected fluid dissipating from the sampling volume enclosure [see D in Figure 5.2 (c)].

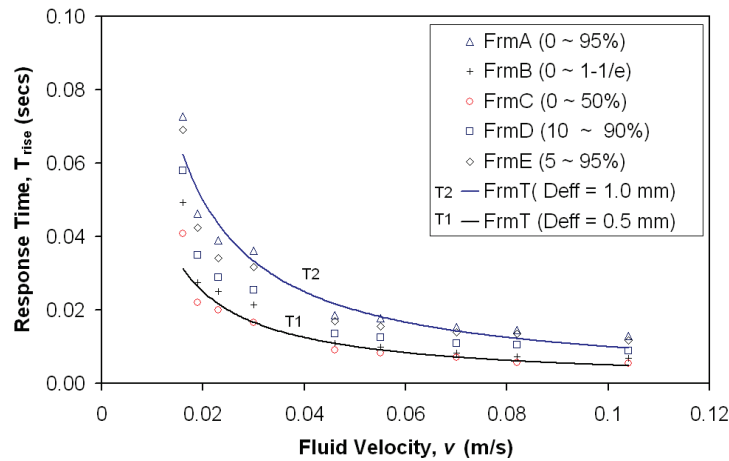


Figure 5.7 Comparison of experimental rise data (FrmA, FrmB, FrmC, FrmD, FrmE) with theoretical frequency response (FrmTs, $D_{\text{eff}} = 0.5$ & 1.0 mm).

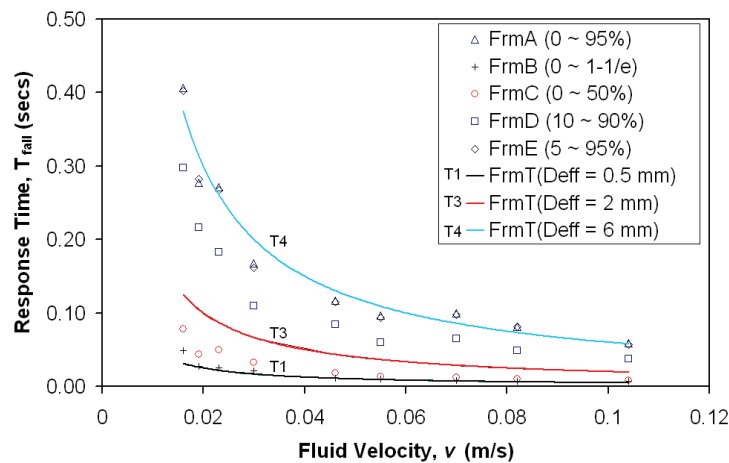


Figure 5.8 Comparison of the experimental fall data (FrmA, FrmB, FrmC, FrmD, FrmE) with theoretical frequency response (FrmTs, $D_{\text{eff}} = 0.5, 2$ & 6 mm).

Table 5.2 Rise and fall time constants using the five methods (see equation 5.2), and E is the measurement uncertainty (equation 5.3).

FrmX	Rise		Fall	
	A_c (mm)	E (%)	A_c (mm)	E (%)
FrmA (0 ~ 95%)	1.05	13.0	5.94	11.0
FrmB (0 ~ 1- 1/e)	0.61	11.0	1.33	13.0
FrmC (0 ~ 50%)	0.49	11.0	0.92	14.0
FrmD (10 ~ 90%)	0.76	12.0	4.00	9.0
FrmE (5 ~ 95%)	0.95	14.0	5.85	11.0

Measurement uncertainties are also noted in areas relating to the probe's orientation with respect to the direction of fluid flow and the surrounding flow disturbance effects. Signal noise levels in the sampling data needed to be addressed. Remedial measures were taken by using differential input connections, grounding the probe casing and using a filtering system to remove unwanted fine particles in the flume. It is unknown to what extent the residual coating of the dye on the surface of the probe casing and sensors' mounts will influence the readings. No cleaning specifications have been supplied by the manufacture to suggest otherwise.

A power law relationship expresses the relationship between velocity and frequency response as follows:

$$FrmX(v) = A_c / v \tag{5.2}$$

where $X = A, B, C, D$ or E , A_c is a constant. The measurement uncertainty (error) is expressed as:

$$E = \frac{FrmX_{predicted} - FrmX_{measured}}{FrmX_{measured}} \times 100\% \tag{5.3}$$

In Table 5.2, the constant A_c and the error (%) are within 95% confidence limits. The maximum and minimum rise and fall trend curves (FrmA-B) are plotted with the theoretical values (FrmT $D_{eff} = 0.5, 1, 2$ and 6 mm) in Figure 5.9 and shows good correlation.

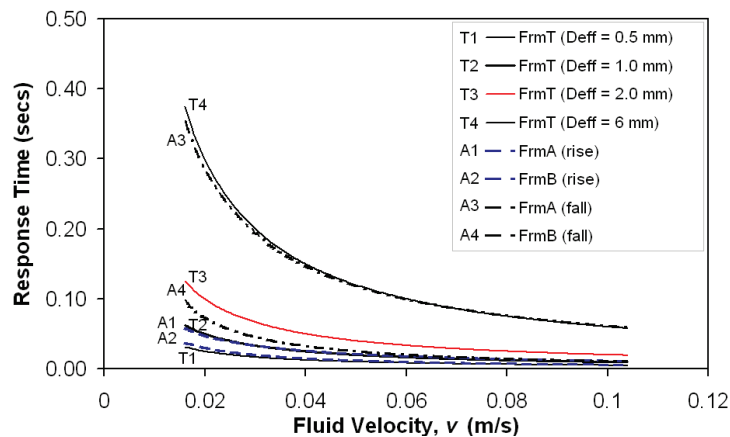


Figure 5.9 Experimental and theoretical frequency response curves (FrmA-B & FrmT $D_{eff} = 0.5, 1, 2$ & 6 mm) with 95% confidence prediction limits.

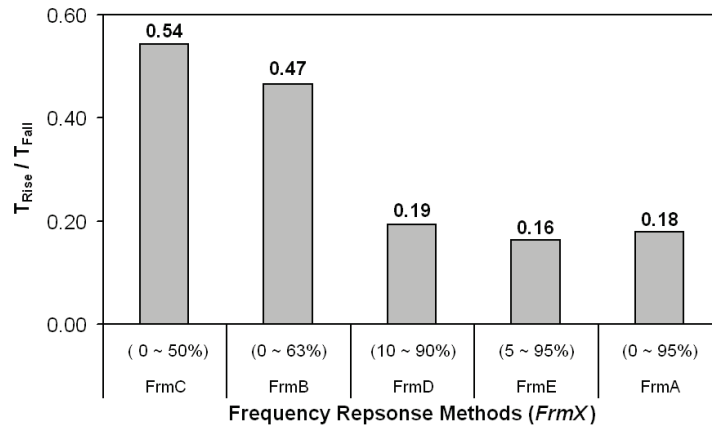


Figure 5.10 A histogram of the rise and fall response time ratio and the corresponding frequency response methods.

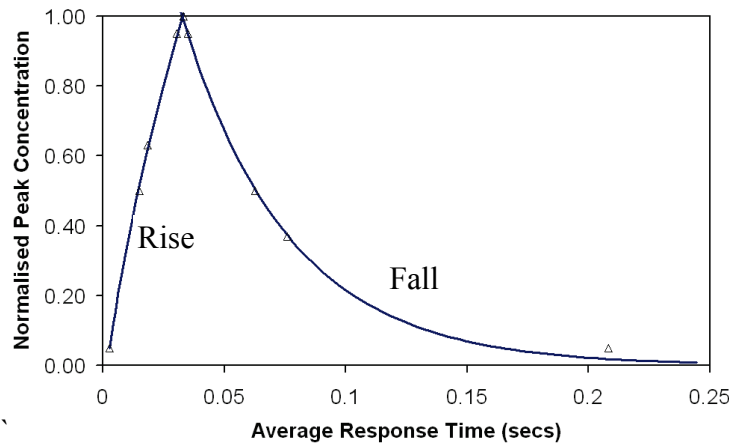


Figure 5.11 Average experimental rise and fall response times.

The ratio between the rise and fall data and the FrmXs are plotted in Figure 5.10. Figure 5.10 initially indicates that for FrmC, the rise time is 54% of the fall time. As the response criteria changes to FrmB, there is a 7% decrease in the ratio between rise and fall data response times. When the bandwidth of response time method increases towards 90% of the measured peak value, there is a rapid increase in the fall data response time. Consequently a stable plateau is reached where the rise time becomes less than 20% of the fall time for the remaining FrmXs i.e. FrmA, FrmD and FrmE. The fall curve has an exponential decaying behaviour towards the tail end. This is also shown in Figure 5.11, where the nominalised peak concentration is plotted against average response time. The rise time increases rapidly unlike the fall time which decreases more slowly. Figure 5.11 also compares favourably with the typical signal curve as shown in Figure 5.5

5.5 CASE STUDIES

As previously mentioned, the Komori probes have been deployed by QUT, to study the effects of mixing and dispersion of pollutants in water, due to outboard motor exhaust emissions, and also to measure the RTD in a blocked gross pollutant trap (GPT). These case studies are respectively described below.

Dispersion of exhaust emissions from an outboard motor



(a)



(b)

Figure 5.12 (a) Measuring the dispersion of blue dye from an outboard motor (b) A closer view of the Komori probes and the boat stern with the outboard motor (Honda).

Exhaust emissions from outboard motors are known to have a detrimental effect on polluting the waterways (Kelly et al., 2005). Field experiments were carried out in a small subtropical creek (Erapah Creek) located at Victoria Point in

Queensland. These measurements are part of an extensive series of measurements by (Chanson et al., 2005; Trevethan et al., 2006). The dispersion rate of exhaust emissions from outboard motors is measured by injecting the tracer (methylene blue dye) into the region of propeller wake from the boat (Figure 5.12). The wake generated by the propeller and boat transports the dye laterally past an array of Komori probes. Here the dye peak concentration is detected in a time series plot as shown in Figure 5.13. The time scale on the horizontal axis relates to point at which the boat passes the probes. Data is recorded on a computer via an A/D converter and the sampling rate is 10 kHz.

A critical aspect of this experiment is to use a probe with an adequate frequency response to detect the peak concentrations that occur in the highly fluctuating flow behind an outboard motor. Results from Section 4 (Figure 5.4) show that the probe is capable of measuring frequency response of up to 100 Hz at velocities of 0.1 m/s. Beyond 0.1 m/s the frequency response of the probe appears to be unaffected by the water velocity. For the outboard field experiments, velocities in excess of this level were noted in certain regions. We need to determine if the frequency response of the probe is sufficient for outboard motor experiments.

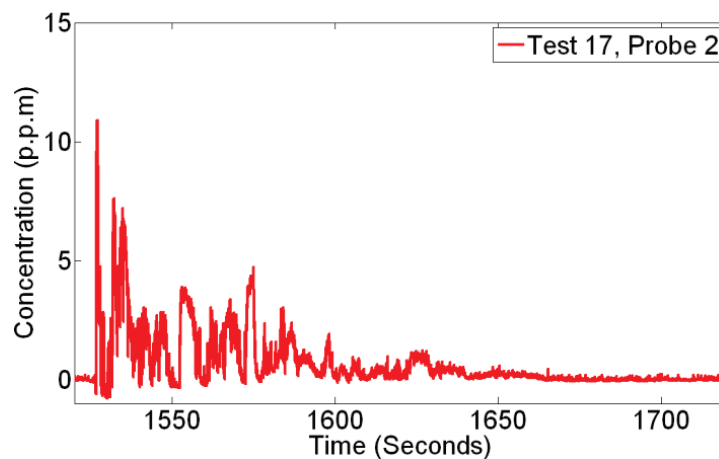


Figure 5.13 An example of a time series graph with peak concentration dye measurement from one of probes shown in Figure 12 (b).

In an attempt to assess the quality of data sampled at the higher frequency, the raw data plotted in Figure 5.13 is re-plotted in Figure 5.14 by finding the maximum (peak) concentration in each successive 10 second window period. In Figure 5.14

consistent peak concentration decay is shown with time. If a number of frequency response points was insufficient close to time = 0 (seconds), the measured peak would be truncated, i.e. the graph would show a plateau and not a sharp peak at time = 0 (seconds). It can be observed that this is not the case indicating that frequency response is adequate for this experiment.

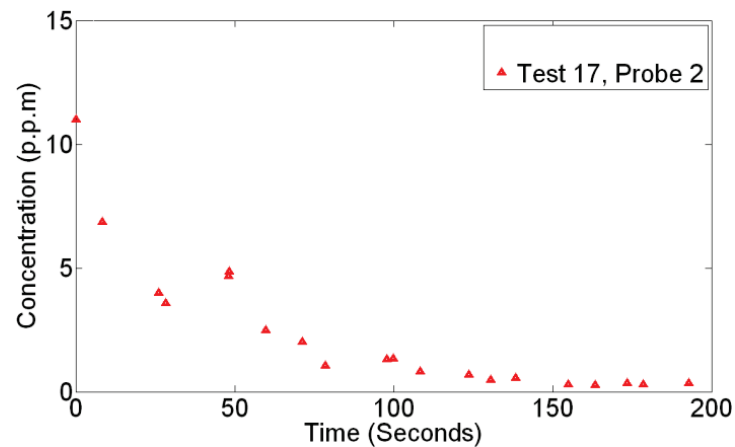


Figure 5.14 Maximum concentration in each successive 10 second window corresponding to the data in Figure 5.13.

Investigating dye mixing and dispersion in a blocked gross pollutant trap (GPT).

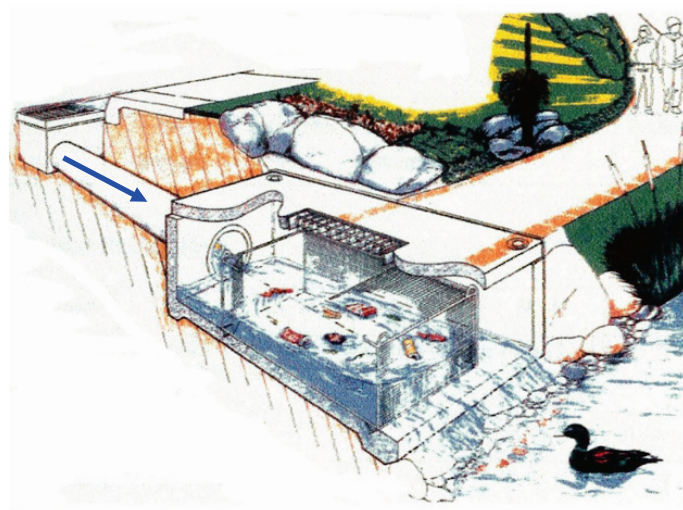


Figure 5.15 SQID (GPT)—*LitterBank* insitu.

Gross pollutant traps (GPTs) are widely used to remove litter from storm water. A GPT *LitterBank* shown in Figure 5.15 was recently developed by C-M Concrete Pty. Ltd in 2004. The *LitterBank* design uses retaining screens to collect gross pollutants from the incoming storm water (Figure 5.16).

Field studies show that retaining screens in GPTs are commonly blocked with organic matter due to infrequent cleaning, and can radically change the litter retention characteristics and flow structure within the GPT, leading to large recirculating flow patterns within the trap area, accompanied by hydraulic short circuiting where the outflow path is via the by-pass channel (Figure 5.16). Dye mixing and dispersion experiments in a GPT with fully blocked screens were carried out to understand the litter retention characteristics in this mode of operation.

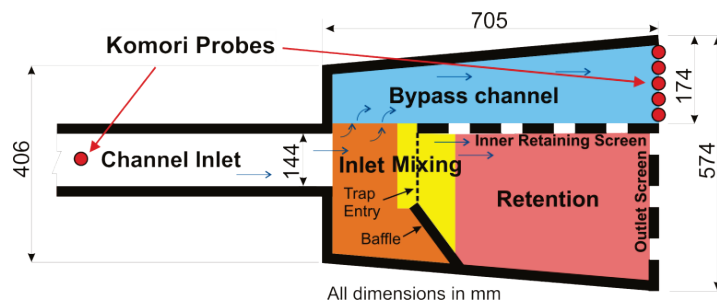
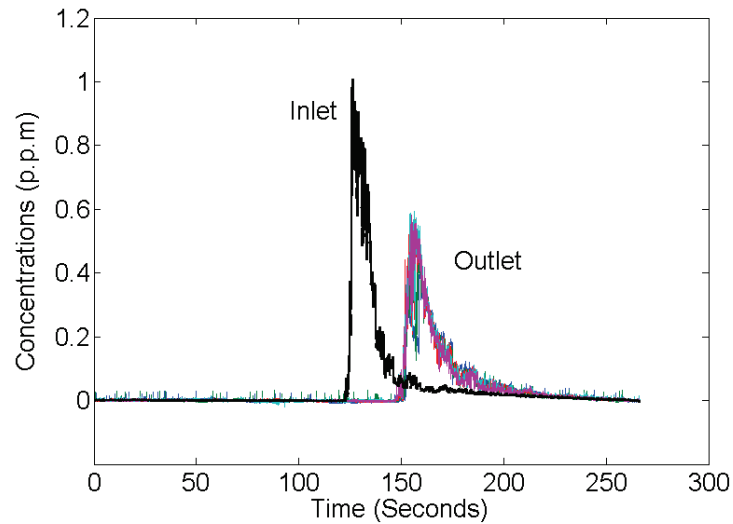
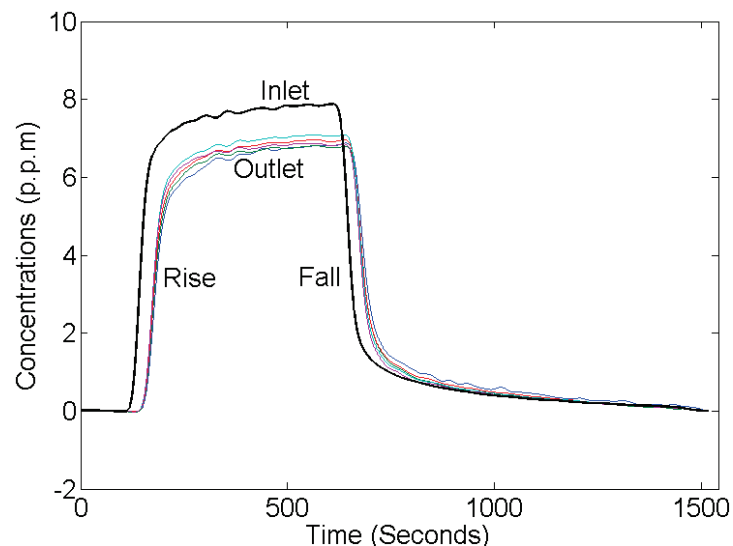


Figure 5.16 Plan view of LitterBank Scale Model with the Komori probes at inlet and outlet.

The experiments were conducted in a 50% scale model placed in a 19m tilting hydraulic flume at QUT. To measure the peak concentrations of dye entering into the scale model, a single Komori probe was placed in the channel inlet whilst an array was positioned at the outlet in by pass channel as shown in Figure 5.16. The blue dye was introduced upstream of the channel inlet in separate experiments using two methods: (a) instantaneously (pulse) and (b) continuously (step). At the inlet, the flow rate was maintained at 1 L/s (i.e. the inlet velocity is 0.07 m/s). The measured peak dye concentration is shown in a time series plots (Figure 5.17) for the two methods of inputs, i.e. pulse and step with a sampling frequency of 200 Hz. There are two parts to the output curve shown in Figure 5.17 (b) i.e. when the dye pump is on (rise) and off (fall). Data plots in Figure 5.17 (b) have been filtered for noise and drift.



(a) Pulse Input.



(b) Step Input.

Figure 5.17 Time series of peak concentration measurements obtained by introducing dye (a) instantaneously (pulse input) and (b) continuously (step input).

The dominant frequency of the inlet and outlet concentration time series in Figures 5.17 (a) and (b) are respectively around 0.03 and 0.02 Hz. Unfiltered data in Figure 5.17 (a) shows additional high frequency fluctuations. It is shown that the probe is well within its frequency response capability to measure the dominant frequencies in this case study. Overall the study shows that the Komori probe is versatile in measuring a range of frequencies and flow velocities.

5.6 CONCLUSION

In this work, the frequency response characteristic of the scalar (dye) concentration probe of Komori is evaluated by injecting methylene blue dye into the flume over a range of typical flow velocities. The data sampled by the Komori probe is subjected to time series analysis and the statistical mean response times for the rise and fall curves are determined. It was found that the frequency response is a strong function of the fluid flow velocity and the maximum frequency response for the rise is higher (100 Hz) than for the fall period (60Hz) for the measured flow velocities (Figures 5.7-5.8). The corresponding minimum values are 60 Hz (rise) and 10 Hz (fall). The theoretical frequency response F_{rmT} is based on the characteristic probe dimension, defined as the effective dimension D_{eff} . It is found that the experimental data fits within an effective dimension of $D_{\text{eff}} = 0.5$ to 6 mm. The slower fall response time may be attributed to the tendency of the injected dye to remain in the sampling volume enclosure after the peak has passed. The injected dye may also be caught in the boundary layer that forms around the probe mirror and associated surfaces. Further investigation is required to determine the influence of the sampling volume.

Two case studies are presented as examples in the usage of the probes to determine the concentration fluctuations: concentration decay in the wake of an outboard motor and in a blocked GPT. It is concluded that the Komori probe's frequency response characteristic is sufficient to measure the relevant concentration fluctuations. Further work is planned to continue measurements in evaluating the data obtained from the Komori probes and compare with other tracer methods.

ACKNOWLEDGEMENTS

The authors would like to thank David Pendrey, Tek-Jin Chin, Nicholas Lee Ming Hong, Armin Liebhardt and Rong Situ for their valuable assistance.

REFERENCES

- Adamsson, A. and Bergdahl, L. (2006). Simulation of temperature influence on flow pattern and residence time in a detention tank. *Nordic Hydrology*, 37(1), 53-68.
- Alkhaddar, R. M., Higgins, P. R., Phipps, D. A. and Andoh, R. Y. G. (2001). Residence time distribution of a model hydrodynamic vortex separator. *Urban Water*, 3(1-2), 17-24.
- Bendat, J. S. and Piersol, A. G. (1971). *Random data: analysis and measurement procedures*. Hoboken, new Jersey, USA: Wiley Interscience.
- Boccelli, D. L., Shang, F., Uber, J. G., Orcevic, A., Moll, D., Hooper, S., Maslia, M., Sautner, J., Blount, B. and Cardinali, F. (2004). Tracer tests for network model calibration. In G. Sehlke, D. F. Hayes and D. K. Stevens (Eds.), *Critical Transitions in Water and Environmental Resources Management: Proceedings of the 2004 World Water and Environmental Resources Congress Salt Lake City, Utah*: American Society of Civil Engineers (ASCE).
- Boxall, J. B. and Guymer, I. (2003). Analysis and prediction of transverse mixing coefficients in natural channels. *Journal of Hydraulic Engineering*, 129(2), 129-139.
- Brown, R. J. (1996). *Experimental investigation of a turbulent reacting plume*. Unpublished Ph.D, University of Sydney, Sydney.
- Chanson, H., Brown, R., Ferris, J., Ramsay, I. and Warburton, K. (2005). Preliminary measurements of turbulence and environmental parameters in a sub-tropical estuary of Eastern Australia. *Environmental Fluid Mechanics*, 5(6), 553-575. Retrieved 16 march 2010, from http://www.uq.edu.au/~e2hchans/reprints/efm05_6.pdf.

- Hart, F. L. (1994). Tracer analysis of a final clarifier and a chlorine contact chamber, *A case study presented at tracer analysis workshop*. Denver, Colorado: American Water Works Association Research Foundation (AWWARF).
- Hart, F. L. and Hom, V. (1996). Wastewater disinfection *MOP FD-10*. Virginia, USA: Water Environment Federation (WEF).
- Kelly, C. A., Ayoko, G. A., Brown, R. J. and Swaroop, C. R. (2005). Underwater emissions from a two-stroke outboard engine: a comparison between an EAL and an equivalent mineral lubricant. *Materials & Design*, 26(7), 609-617.
- Komori, S., Hunt, J. C. R., Kanzaki, T. and Murakami, Y. (1991). The effects of turbulent mixing on the correlation between two species and on concentration fluctuations in non-premixed reacting flows. *Journal of Fluid Mechanics Digital Archive*, 228(-1), 629-659.
- Levenspiel, O. (1999). *Chemical reaction engineering* (3rd ed.). New York: Wiley.
- Lin, A. Y.-C., Debroux, J.-F., Cunningham, J. A. and Reinhard, M. (2003). Comparison of rhodamine WT and bromide in the determination of hydraulic characteristics of constructed wetlands. *Ecological Engineering*, 20(1), 75-88.
- Loberto, A. (2007). *An experimental study of the mixing performance of boat propellers*. Unpublished Master of Engineering, Queensland University of Technology (QUT), Brisbane.
- Loberto, A., Brown, R. J., Kwek, M. K., Iida, A., Chanson, H. and Komori, S. (2004). An experimental study of the jet of a boat propeller. In M. Behnia, W. Lin and G. D. McBain (Eds.), *Proceedings of the 15th Australian Fluid Mechanics Conference* Sydney: University of Sydney.
- Maffiolo, G., Joos, E., Quesnel, R. and Thomas, P. F. (1988). Development and testing of short response time SO₂, NO_x and O₃ analysers. *Journal of Air Pollution and Control Association (JAPCA)*, 38(1), 36-38.

- Martinez, C. J. and Wise, W. R. (2003). Hydraulic analysis of Orlando Easterly wetland. *Journal of Environmental Engineering*, 129(6), 553-560.
- Mudford, N. R. and Bilger, R. W., A (1983). A facility for the study of nonequilibrium chemistry in an isothermal turbulent flow. *The Proceedings of 8th Australian Fluid Mechanics Conference* Newcastle: University of Newcastle.
- Ogata, K. (2002). *Modern control systems*. New Jersey, USA: Prentice Hall.
- Panguluri, S., Krishnan, R., Garner, L., Patterson, C., Lee, Y., Hartman, D., Grayman, W., Clark, R. and Piao, H. (2005). Using continuous monitors for conducting tracer studies in water distribution systems. In R. Walton (Ed.), *Impacts of Global Climate Change: Proceedings of the 2005 World Water and Environmental Resources Congress* (pp. 53-53). Anchorage, Alaska, USA: American Society of Civil Engineers (ASCE).
- Ptak, T., Piepenbrink, M. and Martac, E. (2004). Tracer tests for the investigation of heterogeneous porous media and stochastic modelling of flow and transport-- a review of some recent developments. *Journal of Hydrology*, 294(1-3), 122-163.
- Rabiner, L. R. and Gold, G. (1975). *Theory and application of digital signal processing*. Englewood Cliffs, New Jersey, USA: Prentice-Hall.
- Robinson, S. P., Bacon, D. R. and Moss, B. C. (1990). The measurement of the frequency response of a photodiode and amplifier using an opto-mechanical frequency response calibrator. *Measurement Science and Technology*, 1(11), 1184.
- San, H., Li, L., Li, G., Chen, X. and Feng, B. (2007). Frequency response measurement of high-speed photodetectors using the spectrum power method

in a delay self-heterodyne system. *Applied Physics B: Lasers and Optics*, 88(3), 411-415.

Trevethan, M., Chanson, H. and Brown, R. J. (2006). Two Series of detailed turbulence measurements in a small subtropical estuarine system, *Report No. CH58/06*. Brisbane, Australia: Civil Engineering, The University of Queensland.

Waldon, M. G. (2004). Estimation of average stream velocity. *Journal of Hydraulic Engineering*, 130(11), 1119-1122.

Chapter 6: An experimental and theoretical investigation of flow in a gross pollutant trap

Jehangir T. Madhani¹, Neil A. Kelson² and Richard J. Brown¹

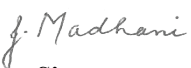
¹School of Engineering Systems

²HPC and Research Support Group

Queensland University of Technology


Publication: Water Science and Technology, 59(6), 117-1127.

This chapter is an exact copy of the above journal paper.

Contributor	Statement of contribution
Jehangir T. Madhani	<p style="text-align: center;">Candidate</p> <p>Experimental design, performed experiments and CFD simulation, collected and analysed the data. Wrote the manuscript and acted as the corresponding author.</p>
 Signature	
8/6/2010 Date	
Neil A. Kelson	<p style="text-align: center;">Associate Supervisor</p> <p>Provided guidance on CFD work/data analysis, assisted in the writing/editing of the manuscript.</p>
Richard J. Brown	<p style="text-align: center;">Principal Supervisor</p> <p>Aided the experimental design, interpretation of flow field results, reviewed and editing of the manuscript.</p>

Principal Supervisor Confirmation

I have sighted email or other correspondence from all Co-authors confirming their certifying authorship.

A/Professor Richard J. Brown		8/6/2010
Name	Signature	Date

ABSTRACT

Flow through a gross pollutant trap (GPT) with fully blocked screens is investigated experimentally and theoretically using computational fluid dynamics (CFD). Due to the wide range of possible flow regimes, an experimental approach is developed which uses a downstream weir arrangement to control the nature of the flow and the variation in free surface height. To determine the overall flow structure, measurements are taken at a fixed depth throughout the trap with an acoustic Doppler velocimeter (ADV), including velocity profile data across three cross sections of the GPT suitable for more detailed comparison with simulations. Observations of the near-wall flow features at the free surface are also taken, due to their likely importance for understanding litter capture and retention in the GPT. Complementary CFD modelling (using Fluent 6.3) is performed using a two-dimensional $k-\epsilon$ turbulence model along with either standard wall law boundary conditions or enhanced near-wall modelling approaches. Comparison with experiments suggest that neither CFD modelling approach could be considered as clearly superior to the other, despite the significant difference in near-wall mesh refinement and modelling that is involved. The experimental approach taken here is found useful to control the flow regime in the GPT and further experiments are recommended to study a greater range of flow conditions.

Keywords Gross pollutant trap, GPT, CFD, Fluent.

6.1 INTRODUCTION

Stormwater is surface water runoff from urban areas discharging into receiving waterways. Pollutants in stormwater are collected on the urban runoff path and consequentially this can have a devastating effect on the environment and its natural habitants. This has led to the development of stormwater quality improvement devices (SQID) to efficiently trap urban waste of varying sizes such as sludge, silt, sediments and solids. Gross pollutant traps (GPTs) are a class of SQIDs that separate pollutants dimensionally greater than 5 mm (Allison et al., 1998) from stormwater. A GPT LitterBank shown in Figure 6.1 was recently developed by C-M Concrete Pty Ltd, and it uses retaining screens (Figure 6.2) to collect gross pollutants prior to the release of stormwater into natural waterways. Currently there are approximately 20 LitterBanks operating at strategic stormwater locations throughout Queensland, Australia.

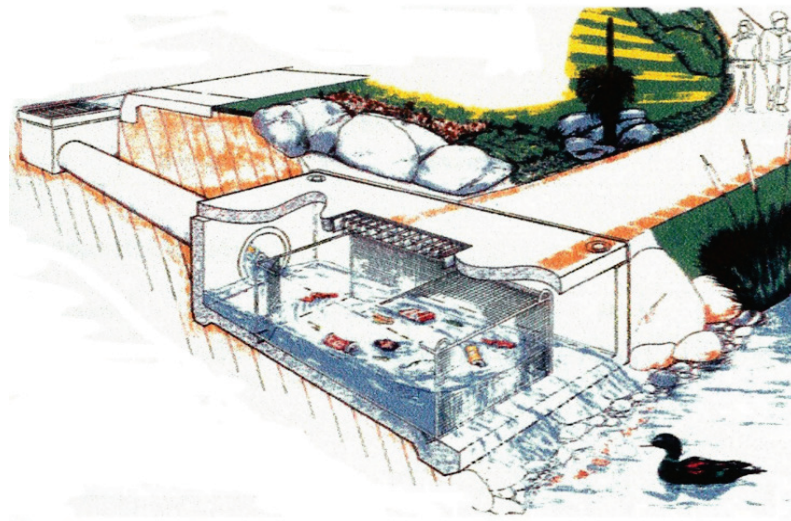


Figure 6.1 GPT—LitterBank in situ.

Field monitoring of GPTs in Brisbane, Queensland, indicates that during wet weather a wide range of inlet, outflow and other operating conditions are encountered. For example, the extent and duration of rainfall will influence the flow rate entering the trap. The tidal or flood levels of the downstream receiving waterways will determine the outflow level in the GPT. Due to infrequent cleaning, the retaining screens are often found to be blocked with organic matter. Partially or

fully blocked screens can radically change the litter retention characteristics and flow structure within the GPT leading, for example, to large recirculating flow patterns within the trap area accompanied by hydraulic short circuiting (Thackston et al., 1987) where the preferred outflow path is via the bypass channel (see Figure 6.2).

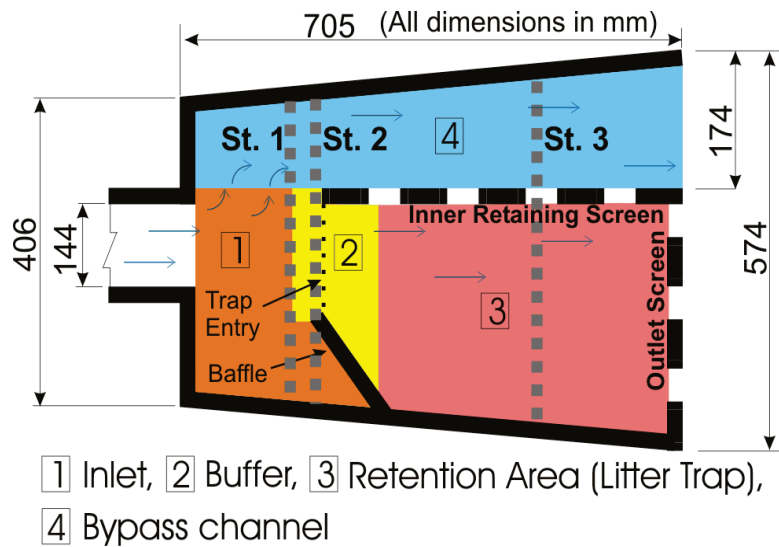


Figure 6.2 Plan view of the LitterBank with the measurement stations St.1 ($x = 137.5$), St.2 ($x = 182.5$) and St.3 ($x = 450$).

Depending on the operating conditions, the possible flow regimes inside the GPT can range from turbulent time dependent free surface flows to more steady state conditions, and this presents significant challenges for either experimental or numerical studies aimed at understanding the flow and litter retention characteristics of the trap. To facilitate the study of steady state flow conditions, an experimental approach is developed here using a downstream weir arrangement to control the nature of the flow and the variation in free surface height in the GPT. The weir height can also approximate the elevated outflow water levels into the receiving waterway due to rainfall or storm events. An experimental rig of a scale model GPT with solid internal walls is used to study pollutant-free flow in a trap with fully blocked screens, and acoustic Doppler velocimeter (ADV) fluid point velocity data is collected at a fixed depth, mainly in the retention area and trap entry. Data is collected in more detail across three cross sections of the GPT (See Figure 6.2) for comparison with simulations. Observations of the near-wall flow features at the free

surface inside the GPT are also taken, due to their likely importance for understanding litter capture and retention. Further details of the experimental approach are provided later.

Supplementary to the experiments, simulations are performed to determine the suitability of CFD as a predictive tool for the case of an assumed steady state flow regime with a quiescent flat free surface. While acknowledging that the flow in the rig is likely to be three-dimensional, a simplified two-dimensional approach is taken in the simulations (using Fluent 6.3) using a $k-\epsilon$ turbulence model with standard and near-wall modelling functions. The simplifications used here avoid the prohibitive computational cost and modelling uncertainties involved in a fully three-dimensional approach, and also permit an investigation of the benefits or otherwise of increased numerical resolution for the prediction of the experimentally observed near-wall flow features at the surface. Details of the modelling are given below.

Regarding earlier research, to the Authors' knowledge, work relating to ADV measurements or CFD on GPTs similar in design to the one studied, has not been published. However, some work in the physical modelling of GPT designs with either real or simulated pollutants exists (Armitage and Rooseboom, 1999; Phillips, 1999). Hydrodynamic details of vector velocity field were not investigated. Combined ADV and CFD studies have been used to understand the hydrodynamic behaviour of fluids in vortex separators, dissolved air flotation (DAF) tanks, sedimentation basins and aquaculture raceways (Huggins et al., 2004; Kwon et al., 2006; Lundh et al., 2001; Park et al., 2006; Ta et al., 2001; Tyack and Fenner, 1999). Also, CFD studies with GPT related devices, such as sewage structures, storage/retention tanks and hydrodynamic separators have provided valuable insights into flow patterns, pollutant mixing and sediment transport behaviour (Faram and Harwood, 2003; Harwood, 2002; Stovin et al., 1999; Stovin et al., 2002; Stovin and Saul, 2000). Two-dimensional CFD models have been used to study global flow structures and sediment retention in invert traps (Buxton et al., 2002; Gupta et al., 2005).

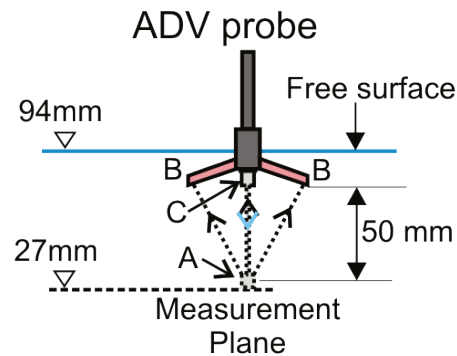
6.2 EXPERIMENTAL METHOD

The experimental rig (50% scale model) was placed in a square section (19 m, 0.6 m width, 0.6 m depth) tilting flume at the QUT hydraulic laboratory. The flume inclination was set to horizontal and a constant flow rate was established via controller settings on the centrifugal pumps which circulate the water from underground storage tanks into the flume. Flow rate readings were checked with periodical measurements in the collection tank at the flume outlet. Flow into the GPT was through a horizontal partially filled 1.8 m section inlet pipe with internal diameter 144 mm. To promote smooth upstream flow conditions, three mesh screens 1 m apart were inserted at the upstream end of the flume. The height of the weir at the downstream end of the flume (not illustrated) was fixed at 92 mm above GPT floor.

Measurements were obtained for a flow rate through the GPT of 1.0 L/s, although some small variations in the flow conditions (± 0.1 L/s) during the course of the experiments were unavoidable as a constant head tank was not fitted to the flume. The flow conditions in the flume were allowed to operate for a minimum of one hour prior to taking measurements, after which the water free surface in the GPT and also downstream was observed to be smooth and free of any obvious wave-like disturbances. Water free surface heights inside the trap and a further 2 m downstream were periodically measured relative to the GPT floor using vernier height gauges (resolution 0.1 mm). The upstream and downstream height measurements were found to be $94 \text{ mm} \pm 1 \text{ mm}$.

Regarding flow data acquisition in the scaled GPT, single point velocity measurements were taken using a Sontek™ UW ADV (10 MHz, serial No. 0510) signal condition module that is joined to a 50 mm downward-facing rigid stem probe (serial No. 0007). The ADV probe (Figure 6.3) uses an acoustic remote sampling volume (using a transmitter and three receivers with 120° separation) based on the Doppler shift to measure the flow component velocities of the seeding particles in the water (Kraus et al., 1994; Lohrmann et al., 1999; McLelland and Nicholas, 2000; Voulgaris and Trowbridge, 1998). The sampling volume is located 50 mm from the probe end (see A in Figure 6.3) and diluted French chalk was used as seeding particles to improve the signal to noise ratios (SNRs). Apart from velocities, the ADV system also records the SNRs and the correlations (CORs) to filter signals that

do not meet certain threshold values. The SNR and COR values indicate the quality of the data sampled. Measurements were taken at or above the Sontek recommended levels of 70% for the minimum COR and 15 dB for the minimum SNR to reduce measurement uncertainties. All measurements were sampled at 25 Hz for the duration of 180 s (time series length of 4500). For batch post processing ADV generated output data files, WinADV version 2.024 was used (Wahl, 2006).



A - Sampling Volume, B - Receivers,
C - Transmitter, ...>... acoustic pulses

Figure 6.3 Front view of upstream inlet structure showing the measured plane.

Due to the internal geometrical configuration of the GPT and the ADV probe, some difficulties were encountered in taking measurements close to the vertical side walls inside the trap, and obtaining data for near-wall distances less than 40 mm was not feasible. Flow data inside the GPT was measured at a fixed depth where the position of the ADV sampling volume was 27 mm from the GPT bed. Although desirable, ADV flow data acquisition closer to the free surface was not possible as the three acoustic receivers and the transmitter on the probe must be submerged for proper operation (SonTek/YSI, 2006). This requirement corresponds to a minimum submerged water depth of at least 60 mm for the ADV sampling volume.

Surface flow structures within the GPT were also observed using neutral buoyant particle seeding (20-50 μm). These were introduced onto the upstream free surface via a feeding system, or sprinkled directly onto the free surface in the retention area and the bypass channel. Repeated observations of the particles on the

free surface were made, and estimates of the lengths of the flow features (estimated error ± 5 mm) recorded, included the zones close to the GPT walls.

6.3 COMPUTATIONAL FLUID DYNAMICS (CFD) STUDY

The modelling approach taken here assumes a steady state turbulent flow regime with a quiescent free surface of constant fixed height h throughout the computational domain. A 2D k- ϵ turbulence model (using Fluent 6.3) with either standard or near-wall modelling functions was used to compute the mean surface flow field $u_i(x, y)$, ($i = 1, 2$) and variation with depth was accounted for via , $u_i(x, y, z) = u_i(x, y) \times s(z)$, where $s(z) = \left(\frac{z}{h}\right)^{\frac{1}{7}}$ is used. The present approach can be thought of as a simplification of the widely used depth-averaged k- ϵ model due to Rastogi & Rodi (1978). For a constant height free surface flow where horizontal shear is much larger than vertical shear, the vertical production terms are negligible compared to the horizontal production, and the Rastogi & Rodi model reduces to the standard 2D k- ϵ model used here (Cea et al., 2007).

While acknowledging that the flow in the rig is likely to be three-dimensional, the simplifications used here permit a computationally feasible investigation of the benefits or otherwise of increased numerical resolution when using enhanced wall modelling (as described below) for the prediction of the experimentally observed near-wall flow features.

Turbulence modelling

To model the turbulence, Cartesian x and y axes were defined along and perpendicular to the primary flow direction in the GPT scale model, and the Reynolds Averaged Navier Stokes (RANS) equations were used to describe the steady incompressible mean flow quantities. The standard two-equation k- ϵ (denoted SKE) turbulence model was used, where the turbulent viscosity, μ_t the turbulent kinetic energy, k and dissipation rate, ϵ are described by the equations:

$$\frac{\partial}{\partial x_i}(\rho k u_i) = \frac{\partial}{\partial x_j} \left[\left(\mu + \frac{\mu_t}{\sigma_k} \right) \frac{\partial k}{\partial x_j} \right] + G_k - \rho \epsilon \quad (1)$$

$$\frac{\partial}{\partial x_i}(\rho \varepsilon u_i) = \frac{\partial}{\partial x_i} \left[\left(\mu_t + \frac{\mu_t}{\sigma_\varepsilon} \right) \frac{\partial \varepsilon}{\partial x_j} \right] + C_{1\varepsilon} \frac{\varepsilon}{k} G_k - C_{2\varepsilon} \frac{\varepsilon^2}{k} \quad (2)$$

In equations (1) and (2) $G_k = \mu_t S^2$ is the turbulent production term, $S \equiv \sqrt{2S_{ij}S_{ij}}$ is the modulus of the mean rate of strain tensor $S_{ij} = \frac{1}{2} \left(\frac{\partial u_i}{\partial x_j} + \frac{\partial u_j}{\partial x_i} \right)$, the turbulent viscosity $\mu_t = C_\mu \frac{k^2}{\varepsilon}$ and the constant values are: $C_\mu = 0.09$, $\sigma_k = 1.0$, $\sigma_\varepsilon = 1.3$, $C_{1\varepsilon} = 1.44$, and $C_{2\varepsilon} = 1.92$.

Regarding the boundary conditions for the SKE model, standard logarithmic wall functions were used, where the near-wall mean velocity is evaluated via:

$$U^+ = \frac{1}{\kappa} \ln(Ey^+) \quad (3)$$

where U^+ and y^+ represent a dimensionless velocity and near-wall distance, and the values of κ and E are set to 0.42 and 9.8 respectively. The above logarithmic wall law is applied at the near-wall cells provided $y^+ \geq 11.225$ (For lower values of y^+ a linear relationship $U^+ = y^+$ is applied).

The influence of near wall modelling in the 2D flow field prediction was also investigated by using an SKE model with enhanced wall treatment (EWT). The EWT is intended to be used with near-wall mesh refinement and features a two layer method where a Reynolds number Re_y based on the near-wall distance is used to divide the flow domain into two regions. In the flow region $Re_y \geq 200$ the SKE turbulence model is employed, while for $Re_y < 200$ the one-equation Wolfshtein turbulence model is used (Wolfshtein, 1969). In the latter model, the k transport equation is retained, while ε and μ_t are expressed as algebraic functions of k and y only (y denoting here the normal distance to the nearest wall):

$$\varepsilon = \frac{k^{3/2}}{L \left[1 - \exp\left(-\frac{Re_y}{A_\varepsilon}\right) \right]} \quad \text{and} \quad \mu_t = C_\mu \rho \sqrt{k} L \left[1 - \exp\left(-\frac{Re_y}{A_\mu}\right) \right] \quad (4)$$

where $L = \kappa C_\mu^{-3/4} y$, $Re_y \equiv \frac{\rho \sqrt{k} y}{\mu}$, $A_\mu = 70$, $A_\varepsilon = 2\kappa C_\mu^{-3/4}$ and $\kappa = 0.41$.

The turbulent viscosity for the EWT model is computed (Jongen, 1998) by blending the viscosities μ_t obtained from the Wolfshtein and the SKE models via:

$$\mu_{t,EWT} = \lambda_\varepsilon (\mu_t)_{SKE} + (1 - \lambda_\varepsilon) (\mu_t)_W \quad (5)$$

$$\text{where } \lambda_\varepsilon = \frac{1}{2} \left[1 + \tanh \left(\frac{\text{Re}_y - \text{Re}_y^*}{A} \right) \right] \quad \text{and} \quad A = \frac{|\Delta \text{Re}_y|}{\tanh(0.98)} \quad (6)$$

Boundary conditions for the EWT model replace the standard logarithmic wall law with wall functions proposed by Kader (1981) based on the blending the linear (laminar) and logarithmic (turbulent) wall laws of the form:

$$u^+ = e^\Gamma u_{lam}^+ + e^{1/\Gamma} u_{turb}^+ \quad (7)$$

$$\text{where } \Gamma = -\frac{a(y^+)^4}{1 + by^+}, \quad a = 0.01 \quad \text{and} \quad b = 5 \quad (8)$$

Further details of the turbulence modelling approach can be found in Fluent (2006).

Numerical method and grid

In the CFD code Fluent, the RANS and turbulence transport equations were discretised using a finite volume method and solved using a point-wise Gauss-Seidel iterative algorithm accelerated by an algebraic Multigrid procedure (Kim et al., 1997; Kim and Rhee, 2002). Second order upwind discretisation was chosen for the convective terms in the transport equations, and the velocity-pressure coupling was resolved via a SIMPLE-type algorithm.

The computational domain consists of three sections. Referring to Figure 6.4, Section A (length 1.845 m = 13D) represents the upstream inlet, Section B (length 0.695 m) models the litter trap and overflow channel of the GPT, and section C (length 6.045 m = 10W) accounts for the downstream outflow region. Across the inlet, a uniform mean axial velocity profile corresponding to a measured flow rate of 1.0 L/s was specified. Inlet turbulence levels were specified using values of 0.144 m (turbulence length scale) and 5% (turbulence intensity). Preliminary computations indicated that varying the upstream turbulence conditions by an order of magnitude had very little influence on the predicted downstream velocity profiles. At the outlet, fully developed uniform flow was assumed by using outflow boundary conditions.

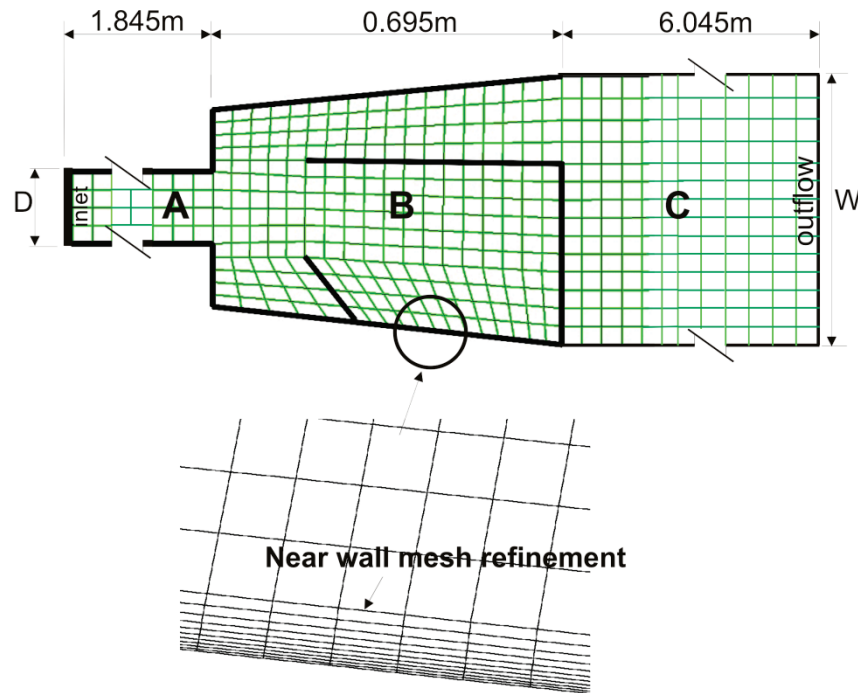


Figure 6.4 The computational domain: uniform 40 mm grid and, detail of near-wall mesh refinement adjoining 6 mm grid

Quadrilateral elements were used to discretise the domain. The internal walls of the trap were modelled as zero thickness and implemented in Fluent as shadow wall boundaries. Two separate grid strategies were employed, depending on the choice of either SKE or EWT turbulence modelling. For the SKE model, nearly uniform grids were used. To investigate the influence of grid refinement on the SKE predictions three grids with mean cell dimensions of 40, 20 and 10 mm (referred to herein as u-gridXX; XX = 40, 20, 10) were created. The coarsest 40 mm grid (u-grid40) is shown in Figure 6.4, and the total number of computational cells for the finer 10 mm grid (u-grid10) was 36236. Initial computations using the SKE model on each of these grids yielded near-wall y^+ values to within the acceptable range of $y^+ = 30$ to 500 (Casey and Wintergerste, 2000).

For the EWT modelling, near-wall mesh refinement was used via the inclusion of 10 transitional layers adjacent to the wetted walls (also shown in Figure 6.4). The near-wall grid spacing was successively increased (from 0.2 mm to 1.03 mm) and then joined with a nearly uniformly spaced grid (mean cell width 6 mm, 101432 cells; denoted bl-grid06) inside the bulk of the computational domain. Initial

computations on bl-grid06 with the EWT modelling, yielded $y^+ < 5$ for the near-wall cell values in the flow domain.

The iterative solver was deemed to have converged and further iterations terminated when a convergence criterion of less than 10^{-5} (c.f. default solver setting of $CC = 10^{-3}$) for the scaled residuals in the computed mean and turbulence quantities was achieved. In addition, the mass flow rates across the inlet and outlet were also monitored and required to be in agreement to five significant figures. Typically, around 6000 iterations were required for the SKE model, and around 10,000 iterations for the EWT model.

Grid independence

A grid sensitivity study was performed and velocity profiles across the trap mouth for the SKE model computed on ugrid-10, ugrid-20 and ugrid-40 are plotted in Figure 6.5. The results on the two finer grids are almost coincident, and consequently ugrid-10 was used. As noted earlier, predictions using EWT modelling were obtained on a grid with maximum spacing of 6 mm (instead of 10 mm) and near-wall mesh refinement, which is also expected to be a satisfactory choice based on the above results.

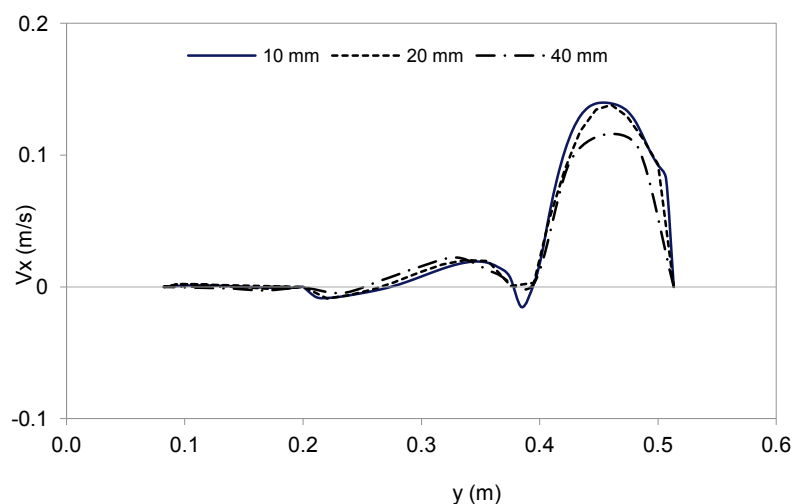


Figure 6.5 Axial velocity profiles at station 2.

6.4 RESULTS AND DISCUSSION

Experimental results

We commence with the discussion of observations of the free surface flow. The main flow structures consist of the deflection of the entry jet into the bypass channel, and the existence of a large inner recirculation flow within the retention area of the trap. Smaller near-wall flow features were also observed. Referring to Figure 6.6 (a), these are a top left corner recirculation (L4) and separation zone (L5) in the GPT bypass channel, and three low velocity corner eddies (L7a, L7b & L7c). Although not shown here (see zone 3 in Figure 6.8 below), a recirculation zone in front of the baffle was also observed. Such areas may play an important role in litter retention and have been identified as flow structures that can be optimised in GPT design.

Experimental length estimates for the secondary flow structures are tabulated in Figure 6.6 (b). These can be described as dead zones detached or separated from the main stream because of the abrupt geometrical changes, thereby forming their own closed paths behind baffles or obstructions. Dead zones have little net forward flow and are slow to mix or interchange fluid with the main stream, retaining their contents for a longer period of time (Thackston et al., 1987).

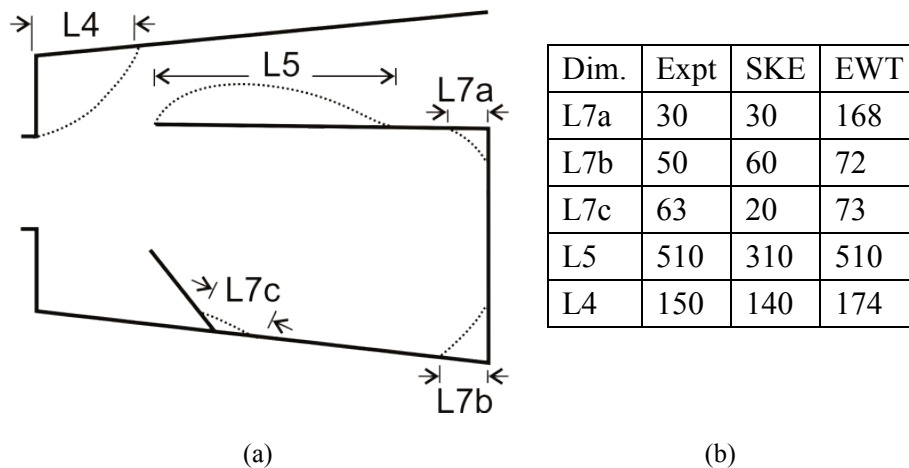


Figure 6.6 (a) Key diagram (see Figure 6.8) (b) experimental and CFD lengths (mm) for the smaller (near wall) flow feature.

The experimentally observed flow structure obtained at a fixed depth of 27 mm from ADV measurements is shown using a vector plot in Figure 6.7 (a). The flow data again shows the strongly deflected jet and the large recirculation zone inside the retention area, as was observed at the free surface. The vector plot also shows a strongly sheared flow across the trap entry which drives the inner recirculation zone. Although near-wall flow data is unable to be measured at this depth due to the limitations of the geometrical configuration of the probe, a dead recirculation zone in front of the baffle can be discerned in the vector plot, similar to the corresponding zone observed at the surface. Qualitatively, the flow structure at this depth is consistent with that observed at the free surface.

Predicted CFD flow structure

Figure 6.7 (b) shows the CFD (SKE) predictions for the overall flow in the GPT in form of vector plots. Here, the vector length scales and colour schemes are identical to those used in Figure 6.7 (a) for ease of comparison with the experimental data. Although direct near-wall comparisons are not possible, away from the boundaries the CFD vector plot is qualitatively similar to the measurements.

The predicted global flow structure at the free surface for both the SKE and EWT models are shown in the form of streamlines in Figure 6.8 (a) and (b), respectively. Both models predict similar large scale and near-wall flow features, although some differences in the predicted size of these features are evident. In addition to the previously discussed flow features inside the GPT, the predicted streamlines of both models also reveal a diverticulum (zone 2) of the inner recirculation. Re-examination of the experimental vector plot in Figure 6.7 (a) also suggests that this flow structure is present at the ADV measurement plane.

In Figure 6.6 (b), the CFD length predictions for the secondary flow features are compared with the experimental estimates. The tabulated results show that the SKE model predictions are either comparable or too low compared to the experimental results. Furthermore, the EWT model predictions are comparable or higher than the experimental estimates for the near-wall flow features. The comparison suggests that neither CFD model could be considered as clearly superior to the other, despite the significant differences in the near-wall mesh refinement and modelling that are involved.

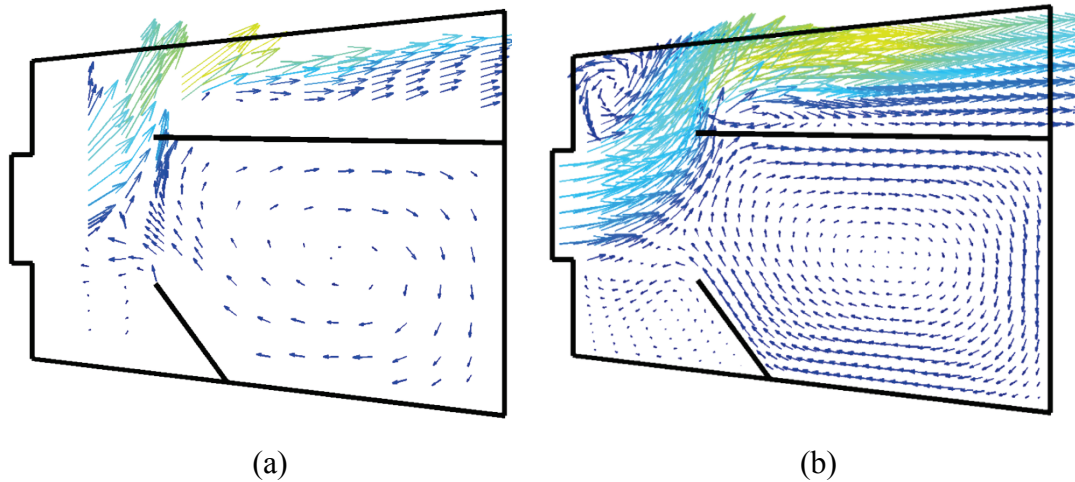
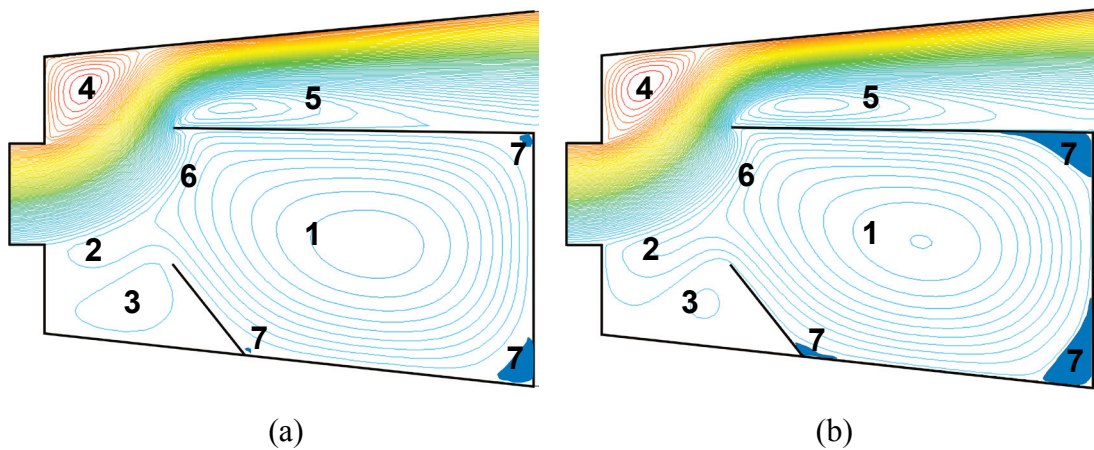


Figure 6.7 Experimental vector plots at 27 mm from the GPT bed for (a) experiment and (b) CFD (SKE)



Feature zones

1, inner recirculation; 2, diverticulum; 3, 4, dead zone (secondary recirculation); 5, flow separation; 6, mixing; 7, low velocity corner eddies.

Figure 6.8 Streamlines illustrating global flow structure for (a) SKE (standard two-equation $k-\epsilon$) or (b) EWT (enhanced wall treatment).

In Figure 6.9, a comparison of CFD predictions with experimental results for the axial velocity across Station 1 is shown. Only small differences between the predicted SKE and EWT profiles are noted, and reasonable agreement between computations and experiment can be seen. Axial velocity flow reversal is evident between $0.2 < y < 0.3$ m, consistent with the presence of the diverticulum shown in Figure 6.8. However, some discrepancies between the computations and measurements are evident with respect to the extent of the reverse axial flow and the magnitude of the peak height.

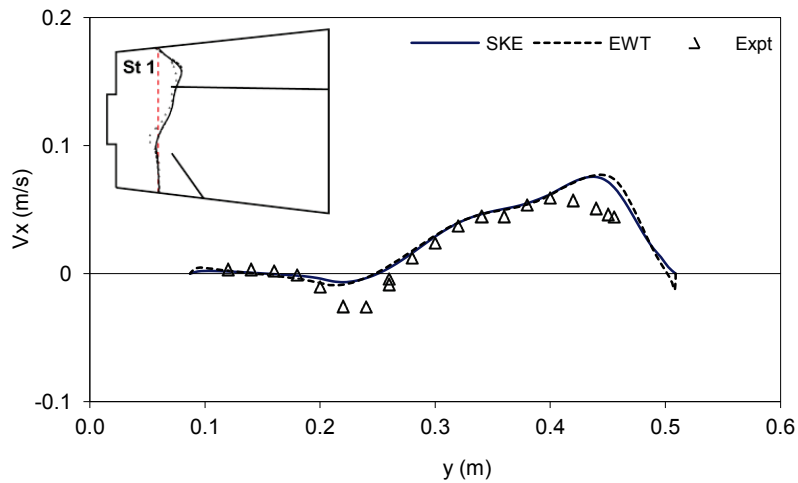


Figure 6.9 Axial velocity profiles at station 1, 27 mm from GPT bed, CFD (SKE: standard two-equation k- ϵ ; EWT: enhanced wall treatment) versus experiment (Expt).

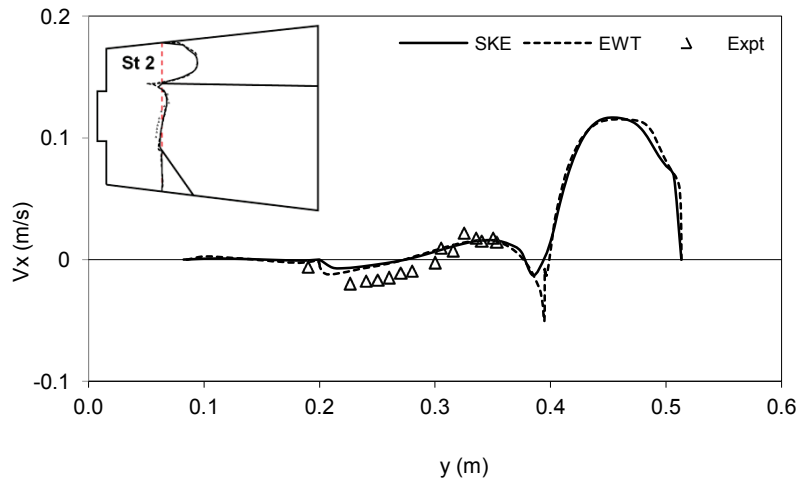


Figure 6.10 Axial velocity profiles at station 1, 27 mm from GPT bed, CFD (SKE: standard two-equation k- ϵ ; EWT: enhanced wall treatment) versus experiment (Expt)

Figures 6.10 and 6.11 show further comparisons of the CFD predictions against experimental axial velocity data stations 2 and 3, respectively. The computed profiles are again little different from each other, and both are in fair agreement with experiments. However, it can be seen that the extent of flow reversal in Figure 6.10, and the strength of recirculation in Figure 6.11, are both under-predicted compared to the experimental data.

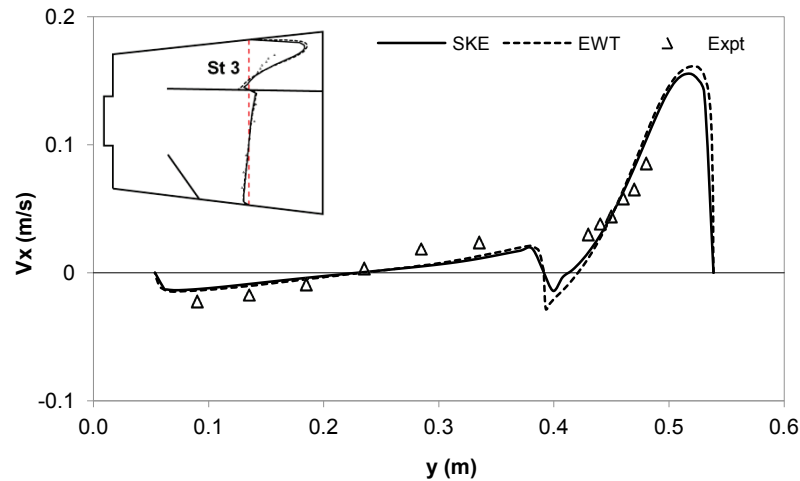


Figure 6.11. Axial velocity profiles at station 3, 27 mm from GPT bed, CFD (SKE: standard two-equation $k-\epsilon$; EWT: enhanced wall treatment ;) versus experiment (Expt).

Analysis of near-wall modelling

As noted above, some differences in the SKE and EWT predictions for the near-wall flow features can be seen in the Figures 6.6 (b) and 6.8. To understand the source of these differences, the relative influence between the two-layer turbulence modelling and the near wall mesh resolution was investigated.

To this end, a numerical experiment was performed where the SKE model prediction was re-computed on the refined bl-grid06 grid, previously used only for the EWT model. Using this grid, the computed near-wall distance at the first computational cell is $y^+ \approx 1$ for both models and, from equation (8), the boundary condition $U^+ = y^+$ is employed for both the SKE and EWT models. Hence, for this numerical experiment, the wall boundary conditions and bulk flow modelling for both models are the same, and any differences that arise can be attributed to differences in the near wall modelling in the region $1 < Re_y \leq 200$. Figure 6.12 (a) shows the near-wall region where the turbulent Reynolds number (Re_y) is in the range 0–200. Inside this region, the SKE model employs the usual transport equations given in equations (1) and (2), whereas the EWT model employs the one-equation Wolfshtein turbulence model described previously in Section 3.

Figure 6.12 (b) shows a comparison of the predicted mean axial velocities inside the retention area at station 3 using grid bl-grid06 for both the EWT and the

SKE models. In the $0 < Re_y \leq 200$ near-wall region [shaded grey in Figure 6.12 (b)], the EWT model predicts somewhat greater near-wall peak values than the SKE model. However, these do not result in any major differences between the two profiles across this station in the *unshaded* $Re_y > 200$ bulk flow region illustrated in the figure. A comparison of axial velocity profiles at stations 1 and 2 for the two models (not shown) also shows similar behaviour.

With regard to the size of the dead zones, an examination of streamlines (also not shown for brevity) indicates that SKE predictions on the bl-grid06 have generally increased compared with the lengths tabulated for the SKE model in Figure 6.6. For example, $L7a = 170$ and $L5 = 500$, and these are now of comparable size to those predicted by the EWT model.

Overall, the above results of this numerical experiment suggest that the use of a refined bl-grid06 mesh with the $U^+ = y^+$ boundary conditions significantly contributes to the change in near-wall flow predictions obtained from the SKE model, while the use of the one-equation Wolfshtein model in the EWT model within the $Re_y \leq 200$ near-wall region contributes a lesser, although noticeable, affect on the peak values.

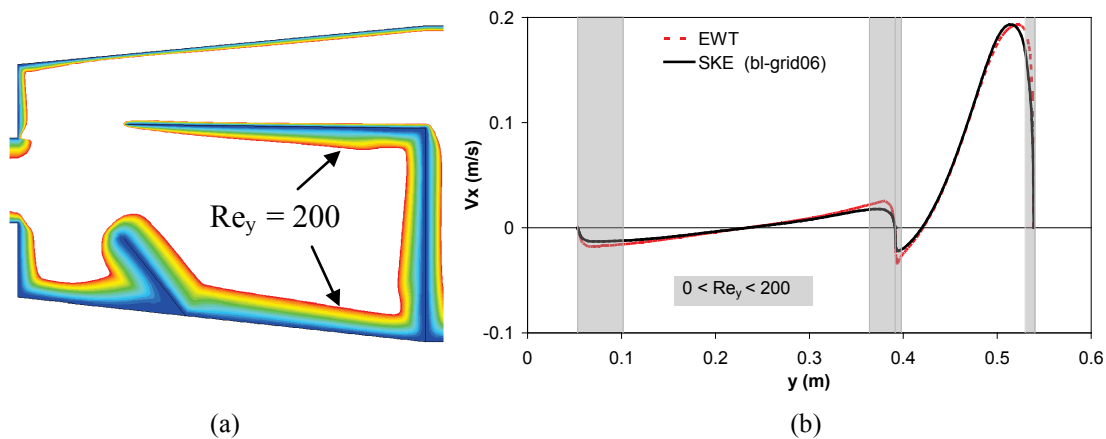


Figure 6.12 (a) near-wall region ($Re_y = 0$ to 200) and (b) mean axial velocity profiles at station 3 for SKE (standard two-equation $k-\epsilon$) and EWT (enhanced wall treatment) models computed on bl-grid06 grid.

6.5 CONCLUSION

In this study an experimental approach was developed which uses a downstream weir arrangement at the flume outlet to control the nature of the flow and variation in free surface height in a 50% scale model gross pollutant trap (GPT) with fully blocked screens. Fixed depth velocity measurements were taken throughout the trap with an acoustic Doppler velocimeter (ADV). Velocity profile data across inlet (station 1), buffer (station 2) and the litter retention (station 3) cross sections of the GPT were taken, suitable for more detailed comparison with simulations. Observations of the near-wall flow features at the free surface were also taken, due to their likely importance for understanding litter capture and retention in the GPT. The experiments showed the existence of main flow structures consisting of a deflected entry jet and a large recirculation zone within the retention area of the GPT. Smaller near-wall flow features were observed and length estimates for these secondary flow structures were made. Qualitatively, the flow structure identified from the fixed depth ADV measurements was consistent with that observed at the free surface.

Complementary CFD modelling (using Fluent 6.3) was performed using a two-dimensional $k-\epsilon$ turbulence model along with either standard wall law boundary conditions or enhanced near-wall modelling approaches. Both models predicted surface flow structures which were consistent with those observed experimentally. However, the results suggest that neither CFD modelling approach could be considered as clearly superior to the other, despite the significant differences in the near-wall mesh refinement and modelling that are involved. Numerical experiments suggest that much of the differences in predictions obtained using standard and enhanced wall modelling can be accounted for by the use of greater near-wall grid refinement, while the use of enhanced near-wall modelling in the $0 < Re_y \leq 200$ region has a lesser, but still noticeable, affect.

The experimental approach taken here was found useful to control the flow regime in the GPT and further experiments are recommended to study a greater range of flow conditions.

ACKNOWLEDGEMENTS

The authors acknowledge C-M Concrete Pty. Ltd, 2004 (Mr Phil Thomas) for their ARC linkage grant support and David Graham and Michael Roomina for their technical support in using Fluent. We also thank the QUT workshop portfolio and the QUT High Performance Computing & Research Support staff for their support with the facilities and services used in this study.

REFERENCES

- Allison, R. A., Walker, T. A., Chiew, F. H. S., O' Neill, I. C. and Mc Mahon, T. A. (1998). *From roads to rivers: gross pollutant removal from urban waterways*. Clayton, Victoria: CRC for Catchment Hydrology. Retrieved 14 January 2010, from <http://www.catchment.crc.org.au/pdfs/technical199806pt1.pdf>
<http://www.catchment.crc.org.au/pdfs/technical199806pt2.pdf>
<http://www.catchment.crc.org.au/pdfs/technical199806pt3.pdf>
<http://www.catchment.crc.org.au/pdfs/technical199806pt4.pdf>
- Armitage, N. P. and Rooseboom, A. (1999). The removal of litter from stormwater conduits in the developing world. *Water Science and Technology*, 39(9), 277-284.
- Buxton, A., Tait, S., Stovin, V. and Saul, A. (2002). Developments in a methodology for the design of engineered invert traps in combined sewer systems. *Water Science and Technology*, 45(7), 133-142.
- Casey, M. and Wintergerste, T. (2000). *Special interest group on quality and trust in Industrial CFD: best practice guidelines*. Switzerland: European Research Community on Flow Turbulence and Combustion (ERCOFTAC).
- Cea, L., Puertas, J. and Vázquez-Cendón, M. E. (2007). Depth averaged modelling of turbulent shallow water flow with wet-dry fronts. *Archives of Computational Methods in Engineering*, 14(3), 303-341.

Faram, M. G. and Harwood, R. (2003). A method for the numerical assessment of sediment interceptors. *Water Science and Technology*, 47(4), 167-174.

Fluent (2006). *Fluent 6.3 user's guide*. Lebanon, USA: Fluent, Inc.

Gupta, K., P., M., Thinglas, T., Tait, S. J. and Stovin, V. (2005). Optimization of sediment trap configuration using CFD modelling for Indian drainage systems. *10th International Conference on Urban Drainage (10ICUD)*, August 21-26, Copenhagen, Denmark.

Harwood, R. (2002). CSO modelling strategies using computational fluid dynamics. In Eric W. Strecker and Wayne C. Huber (Eds.), *Urban Drainage 2002: Proceedings of 9th International Conference on Urban Drainage -9ICUD* (pp. 8-17). Portland, Oregon, USA: American Society of Civil Engineers (ASCE).

Huggins, D. L., Piedrahita, R. H. and Rumsey, T. (2004). Analysis of sediment transport modeling using computational fluid dynamics (CFD) for aquaculture raceways. *Aquacultural Engineering*, 31(3-4), 277-293.

Jongen, T. (1998). *Simulation and modeling of turbulent incompressible flows*. Unpublished Ph.D, Thèse Ecole polytechnique fédérale de (EPF) Lausanne, Lausanne, Switzerland.

Kim, S.-E., Mathur, S. R., Murthy, J. Y. and Choudhury, D. (1997). A Reynolds-Averaged Navier Stokes Solver using an unstructured mesh based finite-volume scheme, *Technical report, TN117*. Lebanon, USA: Fluent Inc.

Kim, S.-E. and Rhee, S. H. (2002). Assessment of eight turbulence models for a three-dimensional boundary layer involving crossflow and streamwise vortices, *Technical report, TN165*. Lebanon, USA: Fluent Inc.

Kraus, N. C., A., L. and R, C. (1994). New acoustic meter for measuring 3D laboratory flows. *Journal of Hydraulic Engineering*, 120(3), 406-412.

- Kwon, S. B., Park, N. S., Lee, S. J., Ahn, H. W. and Wang, C. K. (2006). Examining the effect of length/width ratio on the hydro-dynamic behaviour in a DAF system using CFD and ADV techniques. *Water Science and Technology*, 53(7), 141-149.
- Lohrmann, A., Cabrera, R. and Kraus, N. C. (1999). Acoustic-Doppler velocimeter (ADV) for laboratory use. In C. A. Pugh (Ed.), *Proceeding of Conference on Fundamentals and Advancements in Hydraulic Measurements and Experimentation* (pp. 351-365). Buffalo, New York: American Society of Civil Engineers (ASCE).
- Lundh, M., Jönsson, L. and Dahlquist, J. (2001). The flow structure in the separation zone of a DAF pilot plant and the relation with bubble concentration. *Water Science & Technology*, 43(8), 185-194.
- McLelland, S. J. and Nicholas, A. P. (2000). A new method for evaluating errors in high-frequency ADV measurements. *Hydrological Processes*, 14(2), 351-366.
- Park, N. S., Lim, J. L., Lee, S. J., Lee, K. H. and Kwon, S. B. (2006). Examining the effect of transverse troughs on hydrodynamic behavior in a sedimentation basin with CFD simulation and ADV technique. *Journal of Water Supply: Research and Technology-Aqua*, 55(4), 247-256.
- Phillips, D. I. (1999). A new litter trap for urban drainage systems. *Water Science and Technology*, 39(2), 85-92.
- Rastogi, A. K. and Rodi, W. (1978). Predictions of heat and mass transfer in open channels. *Journal of the Hydraulics Division*, 104(3), 397-420.
- SonTek/YSI (2006). *ADV Field/Hydra acoustic Doppler velocimeter (Field) technical documentation (CDROM: P/ N 6055-00005 rev – E. 6837)*. Nancy Ridge Drive, San Diego, California, USA: SonTek/YSI.

- Stovin, V., R., Saul, A., J., Drinkwater, A. and Clifford, I. (1999). Field testing CFD-based predictions of storage chamber gross solids separation efficiency. *Water Science and Technology*, 39(9), 161-168.
- Stovin, V. R., Grimm, J. P., Buxton, A. P. and Tait, S. J. (2002). Parametric studies on CFD models of sewerage structures. In Eric W. Strecker and Wayne C. Huber (Eds.), *9th International Conference on Urban Drainage : Global Solutions for Urban Drainage* (pp. 312-327). Portland, Oregon, USA: ASCE.
- Stovin, V. R. and Saul, A. J. (2000). Computational fluid dynamics and the design of sewage storage chambers. *Water and Environment Journal*, 14(2), 103-110.
- Ta, C. T., Beckley, J. and Eades, A. (2001). A multiphase CFD model of a DAF Process. *Water Science and Technology*, 39(9), 169-176.
- Thackston, E. L., Shields, J. F. D. and Schroeder, P. R. (1987). Residence time distributions of shallow basins. *Journal of Environmental Engineering*, 113(6), 1319-1332.
- Tyack, J. N. and Fenner, R. A. (1999). Computational fluid dynamics modelling of velocity profiles within a hydrodynamic separator. *Water Science and Technology*, 39(9), 169-176.
- Voulgaris, G. and Trowbridge, J. H. (1998). Evaluation of the acoustic Doppler velocimeter (ADV) for turbulence measurements. *Journal of Atmospheric and Oceanic Technology*, 15(1), 272-289. Retrieved 18 February 2010, from <http://nortek-es.com/biblio/N4000-702.pdf>
- Wahl, T. L. (2006). A window-based viewing and post-processing utility for Acoustic Doppler Velocimeter (ADV) data files. Retrieved 12 December 2006, from http://www.usbr.gov/pmts/hydraulics_lab/twahl/winadv/

Wolfshtein, M. (1969). The velocity and temperature distribution in one-dimensional flow with turbulence augmentation and pressure gradient. *International Journal of Heat and Mass Transfer*, 12(3), 301-318.

Chapter 7: The hydrodynamic investigation of a gross pollutant trap with fully blocked screens

Jehangir T. Madhani¹, Joesph Young² and Richard J. Brown¹

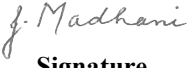
¹School of Engineering Systems

²HPC and Research Support Group

Queensland University of Technology


Publication: To be submitted.

This chapter is an exact copy of the above paper pending a journal submission.

Contributor	Statement of contribution
Jehangir T. Madhani	Candidate Experimental design, performed experiments, CFD simulation and data analysis. Wrote the manuscript and acted as the corresponding author.
 Signature	
8/6/2010 Date	
Joesph Young	Associate Supervisor Provided mathematical guidance, reviewed and edited the manuscript.
Richard J. Brown	Principal Supervisor Assisted in the data analysis, reviewed and edited the manuscript.

Principal Supervisor Confirmation

I have sighted email or other correspondence from all Co-authors confirming their certifying authorship.

A/Professor Richard Brown		8/6/2010
Name	Signature	Date

ABSTRACT

There is no unified approach to the hydrodynamic characterisation of gross pollutant traps (GPTs). This paper considers the specific case of fully blocked screens. Field studies show that internal screens in a GPT are often clogged with organic matter, due to infrequent cleaning. The capture/retention of a channel-inlet-configured GPT with fully blocked internal screens was evaluated by performing a hydrodynamic investigation. This was achieved by conducting experiments in a GPT under a typical range of onsite operating conditions. Using an acoustic Doppler velocimeter (ADV), velocity profiles across three critical sections of the GPT were measured and integrated to examine the net fluid flow at each section. The velocity data was rigorously checked using principle mass conservation and independent checks were made with the measurements at the flume outlet. The data revealed that fully blocked screens radically change the capture/retention characteristics and flow structure within the GPT. For instance, most of the fluid (approximately 80%) will transport the pollutants to the outlet via the bypass for all inlet flow conditions when the GPT is fully blocked. The velocity profiles for the lower flow rate GPT inlet conditions also compared favourably with previous 2D computational fluid dynamic (CFD) simulations. However, some deviations in the velocity profiles were observed, particularly at higher flows near the inlet, due to high shear regions associated with flow separation. Lastly, it was found that when the blockages of the internal screen approached 100%, the head loss of the GPT increased and the gross pollutant capture/retention performance decreased rapidly.

Keywords Gross pollutant trap, GPT, acoustic Doppler velocimeter, ADV, probe orientation

7.1 INTRODUCTION

Gross pollutant traps (GPTs) protect the ecological health of receiving waterways by screening visible street waste from the incoming stormwater. The earliest GPTs were open structures consisting of a large concrete wet basin, a weir and a trashrack [for a historical perspective on GPTs, see Madhani et al., (2009a) other authors are also cited here]. Trashracks are vertical or horizontal bars fitted across the basin in the stormwater flow path to retain gross pollutants. The more recent GPTs are uniquely designed to be compact, more efficient, with their unsightly contents concealed. Their uniqueness is a specific stormwater treatment process. Modern GPTs generally use internal retaining screens to trap pollutants dimensionally greater than 5 mm prior to the release of stormwater into natural waterways. These GPTs are designed either as water retaining or dry devices. Water retaining GPTs have waste biodegradation issues which release toxic substances into downstream waters. A recently developed dry linear screening GPT—the *LitterBank*, (by C-M Concrete Pty Ltd)—is shown in Figure 7.1. Currently, there are twenty *LitterBanks* operating at strategic locations throughout Queensland, Australia.

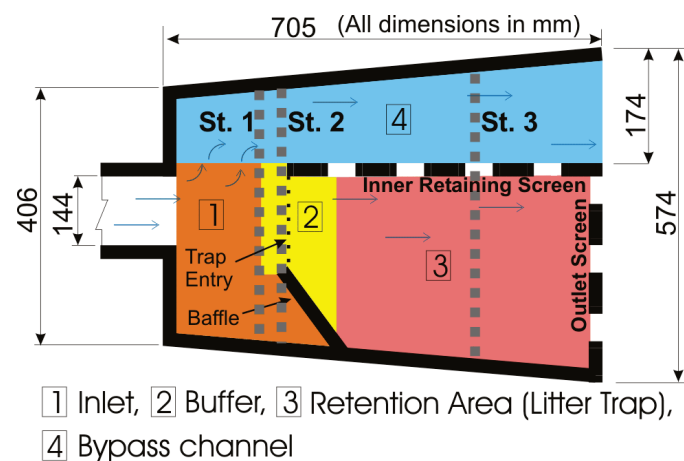


Figure 7.1 Plan view of the *LitterBank* with the measurement stations St.1 ($x = 137.5$), St. 2 ($x = 182.5$) and St. 3 ($x = 450$).

Previous field monitoring of *LitterBank* GPTs in Brisbane, Queensland show that during wet weather a wide range of inlet, outflow and other operating conditions were encountered (Madhani et al., 2009c). For example, the extent and duration of

rainfall influences the flow rate entering the GPT. The outflow level in the GPT is determined by the tidal or flood levels downstream of the receiving waterways. Due to infrequent cleaning, the retaining screens were often found to be blocked with organic matter which influenced the hydrodynamic and the gross pollutant retention characteristics within the GPT. Depending on these operating conditions, the possible flow regimes inside the GPT can range from turbulent time dependent free surface flows to more steady state conditions. This presents significant challenges for either experimental or computational fluid dynamics (CFD) studies aimed at understanding the flow and capture/retention characteristics of the GPT.

To overcome these modelling challenges and to facilitate the study of steady state conditions, an experimental approach was developed earlier. This approach used a downstream weir arrangement to control the nature and the variation in free surface height in the GPT in addition to the elevated outflow levels (Madhani et al., 2009b). With this arrangement, an experimental rig of a scale model pipe-inlet-configured GPT with solid internal walls was previously used to study pollutant-free flow in a trap with fully blocked screens. However, inside the GPT, fluid point velocity data was only collected at a fixed depth and at a single inlet flow rate. Thus, flows across the depth were not investigated which is important when analysing capture/retention characteristics of pollutants particularly those with different densities. Furthermore, the internal geometrical configuration of the GPT and the acoustic Doppler velocimeter (ADV) probe, presented difficulties in taking measurements close to the vertical walls inside the trap. Without such data large errors ($\sim 50\%$) occur when integrity checks are performed (Madhani et al., 2005). Furthermore, the behaviour in these regions cannot be analysed quantitatively.

ADVs are widely used both in laboratory and field applications particularly as the instruments are robust. Scientific evidence shows that ADV signal outputs have had various issues with Doppler noise, signal aliasing and other disturbances (Chanson, 2008). ADV processing methods to minimise these effects have been satisfactorily developed and accepted within the scientific community. Measurement issues in using the ADV in the proximity of solid boundaries have also been reported. For instance, amongst other ADV parameters, streamwise velocity components have been underestimated when validated with other instrumentations (Chanson, 2008). These problems have been widely investigated by analysing the

effect of positioning the ADV probe sampling volume near the boundary with correction strategies. Other authors have reported that the intrusive nature of the ADV probe disturbed the flow which had a dampening effect on the velocity profile and the flow structure during measurements (Lemmin et al., 1999; Tyack and Fenner, 1999). During ADV measurements in narrow channels and near walls, errors associated with wakes produced by the probes have been briefly researched (Abad et al., 2004). These authors have recommended further work on other ADV probes. Other authors have also expressed concerns with the flow disturbances (wake) and the need to seed the water with scattering material to provide adequate signal to noise ratio (SNR) strength in order to accurately measure the velocities (Rusello et al., 2006; Snyder and Castro, 1999). For example, investigations showed substantial deflections of flow near the central transducer particularly when the ADV probe was tilted. Also, introducing seeding material into the flow may interfere with other types of measurements. Consequently, these concerns have led to the development of an improved ADV probe with a new transducer head design. However, the newer designed ADV down-looking probe is not presently suited for measurements next to vertical walls. Overall, scientific investigations on the performance of the intrusive ADV probes in confined flow regions such as inside GPTs with complex internal geometrical wall configuration are not well established. Measurements with ADVs for evaluating the performance of larger stormwater treatment structures are considered essential tools (Klepiszewski, 2009). For example, ADV studies have been used to understand the hydrodynamic behaviour of fluids in vortex separators, dissolved air floatation (DAF) tanks, sedimentation basins, and aquaculture raceways (Huggins et al., 2005; Kwon et al., 2006; Lundh et al., 2001; Park et al., 2006; Ta et al., 2001; Tyack and Fenner, 1999; Viadero et al., 2006).

In this current research, the hydrodynamic behaviour of a channel-inlet-configured GPT with fully blocked screens was comprehensively investigated using ADV measurements. To measure flow across the depth, multi-depth and near-wall measurements under a wider range of typical GPT inlet flow conditions were performed. This was achieved by using a combination of the original designed ADV probes to overcome measurement limitations from earlier hydrodynamic investigations (Madhani et al., 2009b). A technique was developed to perform these measurements in confined flow spaces. The velocity data was checked rigorously

using principle mass conservation and independent checks were made with the measured flow rate at the flume outlet. The integrated data showed good correlation despite ADV measurement difficulties. Furthermore, favourable comparisons were also achieved with previous computational fluid dynamics (CFD) simulation for the GPT experiments with two of the lower flow inlet rate conditions (Madhani et al., 2009b).

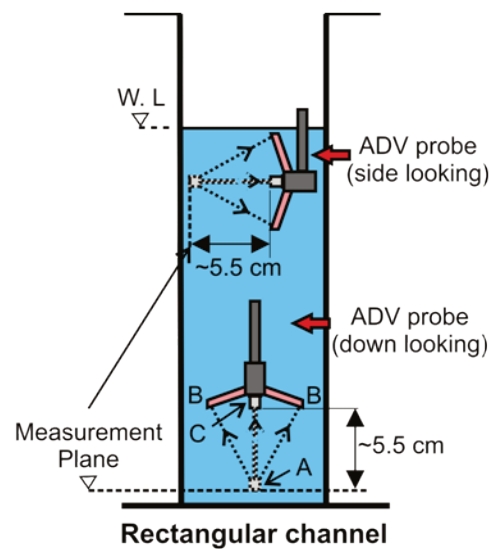
Consequently, for all flow inlet conditions, various sections of the GPT were examined and quantified in terms of flow rates in order to describe its potential capture/retention characteristics. The capture/retention characteristics were also investigated with head loss experiments.

Details of the experimental method, ADV technique and head loss experiments are presented below. As shown subsequently, the ADV technique developed in this paper produced useful results under difficult measuring conditions.

7.2 EXPERIMENTAL METHOD

The experimental rig (50% scale model) was placed in a square section (19 m long, 0.6 m wide and, 0.6 m deep) tilting flume at the QUT hydraulic laboratory. Inside the flume, flow into the GPT was through an upstream channel inlet configuration with its height extended to the full depth of the experimental model and its width 144 mm (see plan view in Figure 7.1). At the flume outlet, an experimental methodology which had been previously developed used a downstream weir arrangement to control the nature of the flow and the variation in free surface height (Madhani et al. 2009b, c). A constant flow rate (Table 7.1) was established through the GPT inlet via controller settings on the centrifugal pumps which circulated the water from underground storage tanks into the flume. At lower flow rates, 1.3 L/s and 3.9 L/s (see Runs 1 and 2, Table 7.1) the corresponding weir heights of 0.1 m and 0.3 m respectively were set above the floor level at the end of the flume terminus raceway. The establishment of these flows during the experiments was based on promoting smooth flow conditions free of any obvious wave-like disturbances (Madhani et al., 2009b). Screens were also placed at the entrance of the raceway to prevent large-scale flow disturbances. Alternatively, at the higher flow regimes, the weir height was set at the floor level of the raceway (zero).

Some variations in these flow conditions ($\pm 10\%$) during the course of the experiments were unavoidable since the constant head tank was not fitted to the flume. However, at the flume outlet, the flow rate was periodically measured in the collection tank with a known height and a stopwatch. The water temperature was also measured at intervals and corrections were made to the ADV software (HorizonADV version 1.04, SonTekTM/YSI, San Diego, USA) when necessary. For further details on the experimental setup for velocity measurements in the GPT see Madhani et al. (2009b, c) which also describe the physical modelling of blocked screens.



A - sampling volume, B - receivers,
C - transmitter, ...>... acoustic pulses

Figure 7.2 Front view of upstream inlet structure showing the measured planes.

Table 7.1 A matrix of flow regimes used in the experimental setup for litter capture.

Run	Flow regime	Weir height (m)	Inlet velocity (m s)	Flow rate (L/s)	Water depth (m)
1	Low	0.108	0.09	1.3	0.1
2	↑	0.286	0.09	3.9	0.3
3	↓	0	0.39	6.1	0.1
4	High	0	2.14	35.4	0.3

Velocity measurements were conducted with three ADVs: (1) SontekTM MicroField-ADV (16 MHz, 3D down-looking probe serial number A813F), (2) SontekTM MicroField-ADV (16 MHz, 3D side looking probe serial number A843F) and (3) SontekTM Micro-ADV (16 MHz, 3D down-looking probe serial number A919F). The approximate minimum submerged distances for proper operations of the 3D down and side-looking probes are respectively 75 mm and 25 mm (SonTek/YSI, 2006). The ADV probes (Figure 7.2) uses an acoustic remote sampling volume (using a transmitter and three receivers with 120° separation) based on the Doppler shift to measure the flow component velocities of the seeding particles in the water (Kraus et al., 1994; Lohrmann et al., 1999; McLelland and Nicholas, 2000; Voulgaris and Trowbridge, 1998). The centre of the sampling volume (see A in Figure 7.2) is located typically 5 cm from the transmitter, but some studies have shown that the distance might change slightly (Chanson, 2008). The current side looking probe was found to be 5.1 cm. The size of the measuring volume is determined by sampling conditions and consists of a cylinder of water with a diameter of 6 mm and a height of 9 mm. The quality of data collected relies on the signal to noise ratios of the measured particles detected in the measuring volume. Diluted French chalk was used as seeding particles to improve the signal to noise ratios (SNRs). Apart from velocities, the ADV system also records the SNRs and the correlations (CORs) to filter signals that do not meet certain threshold values. The SNR and COR values indicate the quality of the data sampled for laboratory conditions, Sontek recommends 70% as the acceptable minimum COR and an SNR above 15 dB to reduce measurement uncertainties (SonTek/YSI, 2006). All measurements were sampled at 50 Hz for the duration of 120 s (time series length of 6000 samples). WinADV version 2.024 was used for batch post processing of ADV generated output data files (Wahl, 2006).

ADV measurement technique

Due to the internal geometrical configuration of the GPT and confined spaces, a combination of differently structured 3D ADV probes was used for three-dimensional velocity measurements. The down-looking probe in Figure 7.3 (a) is capable of taking measurements in the bulk flow and near the GPT bed. The orientation of the coordinate system for this probe was consistent throughout the measurement and the red band was aligned with the streamwise flow, that is x_d in

Figure 7.3 (a) was coordinated with x in Figure 7.4 (a). The second ADV probe offered the additional capability of measuring next to the vertical GPT walls as shown in Figure 7.3 (b). However, the orientation of the local coordinate system with respect to the mainstream flow depended on which vertical wall this probe was facing (Figure 7.4). For measurements with this probe facing the inner wall that is L in Figure 7.4 (a), the local y_s coordinate was aligned with the flow. In the opposite wall face, that is R in Figure 7.4 (a) the local y -axis was negative. To measure the distribution of flow across the width and water depth inside the GPT, the ADV probes (Figure 7.3) were mounted on an instrument carriage placed on the top of the flume rails. The carriage was fitted with fine adjustments on the vertical and transverse positions with 0.1 mm increments. In the horizontal direction, the accuracy of the ADV probe positions was less than 1 mm. The positions of the probes were referenced from the GPT's (x , y and z) global coordinate system as shown in Figure 7.4 (a). The stems of the probes were used as a reference for alignment and positioning in the GPT. The probe sampling volume distances to the solid boundary were reported by the ADV data acquisition software. However, at less than 20 mm the reported distances become unreliable (SonTek/YSI, 2006). Thus the probes distances outside this limit were initially recorded and moved at controlled distances towards the boundary. The SontekTM Beam-Check diagnostic module was also used (SonTek/YSI, 2006) to check the position of the sampling volume with respect to the boundary walls. For a large number of data points this procedure became time consuming and peak signal interferences obscured clarity in accurately interpreting boundary distances. Thus, visual checks were also carried out and other ADV parameters such as SNRs were monitored.

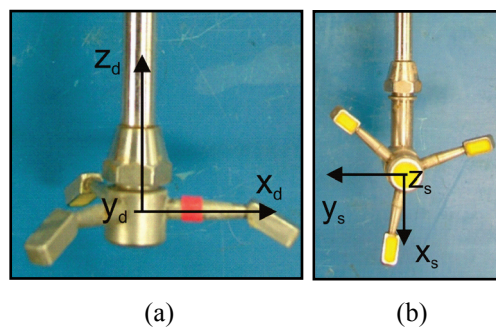


Figure 7.3 Local coordinates systems for the ADV probes, (a) down-looking and (b) side-looking.

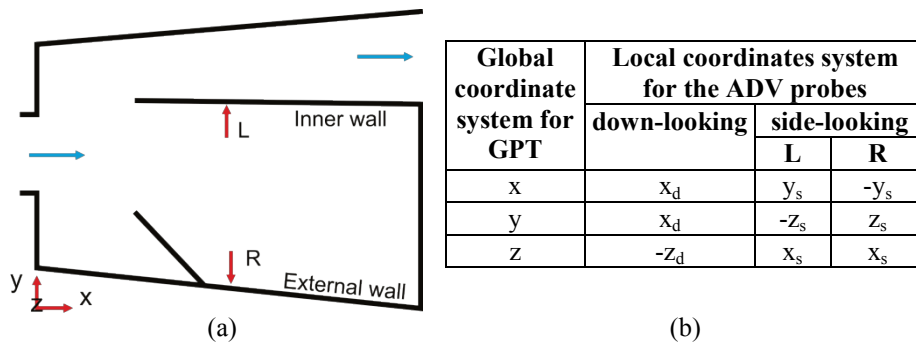


Figure 7.4 (a) Key diagram and (b) global and local coordinate Cartesian system for the GPT and the ADV probes, respectively.

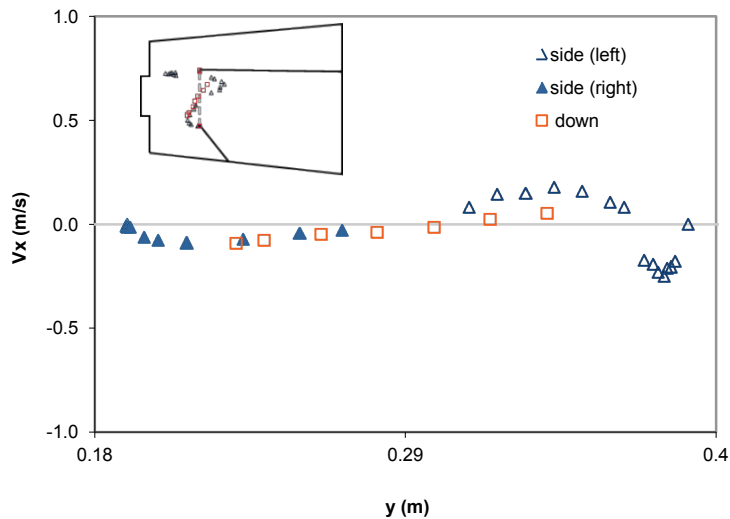


Figure 7.5 Axial velocities (V_x) measured at the trap entry (See 2, in Figure 7.1) using 3 ADV operations. Measurements with the side-looking probe are taken—left facing the inner wall and, right towards the baffle for Run 4 (Table 7.1).

Scientific studies regarding the level of SNRs during ADV measurements as the probe sampling volume enters the proximity of the solid boundary show lack of agreement. A loss of SNRs has been reported while other authors have indicated a rapid rise that reaches a peak value when this volume hits the target (Chanson, 2008; Finelli et al., 1999; Precht et al., 2006). In the current research both a loss and a rise in SNRs were experienced depending on the shear velocity gradients and the particle seeding. However, as the measuring volume changed within 10 mm proximity of the

solid boundary, the SNRs generally rose sharply. This technique was used as a guideline to detect the position of the walls prior to taking measurements.

Figure 7.5 shows a typical outcome of the measurements performed using a combination of the ADV probes in restricted flow areas (Figure 7.3). The two opposing facing and the bulk flow region were measured with 3D side and down-looking probes respectively. In the flow region where $y > 0.3$, the velocity readings were observed to be slightly lower and it was assumed that the probe structure had a damping effect on the data collected. Subsequent calibration checks on these probes in undisturbed flow regions in the flume were generally similar to within 3% to 5%.

Head loss experiments

The head losses from various screen blockages were examined by using various materials (Table 7.2). In Table 7.2, Perspex solid walls were used to model fully blocked screens while perforated sheet metal with 3 mm circular and 5 mm rectangular holes were used to model 68% and 33% screen blockages respectively (Table 7.2). The percentage screen blockages were based on the amount of material obstructing the flow path; no screens represented 0% blockage. The head loss of the blocked screens was recorded using four ultrasonic displacement sensing probes with an accuracy of 0.18 mm: (1) MicrosonicTM +25/IU/TC/E with a response time of 50 ms and (2) MicrosonicTM +35/IU/TC/E with a response time of 70 ms. These probes were mounted across the carriage flume rails, upstream, downstream, in the GPT and at the collection tank. The probe at the collection tank measured the flow rates during transient and steady state flow conditions. The outcome of the experiments is reported in the Results and Discussion Section below.

Table 7.2 Material used in place of normal screens in the GPT to represent percentage of blocked screens.

Material	Screen Blockages (%)
Perspex (solid internal walls)	100
Perforated screens (3 mm holes)	68
5 mm rectangular screen mesh	33

7.3 DATA ANALYSIS

Using conservation of mass to express the net flow at various cross sections (CS) of the GPT (St. 1 to 3 in Figure 7.1) for incompressible steady state conditions:

$$\int_{CS} (\vec{V} \cdot \vec{n}) V \cdot dA = 0, \quad (7.1)$$

where $\vec{V} \cdot \vec{n} = V \cos \theta$ is positive for $\theta < 90^\circ$ (outflow) and negative for $\theta > 90^\circ$ (inflow). Equation (1) represents the net flow rate across the integrated depth of flow. The velocity profile data from ADV measurements across the solid boundary limits is the integral form of equation (1). Let Vx_i , $i = 0, 1, \dots, n$, be the sampled, mean axial velocities at the points x_i , $i = 0, 1, \dots, n$. In order to calculate the net flow, we interpolate the data points (x_i, Vx_i) , $i = 0, 1, \dots, n$ with a smooth C^l function which is continuous and has a continuous derivative on $[x_0, \dots, x_n]$ Vx_i , $x_i = 1, 2, \dots, n$. We require these conditions since we expect the plots of the velocity profiles to be smooth and continuous.

Sets of piecewise cubic polynomials are widely used to create smooth interpolating functions. Cubic polynomials are low order polynomials and display simple local forms. However, sets of cubic polynomials can be used to interpolate complex datasets globally. The integration of spline curves can be computed quickly and easily in a set number of operations, since each polynomial piece is specified analytically. This is useful for the procedure we have developed to approximate accurately (7.1) from the ADV measurements.

A number of different cubic spline interpolants have been developed. However, we are interested in splines curves, which interpolate the data points exactly. They are differentiated from each other in the way the derivate values are computed at each point x_i . We used piecewise cubic Hermite interpolating polynomials to interpolate our sampled velocities. MATLAB's® (2008b, The MathWorks, Melbourne, Victoria, Australia) PCHIP function has been used for the interpolation. PCHIP calculates smooth interpolating function by choosing the derivate values such that (a) the shape of the data is preserved, (b) monotonicity in the data is preserved and (c) local extrema in the data are also preserved (Fritsch and Carlson, 1980). These derivatives were obtained as follows:

Let $\pi : a = x_0 < x_1 < \dots < x_n = b$ be a partition of the interval $I = [a, b]$.

Let $\{Vx_i : i = 0, 1, 2, \dots, n\}$ be a given set of monotone data values at the partition points (knots); that is, we assume either $\{Vx_i \leq Vx_{i+1} (i = 0, 1, 2, \dots, n - 1)\}$ or $\{Vx_i \geq Vx_{i+1} (i = 0, 1, 2, \dots, n - 1)\}$. We construct on π a piecewise cubic polynomial function $P(x) \in C^1[I]$ such that

$$P(x_i) = Vx_i, \quad i = 0, 1, 2, \dots, n, \quad (7.2)$$

and $P(x_i)$ is monotone. In each subinterval $I_i = [x_i, x_{i+1}]$, $P(x)$ is a cubic polynomial which maybe represented as follows:

$$P(x) = Vx_i H_1(x) + Vx_{i+1} H_2(x) + d_i H_3(x) + d_{i+1} H_4(x), \quad (7.3)$$

where $d_i = P'(x_i)$, $j = i, i + 1$, and the $H_k(x)$ are usual Hermite basis functions for the interval I_i :

$$H_1(x) = \phi\left(\frac{x_{i+1}-x}{h_i}\right), \quad H_2(x) = \phi\left(\frac{x-x_i}{h_i}\right), \quad H_3(x) = \psi\left(\frac{x_{i+1}-x}{h_i}\right), \quad H_4(x) = \psi\left(\frac{x-x_i}{h_i}\right),$$

where $h_i = x_{i+1} - x_i$, $\phi(t) = 3t^2 - 2t^3$, $\psi(t) = t^3 - t^2$.

Therefore an algorithm for constructing a piecewise cubic interpolant to $\{Vx_i : i = 0, 1, 2, \dots, n\}$ is essentially a procedure for calculating the derivative values d_0, d_1, \dots, d_n as demonstrated by Fritsch and Carlson (1980) and Matlab's CHIP was used here.

Using these derivative coefficients, Matlab scripts were written to automate the procedure of equation (7.1). The data from the ADV measurements was imported from a spreadsheet and interpolated using equations (7.2) and (7.3). To find the net flow, the positive and negative parts of the integral were evaluated using the limits given by the zero crossing and the real zero roots. These points were added to the original velocity profile dataset (Figure 7.6). The exact area under this profile was analytically obtained by using the Newton-Leibniz method of integration for each interval between these points (Figure 7.6) and summed as follows:

$$\sum_{i=0}^{n-1} \int_{x_i}^{x_{i+1}} P(x) dx. \quad (7.4)$$

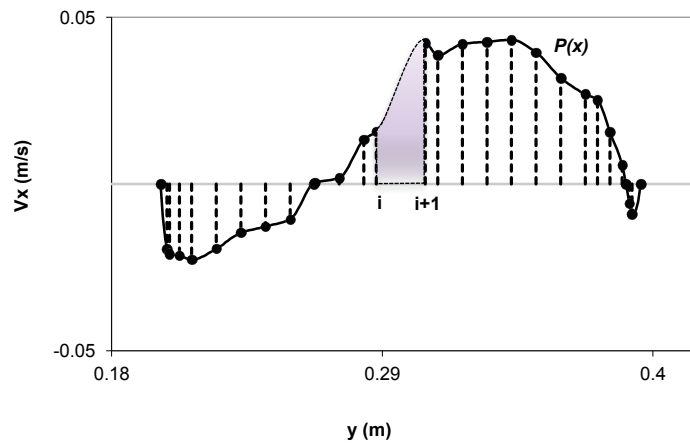


Figure 7.6 Analytically calculating the exact area under a typical spline interpolated velocity profile $[P(x)]$ of a dataset using the definite integral.

7.4 COMPUTATIONAL FLUID DYNAMICS (CFD) STUDY

The current CFD study was based on previous work by Madhani et al. (2009b). The previous 2D simplifications used here avoided the prohibitive computational cost and modelling uncertainties involved in a fully three-dimensional approach, and also permitted an investigation of the benefits or otherwise of increased numerical resolution for the prediction of experimentally observed near-wall flow features at the surface. This modelling approach here assumed a steady state flow regime with a quiescent free surface of constant fixed height throughout the computational domain. A 2D two-equation $k-\varepsilon$ (denoted SKE) turbulence model was deployed (in Fluent® 6.3, ANSYS, Sydney, New South Wales, Australia) with either standard or near-wall modelling functions used to compute the mean surface flow field $u_i(x, y)$ ($i = 1, 2$).

Turbulence modelling

To model the turbulence, Cartesian x and y axes were defined along and perpendicular to the primary flow direction in the GPT scale model, and Reynolds Averaged Navier Stokes (RANS) equations were used to describe the steady incompressible mean flow quantities for a given set of inlet conditions. The standard two-equation $k-\varepsilon$ (denoted SKE) turbulence model was used, where the turbulent viscosity, the turbulent kinetic energy, k and the dissipation rate, ε are described by the equations:

$$\frac{\partial}{\partial x_i}(\rho k u_i) = \frac{\partial}{\partial x_j} \left[\left(\mu + \frac{\mu_t}{\sigma_k} \right) \frac{\partial k}{\partial x_j} \right] + G_k - \rho \varepsilon. \quad (7.5)$$

$$\frac{\partial}{\partial x_i}(\rho \varepsilon u_i) = \frac{\partial}{\partial x_j} \left[\left(\mu + \frac{\mu_t}{\sigma_\varepsilon} \right) \frac{\partial \varepsilon}{\partial x_j} \right] + G_\varepsilon \frac{\varepsilon}{k} G_k - C_{2\varepsilon} \frac{\varepsilon^2}{k}. \quad (7.6)$$

In equations (1) and (2) $G_k = \mu_t S^2$ is the turbulent production term, where $S \equiv \sqrt{2S_{ij}S_{ij}}$ is the modulus of the mean rate of strain tensor $S_{ij} = \frac{1}{2} \left(\frac{\partial u_i}{\partial x_j} + \frac{\partial u_j}{\partial x_i} \right)$, the turbulent viscosity $\mu_t = C_\mu \frac{k^2}{\varepsilon}$, and the constant values are: $C_\mu = 0.09$, $\sigma_k = 1.0$, $\sigma_\varepsilon = 1.44$, and $C_{2\varepsilon} = 1.92$.

Regarding the boundary conditions for the SKE model, standard logarithmic wall functions were used. The influence of near-wall modelling in the 2D flow field prediction was also investigated using an SKE model with enhanced wall treatment (EWT). Both these wall modelling approaches have been previously described in depth, together with the computational grid, numerical method and the outcome of the grid sensitivity analysis (Madhani et al., 2009b). Briefly, across the inlet, a uniform axial velocity profile according to the measured flow rate of 1.3 L/s was specified. Inlet turbulence levels were specified using values of 0.144 m (turbulence length scale) and 5% (turbulence intensity) in the CFD code, Fluent. Here, a second order upwind discretisation was chosen for the convective term in transport equations, and the velocity-pressure coupling was resolved via a SIMPLE-type algorithm. With these solver controls, the time independent velocity flow field was computed. The iterative solver was deemed to have converged and further iterations terminated when a convergence criterion of less than 10^{-5} (c.f. default solver setting of $CC = 10^{-3}$) for the scaled residuals in the computed mean and turbulence quantities was achieved. The outcome of the CFD study predicted the mean flow structure, which consisted of a deflected entry jet and a large recirculation zone within the retention area of the GPT. A detailed discussion on these larger and smaller flow features important for understanding the capture/retention characteristics of the GPT has also been published (Madhani et al., 2009b).

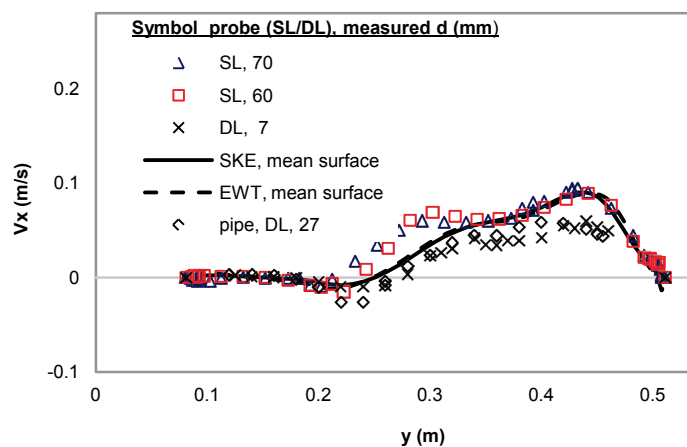
7.5 RESULTS AND DISCUSSION

We commence the discussion by examining the experimental axial velocity profiles across three cross sections of the channel-inlet-configured GPT for the inlet flow conditions described in Table 7.1. Run 1, in Table 7.1 is a repeat of an earlier investigation performed with a pipe-inlet-configured GPT at a fixed depth (Madhani et al., 2009b). Minor differences were noted between the lower profiles of the previous and the current dataset across the inlet region but further inside the GPT these profiles eventually coincided (Figures 7.7-7.9). Overall, the current dataset gives a more detailed distribution of velocities at critical sections of the GPT across the width and depth of flow. For instance, at the inlet region, this data shows the asymmetrical distribution of flow velocities in both directions due to the sudden geometrical expansion of the GPT (See St. 1, Figure 7.7). At the trap entry, the flow entered a narrow opening where the velocities are redistributed to account for outgoing fluid (See St. 2, Figure 7.8). The fluid entering and leaving the retention area results in a near two-dimensional recirculation pattern (See St. 3, Figure 7.9).

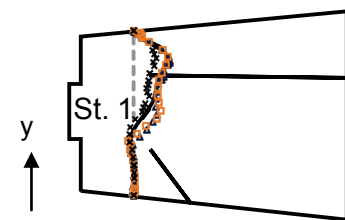
The approximately two-dimensional flow in the experimental setup (Run 1 and 2, Table 7.1) has been previously used to compare measured with the computed values. The computed values from both the SKE and EWT turbulence models are shown in Figures 7.7-7.9 and in general show better comparison with the newer but more comprehensive dataset. In the bulk flow, the computed values, which are not corrected for depth, show good correlations with the measured profiles. Differences were noted in the near-wall velocities, which appear to be higher in most cases for the EWT predictions and lower for the SKE values (Figures 7.7 and 7.8). The differences between the SKE and EWT predictions are mainly attributed to the implementation of the wall boundary conditions (Madhani et al., 2009b). However, both these CFD models under predicted the experimental shear velocity gradients in the retention area and in the bypass (Figure 7.9). A better comparison was achieved with the same inlet velocity but deeper flow conditions (Run 2, Table 7.1), not shown, for the sake of brevity.

Figures 7.7, 7.8 and 7.9 are also typical for the remaining inlet flow rates investigated. It was generally observed with these profiles that maximum velocity did not always occur at the free surface. However, near the inlet with maximum flow rate, profile variations across the depth of water were noted, particularly for the

higher flow rate (Figures 7.10 and 7.11). These flow regions were further complicated by the high negative shear velocity gradients next to the inner wall, as shown on the right of Figure 10 (See $y > 0.29 < 0.4$ m on the abscissa). Such velocities were caused by the detachment of the flow due to the deflection of the entry jet into the bypass (Madhani et al., 2009b). Consequently, the geometrical configuration of the ADV probe disturbed these velocities and shielded the nature of the flow in these regions. To some degree, the shielding was observed visually when measurements were compared between the side and down-looking probes. While in some flow regions the probes gave similar readings, the dampening of the velocities were clearly observed (Figure 7.5). This is further demonstrated by measurements taken at lower inlet flow conditions at similar depths with these two probes (Figure 7.12). The measurement uncertainties were attenuated since the down-looking probe was incapable of measuring close to the walls and the minimum floor distance with the side-looking probe was 30-40 mm. In these sensitive regions, measurements were taken repeatedly to minimise uncertainty.



(a) Velocity profiles at St. 1.

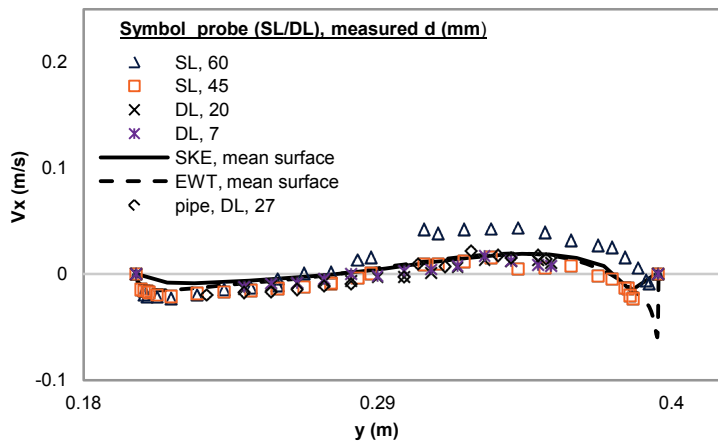


(b) Plan view of St. 1.

Notes for legend Figure 7.7 (a).

(1) Water depth = 100 mm, (2) Distance measured from floor, (3) SKE– 2D CFD/standard wall functions and (4) EWT–2D CFD/enhanced wall functions.

Figure 7.7 (a) Experimental and computed axial velocity profiles (Run 1, Table 7.1) at St. 1 (b). Measurements taken with 3D side (SL) and down-looking (DL) ADV probes. Comparisons are made with the previous dataset (pipe, DL, 27) for the pipe-inlet-configured GPT taken at 27 mm from floor, and with the 2D CFD simulation (Madhani et al., 2009b).



(a) Velocity profiles at St. 2.

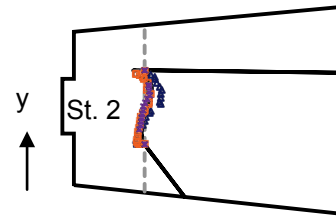


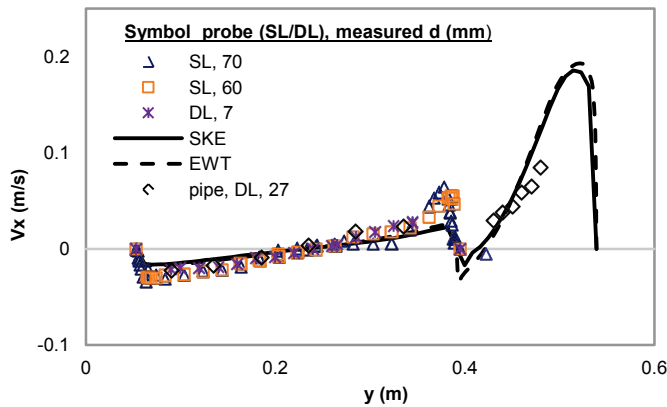
Figure 7.7

(b) Plan view of St. 2.

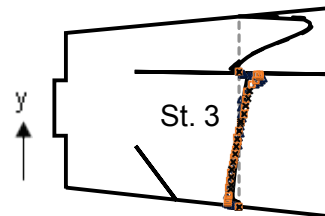
Notes for legend Figure 7.8 (a).

(1) See notes in Figure 7.7.

Figure 7.8 (a) Experimental and computed axial velocity profiles (Run 1, Table 7.1) at St. 2 (b). Measurement taken with 3D side and down-looking ADV probes Comparisons are made with the previous dataset (pipe, DL, 27) for the pipe-inlet-configured GPT taken at 27 mm from floor, and with the 2D CFD simulation (Madhani et al., 2009b).



(a) Velocity profiles at St. 3.

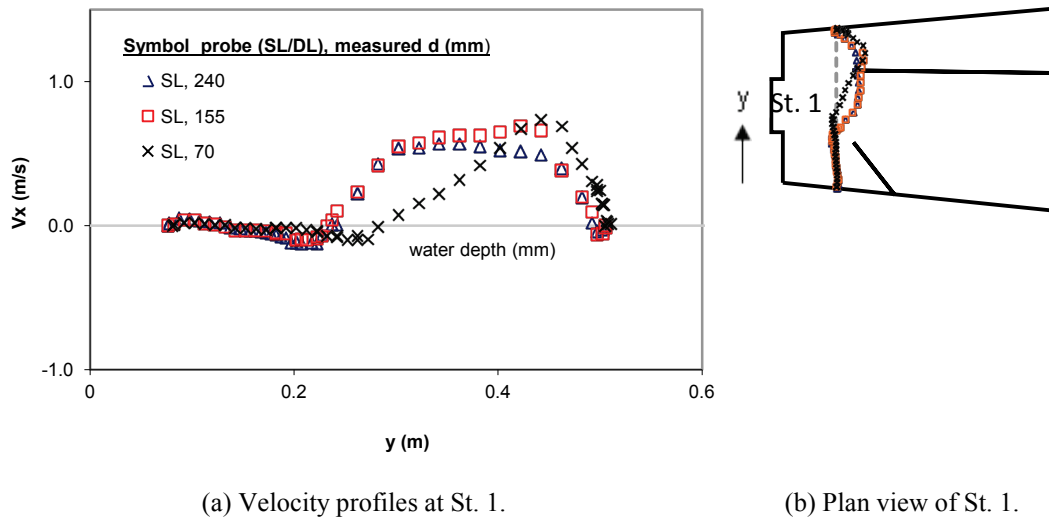


(b) Plan view of St. 3.

Notes for legend Figure 7.9 (a).

(1) See notes in Figure 7.7 (a).

Figure 7.9 (a) Experimental and computed axial velocity profiles (Run 1, Table 7.1) at St. 3 (b). Measurement taken with 3D side and down-looking ADV probes. Comparisons are made with the previous dataset (pipe, DL, 27) for the pipe-inlet-configured GPT taken at 27 mm from floor, and with the 2D CFD simulation (Madhani et al., 2009b).



Notes for legend Figure 7.10 (a).

1. Water depth = 300 mm.
2. See notes in Figure 7.7 (a)

Figure 7.10 (a) Experimental axial velocity profiles (Run 4, Table 7.1) at St. 1 (b). Measurement taken with 3D side and down-looking ADV probes.

In view of the uncertainty, the ADV measurements were examined to investigate the net flow across each station by integrating the velocity profiles as described in the Data Analysis Section. The results for all the runs at the inlet region are tabulated in Table 7.3, good correlations were achieved with the measured flow rate at the collection tank. Figure 7.13 shows the integrated and net flow data for all three stations along with the previous results without near-wall measurements (Madhani et al., 2005). Measurements in the bypass (outlet) were not possible for Runs 2-4 due to the turbulent nature of the flow [see Q_{3out} in Figure 7.13 (a)] and in all cases where the geometry of the passage was restricted for ADV measurements such as at station—St. 2. The results tabulated in Figure 7.13 were based on net percentage error between the positive and negative integrals obtained from the profiles at each station (Table 7.4). In Table 7.4, an overall average error of 10% was achieved due to the complex region under which the measurements were taken. Furthermore, in areas inaccessible to ADV probes such as between the walls and floor, a series of data fits was used to estimate the end conditions for the bottom profiles. In evaluating the percentage of the net flow rate, the average depth of flow

was generally taken between each profile, while in Figure 7.13 (a) the flow at the inlet was assumed to be 100%.

Table 7.3 Integrated data (Q_I) across station St. 1, see key diagram in Figure 12 (b) and the measured flow rate (Q_t) at the collection tank .

Run (Table 7.1)	Q_I (L/s)	Q_t (L/s)	% error
1	1.4	1.3	7.6
2	4.1	3.9	4.8
3	6.1	6.1	<1
4	35.4	33.3	6.2

Table 7.4 Error between positive and negative integrals at St. 1 and 2 (See Figure 7.13).

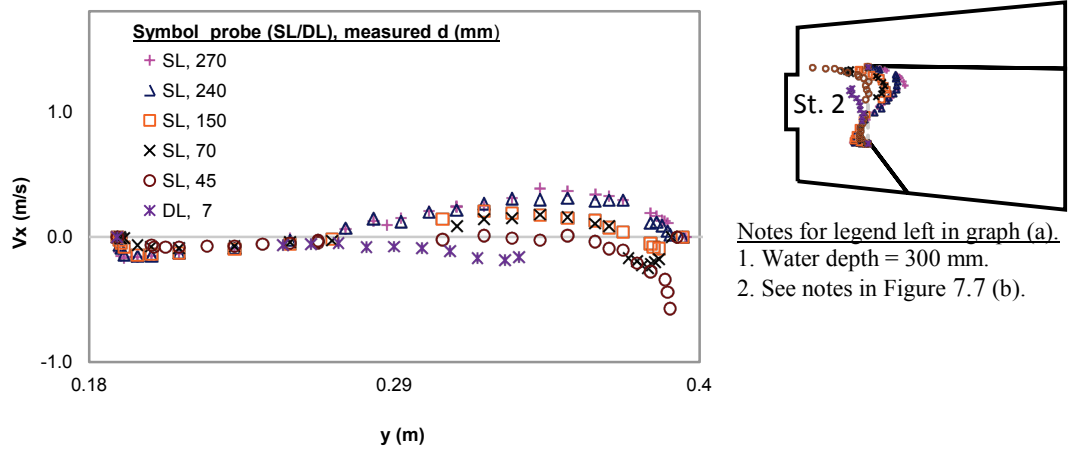
Run (Table 7.1)	Net balance error (%)		
	Q_2	Q_3	Q_{3out}
1	5.1	3.1	1.5
2	8.0	12.4	4.8
3	8.8	2.0	-
4	1.4	6.7	-

The proportion of fluid directly bypassing the retention area of the GPT was estimated by determining the net flow [See $Q_1^+ - Q_2$, Figure 7.4 (a)] between the inlet and trap entry region (St. 1 and 2). This estimation assumes that there is no fluid recirculating at St. 2).

The percentage of fluid directly bypassing the retention area appears to be consistent for all experimental runs with an average of approximately 80%. This trend indicated that the capture and retention characteristics of the GPT with fully blocked retaining screens would be poor. Such indications have since been confirmed by experiments in which an average of 4% capture/retention was achieved for this GPT configuration with fully blocked screens (Madhani and Brown, 2010).

The hydrodynamic experiments also show that a blocked GPT will allow incoming pollutants to escape via the bypass, thus preventing the blockages from extending upstream. The head loss of fully, partially blocked and no screens was also investigated at various flow rates (Figure 7.14). The trends in Figure 7.14 indicate

that the hydraulic performance of the GPT with fully blocked screens is reduced when they are blocked beyond ~70%.



(a) Velocity profiles at St. 2.

(b) Plan view of St. 2.

Notes for legend Figure 7.11 (a)

1. Water depth = 300 mm.
2. See notes in Figure 7.7 (a).

Figure 7.11 (a) Experimental axial velocity profiles (Run 4, Table 7.1) at St. 2 (b). Measurement planes taken with 3D side and down-looking ADV probes.

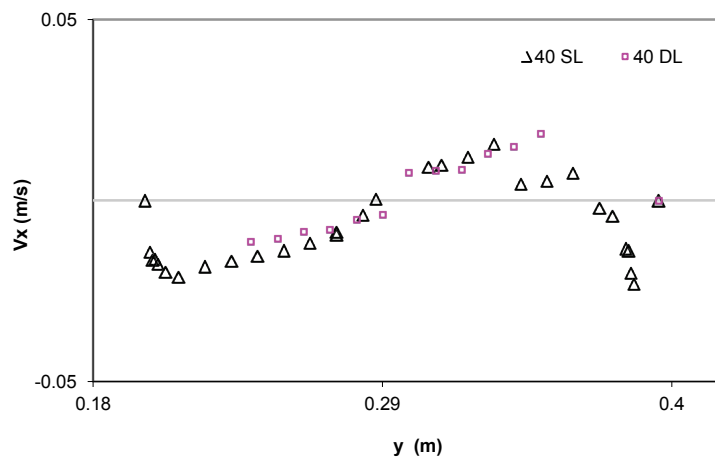
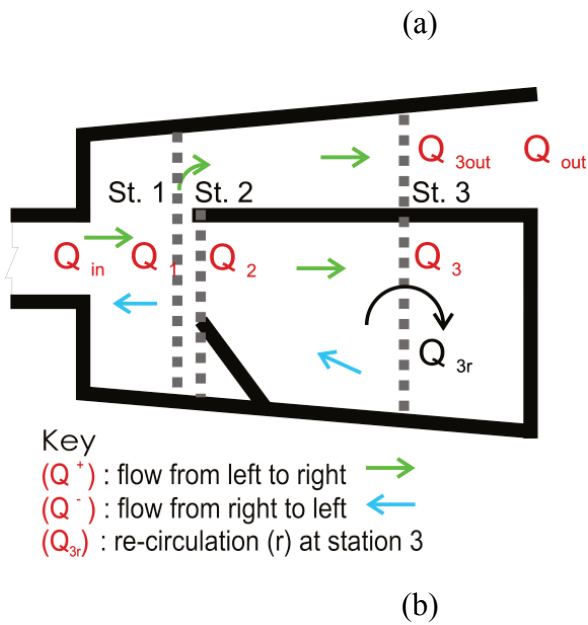


Figure 7.12 Measurement comparison at the trap entry (St. 2) between the side-looking (SL) and the down-looking (DL) ADV probes at 40 mm distance from the floor for Run 1 (Table 7.1).

Run (See Table 7.1)	Percentage (%) of net flow (Q_n)							
	Inlet	St. 1		St. 2	St. 3	**St. 2/St. 3	St. 3	
	Q_{in}	Q_1^+	Q_1^-	Q_2	Q_3	$Q_1^+ - Q_2$	Q_{3r}	Q_{3out}
1	100	97	3	18	19	79	1	97
2	100	96	4	20	21	76	2	97
3	100	93	7	21	33	72	12	-
4	100	94	6	12	19	82	7	-
*	100	-	-	26	22	74	4	-

** $Q_1^+ - Q_2$ estimates the portion of fluid by passing the retention area (assuming that the fluid does not recirculate at St. 2).

* (Madhani et al., 2005)



Note:
The flow rates at the three stations are given by:

$$Q_n = \frac{(Q_n^+ + Q_n^-)}{2}$$

Where Q_n^+ represents the downstream flow at station n (n = 1, 2, 3) and the upstream flow is designated by Q_n^- .

Figure 7.13 (a) Percentage of net flow at the three cross sections of the GPT (St. 1, St. 2 and, St. 3) and, (b) key diagram.

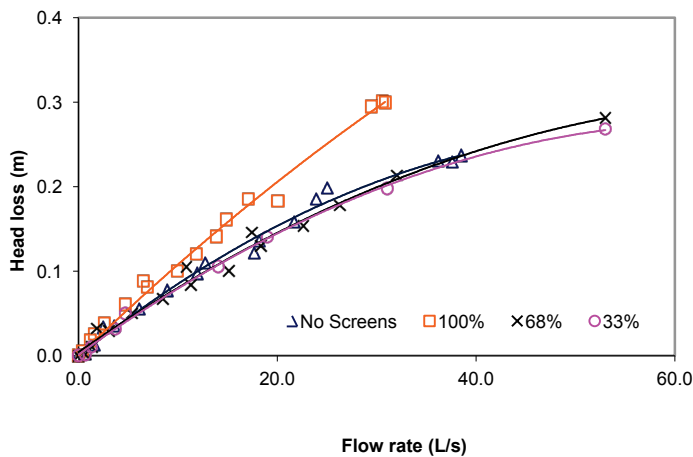


Figure 7.14 Head loss experiments with various screen blockages (100%, 68% and 38%) and no screens.

7.6 CONCLUSION

The potential capture/retention characteristics of a gross pollutant trap (GPT) with fully blocked screens were evaluated using a combination of experimental and data processing methodologies. The methodology developed for this research facilitated a rigorous hydrodynamic assessment of the GPT which can be applied to other treatment devices. This was achieved by conducting detailed velocity measurements at critical sections of the GPT. The collected data was integrated using a mathematical fit with a piecewise cubic interpolating polynomial to analyse the net internal flow. The quality of the data collected was also examined to assess the technique developed for measurements in confined spaces due to the internal configuration of the GPT and the acoustic Doppler velocimeter (ADV) probe. Head loss experiments and computed data were also reported.

The main findings reveal that the hydrodynamic performance rapidly deteriorates when the internal screens of the GPT are blocked. The result showed that less than approximately 80% of the fluid entering the GPT escaped via the bypass for all inlet flow conditions investigated. Subsequently, gross pollutants entering the trap will, in general, follow this flow with the same consequence. The computational fluid dynamics (CFD) velocity profiles were in good agreement with the experimental data for the same inlet flow conditions. Head loss experiments with various screen blockages also indicate that the hydraulic performance of the GPT falls drastically above 70%.

The methodology developed and tested here, demonstrates the usefulness and effectiveness of describing rigorously the hydrodynamic and in turn the capture/retention characteristics of a GPT under typical operating conditions. Similar GPTs have received little attention in scientific research since velocity measurement techniques are generally difficult to perform in these devices, as was demonstrated in this research. This technique is also capable of highlighting positive design features such as a bypass in the case of a fully blocked GPT. Further work is recommended to extend the measurements and the CFD technique in order to investigate a wider range of design configurations.

ACKNOWLEDGEMENTS

The authors acknowledge the sponsors C-M Concrete Pty. Ltd, (2004) for their ARC linkage grant support and the assistance of Sarita Gupta Madhani. We would like to thank under/postgraduates Khoo Jit Hong and Fan Yang for their experimental assistance.

REFERENCES

- Abad, J. D., Musalem, R. A., Garcia, C. M., Cantero, M. I. and Garcia, M. H. (2004). Exploratory study of the influence of the wake produced by acoustic Doppler velocimeter probes on the water velocities within measurement volume. In G. Sehlke, D. F. Hayes and D. K. Stevens (Eds.), *Critical Transitions in Water and Environmental Resources Management: Proceedings of World Water and Environmental Resources Congress 2004* (pp. 267-276). Salt Lake City, Utah, USA: American Society of Civil Engineers (ASCE).
- Chanson, H. (2008). Acoustic Doppler velocimetry (ADV) in the field and in laboratory: practical experiences. In L. Frédérique and C. Hubert (Eds.), *Experiences and Challenges in Sewers: Measurements and Hydrodynamics: International Meeting on Measurements and Hydraulics of Sewers IMMHS'08: Summer School GEMCEA/LCPC* (pp. 49-66). Brisbane, Australia: Department of Civil Engineering, The University of Queensland, Queensland.
- Finelli, C. M., Hart, D. D. and Fonseca, D. M. (1999). Evaluating the spatial resolution of an acoustic Doppler velocimeter and the consequences for measuring near-bed flows. *Limnology & Oceanography*, 44(7), 1793-1801.
- Fritsch, F. N. and Carlson, R. E. (1980). Monotone piecewise cubic interpolation. *Society for Industrial and Applied Mathematics (SIAM) Journal on Numerical Analysis*, 17(2), 238-246.

- Huggins, D. L., Piedrahita, R. H. and Rumsey, T. (2005). Use of computational fluid dynamics (CFD) for aquaculture raceway design to increase settling effectiveness. *Aquacultural Engineering*, 33(3), 167-180.
- Klepiszewski, K. (2009). Sustainable urban water management in Central Europe – how can we prove its treatment efficiency? *Sustainable Water Management: Promoting Internationally Leading Research in Sustainable Urban Water Management at Scottish Universities: Telford Institute Workshop 2009* University of Edinburgh, Edinburgh, Scotland: Telford National Institute.
- Kraus, N. C., A., L. and R, C. (1994). New acoustic meter for measuring 3D laboratory flows. *Journal of Hydraulic Engineering*, 120(3), 406-412.
- Kwon, S. B., Park, N. S., Lee, S. J., Ahn, H. W. and Wang, C. K. (2006). Examining the effect of length/width ratio on the hydro-dynamic behaviour in a DAF system using CFD and ADV techniques. *Water Science and Technology*, 53(7), 141-149.
- Lemmin, U., Lhermitte, R., Nikora, V. I. and Goring, D. G. (1999). ADV measurements of turbulence: can we improve their interpretation? *Journal of Hydraulic Engineering*, 125(9), 987-988.
- Lohrmann, A., Cabrera, R. and Kraus, N. C. (1999). Acoustic-Doppler velocimeter (ADV) for laboratory use. In C. A. Pugh (Ed.), *Proceeding of Conference on Fundamentals and Advancements in Hydraulic Measurements and Experimentation* (pp. 351-365). Buffalo, New York: American Society of Civil Engineers (ASCE).
- Lundh, M., Jönsson, L. and Dahlquist, J. (2001). The flow structure in the separation zone of a DAF pilot plant and the relation with bubble concentration. *Water Science & Technology*, 43(8), 185-194.
- Madhani, J. T. and Brown, R. J. (2010). An investigation of the capture and retention characteristics of a gross pollutant. *Water Research* (Under review).

- Madhani, J. T., Dawes, L. A. and Brown, R. J. (2009a). A perspective on littering attitudes in Australia. *The Environmental Engineer: Journal of the Society for Sustainability and Environmental Engineering, The Institution of Engineers, Australia*, 9/10(4/1), 13-20.
- Madhani, J. T., Kelson, N. A. and Brown, R. J. (2009b). An experimental and theoretical investigation of flow in a gross pollutant trap. *Water Science and Technology*, 59(6), 1117-1127.
- Madhani, J. T., Kwek, L. M. K., Brown, R. J., Kelson, N. A. and Frost, R. L. (2005). Investigating the flow field of a stormwater quality improvement device. Paper presented at the *Environmental Engineering & Sustainability (EES)*. Power House, Sydney: Institution of Engineers Australia.
- Madhani, J. T., Young, J., Kelson, N. A. and Brown, R. J. (2009c). A novel method to capture and analyze flow in a gross pollutant trap using image-based vector visualization. *Water, Air, & Soil Pollution: Focus*, 9(5-6), 357-369.
- McLelland, S. J. and Nicholas, A. P. (2000). A new method for evaluating errors in high-frequency ADV measurements. *Hydrological Processes*, 14(2), 351-366.
- Park, N. S., Lim, J. L., Lee, S. J., Lee, K. H. and Kwon, S. B. (2006). Examining the effect of transverse troughs on hydrodynamic behavior in a sedimentation basin with CFD simulation and ADV technique. *Journal of Water Supply: Research and Technology-Aqua*, 55(4), 247-256.
- Precht, E., Janssen, F. and Huettel, M. (2006). Near-bottom performance of the Acoustic Doppler Velocimeter (ADV)—a comparative study. *Aquatic Ecology*, 40(4), 481-492.
- Rusello, P. J., Lohrmann, A., Siegel, E. and Maddux, T. (2006). Improvements in acoustic doppler velocimetry. *Proceedings of the 7th International*

Conference. on Hydrosience and Engineering (ICHE-2006) Philadelphia, Pennsylvania, USA.

Snyder, W. H. and Castro, I. P. (1999). Acoustic Doppler velocimeter evaluation in stratified towing tank. *Journal of Hydraulic Engineering*, 125(6), 595-603.

SonTek/YSI (2006). *ADV Field/Hydra acoustic Doppler velocimeter (Field) technical documentation (CDROM: P/ N 6055-00005 rev – E. 6837)*. Nancy Ridge Drive, San Diego, California, USA: SonTek/YSI.

Ta, C. T., Beckley, J. and Eades, A. (2001). A multiphase CFD model of a DAF Process. *Water Science and Technology*, 39(9), 169-176.

Tyack, J. N. and Fenner, R. A. (1999). Computational fluid dynamics modelling of velocity profiles within a hydrodynamic separator. *Water Science and Technology*, 39(9), 169-176.

Viadero, J. R. C., Rumberg, A., Gray, D. D., Tierney, A. E. and Semmens, K. J. (2006). Acoustic Doppler velocimetry in aquaculture research: Raceway and quiescent zone hydrodynamics. *Aquacultural Engineering*, 34(1), 16-25.

Voulgaris, G. and Trowbridge, J. H. (1998). Evaluation of the acoustic Doppler velocimeter (ADV) for turbulence measurements. *Journal of Atmospheric and Oceanic Technology*, 15(1), 272-289. Retrieved 18 February 2010, from <http://nortek-es.com/biblio/N4000-702.pdf>

Wahl, T. L. (2006). *Window-based viewing and post-processing utility for Acoustic Doppler Velocimeter (ADV) data files*: U.S. Department of the Interior, Bureau of Reclamation, Denver, Colorado. Retrieved 12 December 2006, from http://www.usbr.gov/pmts/hydraulics_lab/twahl/winadv/

[This page has been left blank intentionally]

Chapter 8: A novel method to capture and analyze flow in a gross pollutant trap using image-based vector visualization

Jehangir T. Madhani¹, Joesph Young², Neil A. Kelson² and Richard J. Brown¹

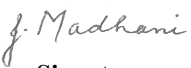
¹School of Engineering Systems

²HPC and Research Support Group

Queensland University of Technology


Publication: Water, Air, & Soil Pollution: Focus, 9(5-6), 357-369.

This chapter is an exact copy of the above journal paper.

Contributor	Statement of contribution
Jehangir T. Madhani	<p>Candidate</p> <p>Experimental design, performed experiments and CFD simulation, collected and analysed the data. Wrote the manuscript and acted as the corresponding author.</p>
 Signature	
8/6/2010 Date	
Joesph Young	<p>Associate Supervisor</p> <p>Guidance on the image based visualisation concepts and assisted with the manuscript.</p>
Neil A. Kelson	<p>Associate Supervisor</p> <p>Assisted with CFD data analysis.</p>
Richard J. Brown	<p>Principal Supervisor</p> <p>Assisted with interpretation of flow field results, reviewed and edited the manuscript.</p>

Principal Supervisor Confirmation

I have sighted email or other correspondence from all Co-authors confirming their certifying authorship.

A/Professor Richard J. Brown		8/6/2010
Name	Signature	Date

ABSTRACT

A novel method is developed to capture and analyze several experimental flow regimes through a gross pollutant trap (GPT) with fully and partially blocked screens. Typical flow conditions and screen blockages are based on findings from field investigations that show a high content of organic matter in urban areas. Fluid motion of neutral buoyant particles is tracked using a high-speed camera and particle image velocimetry (PIV) software. The recorded fluid motion is visualized through an image-based, line integral convolution (LIC) algorithm, generally suitable for large computational fluid dynamics (CFD) datasets. The LIC method, a dense representation of streamlines, is found to be superior to the point-based flow visualization (e.g., hedgehog or arrow plots) in highlighting main flow features that are important for understanding litter capture and retention in the GPT. Detailed comparisons are made between the flow regimes, and the results are compared with CFD data previously obtained for fully blocked screens. The LIC technique is a useful tool for identifying flow structures in the GPT and areas that are subjected to abnormalities difficult to detect by conventional methods. The novel method is found to be useful both in the laboratory and in the field, with little preparation and cost. The enhancements and pitfalls of the LIC technique along with the experimentally captured flow field are presented and discussed.

Keywords Line integral convolution (LIC), Gross pollutant trap (GPT), Litter, Flow visualizations.

Abbreviations

GPT Gross pollutant trap

CFD Computational fluid dynamics

LIC Line integral convolution

ADV Acoustic Doppler velocimeter

PIV Particle image velocimetry

8.1 INTRODUCTION

Stormwater is surface flow runoff from urban areas discharging into receiving waterways. The pollutants collected by stormwater along the path of urban runoff threaten the aquatic and terrestrial ecosystem (Borchardt and Sperling, 1997). This has led to the development of stormwater quality improvement devices (SQIDs) to efficiently trap gross and fine pollutants; for historical overview, see Madhani et al. (2009a). Gross pollutants traps (GPTs) are a class of SQID designed to trap pollutants dimensionally greater than 5 mm. Gross pollutants are defined as visible waste such as litter and organic matter. A linear screening GPT, *LitterBank*, was recently developed by C-M Concrete Pty Ltd. It uses retaining screens to collect gross pollutants prior to the release of the stormwater into natural waterways (Figure 8.1). Currently, there are 20 *LitterBank*s operating at strategic stormwater locations throughout Queensland, Australia.

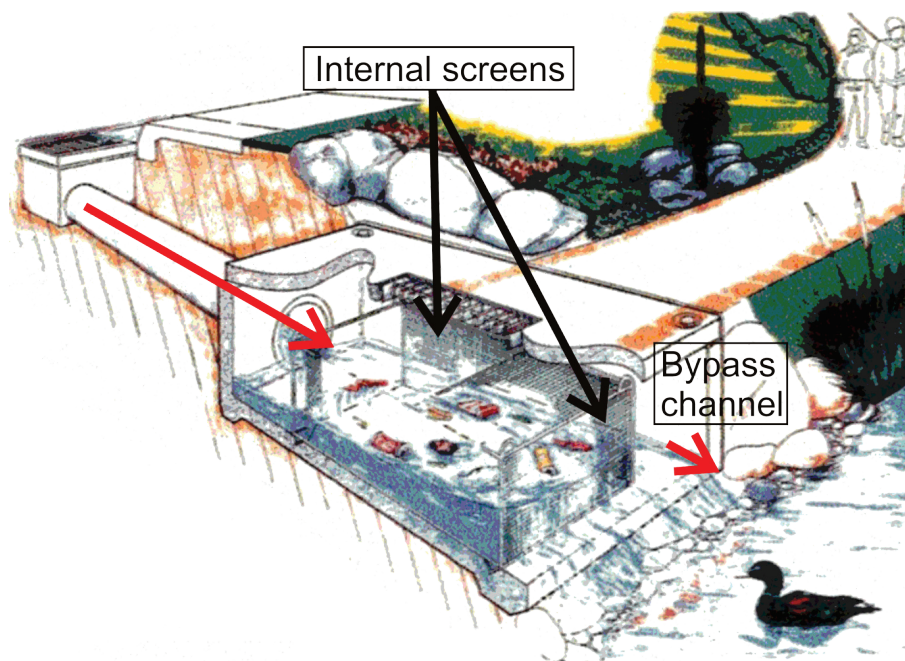


Figure 8.1 GPT—*LitterBank in situ*.

A review of the literature indicates that field monitoring and physical modeling of GPTs with either real or simulated pollutants are well documented, but the hydrodynamic details of velocity vector fields are limited, more so in terms of the flow domain coverage (Madhani et al., 2009b). Engineering flow structures provide

valuable insights into pollutant capture and retention characteristics due to regions of flow recirculation and critical (high and low) velocities. These flow features can cause erosion, containment, and/or mobilization of pollutants (Harwood, 2002). The deposition pattern of particles has been shown to be directly related to the flow pattern observed at the water surface (Stovin et al., 1999). Although computational fluid dynamic simulation is an alternative, modeling uncertainties exist, and validation is often incomplete due to lack of experimental data.

Hydrodynamic characteristics have been investigated previously in an experimental rig consisting of a pipe inlet and a scale model GPT (Madhani et al., 2009b). Velocity profile measurements were taken at a fixed depth throughout the trap with an acoustic Doppler velocimeter (ADV). Full domain flow coverage is extremely laborious using the ADV technique. Furthermore, fluid velocities closer to the free surface are not captured since the ADV probe requires being submerged for proper operations (Madhani et al., 2009b). Consequently, visual observations of surface flow features within the GPT had to be taken due to their likely importance for understanding litter capture and retention.

Advancement of modern optical and digital processing methods has led to capabilities in capturing extensive flow field data rather than single-point ADV measurements in experimental fluid mechanics. Several authors have used a similar particle image velocimetry (PIV) setup to investigate velocity flow fields in other fluidic devices (Hossain et al., 2007; Kandlikar et al., 2009; Li et al., 2009).

In this experiment, a method is developed to analyze several flow regimes through an experimental rig consisting of a rectangular channel inlet and a scale model GPT to study pollutant-free flow in a trap. Typical flow conditions and blocked screens are based on findings from field investigations that show a high content of organic matter in urban areas. Fluid motion of neutrally buoyant particles is tracked using a high-speed camera and PIV software. The recorded fluid motion is visualized through an image-based, line integral convolution (LIC) algorithm.

LIC is widely used in computational fluid dynamic visualization for highlighting both global and local flow features. Direct flow visualization (e.g., hedgehog or arrow plots) may be intuitive but impractical for large 2D or 3D datasets due to visual clutter caused by the dense rendering of arrow glyphs (Telea and van Wijk, 1999). Regions of high velocity where the arrow glyphs become long can also

obscure the clarity of hedgehog visualization; hence, the smaller flow details can be missed. The LIC method, a dense representation of streamlines, is superior to the point-based (direct) flow visualization in providing full spatial flow domain coverage, but the use of streamlines to investigate a whole flow region is difficult since the coverage is highly dependent on the streamline seed points. Kao and Shen (1998) found that LIC images were superior to streamlines in revealing separation and reattachment lines on a model aircraft. However, techniques have been developed that employ streamline-seeding strategies which produce families of streamlines that cover more of the flow domain (Turk and Banks, 1996). Further work is required to test this method on the experimental dataset.

In this investigation, the experimental flow dataset is sufficiently large for an LIC technique to be used. An image-based, LIC algorithm is used to highlight the flow features that are important for understanding litter capture and retention in the GPT. Detailed comparisons are made of the flow regimes and with previously obtained 2D CFD data (Madhani et al., 2009b). The LIC technique with its enhancements and pitfalls, along with the captured flow, are presented and discussed in this paper. Most proprietary GPTs are designed and constructed based on criteria which are often unique to a specific treatment system. Such GPTs will have specific flow structures resulting from their unique patented characteristics that require their own testing program (Rushton et al., 2007). This method is convenient and useful in the preliminary investigation of the flow structure within the GPT, particularly to establish regions of interest.

While acknowledging some uncertainties in the two-dimensional depth coverage, this simplified approach permits the added benefit of investigating a range of flow regimes, which otherwise would be labor intensive.

To the best of the authors' knowledge, work relating to (a) dense, texture-based vector field visualization and (b) flows in GPTs similar to the one studied is limited. This is the first time that texture-based vector field techniques have been used to visualize experimentally collected vector fields.

8.2 FIELD STUDY

Ian Cordery (2005) describes the change in the constitution of gross pollutants in Australian cities over the last 30 years. In the 1970s, street litter was composed of human-derived waste and organic matter in equal quantities. The current trend however exhibits a larger proportion of organic matter. Australian data on gross pollutants first became available in 1986 (Nielsen and Carleton, 1989). An extensive literature review on gross pollutants is conducted from this date and confirms the growing problem of organic matter. For example, volumetric data collected by Nielsen and Carleton (1989) for the Sydney region show that organic matter varied from 22% to 50%. A decade later for the same location, organic matter was found to comprise almost 80% with little variation (Van Drie, 2002).



Figure 8.2 Clippings from grass verge collected at a stormwater drain at Park Road, South Brisbane (2008).

In Melbourne, Allison and Chiew (1995) correlated the composition of gross pollutants in terms of mass with urban land usage. In the two extremes cases, organic matter from light industrial and residential sites varied from 36% to 85% respectively. In mixed commercial and residential areas, organic matter was approximately 65%. Allison et al. (2000) showed volume and mass classifications to be similar and concluded that irrespective of the methods used to analyze the

concentrations of the gross pollutant components, the derived values were usually between 70% and 90% for organic matter and between 10% and 30% for human-derived litter in mixed commercial, industrial, and residential urban centers. A higher trend has been reported for Hobart (Chrispijn, 2004).

Mass data collected from the outer suburbs of Brisbane mainly in residential areas (70-98%) by Brisbane City Council (2004) and Greenway et al. (2002) reveal a similar amount of organic matter (93%) deposited in the GPTs.

The high level of organic matter in stormwater is a cause for concern. Observations during the field study show that grass clippings are often left to accumulate along the roadside (Figure 8.2). Gross pollutants are also a transport mechanism for finer stormwater pollutants. Organic waste blocks stormwater drains and contributes to the nutrients that enter waterways, creating oxygen-depleting substances that are detrimental to the aquatic habitat. Since city planners and architects are promoting the concepts of green walls and roofs in urban centers, buildings clad with vegetation will increase the nutrient load in waterways.

In this field survey, data are collected from the Brisbane central business district (CBD), South Brisbane, and the Burleigh Heads CBD. These sites are chosen to reflect a range of residential and commercial urban activities. The data are collected over a 2-year period which includes photographs and field notes for further analysis. The concentration of gross pollutants is determined by mapping the surface of the littered area on the photograph and using an area ratio method to derive a percentage value. In cases where organic matter and litter were well mixed and difficult to segregate, the waste components were visually approximated.

The results of the field survey consist of data collected from 75 stormwater drains and reveal a high percentage of organic matter (60-70%) in all areas, with the exception of the Brisbane CBD, where human-derived litter such as fast-food packaging, plastic, and beverage containers predominates. The results are on par with findings from other cities (Figure 8.3).

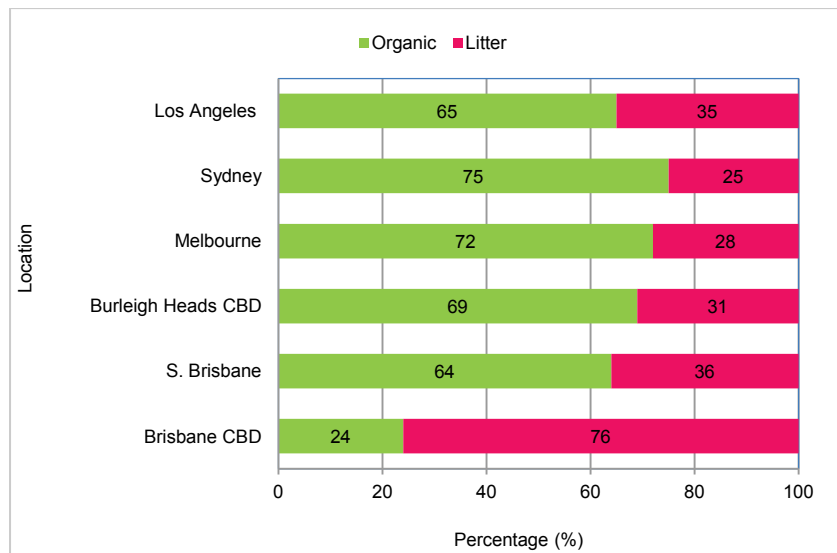


Figure 8.3 Results of the litter field survey taken from 2006 to 2008. Comparison of gross pollutant (organic & litter) data are made with data collected from Sydney (Van Drie, 2002), Melbourne (Lewis, 2002) and Los Angeles (Lippner and Moeller, 2000; Quasebarth et al., 2001).

8.3 PHYSICAL MODELLING

Field monitoring of GPTs in Brisbane indicates that during wet weather, a wide range of inlet, outflow, and other operating conditions occur. For example, the extent and duration of rainfall influence the flow rate entering the trap. The tidal or flood levels of the downstream receiving waterways will determine the outflow level in the GPT (Figure 8.4a). Due to infrequent cleaning, the retaining screens are often found to be blocked with organic matter (Figure 8.4b, c). Partially or fully blocked screens can radically change the litter retention characteristics and flow structure within the GPT, leading, for example, to large recirculating flow patterns within the trap area accompanied by hydraulic short circuiting (Thackston et al., 1987) where the preferred outflow path is via the bypass channel. In this work, fully and partially blocked screens in the GPT are modeled with solid and perforated internal walls, respectively.

Depending on the operating conditions, the possible flow regimes inside the GPT can range from turbulent time-dependent free surface flows to more steady-state conditions, and this presents significant challenges for experimental or numerical studies aimed at understanding the flow and litter retention characteristics of the trap (Madhani et al., 2009b). To facilitate their study of steady-state flow conditions, Madhani et al. (2009b) developed an experimental approach using a down- stream

weir arrangement to control the nature of the flow and the variation in free surface height in the GPT. The weir height can also replicate the elevated outflow water levels into the receiving waterway due to rain or storm events. The experimental approach resulted in a matrix of flow regimes appropriate for a range of low to high operating GPTs (see Table 8.2 below).



(a) Left, high tide downstream causes flooding in the GPT *LitterBank*.

(b) Right, front view of a partially blocked screen with organic matter from incoming stormwater.



(c) Left, fully blocked screens.

Figure 8.4 Field surveys showing the GPT *LitterBank* with (a) high, and (b) low water tidal levels, partially and (c) fully blocked screens.

8.4 EXPERIMENTAL METHOD

The experimental rig (50% scale model GPT) is placed in a square-section (19 m, 0.6 m wide, 0.6 m deep) tilting flume at the QUT hydraulic laboratory. The flume inclination is set to horizontal, and a constant flow rate is established via controller settings on the centrifugal pumps that circulate water from underground storage tanks into the flume. Flow rate readings are checked with periodic measurements in the collection tank at the flume outlet. Flow into the scale model GPT is through a horizontal 1.8-m-length inlet rectangular channel with an internal width of 146 mm. To promote smooth upstream flow conditions, three mesh screens 1 m apart are inserted at the upstream end of the flume.

Table 8.1 Material used in placed of normal screens in the GPT to represent percentage of blocked screens

Material	Blockages (%)
Perspex solid walls	100
Perforated screens (3 mm holes)	68
5 mm mesh	33
No screens	0

Table 8.2 Experimental setup of flow regimes through a GPT with designated blocked screen runs

Flow regime	Weir height (m)	Inlet Velocity (m/s)	Flow Rate (L/s)	Water depth in Trap (m)	Screen blockages %		
					100	68	33
Low	0.108	0.09	1.3	0.1	R1	R3	R5
↑	0.286	0.09	3.9	0.3	R2	R4	R6
↓	0	0.39	6.13	0.1	R7	R9	R11
High	0	2.14	35	0.3	R8	R10	R12

Table 8.1 shows materials used to replace normal screens in the GPT to represent typical blockages found in field studies. The percentage blockages are based on the amount of material obstructing the flow path. To study pollutant-free flow in a trap with fully blocked screens (i.e. 100% blockages) the GPT model is fitted with solid internal walls. A perforated screen with 3 mm circular holes represents 68% blockages while a 5 mm rectangular mesh screen represents 33% blockages.

The measurement runs for the matrix of flow rates based on field investigations are shown in Table 8.2. Flow rates of 1.3 L/s and 3.9 L/s are set with corresponding weir heights of 0.108 and 0.286 m, respectively, at the end of the flume terminus raceway. Some variations in flow conditions ($\pm 10\%$) during the course of the experiments are unavoidable since the constant head tank is not fitted to the flume. Further details on the experimental setup are given by Madhani et al. (2009b). For higher-flow regimes, the weir height is set at the floor level of the raceway (zero).

Flow structures within the GPT are obtained by tracking fluid particle motion with a PIV system supplied by Integrated Design Tools, Inc. (IDT) via SciTech Pty Ltd., Melbourne, Australia. This system comprises a high-speed camera (X-Stream™ XS-4), image acquisition (X-Stream™ Vision version 1.13.05,) and PIV software (proVision-XSTM version 3.08.30). The camera is connected to a PC Pentium 4Mhz, has a 1/4-inch format and is fitted with an 8 mm focal length CCTV lens manufactured by Computar (M0814-MP). The distance from the lens to the GPT floor is 1.5 m, and the vertical view for the maximum water depth coverage is given by: $f \frac{1}{4} vDV$, where f is the focal length, v is the factor dependent on the camera format, D is the distance from lens to object, and V is the vertical (depth) view of field. A vertical view of field of at least 0.5 m is thus obtained for a given factor $v=2.7$. Since the maximum water depth is 0.300 m, adequate focus is achieved for all experimental runs.

The camera is mounted on a tripod and calibrated on a 40-mm gridded paper position inside the scale model GPT (IDT, 2005a). Illumination of the seeded particles is achieved by positioning 1,000-W portable halogen floodlights above the GPT and at the sides. An attempt is made to direct the light in a confined, almost planar area of the intake withdrawal field using slotted sheet metal to enhance the recorded image quality. A polarized lens is also used to reduce the reflection of light from the water surface and internal walls.

The fluid motion of the particles is tracked within the GPT using neutral buoyant particle seeding (20–50 μm), which is introduced into the upstream inlet flow via a feeding system. To avoid clumping of the particles, the outlet seeding tube has to be positioned just below the water surface, and each run is repeated several times. The acquisition rate varies between 30 and 90 Hz depending on the flow rate.

The experimental video recordings from the acquisition software (IDT, 2005b) are exported into the PIV image processing program (IDT, 2005a). A high resolution grid is constructed which covers the entire flow domain within the GPT to generate the x and y coordinates. The PIV program uses tracking algorithms to produce two-dimensional velocity vector fields in terms of the x and y coordinates. The nonuniform velocity data (x , y coordinates and point velocities U_x , U_y) are exported into a text file (filename.plt); typically, each file comprises 5,000 data points.

8.5 THE LINE INTEGRAL CONVOLUTION (LIC)

The line integral convolution method

We begin by describing a vector field and its directional structure in order to define streamlines (Stalling and Hege, 1995). Let v be a vector field, defined by $v : \mathbb{R}^2 \rightarrow \mathbb{R}^2, x^2 \mapsto v(x)$ and let $\sigma(u)$ be an integral path of v , such that:

$$\frac{d}{du} \sigma(u) = v(\sigma(u)) \quad (1)$$

By definition, the tangent vector of $\sigma(u)$ coincides with v and thus $\sigma(u)$ can be used to depict the orientation of v . For our purposes, it is useful to re-parameterize $\sigma(u)$ by its arc-length s . We note that $\frac{ds}{du} = |v(\sigma(u))|$, and hence

$$\frac{d}{ds} \sigma(s) = \frac{d\sigma}{du} \frac{du}{ds} = \frac{v}{|v|} \equiv f(\sigma(s)) \quad (2)$$

In other words, by normalizing v , we can calculate σ as a function of its arc-length s . This re-parameterization is only valid when $|v| \neq 0$, i.e., for non-degenerate curves σ . A streamline through x can be calculated by solving the ordinary differential equation (1).

We describe the LIC method where the flow domain is represented by dense streamlines. This method has received considerable interest because global and local flow details are visualized throughout the spatial domain. The generation of LIC based textures or images of a vector field v can be described as the blurring of a white-noise input texture I along the streamlines of v .

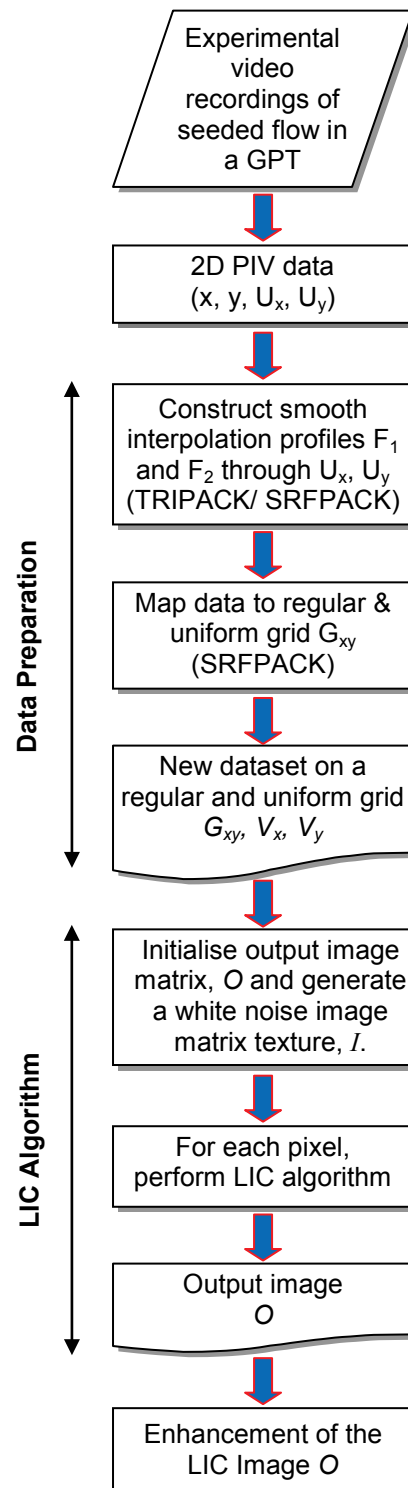


Figure 8.5 Overall view of the steps for producing the LIC image

This method was originally developed by Cabral and Leedom (1993) and the modification proposed by Stalling and Hege (1995) is currently used here. Given a streamline σ , the LIC technique calculates the intensity $O(x_0)$ for a pixel located at x_0 as follows:

$$O(x_0) = \int_{x_0-l}^{x_0+l} k(s)I(\sigma(s))ds \quad (3)$$

Here, I denotes a random noise input texture image (we use a white-noise image) and $k(s)$ is a smoothing one-dimensional filter kernel; l is the length of both the forward and backward streamlines; O is the output (LIC) image. We use a box filter where $k(s) = 1$, $x_0-l \leq s \leq x_0+l$ and 0 otherwise. The convolution integral (3) is discretized by taking L steps of length h along both forward and backward streamlines seeded from x_0 . This leads to the following:

$$O(x_0) = \frac{1}{2L+1} \sum_{i=-L}^L k(x_i)I(x_i), \quad x_i = \sigma(ih) \quad (4)$$

Our method for generating LIC images of the vector field v has two parts: an interpolation process followed by the application of the LIC algorithm as described by Stalling and Hege (1995). The interpolation process allows the vector field v to be mapped onto a uniform Cartesian grid G_{xy} that is amenable to the LIC algorithm. Each point of the uniform grid corresponds to a pixel of the output LIC image O . In this case, the experimental process generates the vector field v with velocities located at irregularly scattered points. An overview of the steps performed in creating a LIC image from a scattered set of experimentally generated sampled velocities is shown in Figure 8.5.

The interpolation process is implemented to use two-dimensional cubic spline interpolations (Renka and Cline, 1992), which are applied successively to the irregularly spaced stream (U_x) and crosswise (U_y) velocities to generate two surfaces F_x and F_y respectively. SRFPACK (ACM, 1996) is a fast, robust code for the interpolation of scattered data; it is used to carry out the interpolations. It is a FORTRAN 77-based code that allows for the triangulation and calculation of a smooth interpolant through scattered data points, optionally defined within a non-convex domain i.e., arbitrary shaped boundaries. The interpolation consists of a set of three cubic surface patches, defined on each triangular element of a Delaunay

triangulation of the scattered data. (Note, each surface patch is defined on a sub-triangle obtained by joining the vertices to the triangle's barycentre). Using the interpolating surfaces F_x and F_y , the stream and crosswise velocity components are calculated on the regular uniform grid G_{xy} , suitable for the LIC algorithm. We denote the interpolated vector field lying on G_{xy} as $V = [V_x, V_y]^T$.

We have typically generated LIC images of 600 x 800 pixels. The method begins with the initialization of the output image matrix O to zeros, the generation a random white-noise input image I and the normalization the vector field velocities $V = [V_x, V_y]^T$ to unity. If $||[V_x, V_y]^T||$ is near zero, $[V_x, V_y]^T$ is set to $[0, 0]^T$. The normalization enables the convolution integral (3) to be approximated using (4) by sampling the input image I at evenly spaced points x_i along σ . The pseudo-code below describes the LIC algorithm:

STEP 1: Initialization

Initialize the output image O to zeros, generate a random white-noise input image I .

Normalize the vector field $V = (V_x, V_y)^T$ to unity – if a zero (or near zero) vector is encountered, set the vector at this location to $[0, 0]^T$.

STEP 2: Streamline generation and convolution

For each pixel p_{ij} in the output image O

Generate a forward streamline S_f of length L , seeded at pixel p_{ij} (see Note 1 below)

Generate a backwards streamline S_b of length L , seeded at pixel p_{ij} (see Note 1 below)

Construct $S = S_f \cup S_b$

Set $Sum = 0$ (accumulates the sum of all pixel values lying on the streamline S)

For each point S_p on the streamline S

determine the value p_v of the underlying pixel p of the white noise image I ,

we choose the closest pixel p to S_p

$Sum = Sum + p_v$

End

Add $Sum / (\text{Number of pixels on the streamline } S)$ to pixel p_{ij} of the output image O

End

STEP 3: Store or display output image O

It should be noted that:

1. If the streamlines S_f or S_b exit the domain or encounter a zero velocity vector, both streamline calculations are terminated after $K < L$ steps.
2. Along the streamline S at evenly spaced points $x_i, i=1, \dots, K \leq L$, not all of the points x_i will lie on the nodes of the uniform grid G . In this case, we use bilinear interpolation across the rectangular cell containing x_i to determine the underlying velocity vector.
3. We use an accurate fourth-order Runge-Kutta integrator (RK4), with a step size $h = 0.5$, to calculate the points x_i lying on the streamline S . The RK4 method is a fourth-order method.
4. With the integration step size set to $h = 0.5$, it is guaranteed that all pixels lying along the streamline S will be sampled, since pixels are separated by a unit distance.

Enhancement of the LIC Image O

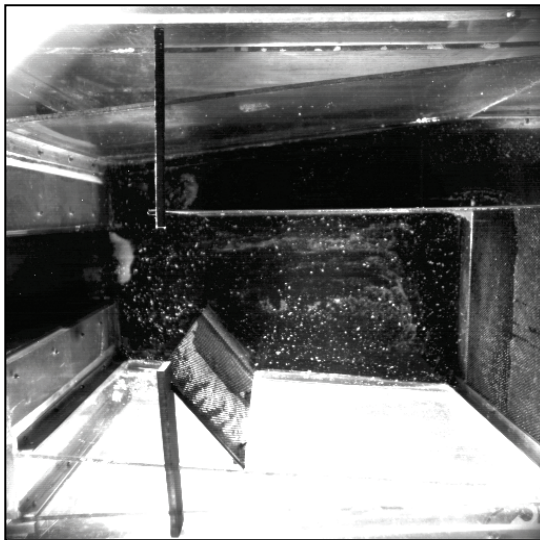
The LIC algorithm repeatedly applies a low-frequency filter [see equation (4)] to the noise input image I . This blurs the image I along the input vector field V . Inherently, the low-pass filter averages the pixel intensities and hence image contrast is lost. One or more image processing techniques are usually applied to the LIC image O to reduce blurring and restore the image contrast. Typical enhancements include high frequency filtering to sharpen the image and histogram equalization to restore contrast. Our implementation allows any general 3x3 image filter to be applied to the LIC image along with histogram equalization. We have experimented with a range of high-pass filters in combination with histogram equalizations and our experience to date indicates that the application of the histogram equalization alone sufficiently enhances image quality. Hence, LIC images included at the end of this paper have been post-processed with histogram equalization.

In the following section, we discuss the application of the LIC algorithm to the experimental PIV data sets.

8.6 RESULTS AND DISCUSSION

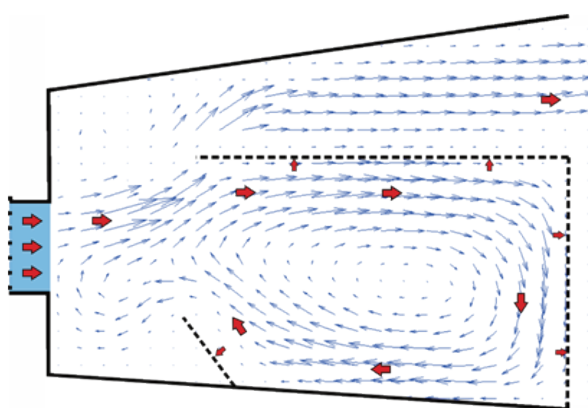
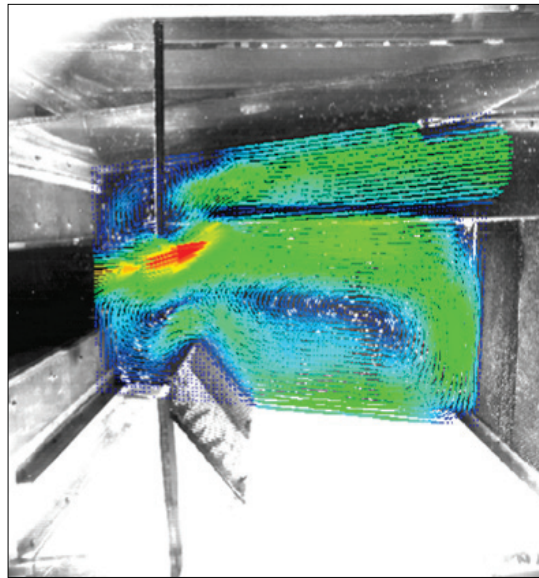
We commence the discussion by choosing an experimental dataset to compare the captured vector field using vector plots with LIC images. Figure 8.6a, b shows a captured flow field for dataset R3, using a camera and a PIV software. Figure 8.6a, a sample of a single frame shot, shows the seeded flow in the GPT with neutrally buoyant particles. Figure 8.6b shows an average statistical image processed PIV vector plot. The vector plot in Figure 8.6b is improved by importing the data into Matlab® (2008b, The MathWorks, Melbourne, Victoria, Australia), and the resulting image is depicted in Figure 8.6c. An attempt to visualize the data using an open-source visualization package (IBM Research Open Visualization Data Explorer, OpenDx version 4.4.0) is also made with no significant improvement in comparison to Figure 8.6c. However, the application of LIC to the same dataset clearly shows superior flow domain coverage particularly for regions of low velocities (R3 in Figure 8.7). The flow structures in the R3 dataset are clear and well defined, indicating sufficient data points were collected. The results demonstrate the potential of the method developed for the purpose of capturing and analyzing flow in a GPT.

To identify flow structures in the LIC images (Figures 8.7 and 8.8), comparisons are made with previous work of the same experimental setup (Madhani et al., 2009b). Here, the main flow structures in a GPT with fully blocked screens for run R1 (Table 8.2) have been theoretically (CFD) and experimentally identified. The CFD flow field is shown in the form of streamlines and a vector plot in Figure 8.9a, b, respectively. The main flow structures consist of the deflection of the entry jet into the bypass channel and the existence of a large recirculation flow within the retention area of the trap (Figure 8.9a). Smaller near-wall features were also observed (Figure 8.9a), such as secondary recirculation (zone 4), flow separation (zone 5), and low-velocity corner eddies (zone 7). These areas may contribute to litter retention and are identified as flow structures that can be optimized in GPT design.



(a) Left, R3.

(b)Right, R3



(c)Left, R3.

Figure 8.6 A single frame capture of the experimental flow for R3 (Table 8.2) with (a) particle seeding, (b) the vector plot from the data processed by the PIV software and (c) the improved vector plot using Matlab (version 2008b) for R3 dataset.

Figures 8.7a and 8.9 generally show good comparisons between the LIC image and the CFD-generated flow domain for the R1 dataset. Most of the smaller flow features are visible unlike the previous ADV-measured flow which lacks spatial flow domain coverage (Madhani et al., 2009b). However, some irregularities or distorted flow patterns are noted behind the baffle (see zone 3 in Figure 8.9a). This area is not clearly sighted by the camera, and the reflective properties of the Perspex baffle would have influenced the low velocities captured. This behavior is not shown for the R3 dataset since the internal structure of the GPT is coated with nonreflective paint. Also, small dark patches are occasionally observed in the LIC images (see corner behind baffle, R1 in Figure 8.7a), which denote very low or zero velocities. Dark patches in the main flow which cause obvious discontinuities are due to either a lack of seeding or to the fact that the overhead structures supporting the baffle and inner wall in the GPT obscure the camera sighting (Figure 8.6a).

In Figures 8.7 and 8.8, the overall flow behavior in the GPT for the given range flow regimes show some similarities in the flow structures for all the experimental runs (see flow feature zone 1, Figure 8.9a). The common flow feature displayed is an inner recirculation in the trap retention area.

For the experimental runs in which the inlet velocities are unaltered, slight differences are observed in the geometrical configuration of the inner recirculation (see flow feature zone 1, Figure 8.9a). These are attributed to the difference in water depth (see R1-R2, R3-R4, and R5-R6, Figure 8.7).

Some distinct differences are noted in the geometrical characteristics of the inner recirculation zones with the 33% blocked screens for the higher-flow regime (Figure 8.7f). Here, the momentum of the entry jet created vortex turbulence motion, resulting in water cascading vertically at the far corner of the retention area (see zone 7, upper right, Figure 8.9a for location in Figure 8.7f) as the water escaped through the screens.

Consequently, the inner recirculation zone is distorted and displaced to the opposite side. Concerning litter capture and retention, preliminary experiments show that a portion of litter rapidly accumulates in this area. However, the turbulence in this flow regime would tend to break up the softer stormwater pollutants.

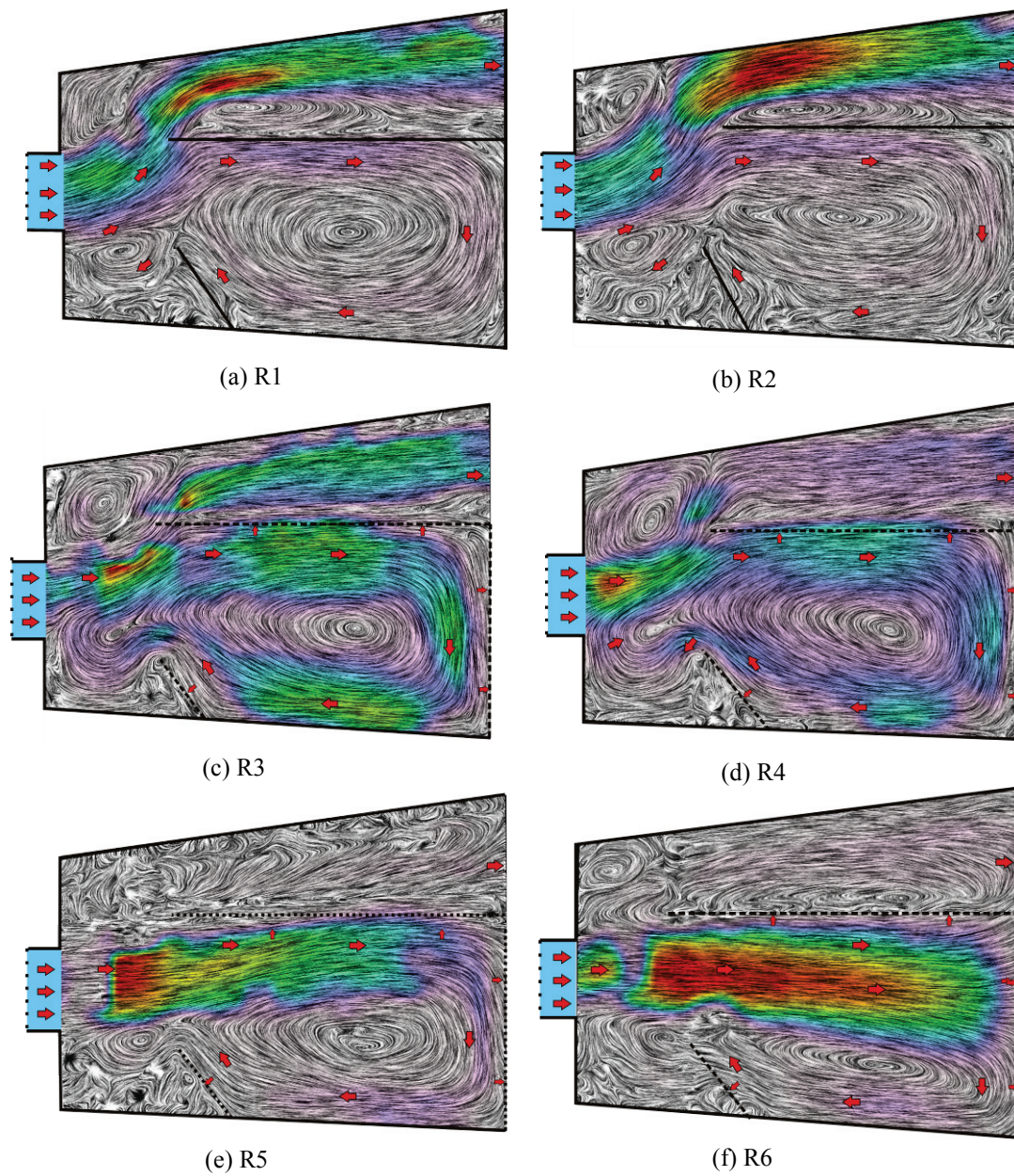


Figure 8.7 Image based vector fields (a) R1, 100% blocked, water depth 0.1m; (b) R2, 100% blocked, water depth 0.3m; (c) R3, 68% blocked water depth 0.1m; (d) R4, 68% blocked water depth 0.3m; (e) R5, 33% blocked water depth 0.1m; (f) R6, 33% blocked water depth 0.3m; (See Table 8.2 for R1 to R6). Color map: red, yellow, green, blue and violet denotes high to low velocities respectively.

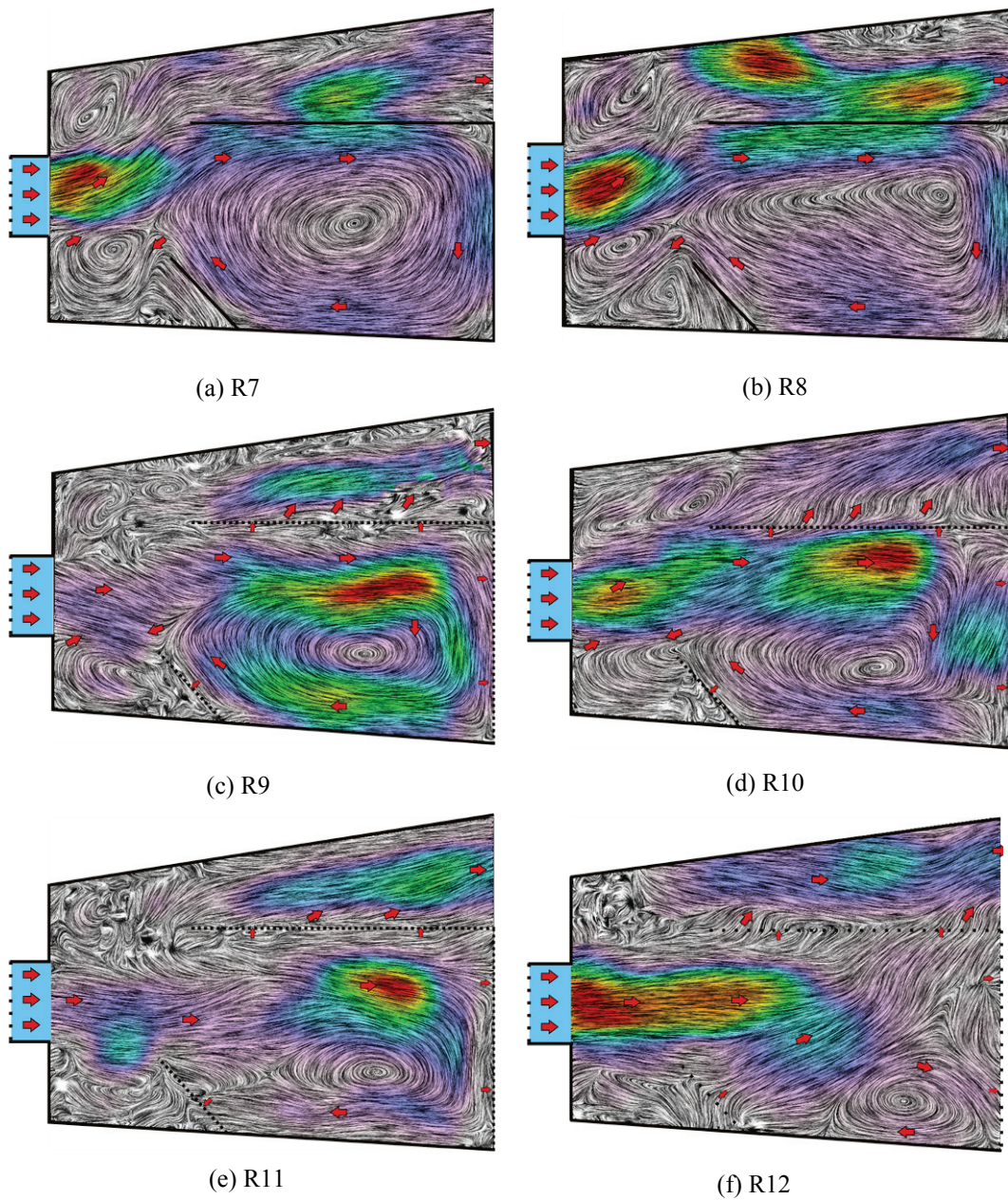
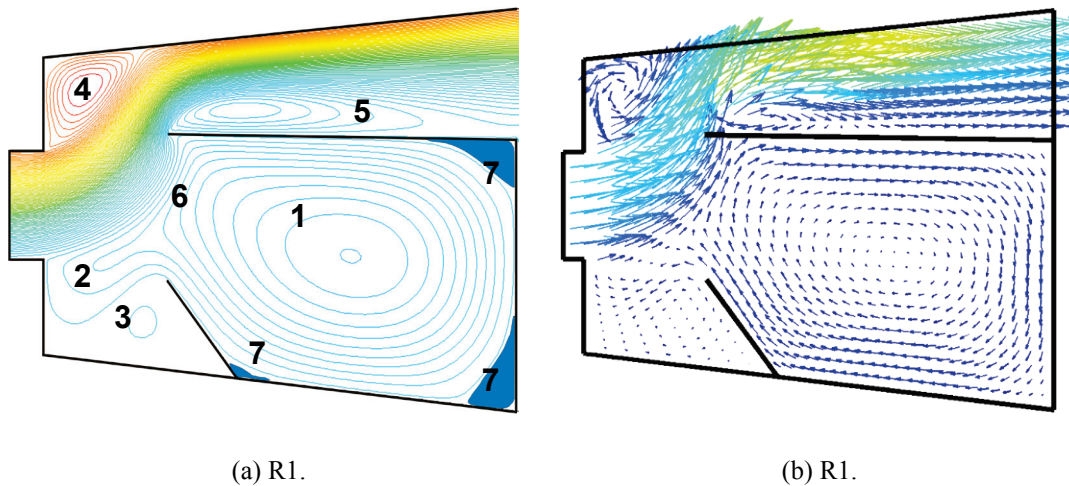


Figure 8.8 Image based vector fields (a) R7, 100% blocked, water depth 0.1m; (b) R8, 100% blocked, water depth 0.3m; (c) R9, 68% blocked water depth 0.1m; (d) R10, 68% blocked water depth 0.3m; (e) R11, 33% blocked water depth 0.1m; (f) R12, 33% blocked water depth 0.3m; (See Table 2 for R8 to R12). Color map: red, yellow, green, blue and violet denotes high to low velocities respectively.

Although the flow structure for the 68% blocked screen (R3 and R4 in Table 8.2) is similar to that of the 100% blocked screen, some differences are observed for the higher inlet flow regimes (6.1 L/s and 35.0 L/s). Unlike the case of a fully blocked GPT (Figure 8.8a and b), the jet entry was not strongly deflected into the bypass channel (Figure 8.8c-f). Hence, the incoming litter is inclined to flow directly into the retention area of the GPT rather than escaping into the bypass channel. Such behavior is observed with the preliminary litter experiments.

Overall, the LIC images are found to be useful in describing the flow structures within the GPT and for better understanding litter capture and retention. The greater flow detail in the LIC images highlighted areas of abnormalities or distortions arising from poor capture techniques caused by issues relating to lighting, particle seeding, or data acquisition rates. Further work is underway to improve the color scheme in order to explore the threshold of the low velocities due to reflected light near the boundaries, which are earmarked by normalized vector plots.



Feature zones

1, inner recirculation; 2, diverticulum; 3, 4, dead zone (secondary recirculation); 5, flow separation; 6, mixing; 7, low-velocity corner eddies.

Figure 8.9 CFD global flow structures for run R1 in Table 2, in form of (a) streamlines and (b) vector plots. Source (Madhani et al. 2009).

8.7 CONCLUSION

A method is developed to capture and analyze several experimental flow regimes through a GPT with fully, partially, and unblocked screens. The recorded fluid motions are visualized through an image-based LIC algorithm and compared with conventional vector plots. The LIC method, a dense representation of streamlines, is found to be superior in highlighting flow features that are important for understanding litter capture and retention in the GPT. Overall, the results demonstrate the potential of the method in capturing and analyzing flow in a GPT. This method was found to be very useful and applicable both in the laboratory and in the field, with little preparation and cost. For the application of field study, further investigation is required using organic particle seeding.

Detailed comparisons are made between the flow regimes, with favorable results compared with the previously defined CFD flow structure for fully blocked screens. The LIC technique is also a useful tool in identifying abnormal flow structures in a GPT, which are often difficult to detect by conventional methods.

The experimental approach previously developed is also found to be useful in controlling a range of flow regimes in the GPT, which are necessary to perform experimental runs. Further work is underway in improving the technique of capturing the flow in the GPT and the method of producing LIC images to address issues with particle seeding and lighting thresholds.

ACKNOWLEDGEMENTS

The authors acknowledge C-M Concrete Pty Ltd. (Mr. Phil Thomas) for its ARC linkage grant support and Ms Sarita Gupta Madhani for assisting with field study and editing.

REFERENCES

Allison, R. A. and Chiew, F. H. S. (1995). Monitoring of stormwater pollution from various land uses in an urban catchment. *Integrated Management of Urban Environments: Proceedings of the Second International Symposium on Urban*

Stormwater Management: Preprints of Papers NCP 95/03 (pp. 511-516). Melbourne, Victoria: Institute of Engineers, Australia.

Allison, R. A., Walter, K. A., Marx, D., Lippner, G. and Churchwell, R. (2000). A method for monitoring and analyzing litter in freeway runoff as part of the Caltrans litter management pilot study. In R. H. Hotchkiss and M. Glade (Eds.), *Building Partnerships: Proceedings of Joint Conference on Water Resource Engineering and Water Resources Planning and Management 2000* (pp. 81-91). Minneapolis, Minnesota, USA: American Society of Civil Engineers (ASCE).

Borchardt, D. and Sperling, F. (1997). Urban stormwater discharges: ecological effects on receiving waters and consequences for technical measures. *Water Science and Technology*, 36(8), 173-178.

Brisbane City Council (2004). Stormwater quality improvement devices (SQIDs) monitoring program summary, *Draft report prepared by Water and Environment City Design for Waterways program*. Brisbane, Queensland: Brisbane City Council.

Cabral, B. and Leedom, L. C. (1993). Imaging vector fields using line integral convolution. Paper presented at the *Proceedings of the 20th annual conference on Computer graphics and interactive techniques*. Anaheim, California, USA: Association for Computing Machinery (ACM).

Chrispijn, J. A. (2004). Assessing different at-source stormwater treatment devices in Hobart: Sullivans Cove and Brooker Highway performance trials. *Stormwater Industry Association (SIA) bulletin* (117), 6. Retrieved 14 January 2010, from <http://www.stormwater.asn.au/tas/Enviro04Paper-Chrispijn.pdf>

Cordery, I. (2005). Field performance of a vortex type gross pollutant trap. *Australian Journal of Water Resources*, 9(1), 49-54.

- Greenway, M., Muth, N. L. and Jenkins, G. (2002). Monitoring spatial and temporal changes in stormwater quality through a series of treatment trains: a case study -Golden Pond, Brisbane, Australia. In Eric W. Strecker and Wayne C. Huber (Eds.), *Urban Drainage 2002: Proceedings of 9th International Conference on Urban Drainage -9ICUD* (pp. 52-68). Portland, Oregon, USA: American Society of Civil Engineers (ASCE).
- Harwood, R. (2002). CSO modelling strategies using computational fluid dynamics. In Eric W. Strecker and Wayne C. Huber (Eds.), *Urban Drainage 2002: Proceedings of 9th International Conference on Urban Drainage -9ICUD* (pp. 8-17). Portland, Oregon, USA: American Society of Civil Engineers (ASCE).
- Hossain, M. Z., Hirahara, H., Nonomura, Y. and Kawahashi, M. (2007). The wake structure in a 2D grid installation of the horizontal axis micro wind turbines. *Renewable Energy*, 32(13), 2247-2267.
- IDT (2005a). *proVision-XSTM user manual for particle image velocimetry (software version 3.08)*. Tallahassee, Florida, USA: Integrated Design Tools, Inc. Retrieved 6 April 2009, from <http://www.idtvision.com>
- IDT (2005b). *X Stream™ Vision cross-platform user manual for high-speed CMOS digital camera (software version 1.13)*. Tallahassee, Florida, USA: Integrated Design Tools, Inc. Retrieved 6 April 2009, from <http://www.idtvision.com>
- Kandlikar, S. G., Lu, Z., Domigan, W. E., White, A. D. and Benedict, M. W. (2009). Measurement of flow maldistribution in parallel channels and its application to ex-situ and in-situ experiments in PEMFC water management studies. *International Journal of Heat and Mass Transfer*, 52(7-8), 1741-1752.
- Kao, D. L. and Shen, H.-W. (1998). Numerical surface flow visualization, *Technical Report, NAS-98-001*. Mountain View, California, USA: National Aeronautics and Space Administration (NASA) Ames Research Center.

- Lewis, J. (2002). *Effectiveness of stormwater litter traps for syringe and litter removal report for Melbourne Water Corporation*. Melbourne, Victoria: Cooperative Reserach Center (CRC) for Catchment Hydrology. Retrieved 14 January 2010, from http://www.clearwater.asn.au/resources/325_1.pdf
- Li, C.-T., Chang, K.-C. and Wang, M.-R. (2009). PIV measurements of turbulent flow in planar mixing layer. *Experimental Thermal and Fluid Science*, 33(3), 527-537.
- Lippner, G. and Moeller, G. (2000). Study quantifies broom sweeper litter pickup ability. *American Sweeper Magazine*, 8(1). Retrieved 14 February 2010, from www.owp.csus.edu/research/papers/papers/PP012.pdf
- Madhani, J. T., Dawes, L. A. and Brown, R. J. (2009a). A perspective on littering attitudes in Australia. *The Environmental Engineer: Journal of the Society for Sustainability and Environmental Engineering, The Institution of Engineers, Australia*, 9/10(4/1), 13-20.
- Madhani, J. T., Kelson, N. A. and Brown, R. J. (2009b). An experimental and theoretical investigation of flow in a gross pollutant trap. *Water Science and Technology*, 59(6), 1117-1127.
- Nielsen, J. S. and Carleton, M. G. (1989). A study of trash and trash interception devices on the cooks river catchment, Sydney. *Investing in Water Futures, the Australian Water Industry in the 1990's:13th Australian Water and Wastewater Association Federal Convention Preprints of Papers NCP No. 89/2* (pp. 23-29). Barton, Canberra, Australia: Institution of Engineers, Australia.
- Quasebarth, T., Schroeder, D., Chappell, R., Churchwell, R. and Lippner, G. (2001). An investigation of factors influencing solids transport and deposition into highway drain inlets. *Bridging the Gap: Meeting the World's Water and Environmental Resources Challenges: Proceedings of World Water and*

Environmental Resources Congress 2001 (pp. 184-194). Orlando, Florida, USA: American Society of Civil Engineers (ASCE).

Renka, R. J. and Cline, A. K. (1992). Scattered data fitting using a constrained Delaunay triangulation. *International Association for Mathematics and Computers in Simulation (IMACS) Transactions on Scientific Computing: AI, Expert Systems, and Symbolic Computation*, 3, 208-214.

Rushton, B., England, G. and Smith, D. (2007). Proposed guidelines for monitoring stormwater gross solids. In K. C. Kabbles (Ed.), *Restoring our natural habitat: World Environmental and Water Resources Congress 2007* (pp. 58-58). Tampa, Florida, USA: American Society of Civil Engineers (ASCE).

Stalling, D. and Hege, H.-C. (1995). Fast and resolution independent line integral convolution. *The 22nd Annual Conference on Computer Graphics and Interactive Techniques-SIGGRAPH 95* (pp. 249-256). Los Angeles, California: Association for Computing Machinery (ACM).

Stovin, V., R., Saul, A., J., Drinkwater, A. and Clifforde, I. (1999). Field testing CFD-based predictions of storage chamber gross solids separation efficiency. *Water Science and Technology*, 39(9), 161-168.

Telea, A. C. and van Wijk, J. J. (1999). Simplified representation of vector fields. In A. C. Telea and J. J. van Wijk (Eds.), *Proceedings of the 10th IEEE Visualization 1999 Conference-VIS 99* San Francisco, California: IEEE Computer Society Washington, DC, USA.

Thackston, E. L., Shields, J. F. D. and Schroeder, P. R. (1987). Residence time distributions of shallow basins. *Journal of Environmental Engineering*, 113(6), 1319-1332.

Turk, G. and Banks, D. (1996). Image-Guided Streamline Placement. In J. Fujii (Ed.), *The 23rd Annual Conference on Computer Graphics and Interactive Techniques-SIGGRAPH 96* (pp. 453-460). New Orleans, Los Angeles:

Association for Computing Machinery (ACM), New York, USA Retrieved 6 April 2009, from <http://lmi.bwh.harvard.edu/~banks/>

Van Drie, R. (2002). Development of a pollutant load algorithm (for Sydney Australia). In Eric W. Strecker and Wayne C. Huber (Eds.), *Global Solutions for Urban Drainage: Proceedings of 9th International Conference on Urban Drainage - 9ICUD* (pp. 207-221). Portland, Oregon, USA: American Society of Civil Engineers (ASCE).

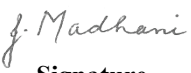
Chapter 9: An investigation of the capture and retention characteristics of a gross pollutant trap

Jehangir T. Madhani and Richard J. Brown

School of Engineering Systems,
Queensland University of Technology


Publication: To be submitted.

This chapter is an exact copy of the above paper pending a journal submission.

Contributor	Statement of contribution
Jehangir T. Madhani	Candidate Experimental design, performed experiments, CFD simulation and data analysis. Wrote the manuscript and acted as the corresponding author.
 Signature	
8/6/2010 Date	
Richard J. Brown	Principal Supervisor Aided in the experimental design conception and data analysis. Reviewed and edited the manuscript.

Principal Supervisor Confirmation

I have sighted email or other correspondence from all Co-authors confirming their certifying authorship.

A/Professor Richard Brown		8/6/2010
Name	Signature	Date

ABSTRACT

A comprehensive methodology and characterisation of gross pollutant behaviour in gross pollutant traps (GPTs) is essential for an efficient design and performance evaluation. Field studies showed that internal screens in GPTs are often blocked with organic matter due to infrequent cleaning. Thus a novel technique was used to investigate the retention characteristic of a GPT with fully and partially blocked internal screens. Custom modified spheres of variable density filled with liquid were released into the GPT inlet and monitored at the outlet. The outlet data shows that the capture/retention performances of a GPT with fully blocked screens deteriorate rapidly. However, screen blockages below 68% approach maximum efficiency during higher flow rates. At lower flow rates, the performance trend is reversed and the variation in behaviour of pollutants with different densities becomes more noticeable. The variable density spheres were characterised further using residence time theory and dye measurements. The experimental dye data is in close agreement with the computational fluid dynamic (CFD) simulation and comparable to the behaviour of partially buoyant pollutants. Additional experiments with a second-upstream-inlet configured GPT showed capture/retention improvements. Intermittent deposits of gross pollutants between rain events were also examined by modelling the blockages in the GPT. Under low flow rates, small changes in residence times were detected indicating little difference in the poor performance between a fully blocked GPT and a partially or empty GPT with fully blocked screens. However, it was also noted that the bypass allows the incoming pollutants to escape when the GPT is blocked. This useful feature prevents upstream blockages between cleaning. Overall, the technique was found to be useful and effective in rigorously describing capture/retention capabilities.

Keywords Dye, gross pollutant trap, GPT, litter, residence time distribution, RTD.

9.1 INTRODUCTION

Gross pollutants are visible waste such as litter and organic matter. Stormwater is surface water runoff from urban areas that is discharged into receiving waterways. Gross pollutants in stormwater collected on the urban runoff path are harmful to the aquatic and terrestrial ecosystem (Madhani et al., 2009a). Consequentially, gross pollutants traps (GPTs) have been developed to play an important role in stormwater treatment [for a historical perspective on GPTs, see Madhani et al. (2009a); other authors are also cited here]. GPTs use internal or retaining screens to trap pollutants dimensionally greater than 5 mm prior to the release of stormwater into natural waterways. A recently developed dry linear screening GPT—the *LitterBank* (by C-Concrete Pty Ltd)—is shown in Figure 9.1 and a plan view with the internal sections is depicted in Figure 9.2. To avoid problems of waste biodegradation and the release of toxic substances, this GPT is designed to be dry.



Figure 9.1 GPT—*LitterBank* in situ.

Dry GPTs such as the *LitterBank* have received little scientific investigation, unlike the water retaining GPTs and other stormwater treatment devices, such as the hydrodynamic separator. To investigate the capture/retention characteristics of these devices experiments have been conducted using mostly real floating litter items

(Phillips, 1999) and artificial pollutants. In those experiments artificial pollutants were chosen for their settling velocities; often, a single type was used for simulating sediment (Luyckx and Berlamont, 2004; Phipps et al., 2004; Phipps et al., 2008). The use of plastic pollutants with different densities has been mentioned briefly elsewhere but no details were given (Armitage and Rooseboom, 1999). Custom modified pollutants with variable densities require lengthy preparation. Thus, tracer dye has been used to study the removal efficiency of hydrodynamic separators and ponds (Persson and Wittgren, 2003; Phipps et al., 2008). However, dye is limited in its representation of varied pollutants, as this research with the GPT *LitterBank* showed.

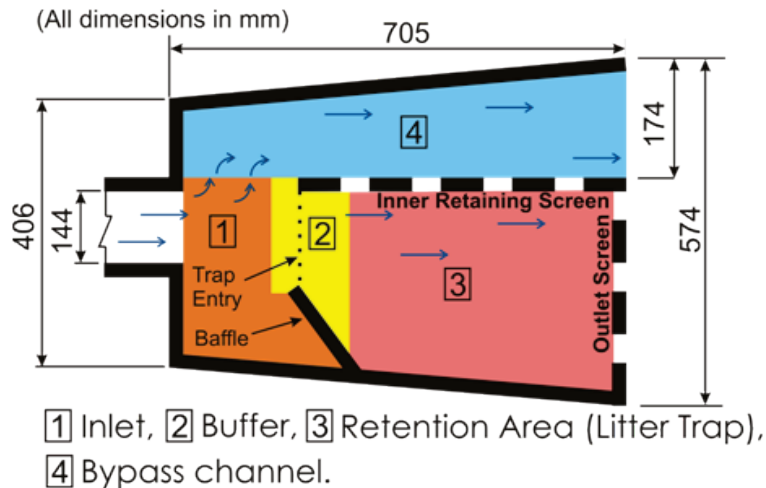


Figure 9.2 Plan view of the gross pollutant trap (LitterBank) with labelled sections.

Previous work (Madhani et al., 2009b) on the dry GPT (*LitterBank*) was based solely on the hydrodynamic aspect of the capture/retention performance of the device using experiments and computational fluid dynamics (CFD). Here, flow features that mobilised and retained gross pollutants have been identified, such as areas of high and low velocities and regions of recirculation. The research has been previously extended to further capture and analyse the pollutant-free flow domain in the GPT for a range of operating and blocked screen conditions (Madhani et al., 2009c). These screen conditions were modelled on findings from field investigations. These

investigations showed that internal screens in GPTs are often blocked with organic matter which can radically change the hydrodynamic and, in turn, the capturing characteristics of the device.

The current experiment comprises the next phase of this broader research where a technique is developed to investigate the capture/retention characteristic of a GPT using artificial pollutants. The custom modified artificial pollutants are large, generic, spherical particles (spheres) filled with liquids to emulate gross pollutants that are floatable, partially buoyant, neutrally buoyant and sinkable. These spheres were released upstream of the channel-inlet-configured GPT either continuously (step function input) or at intervals, and were monitored at the outlet. The capture/retention behaviour of the varied density spheres was investigated using residence time technique and dye measurements.

Dye measurements were performed in a GPT under the worst operating scenario: for example, with fully blocked screens and low flows. Customised scalar dye probes were used in these measurements to monitor the output residence time distribution (RTD) curve, using a step stimulus input function (Madhani and Brown, 2008). The fall (wash-out) method of analysis was used to obtain the experimental RTD curves and the mean residence times (Haas et al., 1997). Comparisons between the experimental data and the CFD predictions were found to be in close agreement and comparable to the behaviour of partially buoyant spheres. These measurements were extended to facilitate the comparison of data from blocked screens with blockages from intermittent deposits of gross pollutants.

The deposits of gross pollutant profiles between rain events were examined by modelling blockages in the GPT. Under low flow rates, small changes in residence times were detected indicating that there was little difference in the poor performance between a fully blocked GPT and a partially or empty GPT with fully blocked screens.

Details of the experimental method (gross pollutant capture and tracer dye measurements), CFD and the residence time theory are presented below. As shown subsequently, overall the method was found to be useful and effective for rigorous description of the GPT's capture/retention capabilities.

9.2 EXPERIMENTAL METHOD

The preparation for the experiments is presented in three stages: the experimental GPT rig and the establishment of flows in the flume, the gross pollutant capture/retention experiments and the tracer dye measurements. The last two are described below under their respective headings. The experimental rig (50% scale model) was placed in a square section (19 m long, 0.6 m wide and 0.6 m deep) flume at the QUT hydraulic laboratory. Inside the flume, flow into the GPT was through an upstream channel inlet configuration with its height extended to the full depth of the experimental model and with a width of 144 mm (See plan view in Figure 9.2). Experiments were also conducted with an upstream inlet pipe with a 100 mm circular cross section and terminating in a small invert level of 40 mm at the entrance to the GPT (Figure 9.1). Both these GPT inlet configurations are commonly used in stormwater applications. A constant flow rate was established through the GPT inlets via controller settings on the centrifugal pumps, which circulated the water from underground storage tanks into the flume. Flow rate readings were checked with periodical measurements in the collection tank at the flume outlet using a stop-watch.

Table 9.1 Matrix of flow regimes used in the experimental setup for litter capture

Run	Flow regime	Weir height (m)	Inlet velocity (m s)	Flow rate (L/s)	Water depth (m)
1	Low	0.108	0.09	1.3	0.1
2		0.286	0.09	3.9	0.3
3		0	0.39	6.1	0.1
4	High	0	2.14	35.4	0.3

Table 9.2 Material used in placed of normal screens in the GPT to represent percentage of blocked screens

Material	Screen Blockages (%)
Perspex (solid internal walls)	100
Perforated screens (3 mm holes)	68
5 mm rectangular screen mesh	33

At the flume outlet, an experimental methodology had been previously developed which used a downstream weir arrangement to control the nature of the flow and the variation in free surface height (Madhani et al., 2009b, c). A matrix of

flow regimes investigated is shown in Table 9.1. The lower flow regimes—1.3 L/s and 3.9 L/s—were set with corresponding weir heights of 0.1 m and 0.3 m respectively above and at the end of the flume terminus raceway. The establishment of the lower flow regimes in the GPT was based on promoting smooth flow conditions and free from obvious wave-like disturbances. Alternatively, at the higher flows regimes, the weir height was set at the floor level of the raceway (zero). Some variations in these flow conditions ($\pm 10\%$) during the course of the experiments were unavoidable since the constant head tank was not fitted to the flume. For further details on the experimental setup see Madhani et al. (2009b, c) which also describes the modelling of blocked screens (Table 9.2).

In Table 9.2, to model fully blocked screens, normal GPT screens were replaced with Perspex solid walls. Perforated walls with 3 mm circular and 5 mm rectangular holes were used to model 68% and 33% screen blockages respectively (Table 9.2). The percentage screen blockages were based on the amount of material obstructing the flow path and no screens represented 0% blockage.

Gross pollutant capture/retention experiments

In the gross pollutant capture/retention experiments, generic and custom modified large (~ 40 mm) celluloid spherical particles (table tennis balls) were used to model gross pollutants with four different relative densities (see RD in Table 9.3). These densities were chosen to represent the hydrodynamic characteristics of positive, neutral and negative buoyant gross pollutant particles, and each density batch consisted of 300 spheres. Preliminary experiments indicated that 300 spheres were sufficient to fill the retention area of the GPT. These spheres were used in the gross pollutant capture/retention experiments for the established flow regimes (Table 9.1) and the three different screen blockages. However, experiments relating to the upstream circular pipe inlet configuration were restricted to two of the four flow regimes due to time constraints (Runs 1 and 3 in Table 9.1). The preparation of the spheres for these experiments was lengthy (~ 200 hours) and was performed under strictly controlled procedures to minimise measurement error.

The authors de Souza and Brasil (2009) describe procedures to measure the physical properties of the spheres (table tennis balls) both empty and filled with water. A similar method was followed and the process intensified with the number of

spheres used in the current experiments. Each sphere was numbered, repeatedly measured and filled to its correct weight for the desired densities, to an estimated error of $\pm 2\%$. The external diameter was measured to ± 0.01 mm and weighed to within ± 0.001 g. To fill the spheres to the required density, two types of syringes were used (30 cc and 5cc), the larger for the initial filling and the smaller to allow finer weight adjustments. Some difficulties were encountered in expelling the minute air pockets. The holes were sealed with a waterproofed sealant, an epoxy resin for the heavier particles and a silicon based substance for the lighter spheres. After the sealant had set, the spheres were kept under moisture in a container to avoid swelling and shrinking.

Table 9.3 Generic spherical particles used in the litter capture experiments

Description	Relative Density (RD)	Physical properties
Floatable	0.10	empty
partially buoyant	0.90	Filled with tap water
neutrally buoyant	1.00	Filled with tap water
Sinkable	1.10	Filled with salt water

Janosi et al (2004) reported the swelling and shrinking of the celluloid skin when in contact with water or a dry atmosphere. To minimise these effects, the physical properties of the spheres were randomly monitored prior to commencing the experiments. Also, at the collection points such as the net, the spheres were inspected for damage after each experiment.

Downstream of the GPT experimental rig, a net was installed prior to the flume terminus raceway to prevent the spheres from escaping. To monitor and capture the motions of these spheres during the experiments, a digital video camera (Panasonic SDR-H280) was mounted on a tripod above the experimental rig and connected to a computer via a USB port. Microsoft Window Movie Maker Version 5 was used to record and analyse the motions of these spheres as they were released into the GPT inlet.

During the experiments, the spheres were released upstream of the GPT inlet, either continuously or intermittently. In the continuous mode, a temporary mesh screen placed upstream of the GPT inlet was lifted to simultaneously release all the

spheres. For the intermittent feed, small batches (3 or 5) of the spheres were introduced into the inlet at a time rate. At lower flows, a longer interval was selected to avoid the spheres from colliding between successive feedings. Overall, a total of 106 experimental runs were performed. An Excel spreadsheet template was constructed to analyse these runs by obtaining the output time series of the spheres entering and leaving the GPT. The GPT capture/retention efficiencies and the RTD were evaluated from the output data.

Tracer dye measurements

Tracer measurements were performed by injecting dye into the incoming fluid to continuously (as a function of time) monitor its concentrations at the GPT outlet. The outlet time series data was used to obtain the RTD curve and calculate the average time it took the fluid to pass through the system boundaries (Levenspiel, 1999). In this experiment, the RTD data was obtained for the rectangular channel-inlet-configured GPT with fully blocked screens (Table 9.2). The RTD measurements were taken in a pollutant-free water flow, while the turbulent nature of the flow in the bypass channel restricted the use of the dye sensing probes to the lower flow regimes (flow types 1 and 2, Table 9.1). The RTD measurements were extended to include the physical modelling of the captured gross pollutants between rain events using polystyrene blocks (Figure 9.3).

Table 9.4 Shaped polystyrene blocks and the corresponding percentage of GPT volume reduction

Block type	GPT Vol. blockages (%)	Cumulative GPT Vol.
0	0	0
1	17	17
1-2	10	27
1-3	17	44
1-4	6	50
1-5	9	59

The shaped blocks in Figure 9.3 are based on snapshots taken from litter experiments with tin cans and bottle caps. These snapshots capture the five stages of litter deposits in the retention area. The third and last stages are Figures 9.4 and 9.5, respectively. The first stage L shaped block represents the initial stage of gross pollutant deposits next to the retaining screens (block 1, Figure 9.3). The inward progressions of deposits were represented by the remaining blocks, four rectangular and one quadrilateral. The blocks and their corresponding GPT volume percentage of blockages are shown in

Table 9.4. Here the height of the blockages was equated to the water depth (0.1 m). In

Table 9.4, 61% is considered a fully blocked GPT. The remaining 39% consisted of the inlet and bypass areas which were blockage-free and the concentration of dye was monitored at the outlet.

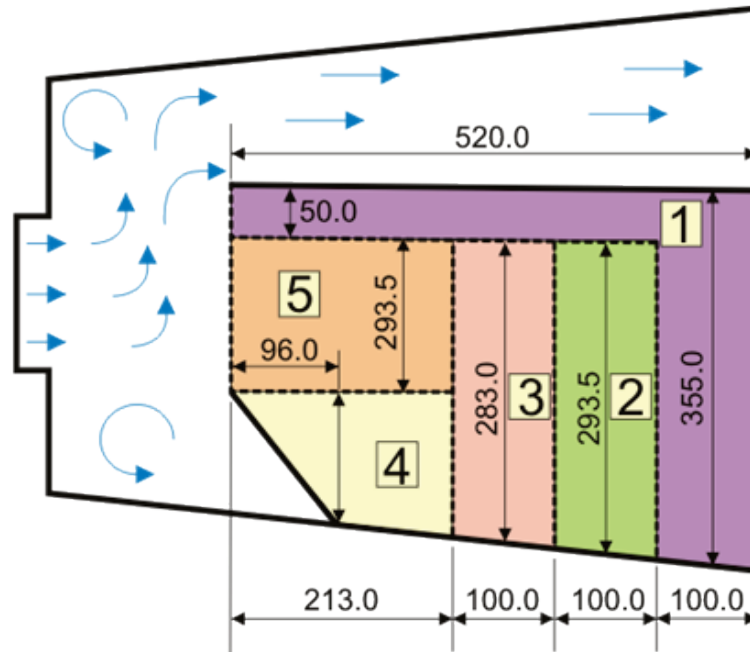


Figure 9.3 Deposits of gross pollutants modelled with polystyrene blocks (1- blocks (1-5) to represent partial and a fully blocked GPT. Only the retention retention area is considered (See also

Table 9.4).

The dye measuring system comprised: a voltage supply with zero adjustment, Komori probes, an injection unit and a data acquisition system (Data Translation DT9802). The injection unit consisted of a volumetric infusion pump (Alaris Medical Systems—formerly IVAC Corporation Model 597), a dye outlet probe/ injector tube and an intravenous (IV) /infusion bag filled with blue dye. Further details on the applications and usage of the Komori probes are given by Madhani and Brown (2008). The concentration of dye is approximated as follows:

$$C \cong \frac{m_d}{m_s} (10^{-6}) \text{ ppm.} \quad (9.1)$$

In the equation above, C is the dye concentration, m_d is the dye mass and m_s is the solution mass. In this case, the concentration of methylene organic blue dye was diluted to 25.000 parts-per-million (ppm); this was sufficient to allow a maximum detection of 8 ppm when the dye was injected and mixed into a volume of water inside the flume. The 8 ppm is the maximum detection range of the Komori probe. Before and after measurements, the Komori probes were calibrated by measuring several times the output sensing voltage in clean water (0 ppm), and in a solution of known concentration (8 ppm). During measurement, the dye was injected upstream of the experimental rig in a step function, with the volumetric pump set to disperse 110 ml at a maximum rate of 999 mL/ h. To aid mixing with the fluid entering the GPT, at the dye injection point, compressed air was passed through a ball-shaped filter to create bubbles. Also, to promote a homogenous fluid entering the GPT, a few bricks were placed crosswise either side of the flume walls with offsets to produce a slight meandering flow path.

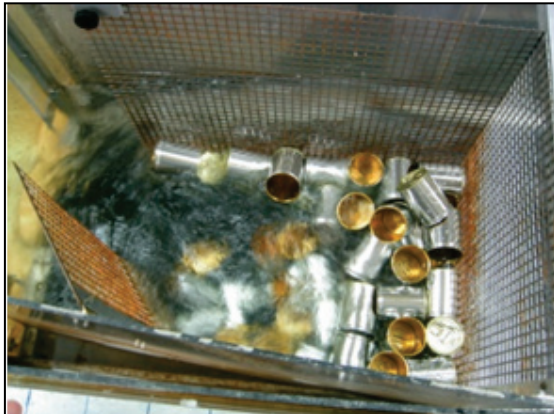


Figure 9.4 Left, a snapshot of the preliminary litter deposit experiments with tin cans. The partially blocked GPT is modelled with three polystyrene blocks (see blocks 1, 2 and 3, Figure 9.3).



Figure 9.5 Left, A snapshot of a fully blocked GPT taken from litter deposit experiments with tin cans. The partially blocked GPT is modelled with all five polystyrene blocks (see blocks 1-5, Figure 9.3).

To measure the peak concentrations of dye in the homogeneous fluid, a Komori probe was placed at the channel inlet and an array was positioned at the

outlet in the bypass channel (Figure 9.2) to capture the dye at outgoing velocity profile peaks and troughs. Data was sampled at 200 Hz and the rise (hold-down) and the complementary fall (wash-out) concentrations were measured with respect to time. The experiments were terminated when the GPT was visibly free from dye. For further details on the measurement technique, see Madhani and Brown (2008).

9.3 COMPUTATIONAL FLUID DYNAMIC (CFD) STUDY

The current CFD study is based on previous investigation which predicted the mean flow structures in a fully blocked GPT. These structures consisted of a deflected entry jet and a large recirculation zone within the retention area of the GPT. The characteristics of these flow structures in terms of mixing, channelling or recycling of fluid and stagnant properties were investigated using dye experiments. In the current research, dye simulation is conducted using the previously defined computational flow field (Madhani et al., 2009b). This flow field was obtained using a 2D modelling approach which assumed a steady state turbulent flow regime with a quiescent free surface of constant fixed height through the computational domain. The standard two-equation k - ε (denoted SKE) turbulence model was deployed (in Fluent® 6.3, ANSYS, Sydney, New South Wales, Australia) to compute the mean surface flow field $u_i(x, y)$ ($i = 1, 2$). To model the turbulence, Cartesian x and y axes were defined along, and perpendicular to, the primary flow direction in the GPT scale model, and the Reynolds Averaged Navier Stokes (RANS) equations were used to describe the steady incompressible mean flow quantities. In the standard two-equation k - ε (denoted SKE) turbulence model, the turbulent viscosity, the turbulent kinetic energy k , and dissipation rate ε , are described by the equations:

$$\frac{\partial}{\partial x_i}(\rho k u_i) = \frac{\partial}{\partial x_j} \left[\left(\mu + \frac{\mu_t}{\sigma_k} \right) \frac{\partial k}{\partial x_j} \right] + G_k - \rho \varepsilon. \quad (9.2)$$

$$\frac{\partial}{\partial x_i}(\rho \varepsilon u_i) = \frac{\partial}{\partial x_j} \left[\left(\mu + \frac{\mu_t}{\sigma_\varepsilon} \right) \frac{\partial \varepsilon}{\partial x_j} \right] + G_\varepsilon \frac{\varepsilon}{k} G_k - C_{2\varepsilon} \frac{\varepsilon^2}{k}. \quad (9.3)$$

In equations (9.2) and (9.3) $G_k = \mu_t S^2$ is the turbulent production term, $S \equiv \sqrt{2S_{ij}S_{ij}}$ is the modulus of the mean rate of strain tensor $S_{ij} = \frac{1}{2} \left(\frac{\partial u_i}{\partial x_j} + \frac{\partial u_j}{\partial x_i} \right)$, the turbulent viscosity $\mu_t = C_\mu \frac{k^2}{\varepsilon}$ and the constant values are: $C_\mu = 0.09$, $\sigma_k = 1.0$, $\sigma_\varepsilon = 1.44$, and $C_{2\varepsilon} = 1.92$.

Across the inlet, a uniform axial velocity profile according to the measured flow rate of 1.3 L/s was specified. Inlet turbulence levels were specified using values of 0.144 m (turbulence length scale) and 5% (turbulence intensity). The boundary conditions for the SKE for the mean velocity and turbulence quantities were determined by the near-wall modelling approaches. Results from previous studies showed that neither the SKE with standard wall law boundary conditions or enhanced near-wall approaches were clearly superior (Madhani et al., 2009b). For the sake of brevity, the enhanced wall treatment (EWT) approach was currently deployed (in Fluent 6.3); this uses a near-wall refinement mesh in the computational domain. Details of implementing the EWT and the near-wall refined grid are described previously by Madhani et al. (2009b). Additionally, the numerical method and grid to predict the velocity flow field are reported, together with the outcome of a grid sensitivity analysis. Basically, in the CFD code Fluent, a second order upwind discretisation was chosen for the convective term in transport equations, and the velocity-pressure coupling was resolved via a SIMPLE-type algorithm. With these solver controls, the time independent velocity flow field was computed. The iterative solver was deemed to have converged and further iterations terminated when a convergence criterion of less than 10^{-5} (c.f. default solver setting of $CC = 10^{-3}$) for the scaled residuals in the computed mean and turbulence quantities was achieved. With the converged flow field solution, the transient species calculation for the dye simulations was executed and the output data was used for RTD analysis. For the dye simulations, the temporal and spatial distributions of the tracer dye concentrations were obtained from the solution of the Reynolds-averaged species transport equation in the predicted incompressible flow field. For a non-reacting species, the equation takes the following form (Fluent, 2006; Javed et al., 2006):

$$\frac{\partial C}{\partial t} + \frac{\partial}{\partial x_i} (u_i C) = \frac{\partial}{\partial x_i} \left(D_m \frac{\partial C}{\partial x_i} \right) - \frac{\partial}{\partial x_i} (\overline{u_i' C'}), \quad (9.4)$$

where C and C' are the mean and fluctuating tracer dye concentrations respectively, D_m is the laminar diffusion coefficient and a default value of $2.88 \times 10^{-5} \text{ m}^2/\text{s}$ was used for methylene blue dye. However, this term is insensitive (Fluent, 2006) compared to the turbulent mass fluxes, $(\overline{u'_i C'})$ which takes the following form (Launder and Spalding, 1974):

$$\overline{u'_i C'} = - \left(\frac{\mu_t}{Sc_t} \right) \frac{\partial C}{\partial x_i}, \quad (9.5)$$

where μ_t is the turbulent viscosity $\left(C_\mu \frac{k^2}{\varepsilon} \right)$ where C_μ is a constant and the turbulent Schmidt number (Sc_t) was taken as 0.7 (Daily and Harleman, 1966).

A zero-gradient (zero-flux) boundary condition was specified at the walls. At the inlet boundary condition, a uniform stream of dye concentration (representing a step input), which had similar properties to water, was released by a convection and diffusion process. This was achieved by setting the concentration of dye to unity and the initial condition set to: $C(x_i, y_j, 0) = 0$. A transient calculation was performed using time steps of 0.1 second with 20 iterations per time step (Stovin et al., 2008). The second order implicit calculation was terminated when 98% of the dye was recovered at the outlet.

9.4 DATA ANALYSIS

Residence time theory

Danckwerts (1953) originally described the residence time distribution (RTD) of F-diagrams using continuous flow systems and gave typical cases namely, piston flow, piston flow with longitudinal mixing, complete mixing and dead water. An example of an experimentally obtained F-diagram is given in Figure 9.6 and has a similarity with the dead water case. Here, a considerable fraction of the fluid is trapped in eddies, and spends much more than the average length of time in the vessel whilst most of the flow takes place through a restricted channel (Danckwerts, 1953). In Figure 9.6, the average or mean residence time (\bar{t}) is denoted by the area A above the F diagram (Levenspiel, 1999).

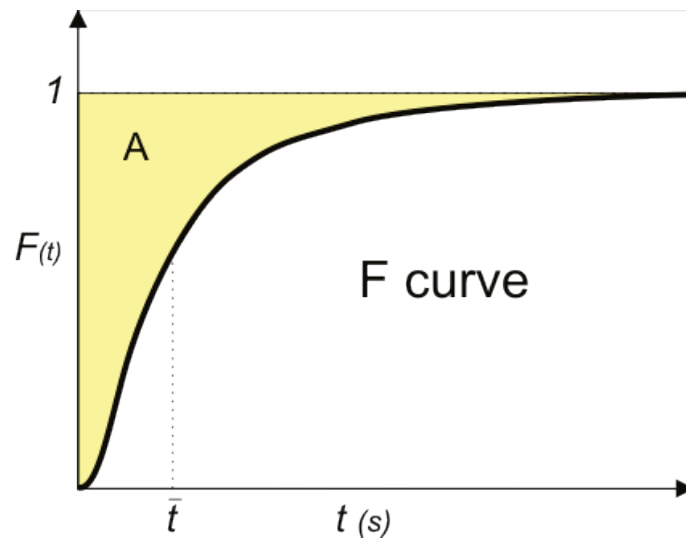


Figure 9.6 A typical residence time distribution (RTD) normalised F curve.

The F-diagram or RTD function $F(t)$ is directly obtained from the tracer concentration at the outlet following a step change at the inlet, using either the hold-down or wash-out method of measurements (Haas et al., 1997; Naor and Shinnar, 1963). In the hold-down (rise) method the tracer concentrations C_t rises from zero to a maximum value C_0 , the RTD function

$$F(t) = \frac{C_t(t)}{C_0}. \quad (9.6)$$

In the wash-out (fall) method, the complementary function $F^*(t)$ decreases asymptotically to zero with time where

$$F^*(t) = 1 - \frac{C_t(t)}{C_0}. \quad (9.7)$$

For the retention/ capture experiments, C_t represents the number of pollutants escaping, and C_0 is the maximum number fed into the GPT. The density function $f(t)$ is the derivative of the function $F(t)$ (Naor and Shinnar, 1963):

$$f(t) = \frac{d F(t)}{dt} = -\frac{d F^*(t)}{dt}. \quad (9.8)$$

The r^{th} moment of the distribution function is defined as:

$$E_f(t^r) = \int_0^{\infty} t^r f(t) dt. \quad (9.9)$$

For the mean value of distribution, $r = 1$, equation (9.9) yields:

$$\bar{t} = E_f(t) = \int_0^{\infty} t^1 f(t) dt. \quad (9.10)$$

The variance (σ^2), skewness (s^3) and kurtosis (k^4) are defined respectively

$$\sigma^2 = E_f(t^2) = \int_0^{\infty} t^2 f(t) dt - \bar{t}^2. \quad (9.11)$$

$$s^3 = \frac{\int_0^{\infty} t^3 f(t) dt}{(\sigma^2)^{\frac{3}{2}}}, \quad k^4 = \frac{\int_0^{\infty} t^4 f(t) dt}{(\sigma^2)^2}. \quad (9.12)$$

The mean holding time or the plug flow/theoretical residence time, τ for ideal flow (Levenspiel, 1999) is

$$\tau = \frac{\text{Volume of GPT (m}^3\text{)}}{\text{Inlet flow rate (}\frac{\text{m}^3}{\text{s}}\text{)}}. \quad (9.13)$$

Equations (9.9-9.12), the moments of distribution functions were used to calculate the mean, variance, skewness and kurtosis, respectively. The trapezoidal integration rule was also used to calculate the shaded area (A) in Figure 9.6. Since the sample record is sufficiently long, both methods are in close agreement (< 1%). A procedure for calculating the RTD parameters using experimental data is given by

Hass et al. (1997), and a similar approach was taken in this current experiment. The data was processed using Matlab® (R2008b, The MathWorks, Melbourne, Victoria, Australia) and signal processing routines were implemented for smoothing and curve fitting operations (Madhani et al., 2010).

Using Equations (9.6) or (9.7), (9.8) and (9.9) we calculate the mean residence time (\bar{t}) with a discrete data (size n) from:

$$\bar{t} = \frac{1}{C_0} \sum_0^n t \Delta C_t. \quad (9.14)$$

Similarly the other RTD parameters are computed from:

$$\sigma^2 = \frac{1}{C_0} \sum_0^n t^2 \Delta C_t - \bar{t}^2, \quad s^3 = \frac{\frac{1}{C_0} \sum_0^n t^3 \Delta C_t}{(\sigma^2)^{\frac{3}{2}}} \quad \text{and} \quad k^4 = \frac{\frac{1}{C_0} \sum_0^n t^4 \Delta C_t}{(\sigma^2)^2}. \quad (9.15)$$

Capture/ retention efficiency

The time series data from the capture/ retention experiments relate to the number of pollutants capture and retained during and after feeding. The retention efficiency (R') is expressed as

$$R' = \frac{\text{Total} - \text{escaped}}{\text{Total}}. \quad (9.16)$$

9.5 RESULTS AND DISCUSSION

Gross pollutant capture/retention experiments

We commence the discussion by comparing the earlier hydrodynamic investigations with the current capture/retention results. Earlier investigations (Madhani et al., 2009b, c) revealed that a GPT with fully blocked screens can radically change the hydrodynamic and capture/retention characteristics of a GPT. This can lead to large recirculating flow patterns within the GPT, accompanied by

hydraulic short circuiting where the preferred outflow path is via the bypass channel (Figure 9.2). A visual snapshot showed the neutrally buoyant spheres escaping via the outflow path upon entry into the channel inlet GPT (Figure 9.7). Here, a large number of spheres entered the inlet within a very short time. This behaviour described the continuous or step input method of introducing the spheres into the inlet. The snapshot in Figure 9.7 revealed the poor capture/retention performance, since the majority of the spheres escaped the GPT. The data point (RD = 1.0, 1.3 L/s) for this snapshot is graphically represented by A in Figure 9.8.

Overall, the capture/retention versus flow rate plots indicate poor performance for experiments with fully blocked screens (Figure 9.8). These plots highlight the capture/retention trends of the variable density spheres (RD = 0.1, 0.9, 1.0 and 1.1) and 1.0 on the vertical axis represents 100%. The total average capture/retention for these experiments was 4%. Below this average, the sinkable and neutrally buoyant spheres (RD = 1.0 and 1.1) appear to be the worst performers. It is unclear whether the high shear velocity gradients causing the flow separation feature next to the inner wall (See B, Figure 9.7) contribute to this poor behaviour. This feature was caused by the turning motion of the deflected entry jet into the bypass and peaks nearer the GPT floor (Madhani et al., 2009b). Here, the high shearing velocities were seen to force the spheres to escape into the bypass. However, this feature is not prominent in lower screen blockages.

To investigate the lower screen blockages (33% and 68%), the solid internal walls were replaced with perforated screens in the GPT (Table 9.2). The GPT performance dramatically improved with these blockages particularly at higher flow rates where the entry jet transported the spheres further into the retention area of the trap (Figure 9.9). Although the capture/retention trends were similar in both cases, the 68% blocked screen performed slightly better at the higher flow rate (Figure 9.10). For the sake of brevity, Figure 9.10 only shows the capture/retention trends for this case. This finding is of practical significance for the maintenance of the GPT since the device can operate efficiently with at least 68% of the screens blocked.

At lower flow rates these high performance for the heaviest spheres (RD = 1.1) which rolled setback reduced the average performance trends cases to 46% and 57%, respectively (

Table 9.5). A noticeable feature is that the performance trends for the lighter spheres were better in the lower flow regime with a shallower water depth (Run 1, Table 9.1), despite the same inlet velocities. Furthermore, at lower flow regimes (< 6 L/s), the capture/retention characteristics of spheres with different densities tended to vary. The varied capture/retention characteristics between the higher and lower regimes also tended to influence the deposition patterns of the spheres (Figures 9.9 and 9.11).

Table 9.5 The average capture/retention efficiencies for the four spheres with different densities using the step input function (continuous feed)

Screen blockage (%)	Retention eff. (%)	
	Inlet configuration	
	channel	pipe
33	46	76
68	57	83
100	6	1

In the higher flow regime the spheres were stacked in layers (Figure 9.9). Otherwise, at low flow rates, the motion of the spheres was sufficiently slow for them to form queues, resulting in a single layer deposition inside the GPT (Figure 9.11). Further comparisons showed similarities in deposition patterns in an infield GPT operating intermittently between rain events (Figure 9.12). This GPT had a circular pipe inlet, and a similar model was partially tested in the laboratory. This pipe inlet entered above the GPT floor with a small invert level and was partially tested using two flow regimes (see Run 1 and 3, Table 9.1).

Table 9.6 The average capture/retention efficiencies for the three blockage conditions and both the continuous and intermittent methods of input

Artificial pollutants (spheres) RD	Retention eff. (%)	
	Inlet configuration	
	channel	pipe
0.1	34	48
0.9	49	56
1.0	43	55
1.1	24	58

The results of the circular pipe and channel inlet configured GPT are summarised in tables 9.5 and 9.6. These results clearly show that overall the raised inlet—circular pipe—had better gross pollutant capture/retention efficiencies for 33% and 68% blocked screens. Also, the variable density gross pollutants performed better for this inlet.

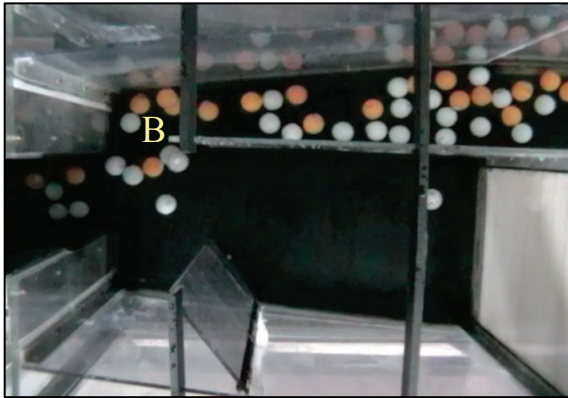


Figure 9.7 Left, experiments with fully blocked screen show the neutrally buoyant spheres (RD =1.0) escaping the GPT via the bypass (See data point A in Figure 9.8 at 1.3 L/s on the abscissa). B (See left of figure) denotes the existence of large negative horizontal velocities (right to left).

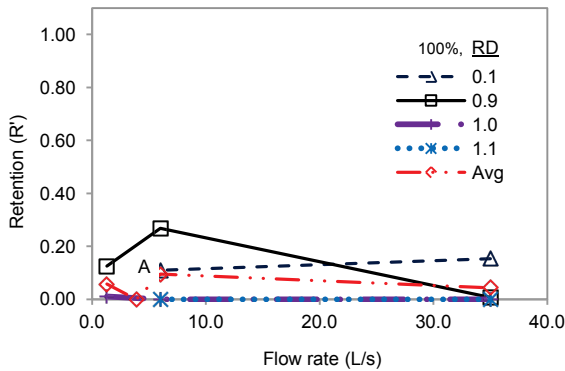


Figure 9.8 Normalised capture/retention profiles (R') for continuously fed variable density spheres (RD) = 0.1, 0.9, 1.0 and 1.1. The channel-inlet-configured GPT experiment is with fully blocked screens tested under varying flow rates (See Figure 9.7 for B).



Figure 9.9 Deposition pattern for the GPT with 68% blocked screen shows total (100%) capture/ retention of the lightest pollutants (RD = 0.1) at a high (35 L/s) flow rate (See C, Figure 9.10).

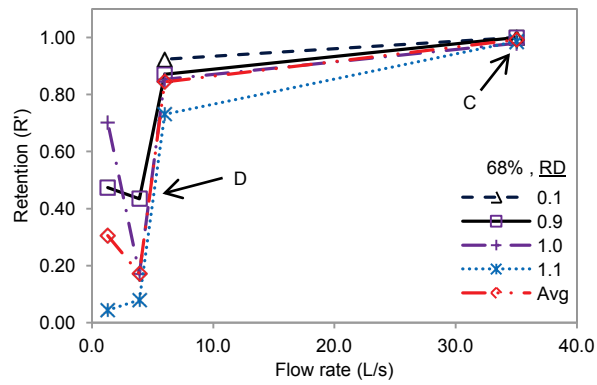


Figure 9.10 Normalised capture/retention profiles (R') for continuously fed variable density spheres (RD) = 0.1, 0.9, 1.0 and 1.1. The channel-inlet-configured GPT experiment is with 68% blocked screens tested under varying flow rates. See Figures 9.9 and 9.11 for C and D, respectively.



Figure 9.11 Single layer deposition pattern for the GPT with 68% blocked screen capture/retention of the lightest pollutants (RD = 0.9) at a low (3.9 L/s) flow rate (See D, Figure 9.10).



Figure 9.12 A snapshot of a field investigated GPT showing deposits of sediments which are similar to the pattern from the gross pollutant capture/retention experiments with partially buoyant spheres (See Figure 9.11). Note the blocked inlets in both cases.

Residence time measurements

To obtain the RTD function $F(t)$, it is not necessary to measure the residence time of a large number of particles entering at different times; it is sufficient to study the RTD of a large number of particles all entering at the same time (Naor and Shinnar, 1963). Table 9.7 tabulates this continuous or step stimulus RTD data in the form of residence times for spheres and dye entering the GPT. This data was taken from the gross pollutant and dye experiments with fully blocked screens operating under low flows (Run 1 and 2, Table 9.1). The last column in Table 9.7 shows the amount of dye/spheres recovered at the outlet of the GPT when released into the GPT inlet during the experiments.

The less than 100% recovery rate meant that some of the spheres were trapped in the GPT. However, the recovery rate at the outlet (greater than $\sim 90\%$) for the spheres and the dye were generally sufficiently high for direct comparisons to be made. Otherwise, high capture/retention represents infinite residence time, thereby requiring no further analysis.

Table 9.7 Residence times (\bar{t}) obtained from capture/ retention experiments using spheres, dye measurements and CFD simulation. Key: Water depth (WD), relative density (RD), inlet flow rate (Qin), variance (σ^2), skewness (s^3) and kurtosis (k^4).

No.	Material-Expt/CFD	Inlet Config.	RD	Qin (L/s)	WD (m)	(\bar{t}) (secs)	σ^2	s^3	k^4	Recovered (%)
1	Expt-spheres	channel	0.9	1.3	0.1	107.9	18387.3	5.7	24.4	87.5
2	Expt-spheres	channel	1.0	1.3	0.1	59.1	711.9	17.6	56.7	98.9
3	Expt-spheres	pipe	0.9	1.3	0.1	101.2	8720.8	6.4	22.6	96.5
4	Expt-spheres	pipe	1.0	1.3	0.1	51.6	3821.3	6.7	34.0	99.3
5	Expt/spheres	pipe	1.1	1.3	0.1	132.5	3018.5	22.4	85.8	99.7
6	Expt-dye	channel	n/a	1.3	0.1	91.2	25121.4	19.9	4.8	96.0
7	Expt-dye	channel	n/a	3.9	0.3	94.2	31661.8	14.3	4.1	92.0
8	CFD-dye	channel	n/a	1.3	surface	94.7	7786.5	6.5	25.0	98.0

Experiments with spheres entering a pipe or channel-inlet-configured GPT show similar residence times (Table 9.7). In Table 9.7, data pertaining to sinkable spheres is only available for the pipe-inlet-configured GPT at this flow rate (1.3 L/s) which produced the longest residence time (132.5 seconds). Otherwise, at this flow rate, experiments with the channel-inlet-configured showed that the sinkable spheres could not be mobilised passed the inlet. The neutrally buoyant spheres (RD=1.0) inherited the shortest residence times (59.1 and 51.6 seconds). The experimental dye residence times for both flow regimes and the CFD simulation were in close

agreement, irrespective of the water depth. These residence times were within 15% of the values for the partially submerged spheres ($RD = 0.9$). The RTD F diagrams for these spheres and dye show similar trends in relation to fully blocked screens (Figure 9.13). Additional RTD data was also collected for GPT (three-dimensional) blockages for comparisons with blocked screens.

Figure 9.14 shows the experimental (\bar{t}) and theoretical (τ) residence times with retention area blockages. Despite the similarity of the trends observed between the experimental and theoretical residence times, their ratio increases from 4 to 7 corresponding with the blockages. As this ratio (\bar{t}/τ) increases from unity, the longer experimental residence time is attributed to the flow paths of the recirculation and dead zones in the GPT (Levenspiel, 1999). These flow features have been previously described (Madhani et al., 2009b). As blockages in the GPT increases, the fluid exchange or interaction between the dead zone behind the baffle and the entry jet becomes less; hence, this ratio becomes larger. Although this is generally an important consideration in the retention/capture characteristics of the GPT, the overall trends show an insignificant change in residence times (Figure 9.14).

The small change suggests there is little difference in the poor performance between a fully blocked and an empty or partially filled GPT with 100% screen blockages. Despite these differences, the experiments show generally that a blocked GPT will allow incoming pollutants to escape via the bypass, thus preventing the blockages to extend upstream. Overall, confidence in the data collecting and processing methods increased due to the sensitivity of the dye measurement technique in detecting the small changes.

During data processing it was found that the residence times calculated during the hold-down and wash-out periods differed significantly. This difference was due to the length of time allowed to measure the tail characteristic of the hydraulic dead zones. Consequently, it was more practical to use the wash-out method to prevent the unnecessary overuse of dye.

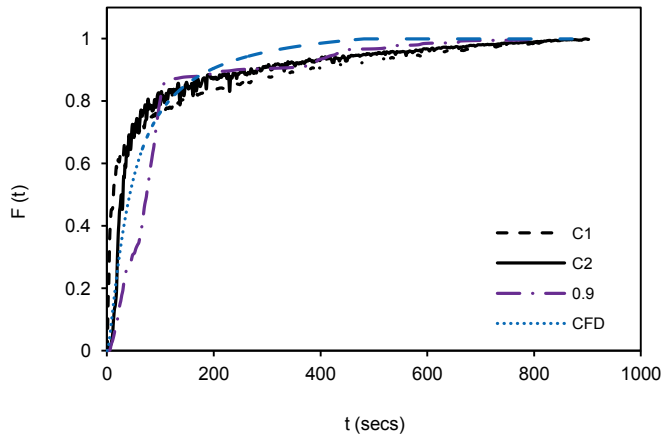


Figure 9.13 Normalised escaped artificial pollutants (spheres, RD = 0.9), and experimental dye concentration residence time profiles C1 (Run 1, Table 9.1), C2 (Run 2, Table 9.1) and CFD for 100% blocked screen.

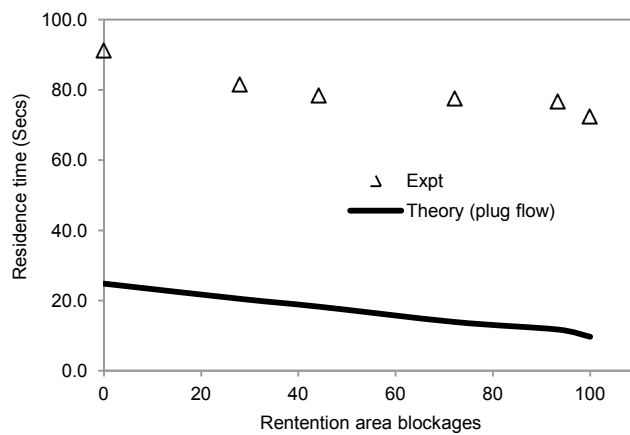


Figure 9.14 Comparisons of residence times obtained with GPT blockages using polystyrene shapes and plug flow theory.

9.6 CONCLUSION

A novel technique was developed to assess the retention/capture characteristics of a GPT with fully and partially blocked screens. This technique facilitates a rigorous GPT assessment and can be used on other treatment devices. The mainly experimental technique used custom modified spheres with variable densities and tracer dye. The spheres were modified to represent floatable, partially buoyant, neutrally buoyant and sinkable gross pollutants in the capture/retention experiments. During the experiments, the spheres were released into the GPT inlet, while the outlet was monitored with time. The experiments consisted of a range of flow regimes, two different inlet designs, and different screen blockage conditions. The outlet data was used to assess the GPT performance and to investigate the capture/retention characteristics of the variable ball densities with dye measurements.

The main findings reveal that the retention/capture characteristics rapidly deteriorate when the internal screens are fully blocked. However, below 70% screen blockage, the GPT performance improves dramatically, particularly at higher flow rates. The practical significance of this finding is important for the maintenance of the GPT which can be scheduled when this percentage of blocked screen is reached.

During lower flow rates, the high performance trends are reversed. Also, a raised inlet GPT offers greater capture/retention capabilities. Experiments with this inlet showed that spheres of variable density have similar retention/capture characteristics. The density characteristics of these spheres were quantified with residence time measurements. The residence times of the dye from both the experiments and computational fluid dynamic (CFD) simulation were in good agreement, and comparable to partially buoyant pollutants. There was also little difference in the poor performance between a fully blocked and an empty or partially filled GPT with 100% screen blockages.

The technique developed and examined here, demonstrates the usefulness and effectiveness of rigorously describing the capture/retention capabilities of a GPT under various operating conditions. Similar GPTs have received little attention in scientific research since experimental techniques have not been fully established. This technique is also capable of highlighting possible GPT inlet improvements and positive design features such as the bypass channel. Furthermore, this research shows that testing GPTs with dye alone is insufficient to assess the full capabilities in the capture/retention of a range of pollutants. Further work is recommended to refine the measurement process and to extend the CFD technique to reduce the labour intensiveness of experiments. This will provide opportunities to investigate a wider range of design configurations and operating conditions.

ACKNOWLEDGEMENTS

The authors acknowledge C-M Concrete Pty. Ltd, 2004 (Mr Phil Thomas) for their ARC linkage grant support and the assistance of Ms Sarita Gupta Madhani, and Dr Glenn Fulford for his mathematical advice. We also would like to thank under/postgraduates Mr Siang Hor Sim, Mr Khoo Jit Hong, and Mr Fan Yang for their experimental assistance.

REFERENCES

- Armitage, N. P. and Rooseboom, A. (1999). The removal of litter from stormwater conduits in the developing world. *Water Science and Technology*, 39(9), 277-284.
- Daily, J. W. and Harleman, D. R. F. (1966). *Fluid dynamics*. Reading, Massachusetts, USA: Addison-Wesley Publishing Company.
- Danckwerts, P. V. (1953). Continuous flow systems. *Chemical Engineering Science*, 2, 1-13.
- de Souza, P. A., Jr. and Brasil, G. H. (2009). Assessing uncertainties in a simple experiment. *European journal of physics*, 30, 615-622.
- Fluent (2006). *Fluent 6.3 user's guide*. Lebanon, USA: Fluent, Inc.
- Haas, C. N., Joffe, J., Heath, M. S. and Jacangelo, J. (1997). Continuous flow residence time distribution function characterization. *Journal of Environmental Engineering*, 123(2), 107-114.
- Jánosi, I. M., Szabo, G. and Tél, T. (2004). Swelling of ping-pong balls. *European journal of physics*, 25, 303-310.
- Javed, K. H., Mahmud, T. and Zhu, J. M. (2006). Numerical simulation of turbulent batch mixing in a vessel agitated by a Rushton turbine. *Chemical Engineering and Processing*, 45(2), 99-112.
- Lauder, B. E. and Spalding, D. B. (1974). The numerical computation of turbulent flows. *Computational Methods Applied Mechanical Engineering*, 3, 269-289.
- Levenspiel, O. (1999). *Chemical reaction engineering* (3rd ed.). New York: Wiley.

Luyckx, G. and Berlamont, J. (2004). Removal efficiency of swirl/vortex separators. *Urban Water Journal*, 1(3), 251-260.

Madhani, J. T. and Brown, R. J. (2008). A scalar concentration (Komori) probe for measuring fluctuating dye concentration in water. *WSEAS Transactions on Fluid Mechanics*, 3(3), 224-233. Retrieved 15 February 2010, from <http://www.worldses.org/journals/fluid/fluid-2008.htm>

Madhani, J. T., Dawes, L. A. and Brown, R. J. (2009a). A perspective on littering attitudes in Australia. *The Environmental Engineer: Journal of the Society for Sustainability and Environmental Engineering, The Institution of Engineers, Australia*, 9/10(4/1), 13-20.

Madhani, J. T., Kelson, N. A. and Brown, R. J. (2009b). An experimental and theoretical investigation of flow in a gross pollutant trap. *Water Science and Technology*, 59(6), 1117-1127.

Madhani, J. T., Young, J. and Brown, R. J. (2010). The hydrodynamic investigation of a gross pollutant trap. *Water Research*, (Under review).

Madhani, J. T., Young, J., Kelson, N. A. and Brown, R. J. (2009c). A novel method to capture and analyze flow in a gross pollutant trap using image-based vector visualization. *Water, Air, & Soil Pollution: Focus*, 9(5-6), 357-369.

Naor, P. and Shinnar, R. (1963). Representation and evaluation of residence time distributions. *Industrial & Engineering Chemistry Fundamentals*, 2(4), 278-286.

Persson, J. and Wittgren, H. B. (2003). How hydrological and hydraulic conditions affect performance of ponds. *Ecological Engineering*, 21(4-5), 259-269.

Phillips, D. I. (1999). A new litter trap for urban drainage systems. *Water Science and Technology*, 39(2), 85-92.

Phipps, D. A., Alkhaddar, R. M., Dodd, M. J., Faram, M. G., Andoh, R. Y. G. and Roberts, M. C. (2004). Experimental investigation into solids re-entrainment in hydrodynamic vortex separators. *Novatech: 5th International Conference on Sustainable Techniques and Strategies in Urban Water Management* (pp. 69-76). Lyon, France.

Phipps, D. A., Alkhaddar, R. M., Loffill, E., Andoh, R. Y. G. and Faram, M. G. (2008). Efficiency testing of a hydrodynamic vortex separator. Paper presented at the *Proceedings of the 11th International Conference on Urban Drainage*. Edinburgh, Scotland, UK. Retrieved 14 January 2010, from http://plc.hydro-intl.com/index2.php?option=com_docman&task=doc_view&gid=16&Itemid=88

Stovin, V. R., Grimm, J. P. and Lau, S. T. D. (2008). Solute Transport Modeling for Urban Drainage Structures. *Journal of Environmental Engineering*, 134, 640.

Chapter 10: General Discussion

This chapter discusses the key aspects of the research as documented in Chapters 3-9 together with any additional considerations and issues not previously raised in these chapters.

In this thesis, the chapters are arranged as shown in Figure 10.1, which is an extended version of the flow chart presented and discussed in Chapter 1. Figure 10.1 includes the experimental setup parameters (denoted R1-R12, in this figure) with key operational characteristics of the GPT with fully or partially blocked screens. Table 10.1 tabulates these parameters, R1-R2 in terms of experimental setup conditions of weir height, inlet velocity, flow rate, water depth and screen blockages.

The chapters in this figure essentially relate to: Field Studies and the Extended Literature Review, Calibration of Equipment, Hydrodynamic Studies and Gross Pollutant Capture/Retention Investigations.

The general discussion below commences with the modelling considerations for conducting a detailed investigation on the GPT.

10.1 MODELLING CONSIDERATIONS OF THE GPT

Since there are no established guidelines for testing GPTs, stakeholders—including researchers, local city councils and the stormwater industry—tend to rely on their previous experiences in procuring or managing GPTs which have been occasionally reported in the literature.

It is reported that the design of GPTs should consider: site constraints; inlet flows; operations under adverse conditions; prevention of flooding when fully blocked by introducing a bypass system; the scouring of the captured/retained pollutants; high capture/retention efficiency; minimal adverse hydraulic properties such as low head losses, and inexpensive and infrequent maintenance (Field and Sullivan, 2003; Wong et al., 2000).

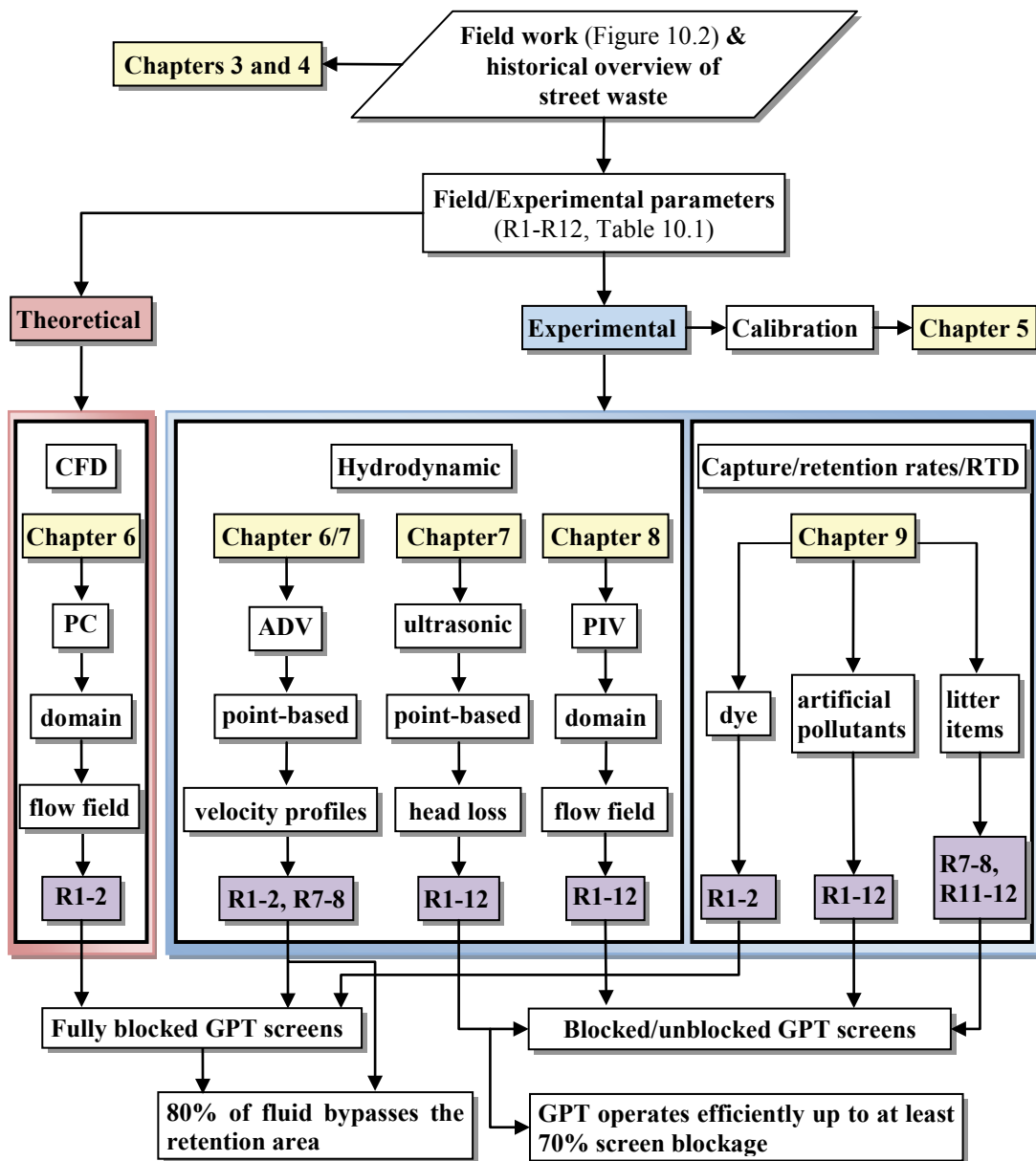


Figure 10.1 An overview of the current research with main subdivisional headings is shown in the flowchart. The experimental setup parameters are grouped under R1–R12 in Table 10.1.

Table 10.1 Experimental setup parameters for the GPT rig

Flow regime	Weir height (m)	Inlet velocity (m/s)	Flow rate (L/s)	Water depth (m)	Screen blockages %		
					100	68	33
Experiment numbers							
Low	0.108	0.09	1.3	0.1	R1	R3	R5
↑	0.286	0.09	3.9	0.3	R2	R4	R6
↓	0.000	0.39	6.1	0.1	R7	R9	R11
High	0.000	2.14	35.0	0.3	R8	R10	R12

Scientific findings also indicate that most of the gross pollutant load is transported during peak discharges (Allison et al., 1998). For example, strong correlations between litter volume and rain intensity have also been observed (Kayhanian et al., 2002).

These suggested guidelines and findings have been incorporated as part of the developed testing approach for GPTs in this research. The GPT under investigation was tested during peak discharges, adverse operating conditions such as screen blockages and flood conditions which were interpreted as low and high tidal waters. These conditions were initially explored during field observations as documented in Chapter 4.

10.2 FIELD STUDIES AND THE EXTENDED LITERATURE REVIEW

To fill a research gap, the comprehensive literature review in Chapter 2 was extended to include a historical overview of street waste and SQIDs (as documented in Chapter 3). The nature of this evaluation involved collecting historic material from the websites of local city councils, the National Library of Australia and educational institutions.

The historical data together with the field results presented in Chapter 4 were used to analyse the past and current gross pollutant trends in Australia to inform the future management of street waste.

Chapter 4 also describes the use of the of geographic information system (GIS) web interface software (www.maps.google.com), to store the results of the field study. Further work is required to import the remaining 300 photographic results into the existing GIS database with the 80 inspected stormwater drains and GPTs.

Unlike this research, other scientific investigations of GPTs and SQIDs generally do not include comprehensive field work. An overview of the field work conducted as part of this research is shown in Figure 10.2. Here, photographic snapshots of the gross pollutants at the centre of this figure, is taken from the southern inner suburbs of Brisbane. These snapshots typically reveal gross pollutants—organic matter and anthropogenic litter—found in street and stormwater systems during the course of the field investigation (See left and right of the circular picture in Figure 10.2. An example of public littering habits at public places such as

bus stops is shown on the upper left of this picture in Figure 10.2. A partial view of the field study urban catchment area (upper right) is also shown in this figure.

It was concluded from Chapters 3 and 4 that street waste is a growing problem in Australia. Field inspections showed that a large amount of sediments were deposited in GPTs and in the inlet structure during low and intermittent flows when placed in residential areas in the outer suburbs of Brisbane (as discussed in Chapter 9).

It was also noted that gross pollutants with water absorbing surfaces such as leaves and paper appeared to be more efficient carriers for the finer and more harmful pollutants. It is recommended that further investigations are required to quantify these gross pollutant findings.

The high amount of waste found on streets and in stormwater systems generally consists of anthropogenic litter and organic matter. Floating masses accumulating in our oceans due to the non-biodegradable street litter entering stormwater systems have caused recent scientific and public concern.

There is also the issue of the high amount of organic matter found on streets and in stormwater systems. Organic matter causes blockages in stormwater systems such as roadside drains and GPTs, and these result in upstream flooding.

Organic matter such as grass clippings may also constitute a fire hazard. With the advent of new urban design and planning concepts such as green roofs and walls it is envisaged that the increase in organic waste will cause further problems in the management of stormwater pollution. Consequently, there is a need to address the long term management of street waste and hence GPTs will have a vital role to play in the future management of gross pollutants.

With regards to conducting tests in the laboratory, field studies also indicated that GPTs should be tested for abnormal or adverse conditions such as blockages caused by organic matter (Figure 10.2).

Consequently, the focus of this investigation has been on the operating efficiency of a GPT under screen blockage conditions using hydrodynamic and capture/retention experiments and CFD as shown in Figure 10.1.

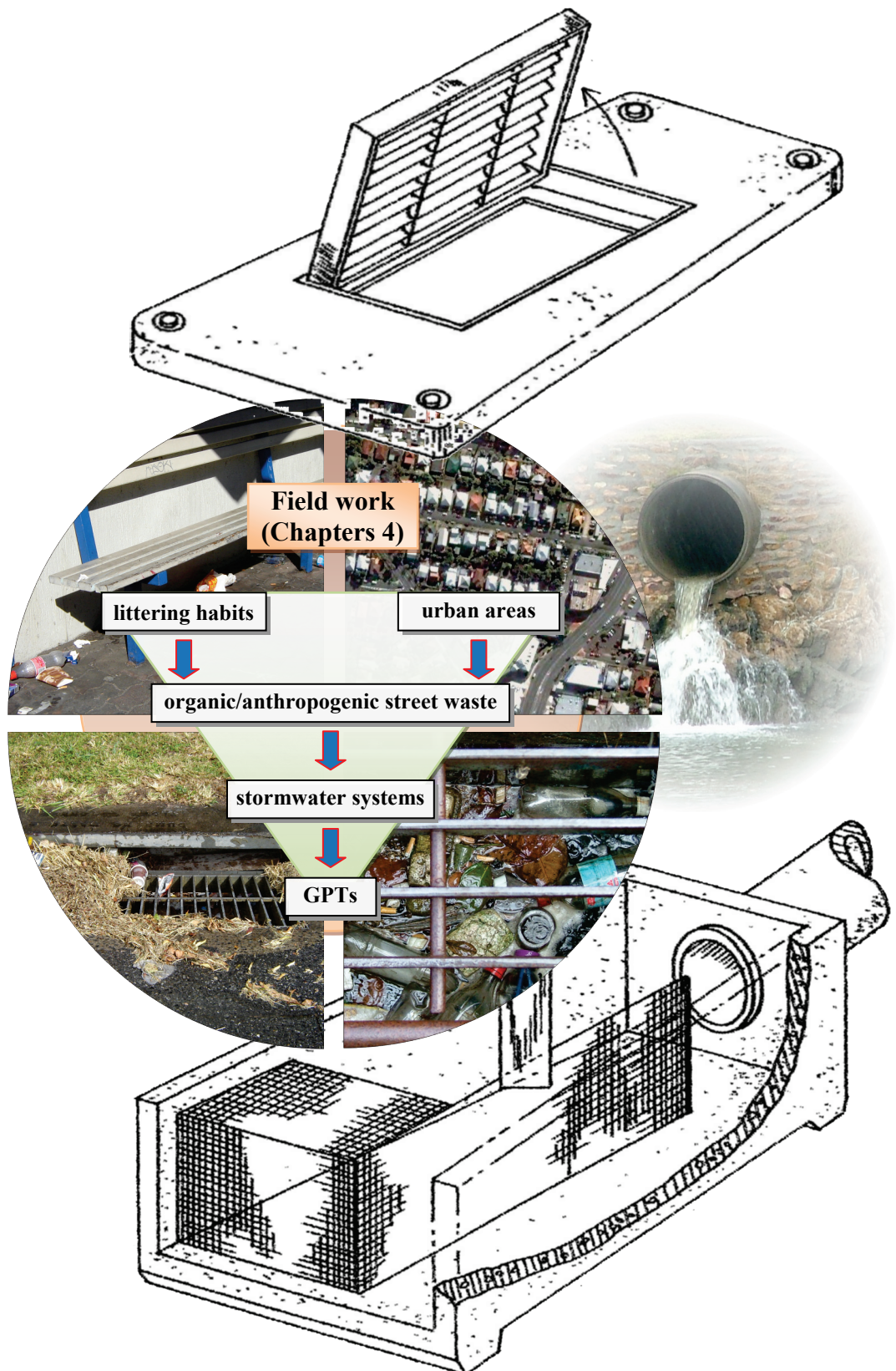


Figure 10.2 An overview of the field work and associated areas of investigations, namely: littering habits in urban areas and street waste which enters stormwater systems and is eventually captured by GPTs. The illustrated removable cover and internal view of the GPT *LitterBank* are shown at the top and bottom of this figure. The figure on the upper right is the view of the stormwater outlet from the South Bank urban catchment discharging into the Brisbane River.

10.3 CALIBRATION OF EQUIPMENT

Preparatory work for the hydrodynamic and capture/retention experiments included the calibration and performance assessments of equipment where necessary (Figure 10.1). For example, the scalar dye concentration probe was investigated and calibrated, since this equipment was custom made and little was known of its true performance.

Most commercial probes are bulky and cannot be used in confined spaces. The slender custom designed scalar dye concentration (Komori) probes were ideally suited for such measurements in the GPT rig. Consequently, Chapter 5 documents the calibration techniques and their overall performance under varied flow conditions.

The Komori probes were found to have a frequency 100 Hz—which is dependent upon fluid velocities—and this was adequate to measure the relevant fluctuations of dye introduced into the GPT flow domain. Although the overall results were satisfactory, a number of measurement issues had to be addressed. These issues related to the orientation of the probe with respect to downstream flow, noise levels, electrical drift, spiking and fluid turbulence. Initial efforts were focused on the rewiring of the sensor input terminals in which a resistor (470 ohms) was used to minimise the effect of signal noise. The sensor inputs were connected using a differential system as shown in Appendix B.

In addition to making hardware modifications on the data acquisition system to address the above mentioned measurement issues, a signal processing program was also developed using Matlab (2008b, The MathWorks, Melbourne, Victoria) to address the voltage offsets and the instantaneous spikes. A flowchart in Figure 10.3 provides an overview of this program which consists of five main signal processing algorithms/modules.

The first module (See item 1, Figure 10.3), performs initial checks on the input of the measured dye concentration data. This data is rejected if the voltage offsets/drifts exhibits erroneous fluctuations. Otherwise, the calibration input file is read into the program to correct the drift (See item 6, Figure 10.3). The calibration file contains the recordings of the voltage offsets. The program performs a statistical averaging of these recordings and makes the necessary adjustments to the input data.

The second module is used to extract the rise and fall data (See item 2, Figure 10.3) using the input definition file. The cut-off points for rise and fall signals are stored in this file (See item 7, Figure 10.3). The cut-off points can be manually inserted or evaluated by the program.

The smoothing operation of the experimental data was provided by the third program module (See item 3, Figure 10.3). In this module, an option was made available in this program to graphically inspect the raw with the filtered signals for the removal of spikes and to ensure that data clipping was avoided due to excessive curve smoothing as shown in Figure 10.4. Figure 10.4 (a) shows a menu for selecting various options for displaying the raw and filtered signals. An example of a comparative plot between these signals and removal of spikes is given in Figure 10.4 (b). The spikes were caused either by dirt particles or dye unmixed with water passing through the sensing probes. A set of screens was placed at the entrance to the flume to filter the incoming water from dirt particles to prevent spiking and reduce downstream turbulence.

In the residence time calculations, the plotting of the RTD curve is provided by the fourth module (See items 4, Figure 10.3) and the fifth module checks the balance between the measured dye concentrations at the inlet and outlet (See items 5, Figure 10.3). Examples of output display from these modules are shown in Appendix E.

In addition to the dye concentration probes, the ultrasonic sensors and the ADVs were also used in the flume to measure water depths and velocities respectively. Generally, these robust devices require minimal calibration. However, in this case, difficulties were encountered with the new ADV probes during the course of measurements, and this prompted further investigation. This involved a series of checks in the flume with the ADVs mounted on the carriage and tested, as shown in Appendix C.

The method used to perform these calibration checks was as per the manufacturer's recommendation, with the carriage moving at a constant velocity along the length of the flume. The correlated mean velocities measured by the ADVs were between 0.3% and 5%. Later, a larger margin was noted (15%) and the ADV probes were returned to the manufacturer. Considerable time and effort was spent in repeating ADV measurements with a replacement probe to ensure repeatability; thus,

the quality and standard of data collected from the hydrodynamic investigations of the GPT was maintained.

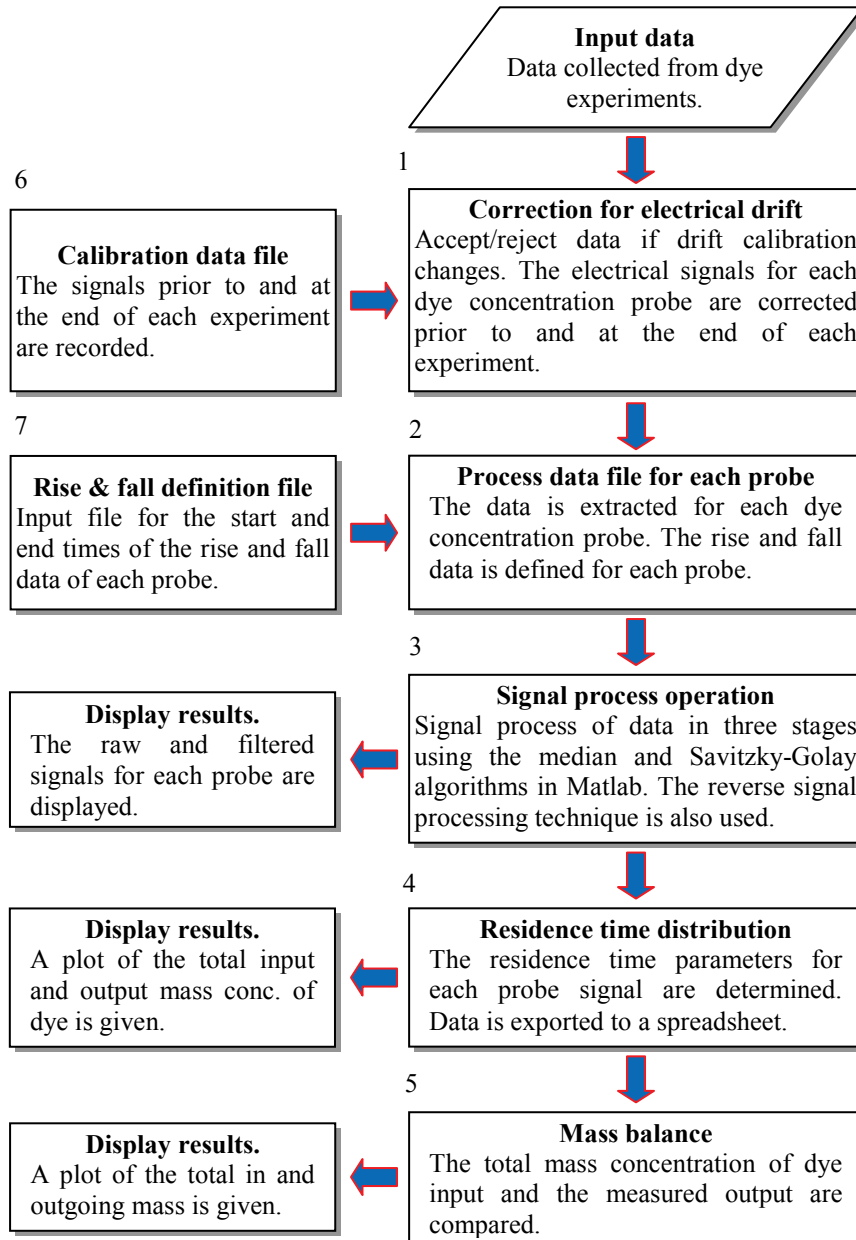


Figure 10.3 A flowchart to show the signal processing methodology used on data collected from dye experiments. In addition to addressing the spikes, the integrity of data was checked using the mass balance routine (see last box in the above flowchart).

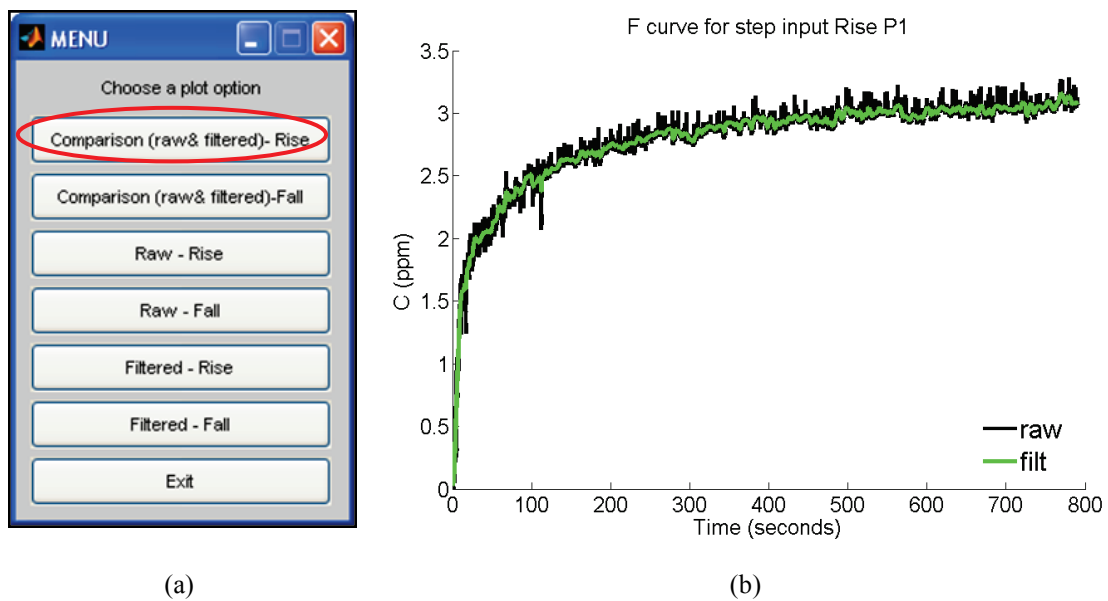


Figure 10.4 The signal processing routine in Figure 10.3 provides (a) an option menu to compare the raw with filtered data as shown in (b) in the form of a comparative plot.

10.4 HYDRODYNAMIC STUDIES

Hydrodynamic data was collected from a 50% scale model rig which was placed in a 20m flume, and an experimental method was developed to simulate a range of typical steady state flow conditions as described in Chapter 7 (Figure 10.1).

The outcome of initial hydrodynamic investigations resulted in a 3D overview of the flow entering a circular pipe inlet of the GPT model with fully blocked screens—that is 100% (Figure 10.5). The flow structure in Figure 10.5 was based on a spatial resolution of 500 ADV measured velocity points spanning four horizontal planes. These points were sparsely spaced at 50 mm, and only the outlining details of the smaller flow features were barely visible.

This method of obtaining data was revised (as discussed in Chapter 6) by refocusing solely on local areas of the fluid domain important to the overall capture/retention characteristics of the GPT. The GPT domain was divided into three distinct areas where measurements of cross sectional velocity profiles were manageable in the slotted timeframe. The revised approach also consisted of less

sampling time. For example, the original sampling time was 5 minutes. Tests showed that 2 minutes were adequate for measuring the average velocity (See Appendix C).

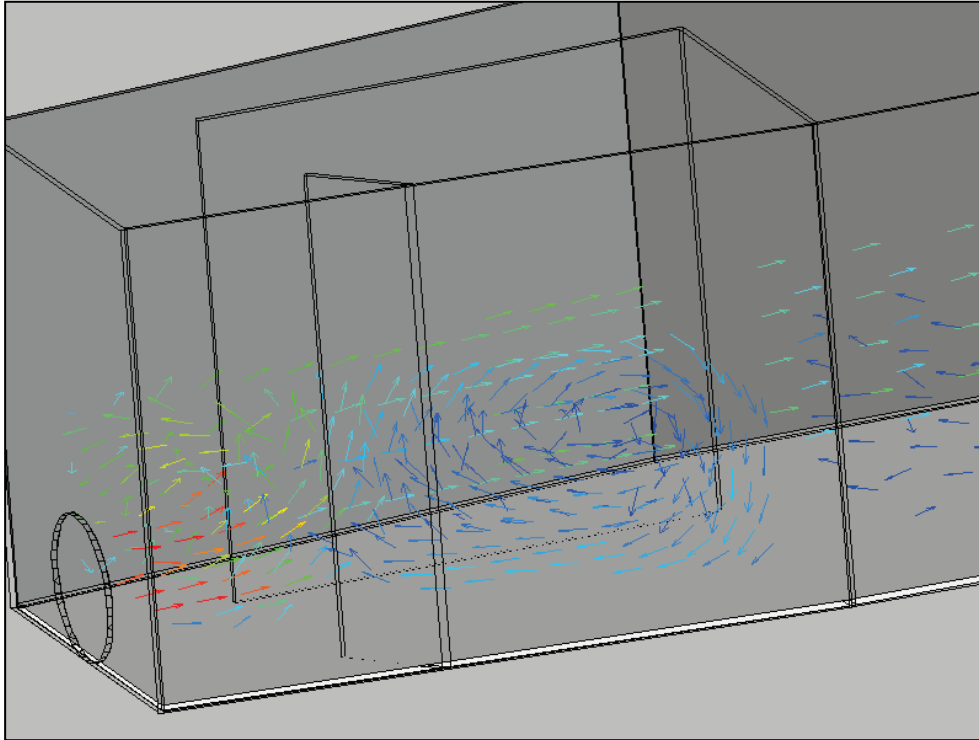


Figure 10.5. A 3D overview of the visualised flow in the GPT with fully blocked screens, obtained from initial hydrodynamic investigations. The sparsely spatial resolution of the velocity points (50 mm) does not capture the local flow features.

The outcome of the revised measurements—which also included some flow visualisations of the smaller flow structures—compared well with 2D CFD simulations (Figure 10.1). The CFD comparison was based on the assumption that measurements were taken under a steady state flow regime with a flat free surface. The approximately 2 m long inlet structure from the GPT prevented the occurrence of large-scale turbulent disturbances and allowed the development of a quasi-constant water depth flow.

The turbulent velocity spectra were also investigated by taking measurements in several locations within the GPT for a period of up to one hour (Appendix C). During this period, no low frequency spikes were observed, indicating no measurable resonance in the flume, pump and reservoir system as a whole, as indicated in the turbulent spectra plots given in Figures C.16-19, Appendix C.

In these figures, the turbulent spectra were identified by an inertial sub-range which is close to $-5/3$ slope as per Kolmogorov theory (Launder and Spalding, 1974). This slope describes the rate at which turbulent energy ε dissipates to smaller eddies and meets the hypothesis of the standard two equation k - ε turbulence model used in the CFD simulation. This outcome gave additional confidence in the measured data, particularly in view of the earlier ADV problem.

The measured and CFD data revealed several unique flow features important in understanding capture/retention characteristics of the GPT (as described in Chapter 6). Further 2D assessments were made (as documented in Chapter 7) by repeating the measurements in a rectangular channel inlet configured GPT across the water depth. The assessment was particularly enhanced since the new ADV probes revealed high shear velocity gradients next to the walls. These velocities were previously undetected since the older probes were based on a minimum wall stand-off distance. The high shear velocities were caused by the internal geometric configuration of the GPT, particularly at the bypass entrance. This had some effect on the overall 2D assessment. For example, some variations were observed in the multi-depth velocity profiles near the inlet and neighbouring regions. Despite these variations, good comparisons were obtained with the 2D CFD simulations.

At this stage, it was decided not to proceed with 3D CFD modelling, since further measurements revealed similar trends for all inlet flow rates. However, at higher flow rates, some 3D characteristics were observed in the bypass channel.

The hydrodynamic investigation using ADVs (as seen in Chapter 7, and Figure 10.1) indicated that under fully blocked conditions approximately 80% of the fluid bypasses the retention area of the GPT. This suggests that the majority of the gross pollutants entering the GPT would eventually escape through the bypass channel. This assumption holds true, provided the fluid does not recirculate at the entry to the retention region. Under the same GPT operating conditions, it was also noted that the capture/retention experiments (as discussed in Chapter 9) for the partially submerged particles ($RD = 0.9$) resulted in a maximum of 75% of pollutants escaping the GPT. In both cases the ADV and gross pollutant capture/retention results are comparable.

Point based ADV measurements can be lengthy and require considerable time and effort in capturing flows in a larger fluid domain. Thus, as seen in Chapter 7, the collection of data was limited to a GPT with fully blocked screens.

Chapter 8 describes a novel approach which was developed to capture flow in a GPT using a PIV technique. Such a technique facilitated a greater fluid coverage (with minimum effort) to include a variety of screen blockages and flow inlet conditions.

The large PIV flow dataset collected was visualised using image-based LIC algorithms. The image-based visualisations are suited to large datasets and the resulting images are considered more superior than conventional point-based visualisations such as vector or hedgehog plots, as demonstrated in Chapter 8. For example, point-based visualisations using large datasets often result in clutter.

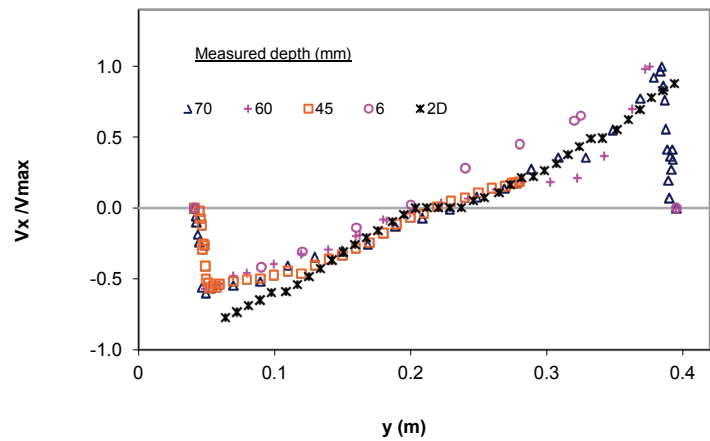
An initial attempt was made to address the cluttering issue in the current research when using the conventional vector plot routines. Data reduction techniques were used to remove clutter, but often at the expense of losing the finer flow features. A program was developed to sequentially remove clutter by spatially mapping alternate rows, columns and points from the scattered dataset. A tolerance was also introduced to remove neighbouring points. When the concentration of data varied, the fluid domain was subdivided and treated accordingly to obtain a uniform plot throughout.

For the plotting of streamlines, further problems were encountered since the scattered and irregular data had to be mapped onto a regular structured grid. This process—using generic scientific software—often inherits inaccuracies due to the low order interpolation schemes when mapping data.

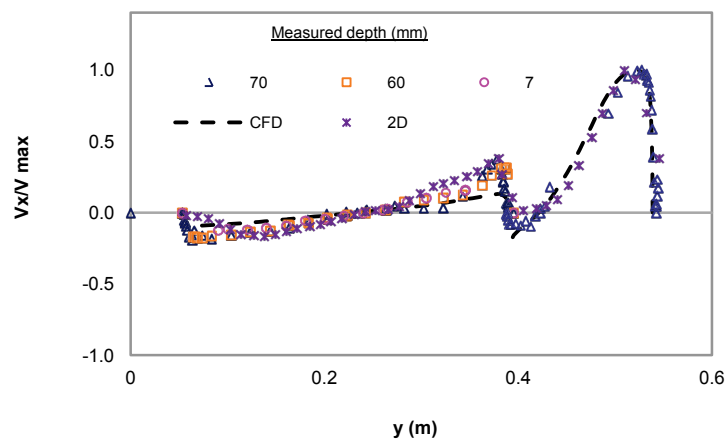
The issue of clutter and interpolation was addressed when using image-based visualisations. Image-based visualisations use higher order interpolation schemes such as cubic splines and minimising errors when producing flow images. Such an interpolation process with a large dataset usually requires high computing resources.

Chapter 8 documents the production of LIC visualisations using the supercomputing facilities at Queensland University of Technology. These PIV dataset visualisations compared favourably with the previously defined CFD flow structures for the GPT with fully blocked screens (Chapter 6).

This dataset also favourably compared with ADV measurements recorded in Chapter 7. Comparisons were made using velocity profiles of the GPT retention area for high and low inlet flow rates, as shown in Figures 10.6 (a) and (b), respectively. In Figure 10.6 (b), the CFD generated profiles are also shown. The good comparisons between the ADV and PIV profiles were attributed to the uniform seeding across the fluid domain in this retention area. Similar results were obtained from the experiments of the GPT with fully blocked screens operating under various inlet flow rates. However, some inconsistencies were observed in the inlet area of the GPT due to the non-uniform particle seeding distribution. This is a subject for further improvement.



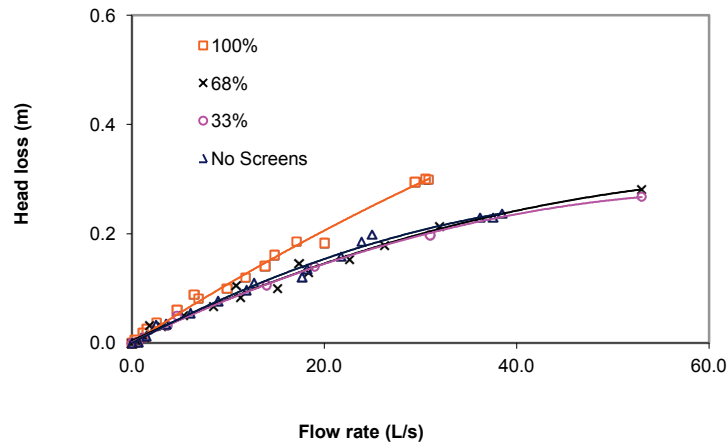
(a)



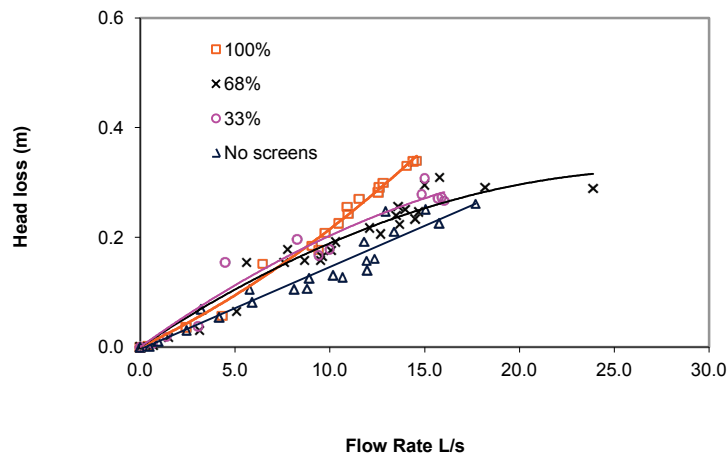
(b)

Figure 10.6. Velocity profiles from ADV and 2D PIV measurements in the retention area of the GPT are shown for a high (a) and (b) low flow inlet rates. The CFD profile for the lower flow rate is also included.

The outcome of the hydrodynamic studies documented in both Chapters 7 and 8 demonstrates the necessity of the two different experimental approaches which provided complementary results.



(a)



(b)

Figure 10.7 Head loss for (a) the rectangular and (b) the circular-pipe-inlet-configured-GPT measured under various screen blockages and no screens.

The integrated ADV results from Chapter 7 were shown to be consistent with data obtained from flow measurements taken downstream at the collection tank. This meant that, apart from obtaining localised flow features, the ADV measurements

could also be used as a comparative reference source for other dataset such as the PIV.

The PIV images in Chapter 8 were useful to compare the set of flow features in the GPT from various operating conditions which was not possible with the ADV data. The PIV images showed that beyond at least 70% screen blockages, the streamlines in the retention area of the GPT, were weaker than the flow entering the bypass. This suggests that the capture/retention performance will rapidly deteriorate as confirmed by the capture/retention experiments (Chapter 9).

Similarly, the irregularity in the rotational flow pattern of the deeper water flow regimes also suggests a poorer capture/retention performance. This behaviour was also observed in the capture/retention experiments with the exception of the sinkable pollutants (RD = 1.1). The sinkable pollutants were influenced by high negative shear velocity gradients—obtained with ADV measurements—in the lower vicinity of the inner wall. Consequently, the GPT capture/retention results for this pollutant tend to differ, as discussed in Chapter 9.

The hydraulic head loss for the pipe and channel-inlet-configured GPT were also investigated (Figure 10.7). The head loss and—by implication—the hydrodynamic flow field and capture/retention characteristics of the GPT for both inlet structures appeared not to be affected until at least 70% of its internal screens were blocked.

The gross pollutant capture/retention investigation is further discussed in Chapter 9 and below in Section 10.5.

10.5 GROSS POLLUTANT CAPTURE/RETENTION INVESTIGATION

Prior to the work reported in Chapter 9, preliminary experiments were conducted with real litter such as varied size tin cans, plastic caps and bags. Various sizes of litter were chosen to overcome the scaling issue that some researchers may dispute, since a 50% scale model GPT rig was deployed.

The various sizes provided a useful indication of the GPT performance. For example, the GPT captured the larger sizes more efficiently than the smaller cans at lower inlet flow rate (10 L/s); the plastic bags were the worst performers and, at

higher flow rates (21-26 L/s), all litter was captured efficiently. However, these experiments were insufficient in evaluating the performance of the GPT since other pollutant properties also needed to be considered.

Thus, Chapter 9 documents a novel approach which was taken to finally assess the capture/retention efficiency of the GPT with variable density artificial pollutants (See Figure 10.1). These pollutants were prepared in the laboratory using generic spherical particles which were filled with liquid to represent floatable, partially buoyant, neutrally buoyant and sinkable gross pollutants.

During the capture/retention experiments, these pollutants were released into the GPT inlet, while the outlet was video recorded. Major findings showed the rapid deterioration of the capture/retention efficiency when the internal screens were fully blocked.

Table 10.2 A comparison of the capture/retention results for the channel and the pipe-inlet configured GPT

Screen blockages (%)	Inlet flow rates (L/s)	Percentage of pollutants retained (%)	
		rectangular channel	raised pipe
33	1.3	11.0	61.6
33	6.1	81.7	90.1
68	1.3	30.5	69.8
68	6.1	84.4	96.2
100	1.3	3.3	1.1
100	6.1	9.5	0.6

At up to 70% screen blockage, the capture/retention performance of the GPT remained efficient, particularly during the higher flow rates. Further experiments may be necessary to investigate the performance between 70% and 100% screen blockages. However, the 70% screen blockage performance is also similar to findings from the hydraulic head loss experiments which suggest that this limit has been reached.

The high capture/retention performance of the GPT at this blockage is more likely due to the initial deposits of organic matter (such as grass clippings) which matted the screens. As the thickness of the mat increased, the capturing of the smaller particles was more efficient as noted during field observations. However, during lower flow rates, the performance trends of the GPT were reversed, regardless

of the screen conditions. Furthermore, there was little difference in the poor performance between a fully blocked GPT and a partially or empty GPT with fully blocked screens.

The practical significance of the above mentioned findings revealed that the GPT does not require cleaning until at least 70% of screens are blocked. This information is important for the management and maintenance of the GPT in the field whereby cleaning operations could be less frequent.

With regards to design improvements, the gross pollutant capture/retention experiments were partially repeated with a raised circular pipe inlet GPT. Based on the discussion with the manufacturer, this inlet configuration was chosen to provide additional momentum to propel the spheres into the retention area of the GPT, particularly during low flows. The results showed a marginal capture/retention improvement (16.5%), as shown in Table 10.2.

10.6 SUMMARY

In this chapter, the four specific areas of this research are presented and discussed as follows: Field Studies and the Extended Literature Review, Calibration of Equipment, Hydrodynamic Investigations and Capture/Retention Investigation as shown in Figure 10.1. These areas played a supporting role in constituting a comprehensive approach to evaluate the performance of GPTs.

The Field studies and extended literature review showed that there is a need to address the long term management of street waste, and GPTs will have a vital role to play in the future management of gross pollutants. Field studies also indicated that GPTs should be tested for abnormal or adverse conditions such as blockages caused by organic matter.

Prior to testing, equipment was prepared for the hydrodynamic and capture/retention experiments. Experimental methodologies and data processing techniques were developed and refined to address the measurement issues associated with the dye concentration probe. Here, issues relating to noise levels, electrical drift, spiking and fluid turbulence were also addressed. The use of ADV semi-intrusive probes in awkward and tight spaces and the flow disturbance due to their geometrical configuration were also addressed when measuring velocities.

The hydrodynamic data was used to complement the capture/retention experimental results. These results showed that when the internal screens of the GPT are fully blocked capture/retention efficiency rapidly deteriorates. Up to at least 70% screen blockages, the capture/retention performance of the GPT remained efficient, particularly during the higher flow rates. At lower flow rates, the performance trends of the GPT were reversed, regardless of the screen conditions.

The practical significance of this finding implies that the GPT can operate until the screens are approximately 70% blocked without prior maintenance. This is valuable information for the management of the maintenance schedules of the *LitterBank* GPT.

Table 10.3 Summary of data collected for the current scientific research of a GPT

Investigation/ preparation	Data collected	Methodology	Duration	Total
Field survey	300 photographs/notes	area measurements	n/a	3 mths over 2 yrs
Dye	180 pts measured	scalar dye concentrations	10 mins/pt	30 hrs
ADV	4000 pts measured	velocities	5 mins/pt	333 hrs
Flow visualisations	36 real time videos	flow field velocities	30 mins/video	18 hrs
Capture/retention	72 real time videos 21600 particles	capture efficiency/ residence time	45 mins/video	54 hrs
Head loss	120 pts measured	water height measurements	8 mins/pt	16 hrs
Artificial pollutants (preparation)	900 spherical particles	preparation of variable buoyancy pollutants	20 mins/particle	300 hrs
CFD	30 simulated flow fields	simulation runs	3 hours/run	90 hrs

The hydrodynamic and capture/retention data collected and the time taken for this research are summarised in Table 10.3. Here, the duration does not include data preparation or analysis time. This data consisted of approximately 100 Gigabytes of computer file storage disk space. The current research data showed that the GPT is

designed with an efficient high flow bypass to prevent scouring of gross pollutants and upstream blockages. The GPT was also satisfactorily tested under adverse operating conditions, with high and low tidal waters. The outcome is consistent with most design guideline criteria quoted in the literature (Wong et al., 2006).

REFERENCES

- Allison, R. A., Walker, T. A., Chiew, F. H. S., O' Neill, I. C. and Mc Mahon, T. A. (1998). *From roads to rivers: gross pollutant removal from urban waterways*. Clayton, Victoria: CRC for Catchment Hydrology. Retrieved 14 January 2010, from <http://www.catchment.crc.org.au/pdfs/technical199806pt1.pdf>
<http://www.catchment.crc.org.au/pdfs/technical199806pt2.pdf>
<http://www.catchment.crc.org.au/pdfs/technical199806pt3.pdf>
<http://www.catchment.crc.org.au/pdfs/technical199806pt4.pdf>
- Field, R. and Sullivan, D. (2003). *Wet-weather flow in the urban watershed: technology and management*. Boca Raton, Florida: Lewis Publishers.
- Kayhanian, M., Kummerfeldt, S., Kim, L.-H., Gardiner, N. and Tsay, K. (2002). Litter pollutograph and loadograph. In E. W. Strecker and C. H. Wayne (Eds.), *Global Solutions for Urban Drainage: Proceedings of 9th International Conference on Urban Drainage (9ICUD)* (pp. 218-218). Portland, Oregon, USA: American Society of Civil Engineers (ASCE).
- Lauder, B. E. and Spalding, D. B. (1974). The numerical computation of turbulent flows. *Computational Methods Applied Mechanical Engineering*, 3, 269-289.
- Wong, T., Wootton, R., Argue, J. and Pezzaniti, D. (2000). Bringing order to the pollution control industry-issues in assessing the performance of gross pollutant traps. *Australian Civil Engineering Transactions*, 42, 57-62.
- Wong, T. H. F., Allison, R. A., Argue, J., R., Breen, P., Brown, R., Coombes, P., Duncan, H., Evangelisti, M., Fletcher, T., Lawrence, I., McAlister, T., Mitchell, G., Mouritz, M., Pezzaniti, D., Phillips, B. and Taylor, A. (2006).

Australian runoff quality—a guide to water sensitive urban design. Crows Nest, New South Wales: Engineers Australia.

Chapter 11: Conclusion

This research is presented in a series of publications which forms the main body of the thesis. Here, a novel and comprehensive testing approach has been developed to examine a recently manufactured dry sump GPT. The linear fluid motion characteristic GPT is designed with internal screens to capture gross pollutants—organic matter and anthropogenic litter—and has not been previously investigated.

Alongside the literature review of GPTs and gross pollutant data, there are four specific methodologies employed in this testing approach, and these are: field work and an historical overview of street waste/stormwater pollution, calibration of equipment, hydrodynamic studies and gross pollutant capture/retention.

These studies are the first comprehensive investigations of their kind and provide valuable information for this research and for any future work pertaining to the operations of GPTs and management of street waste in the urban environment.

The novel and comprehensive testing approach employed, addresses the current limitations in the evaluation methodologies of GPTs. This approach uses a combination of physical and theoretical models to examine in detail the hydrodynamic and capture/retention characteristics of the GPT.

The hydrodynamic assessment employed point-based ADV measurements, and flow field PIV capture, head loss experiments and CFD simulation.

The gross pollutant capture/retention assessment included the use of anthropogenic litter components, tracer dye and custom modified artificial gross pollutants.

The hydrodynamic and capture/retention performance assessments of the GPT were carried out under various in-field operating conditions which included fully and partially blocked screens. Two different inlet configurations—circular pipe and rectangular channel—were also examined under likely operations of the GPT in real settings, which were informed by field work.

The results of these assessments together with the measurement methodologies for deploying ADVs and dye concentration (Komori) probes are reported in the next section under the heading ‘Research Outcomes’.

11.1 RESEARCH OUTCOMES

Field work revealed that some GPTs were inappropriately placed and their intended purpose to capture gross pollutants was not effectively utilised. Other findings showed that the finer and more harmful pollutants—traffic-generated dust and nutrients—are likely to be attached to gross pollutants which become carriers when transported into the environment. Gross pollutants found on streets and in stormwater systems are on the rise. Furthermore, with the implementation of green walls and roofs in new urban design concepts, the resulting increase in organic street waste will further complicate the management of stormwater pollution. Consequently, GPTs will continue to play a role in protecting the environment. The demand for these GPTs calls for stringent quality control and this research provides a foundation to rigorously assess these devices.

In order to assess the GPT, experimental methodologies for using equipment such as the ADVs and the Komori dye concentration probes were successfully developed which also overcame the issues arising from measurements. This was the first attempt to perform hydrodynamic and gross pollutant capture/retention assessments of a dry sump GPT with these instruments. Consequently, a rigorous assessment of the frequency response characterisation of the Komori probe was carried out since it has not been previously reported.

The assessment revealed that the Komori probes were found to have a frequency response of up to 100 Hz—which is dependent upon fluid velocities—and this was adequate to measure the relevant fluctuations of dye introduced into the GPT flow domain.

The initial hydrodynamic assessment was based on a circular pipe and rectangular channel inlet GPT with fully blocked screens. Velocity profiles across the three cross sectional width of the GPT were assessed. The results of this assessment revealed good comparisons between the CFD and the measured ADV point-based velocity data.

In the CFD flow field simulation result, global and local flow structures important for understanding capture/retention characteristics of a GPT were identified. Furthermore, the simplification of the 2D CFD simulation was sufficient to capture the major flow features of the flow.

The good correlation between the CFD and experimental data, demonstrated that the measurement technique developed to use the semi-intrusive ADV probe in confined spaces within the GPT produced satisfactory results. Although, during measurements in limited spaces, some flow disturbances were noted in the fluid surrounding the ADV probes. Here, small variations in these measurements were observed and reported as a result of using different geometrical ADV probe configurations.

Apart from ADV measurements, the flow field PIV, the head loss and the gross pollutant capture/retention data were used to investigate the GPT under various screen blockages. The results of the investigation revealed that the capture/retention performance of the GPT rapidly deteriorates when the internal screens are fully blocked.

The results also showed that the GPT will operate efficiently until at least 70% of the screens are blocked, particularly at high flow rates; that is, above 6 L/s. At lower flow rates, the high capture/retention performance trends were reversed. There is little difference in the poor capture/retention performance between a fully blocked GPT and an empty or partially filled GPT with 100% screen blockages.

With regard to the design and performance assessments, further investigation showed that a raised inlet GPT offers better capture/retention performance, particularly at lower flow rates.

It was shown from this investigation that the GPT meets the general WSUD design guidelines. The assessment revealed that the GPT is designed with an efficient high flow bypass system to avoid upstream blockages. The capture/retention performance of the GPT at medium to high inlet flow rates (inlet velocity > 2 m/s) is close to maximum efficiency—100%.

The practical significance of the above mentioned findings revealed that the GPT does not require cleaning until at least 70% of screens are blocked. This information is important for the management and maintenance of the GPT in the

field, whereby cleaning operations could be less frequent. This research also shows that field work plays an important role in collecting gross pollutant data for the management and appropriate placement of GPTs.

11.2 FUTURE WORK

This section recommends specific areas of this research to be extended in consideration for future work.

Firstly, the outcome of this research pertains to the development of a comprehensive testing approach which has been used to investigate a dry sump, linear fluid motion GPT. Further evaluation is necessary to determine the broader viability and application of the comprehensive testing approach developed here by undertaking investigations of other GPTs or SQIDs.

Secondly, the experimental work involves a number of labour-intensive tasks which could be reduced by using: commercially manufactured artificial pollutants, an automatic feeding mechanism for introducing the artificial pollutants into the GPT during the capture/retention experiments, and a program to analyse video recordings of the outlet. Additionally, a program using Simulink® (2008b, The Mathwork, Melbourne, Victoria) has been developed by the author to monitor the artificial generic pollutants escaping the GPT and is nearing completion.

These above mentioned improvements would make the testing methodologies viable for the commercial application of assessing GPTs and other SQIDs.

Thirdly, the maintenance of the GPT is an important consideration which requires further investigations based on the findings of this research. Currently, there is scant data in relation to the modelling and prediction of the maintenance schedule for GPTs.

Fourthly, this research was partly based on the capture/retention results of the GPT using hard, generic artificial pollutants. However, field work showed that a large amount of organic matter is found on streets and in stormwater systems. Organic matter is a soft pollutant and its physical properties often change when transported in water. Anthropogenic litter such as paper and plastic are also classed

as soft pollutants. Preliminary experiments with plastic bags indicated their poor capture/retention behaviour in comparison to solid litter items.

Consequently, it is necessary to explore the physical modelling of the softer pollutants with variable densities. Such artificial pollutants could be constructed from miniature water—proofed sacks filled with liquid and introduced to the capture/retention experiments of GPTs. This would provide a better indication of their field performance.

Fifthly, the data collected from field studies was partially stored in a GIS database and further work is necessary to incorporate the remaining photographic results. It is envisaged that this database will be beneficial to the public and scientific community and will also encourage participation of stakeholders and local city councils.

Lastly, sufficient experimental data has been collected from this research to validate investigations of a 3D flow in a GPT using CFD simulation. Preliminary 3D CFD flow field simulation has been carried out for the GPT with the rectangular channel inlet configuration, indicating that further modelling assessments are required. This should also include design optimisation studies for different GPT inlet and screen configurations.

For example, the partial results for the raised circular pipe inlet GPT showed improved capture/retention performance and further investigations are also necessary in this regard. The flow characteristics of this inlet configuration are predominantly three-dimensional. Thus, this warrants 3D CFD modelling and PIV techniques to capture the comprehensive characteristics of these flows in the GPT.

The CFD work could also be extended to include the modelling and simulation of gross pollutant particles for subsequent comparisons with the current experimental gross pollutant capture/retention results.

[This page is left blank intentionally]

Appendices

[This page has been left blank intentionally.]

APPENDIX A: RAINFALL DATA

This appendix contains rainfall data over a two year period in which gross pollutant data was collected for the field study in Chapter 2.

Table A.1 Daily Rainfall (millimetres), BRISBANE Station Number: 40913; State: QLD; Latitude: 27.48°S (<http://www.bom.gov.au/climate/averages/>)

2006	Jan	Feb	Mar	Apr	May	Jun	Jul	Aug	Sep	Oct	Nov	Dec
1st	0	0	1	25.2	5.8	0	0	0	9	0	0	0
2nd	0	0	4.4	0	0	0	0	0	5	0	0	0.2
3rd	0	0	27.2	0	0	0	0	0	0	0	0	0
4th	24.4	0	11.2	0	0	0	0	0	0.2	0	2.6	40.4
5th	17.2	1.4	15.4	21.4	0	0	0	0	0.2	0	46.4	0
6th	1.4	0.8	0.4	1.6	0	0	0	0	1	0	0.2	0
7th	45.4	0.2	0	0.2	0	0	0	0	0	0	15.8	0
8th	3.4	1.2	0	0	0	0	0	0	0	0	0	1
9th	2.2	0	0	0	0	0	0	0.2	0	0	5.8	0.2
10th	13.6	0	0.4	0	0	1.2	0	0	0	0	0	0
11th	4.6	1.8	0	0	0	12	0	0	16.2	4	0	0.2
12th	0	17	0	0	0	0	0	0	0.2	0	0	0
13th	0	1.8	0	0	0	0	0	0	0.2	0	0	1.8
14th	0	0.2	0	0	0	0	0	0	0	0	0	0
15th	0	22.4	0	0	0	0	0	0	0	0	0	0
16th	0	5.6	0	0	4	0	1.8	0	0.8	0	14	2
17th	0	10.8	0	0	0.2	0	0	0	9.6	4.6	0	4.8
18th	0	0	0	0	0	0	0.2	0	0	0	0	1.2
19th	0	0	0	0		1	0	0	0.2	0	0	0
20th	30.2	0	0	0	0	1.2	0	0	0.2	0.8	0	0
21st	31.2	0	0	0	0	20.8	0	0	0	0	0	0
22nd	0.2	1.2	0.4	0	0	3.6	0.4	0	0	12	0	5.4
23rd	0	11.2	0.8	0	0	1.4	0.6	0	0	0	0	0
24th	0	8	15.8	0	0	0.4	0	0	0	0	0	0
25th	0	5.4	1.2	0	0	0.2	2.6	0	0	0	0	0
26th	0	0	0.2	0	0	0	0.2	0	0	0	0	1.8
27th	0	11.4	0	0	0	1.8	0	0	0	0	0	16
28th	0.2	6.2	0	0	0	0	9.6	20.2	14.2	0	0	7.4
29th	0	-	0	0	0	0	16.8	24.2	0	0	0	0.2
30th	0	-	0	0	0	0.2	0.2	0	0	0	0.6	0
31st	0	-	0.4	0	0	-	-	10.6	0	0	-	0
Highest daily	45.4	22.4	27.2	25.2	5.8	20.8	16.8	24.2	16.2	12	46.4	40.4
Monthly Total	174	106.6	78.8	48.4	10	43.8	32.4	55.2	57	21.4	85.4	82.6

Annual total for 2006 = 795.6 mm

	Jan	Feb	Mar	Apr	May	Jun	Jul	Aug	Sep	Oct	Nov	Dec
Highest daily	0	0	1	25.2	5.8	0	0	0	9	0	0	0
Date of highest	16th	2nd	3rd	10th	20th	3rd	27th	22nd	5th	18th	20th	31st
daily rainfall	2004	2001	2001	2009	2009	2008	2001	2002	2008	2001	2008	2001

Table A.2 Daily Rainfall (millimetres), BRISBANE Station Number: 40913; State: QLD; Latitude: 27.48°S (<http://www.bom.gov.au/climate/averages/>)

2007	Jan	Feb	Mar	Apr	May	Jun	Jul	Aug	Sep	Oct	Nov	Dec
1st	4.2	0	1.6	0	0	0	0	0	0	0	2.2	0.2
2nd	9.2	8	0.4	0.2	0	0	0	0	0	0	0.2	1
3rd	23.8	0.4	0	0	0	0	0	0	0	0	0	7
4th	8.4	0	0	0.2	0	0.2	0	0	0	0	0	0
5th	7.4	0.2	0.2	0	0	0	0.2	0	14.2	0	0	1.2
6th	0.6	0	4.2	0	0	52.6	0	0	10.4	0	10	2.2
7th	0	0	8.4	0	0	18	0	0	2.4	0	0.2	0.2
8th	0	0	0.6	0.4	6	0	0	0	1.6	3	18.6	27
9th	0.2	0	3.6	0.6	0.2	0.2	0	0	0.2	10.2	0.6	0.2
10th	0	0	0	0	0	0	0	0	0	0.2	0	0
11th	0.2	15	0	0	1.4	0	0	0	0	10	0.2	0.2
12th	0	0.4	0	0	0.2	0	0	0	0	0.2	3.6	9.8
13th	0	16.6	0	0	2.6	0	0	0	0	0	2.6	10
14th	0	5.6	0	0	0.2	0	0	0	0	0	0	0
15th	0	0.8	0	0	0	0	0	0	0	0	0	0
16th	0	0	0	0	0	0	0	1.2	0	0	0	0
17th	0	1	0	0	0	0	0	0.2	0	0	9.6	0
18th	0	1.2	0	0	1.6	0	0	0	0	0	2.6	1
19th	0.6	1.6	0	0	0	0.2	0	0	0	0	0	0.2
20th	0.2	0	0	0	0	0	0	28.6	0	0	0	0
21st	0	1.6	0	0	0.2	0	0	1.6	0.2	0	0	0
22nd	0	0.8	0	0	0.2	0	0	11.8	0	0	1.2	0
23rd	0.2	0	0	0.8	0	0	0	5	1.2	0	0.8	0
24th	0	2	0	0	0	4.6	0.4	35.8	0.2	0	3.8	5
25th	0.6	2	0	0	0	2	0.4	5.8	0	0	0.6	0.2
26th	22.4	0	1.6	0	7.2	20.2	0	1	0	18.8	1.4	0
27th	0.2	0	0	0	3.8	14.6	0	0.2	1.8	0.4	1	3.8
28th	0	0	0	0	9.2	0	0	0	0.2	0	0.8	2.6
29th	0	0	0	1	2.4	0	0	0	0	12.2	0.2	0.4
30th	20.8	0	0	0	0.2	0	0	0	0	0.2	1.6	0
31st	0	0			3.6	0	0	0	0	0	0	7
Highest daily	23.8	16.6	8.4	1.0	9.2	52.6	0.4	35.8	14.2	18.8	18.6	27.0
Monthly Total	99.0	57.2	20.6	3.2	39.0	112.6	1.0	91.2	32.4	55.2	61.8	79.2

Annual total for 2006 = 652.4 mm

	Jan	Feb	Mar	Apr	May	Jun	Jul	Aug	Sep	Oct	Nov	Dec
Highest daily	0	0	1	25.2	5.8	0	0	0	9	0	0	0
Date of highest	16th	2nd	3rd	10th	20th	3rd	27th	22nd	5th	18th	20th	31st
daily rainfall	2004	2001	2001	2009	2009	2008	2001	2002	2008	2001	2008	2001

Table A.3 Daily Rainfall (millimetres), BRISBANE Station Number: 40913; State: QLD; Latitude: 27.48°S (<http://www.bom.gov.au/climate/averages/>)

2007	Jan	Feb	Mar	Apr	May	Jun	Jul	Aug	Sep	Oct	Nov	Dec
1st	0	0	0	0	1	0	0	1.6	0	0	0	0
2nd	5.4	0	0	0	0	44.2	0	0	0	0	0	0
3rd	3.2	42	0	0	0	60	0	0	0	0	0.2	0
4th	36.2	42	0	0	0	0.2	0.8	0	6	0	2.8	3.6
5th	27.4	10.6	0	0	0	0	0	0	41.6	0	0	9.6
6th	0	5.2	0	0	0	0	16.2	0.2	3.8	0	23.6	7.8
7th	42.2	41.6	0	6.2	0	5.6	0	0	0	0	0	12.4
8th	0	0	0	0	0	0	24.2	0	0	0	0	0
9th	0.6	5	0	2.2	0	0.8	3.8	0	0	0	8.6	0.2
10th	1.2	0	1.2	0	0	2.4	0.2	0	0	22.6	0	0.6
11th	0	0	0.6	0.2	0	0	0	0	0	7.6	0	0
12th	0.8	10.2	0	0	0	0	0	0	0	2	0.4	9.6
13th	0	15.6	0	0	0	0	0	0	0.4	1.2	8.8	0
14th	0	8	0	0	0	0	0	0	0.2	0	1	0.4
15th	8.4	0.2	0	0	0	0	0	0	1	0.2	0.2	0
16th	11.2	0	0.4	0	0.2	0	5.4	0	0	14.4	0	0
17th	0.8	1.4	2.8	0	0	0	2.8	0	0	0.2	31.8	0
18th	0.6	2.2	2.4	0.8	5.4	0	0	0	0	0	14.6	0
19th	0.2	16.6	1.4	7	0	3.6	0	0	0.4	0	77.2	2
20th	0	0.2	1.2	0.4	0.2	0	0	0	0.2	0	79.4	0
21st	0.4	0	3.6	0	0	3.8	0	0	0.4	0	28.8	0
22nd	0	0	0	0	0	0.2	0	0	0	6.6	0.2	0
23rd	0	0	0	0	0	0	0.2	10	0	0	6.6	0
24th	0	0	0.8	0	0	0	12.6	0	0	0	0	0
25th	0	0	0.6	0	0	0	22.4	0	0	0	0	0
26th	0	1.2	0	0	0	0	0.4	0	0	0	11.6	0.8
27th	0	14.8	5.4	0	0	0	0	0.2	0	0	25.2	0.6
28th	0	0	15	0	0	0	2.4	0	0	0	2.2	4.2
29th	0.8		6.4	0	0.6	0	0	5	0	0	0	0.2
30th	35	0	0	0	31.8	0	0	0.4	0	0.4	3.4	6.6
31st	3	0	0	13.8	0	0	0	0	0	0	0	4
Highest daily	42.2	42	15	7	31.8	60	24.2	10	41.6	22.6	79.4	12.4
Monthly Total	184.4	216.8	41.8	16.8	52	121.8	91.4	15.8	55.6	55.2	326.6	62.6

Annual total for 2006 = 1240.8 mm

	Jan	Feb	Mar	Apr	May	Jun	Jul	Aug	Sep	Oct	Nov	Dec
Highest daily	0	0	1	25.2	5.8	0	0	0	9	0	0	0
Date of highest	16th	2nd	3rd	10th	20th	3rd	27th	22nd	5th	18th	20th	31st
daily rainfall	2004	2001	2001	2009	2009	2008	2001	2002	2008	2001	2008	2001

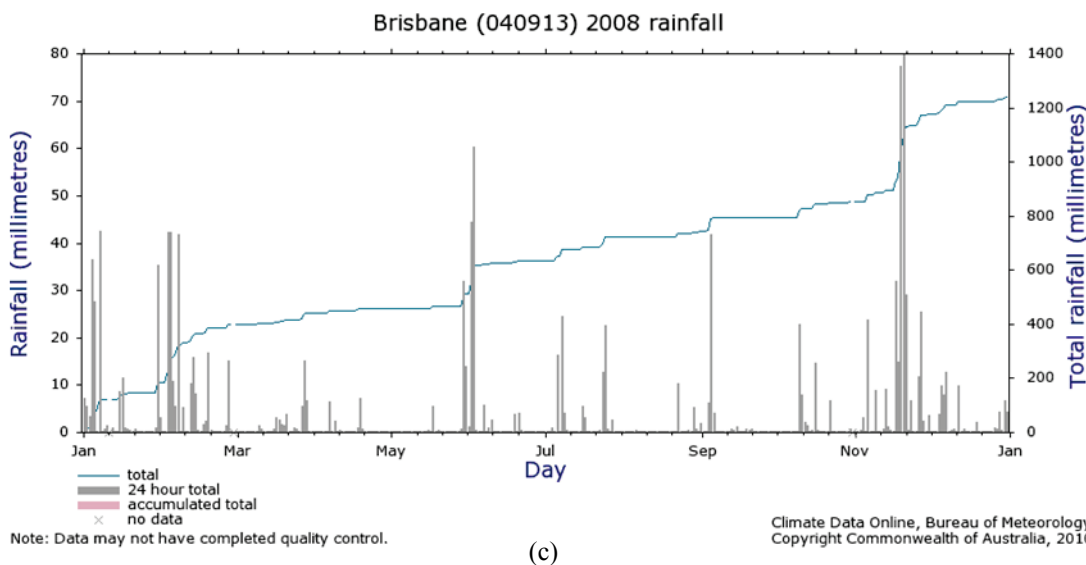
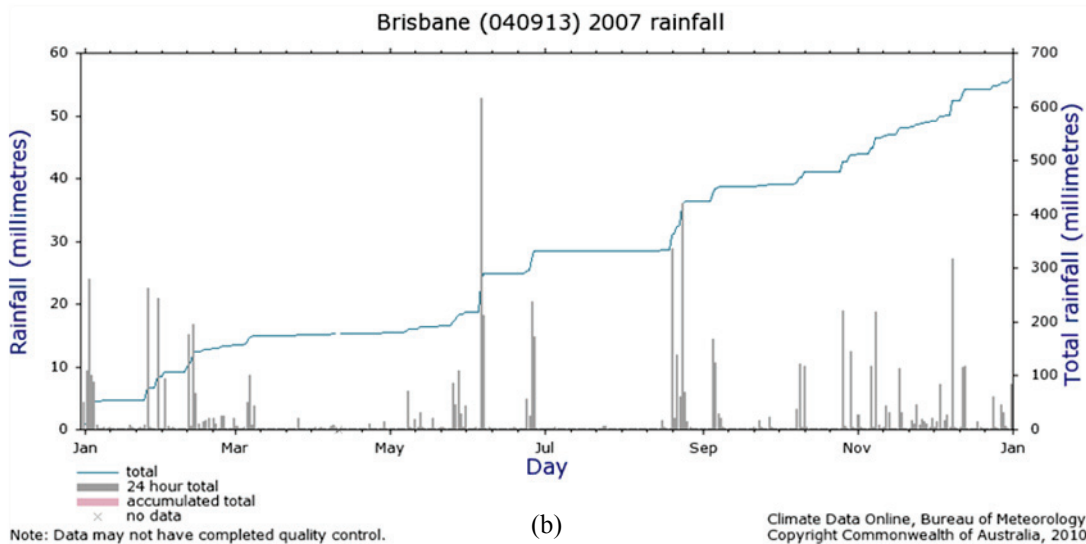
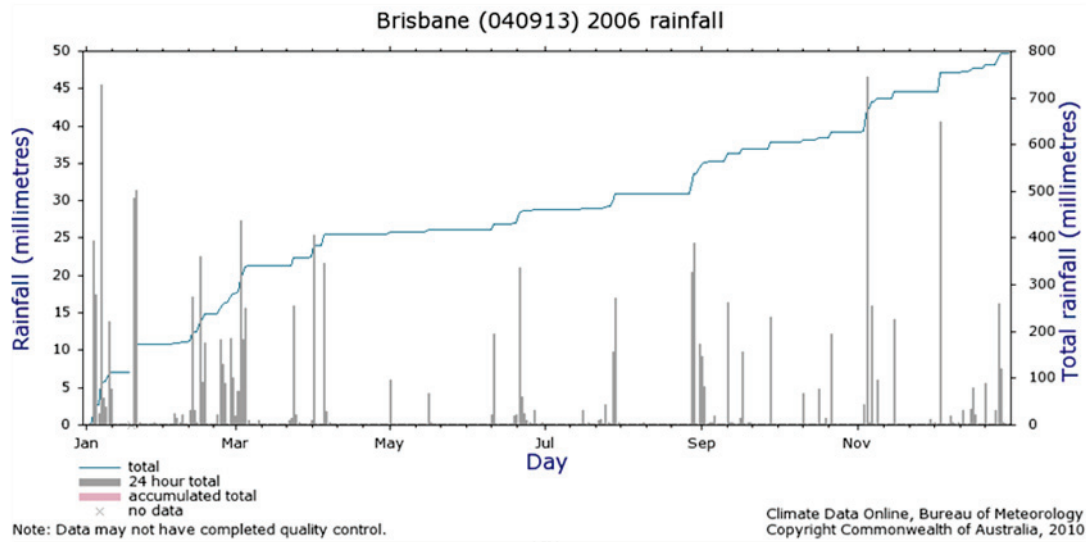


Figure A.1 Monthly rainfall data for Brisbane (a) 2006, (b) 2007 and (c) 2008. (<http://www.bom.gov.au/climate/averages/>).

APPENDIX B: WIRING DIAGRAM

This appendix details the wiring diagram for the Komori (dye concentration) probes (Section B.1) and the ultrasonic sensors (Section B.2). Figure B.1 is a photograph showing the housed connections of these instruments to the data acquisition board.

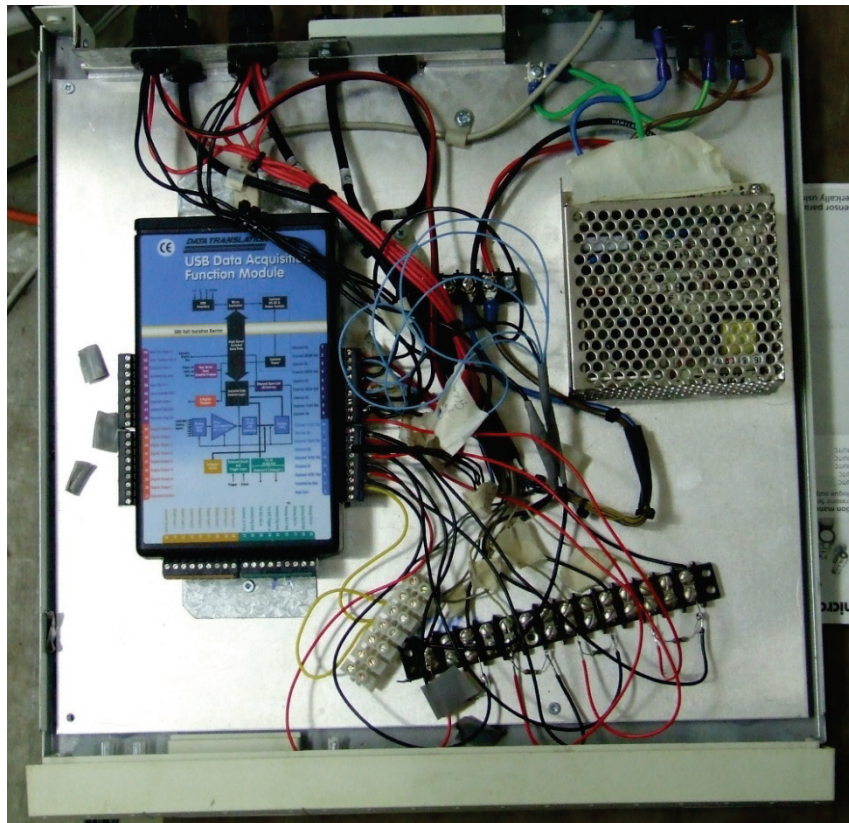


Figure B.1 Inside the housing showing the connections of the instrumentation to the data acquisition system.

B.1 Komori probes

Pin connections (probes labelled P1-6) for the dye concentration probes to the data acquisition instrumentation DT9800 series is shown in Figure B.2

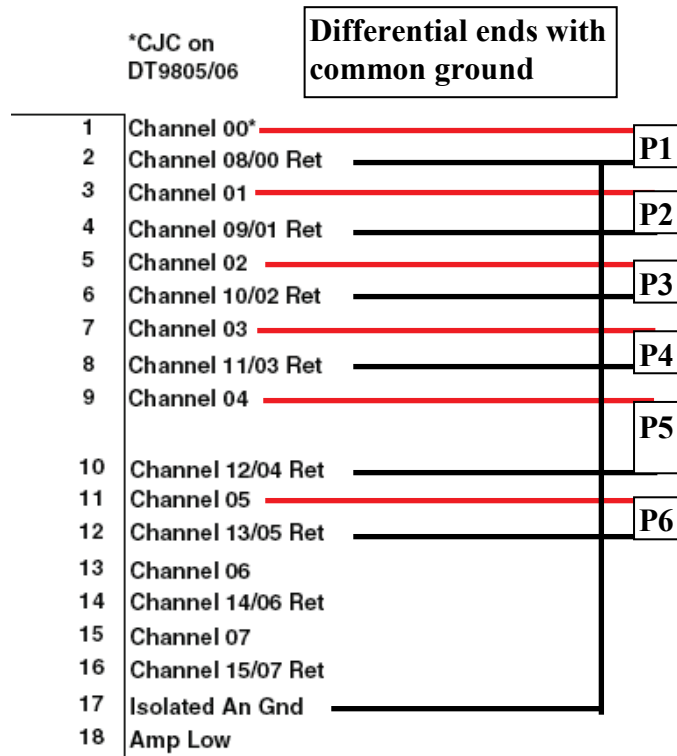


Figure B.2 Pin connections for the Komori scalar dye probes (P1-P6) to the DT9800 connection board.

B2. Ultrasonic probes

Water depth measurements were taken to monitor the flow conditions in the flume during the hydrodynamic, gross pollutant capture/retention and the head loss experiments. Ultrasonic probes were fitted at various points in the flume (as documented in Chapter 7) to take the water depth measurements.

Two model types of the ultrasonic displacement sensing probes with an accuracy of 0.18 mm were used: (1) Microsonic™ +25/IU/TC/E with a response time of 50 ms and (2) Microsonic™ +35/IU/TC/E with a response time of 70 ms.

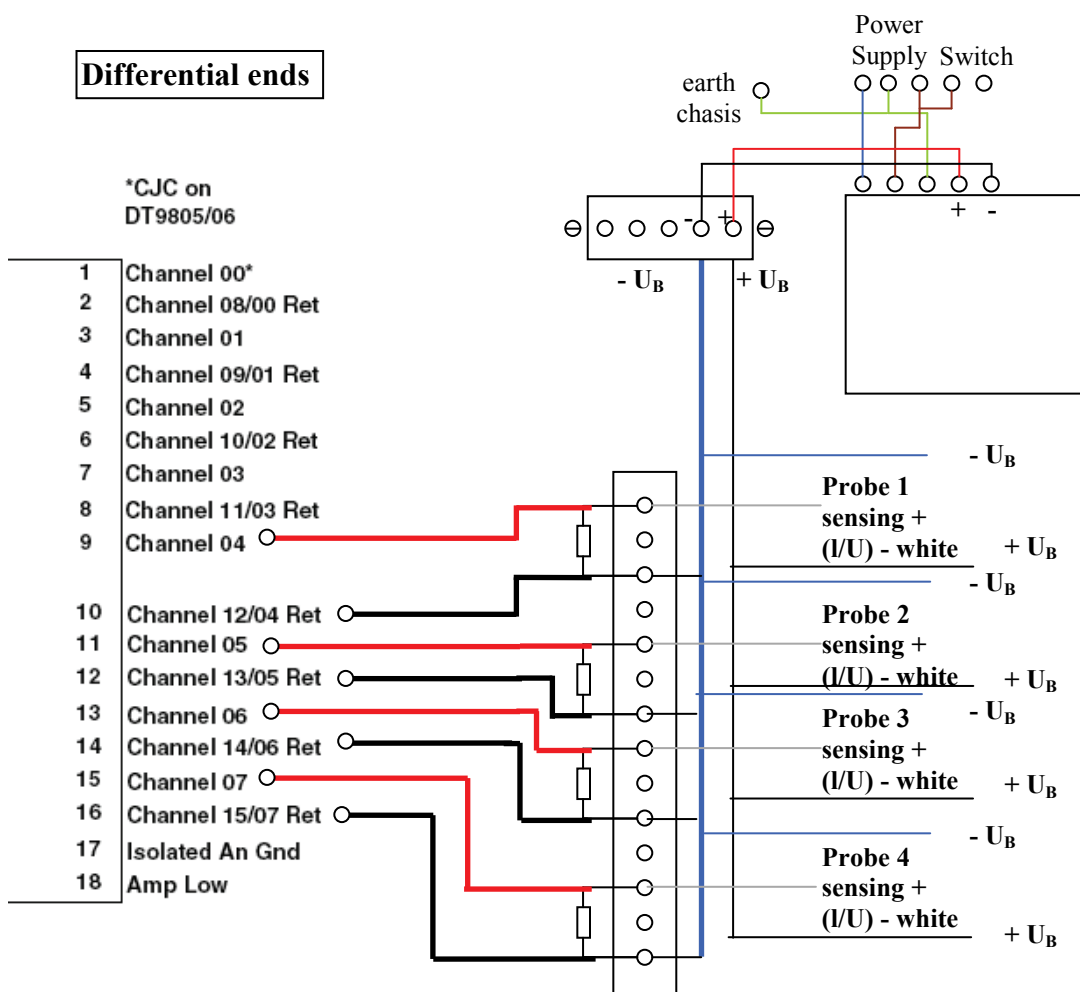


Figure B.3 Wiring diagram for the connection of the ultrasonic probes to the acquisition data system DT9800.

The wiring diagram for the connection to the data acquisition instrumentation DT9800 series is shown in Figure B2.1. The five core wires from the probe main cable. $-U_{\text{Blue}}$ (No. 3) connects to the negative terminal on the 30V power supply and also to the DAQ negative terminal. $+U_{\text{Black}}$ (No. 1) connects to the positive terminal of the power supply. (No. 2) white, is the sensing + connects to the DAQ positive terminal. Pin numbers 4 are joined together from each probe. Likewise for pin numbers 5 from each probe are joined together.

APPENDIX C: ADV DATA ANALYSIS

The ADVs used in this research are widely used and suitable for field and laboratory measurements. Scientific evidence shows that ADV measurement issues, if not correctly addressed, can affect the reliability and accuracy of the results obtained. These inherent issues relate to spike events caused by the aliasing of the Doppler signals, velocity shear, noise and hardware errors (Trevethan, 2007; Lemmin and Lhermitte, 1999; Goring and Nikora, 2002).

Generally, ADV processing methods have been satisfactorily developed and accepted within the scientific community. For example, the widely used industrial software programs such as WinADV (http://www.usbr.gov/pmts/hydraulics_lab/twahl/winadv/) and Horizon ADV (<http://www.sontek.com/>) were successfully used in this research to process raw ADV files. However, the quality of data collected also relies on other measurement variables such as sample size, noise levels and the intrusive nature of the ADV probe.

A sensitivity analysis on the effect of the sample size was carried out on the time-averaged velocity data, the turbulent velocity spectra and the measurement comparisons of the side and down-looking ADV probes. A series of stationary tests were conducted to investigate the variation of the stationary statistical properties of the velocity data over the sampling period.

The first four statistical moments were respectively investigated, namely: time-averaged mean (\overline{Vx}), standard deviation (σ), skewness (Sk) and kurtosis (Kt). These were calculated using the definition of statistical moments of the instantaneous velocity variable Vx as:

$$\overline{Vx} = \frac{1}{N} \sum_{i=1}^N Vx_i . \quad C.1$$

$$\sigma = \sqrt{\frac{1}{N-1} \sum_{i=1}^N (Vx_i - \overline{Vx})^2} . \quad C.2$$

$$Sk(Vx) = \frac{1}{N-1} \sum_{i=1}^N \left(\frac{Vx_i - \overline{Vx}}{\sigma} \right)^3, \quad C.3$$

and

$$Kt(Vx) = \frac{1}{N-1} \sum_{i=1}^N \left(\frac{Vx_i - \overline{Vx}}{\sigma} \right)^4, \quad C.4$$

or the excess Kurtosis where it is zero for a Gaussian distribution and is defined as

$$Ku(Vx) = \left[\frac{1}{N-1} \sum_{i=1}^N \left(\frac{Vx_i - \overline{Vx}}{\sigma} \right)^4 \right] - 3, \quad C.5$$

where N = total number of data samples, i is the data sample number and Vx_i is the velocity value at sample number, i . The statistical moments from the above equations characterises the turbulent flow properties.

The standard deviation in equation C.2 measures the dispersion or the magnitude of fluctuations about the time-averaged mean.

The skewness and kurtosis denotes the temporal distributions or fluctuations about its mean value and the Gaussian distribution.

Skewness describes the asymmetry in the probability density function of turbulent fluctuations (Balachandar and Bhuiyan, 2007). Skewness other than zero indicates the degree of temporal asymmetry of the turbulent fluctuations associated with ejection events. Ejection is the process when a low-speed fluid parcel or streak lifts away from the wall, oscillates in three dimensions, and then breaks down so that fluid is expelled into the outer flow. The ejected fluid that remains as a result of retardation is swept away by high-speed fluid that approaches the wall in a process called the sweep. The point of change of sign in the skewness profile is related to the crossover from sweep to ejection motions (Balachandar and Bhuiyan, 2007).

The fourth-order moment—that is the kurtosis—relates to the flatness factor which describes the intermittency of turbulence. A kurtosis (K_t) greater than 3 indicates an association with a peaky signal characteristic of intermittent turbulent events (Balachandar and Bhuiyan, 2007).

The four ordered moments were calculated using equations C1-C4 to investigate the signal characteristics for the collected velocity time series at various locations in the GPT (Table C.1 and Figure C.1).

The GPT was divided into four locations each with its unique flow characteristics, namely the inlet, trap mouth, retention area and the outlet as denoted respectively, by A, B, C and D in Figure D1. Upon the flow entering the GPT and reaching the water depth required, the velocities at these points were monitored and recorded for a period of up to one hour.

The statistical properties of the measured velocity dataset were calculated and plotted for the period as shown in Figures D2 to D10. These figures report the statistical average (A_v), standard deviations (σ), skewness (S_k) and the kurtosis (K_t), respectively for each sampling period up to a duration of one hour.

All measurements were taken after a one hour period, thereby allowing the flow in the flume to reach steady state conditions (Figures C.2 – C.10). Towards the end of the time series, a set of sampling periods and the corresponding statistical moments were replotted in Figures C.11-C.14. Overall, the statistical mean and higher moments of the measured data showed little variations when compared with various sampling periods.

Table C.1. The locations at which data was collected for the investigation of

Point	Serial number	x (mm)	y (mm)	Description
A	A919F	000	297	inlet
B	A919F	200	318	trap mouth
D	0007F	450	318	retention area
B	0007F	670	470	trap mouth

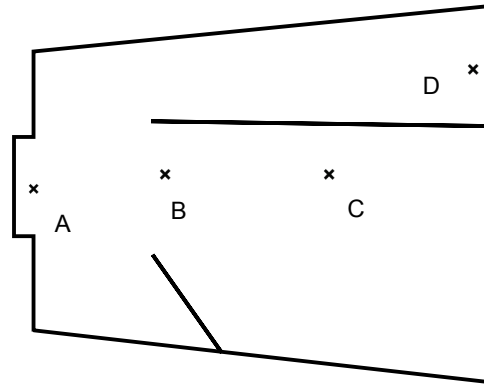
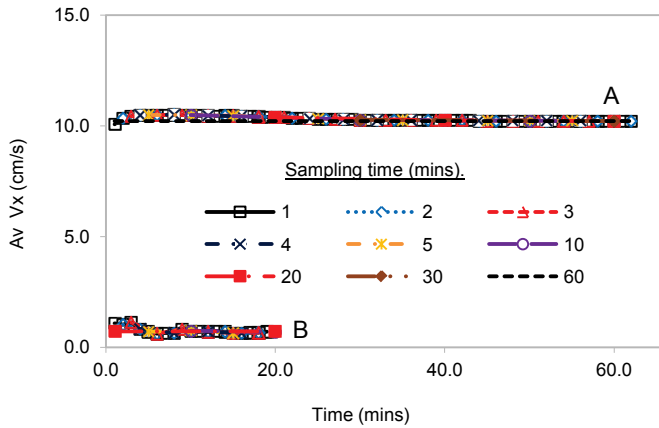
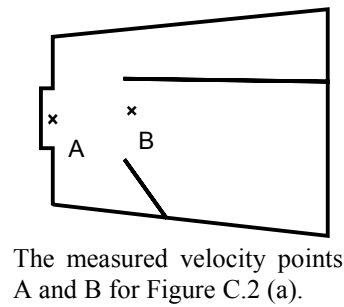


Figure C.1 The plan view of the GPT under investigation and the four locations (A-inlet; B-trap mouth; C-retention area; D-outlet) in which the turbulent statistical properties were measured over a period of up to one hour.

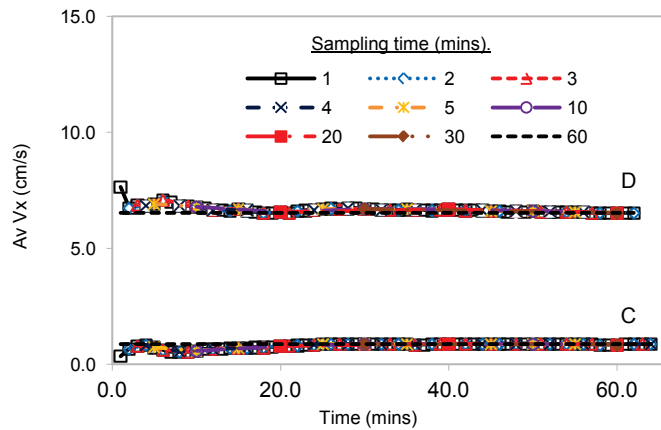


(a)

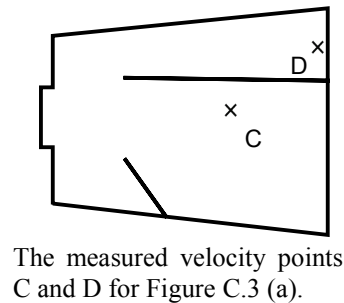


(b)

Figure C.2 The measured average velocities at points A and B since commencing the experiments, (a) the average velocities for the sampling time and (b) the locations of the points.



(a)



(b)

Figure C.3 The measured average velocities at points C and D since commencing the experiments, (a) the average velocities for the sampling time and (b) the locations of the points.

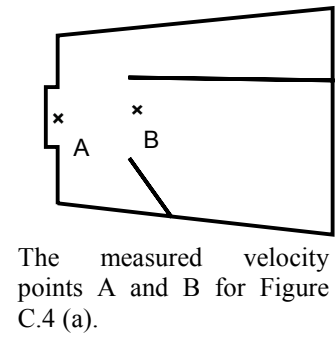
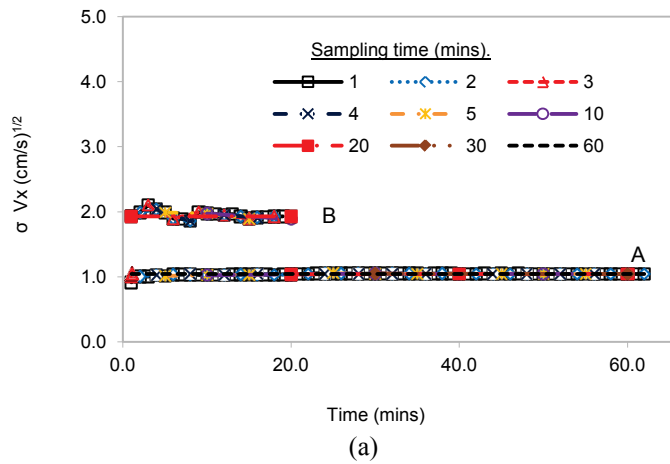


Figure C.4 (a) The standard deviation of the measured velocities at points A and B from commencing the experiments for the sampling times and (b) the locations of the points.

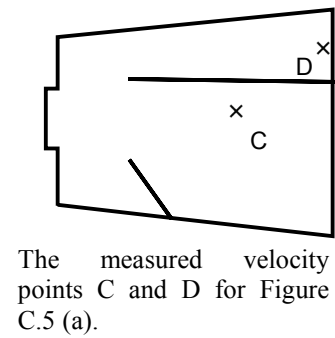
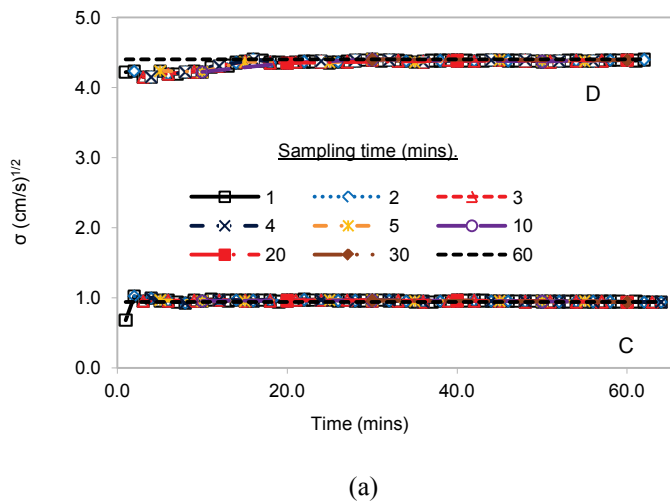
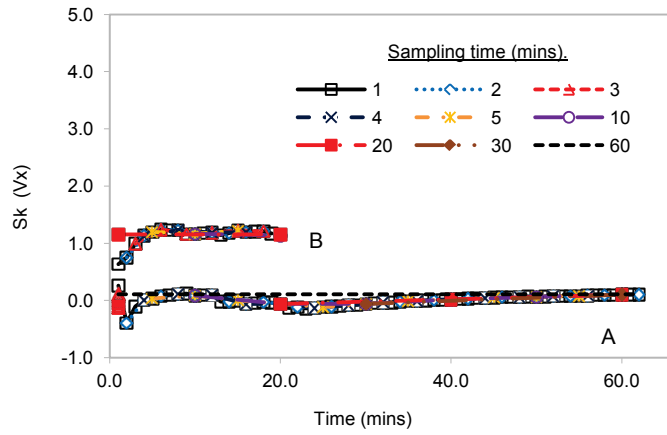
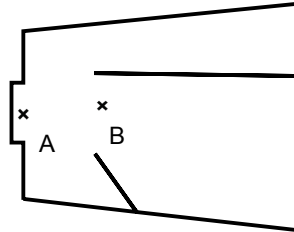


Figure C.5 (a) The standard deviation of the measured velocities at points C and D from commencing the experiments for the sampling times and (b) the locations of the points.



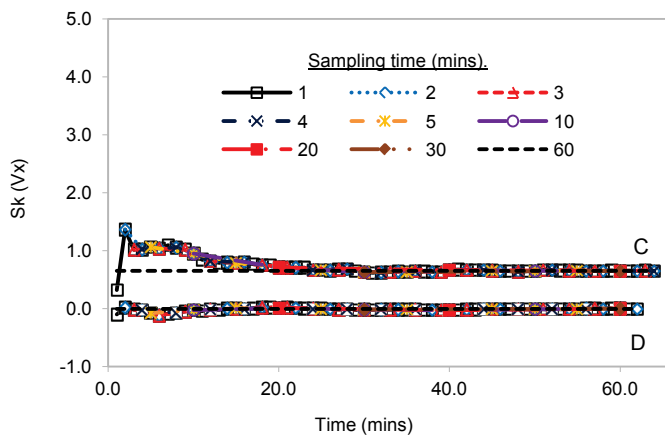
(a)



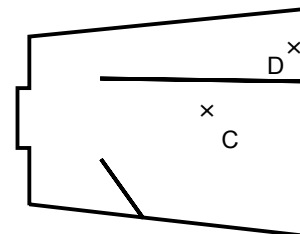
The measured velocity points A and B for Figure C.6 (a).

(b)

Figure C.6 (a) The skewness of the measured velocities at points A and B from commencing the experiments for the sampling times and (b) the locations of the points.



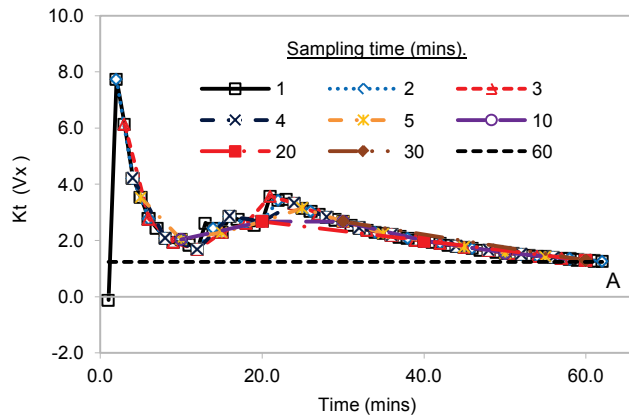
(a)



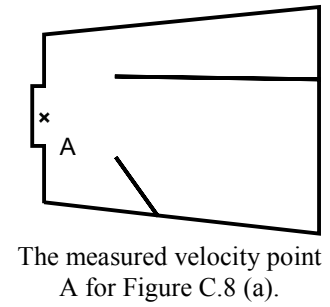
The measured velocity points C and D for Figure C.7 (a).

(b)

Figure C.7 (a) The skewness of the measured velocities at points C and D from commencing the experiments for the sampling times and (b) the locations of the points.

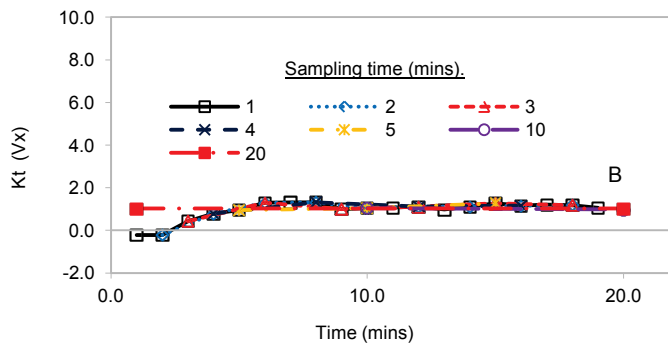


(a)

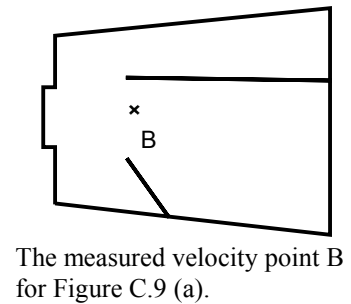


(b)

Figure C.8 (a) The kurtosis of the measured velocities at points A from commencing the experiments for the sampling times and (b) the locations of the points.

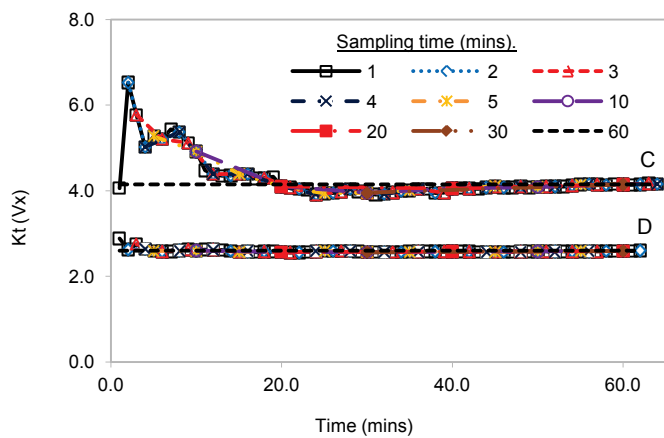


(a)

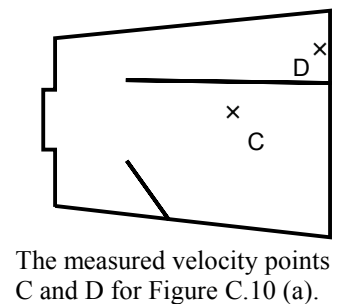


(b)

Figure C.9 (a) The kurtosis of the measured velocities at points B from commencing the experiments for the sampling times and (b) the locations of the points.

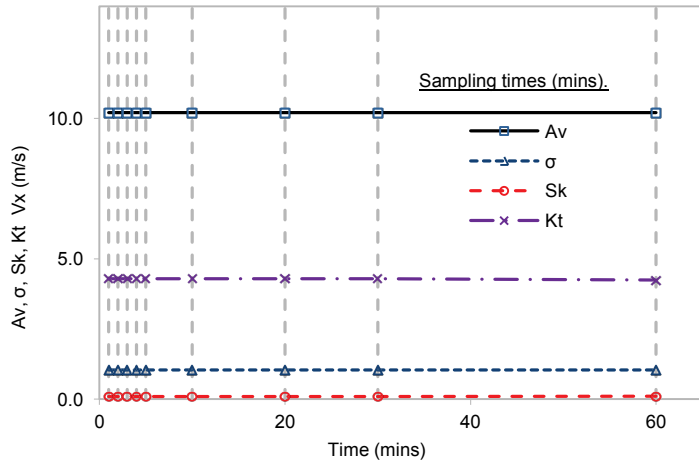


(a)

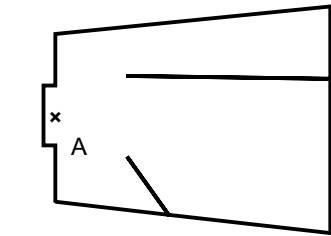


(b)

Figure C.10 (a) The kurtosis of the measured velocities at points C and D from commencing the experiments for the sampling times and (b) the locations of the points.



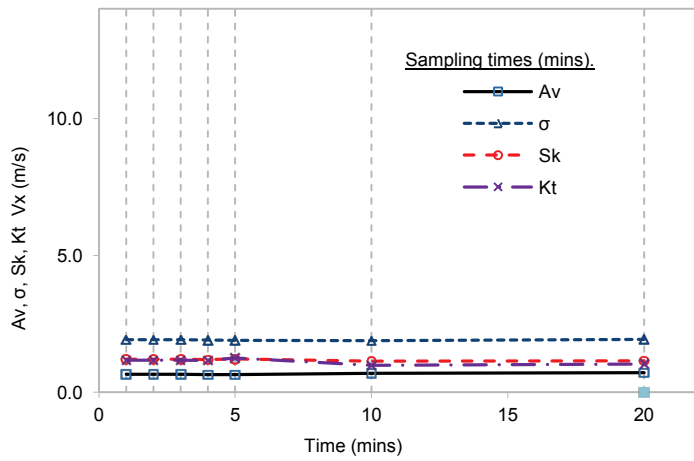
(a)



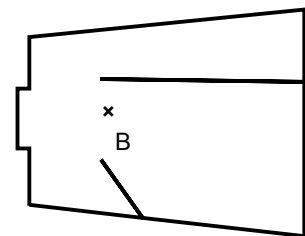
The measured velocity point A for Figure C.11 (a).

(b)

Figure C.11 (a) A plot of the statistical moments of data sampled after 55 minutes for the stationary test conducted at point A as shown in (b).



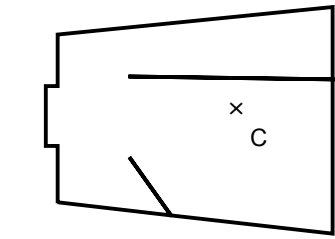
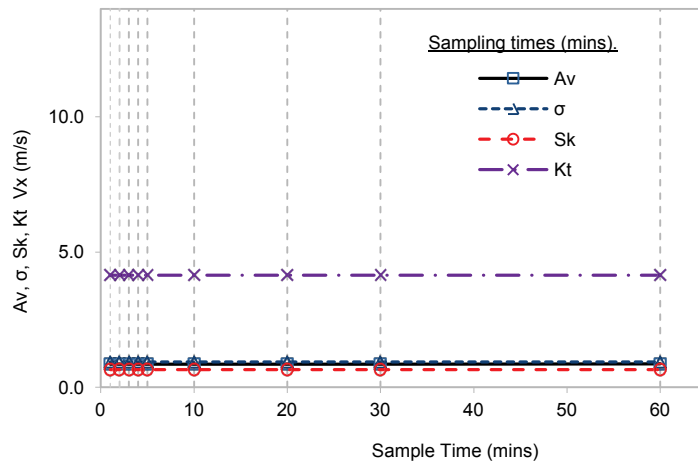
(a)



The measured velocity point B for Figure C.12 (a).

(b)

Figure C.12 (a) A plot of the statistical moments of data sampled after 55 minutes for the stationary test conducted at point B as shown in (b).

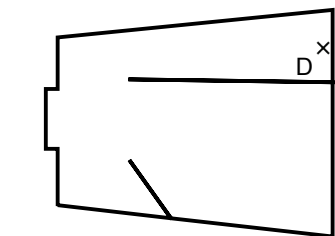
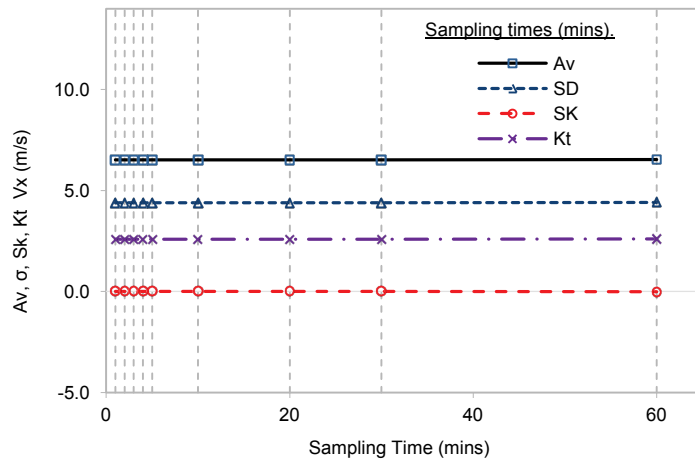


The measured velocity point C for Figure C.13 (a).

(a)

(b)

Figure C.13 (a) A plot of the statistical moments of data sampled after 55 minutes for the stationary test conducted at point C as shown in (b).



The measured velocity point D for Figure C.14 (a).

(a)

(b)

Figure C.14 (a) A plot of the statistical moments of data sampled after 55 minutes for the stationary test conducted at point D as shown in (b).

The Turbulent velocity spectra

The turbulent velocity spectra were also investigated and Gordon et al. (2000) describes different parts of a typical spectrum (Figure C.15). Figure C.15 is a log-log plot and here the turbulent spectra can be identified by an inertial sub-range which falls with a $-5/3$ slope as per Kolmogorov theory (Launder and Spalding, 1974). This slope describes the rate at which turbulent energy, ε dissipates to smaller eddies and meets the hypothesis of the standard two equation k - ε turbulence model used in the CFD simulation. In Figures C.16-19 the turbulent velocity spectra are plotted for the corresponding measured points.

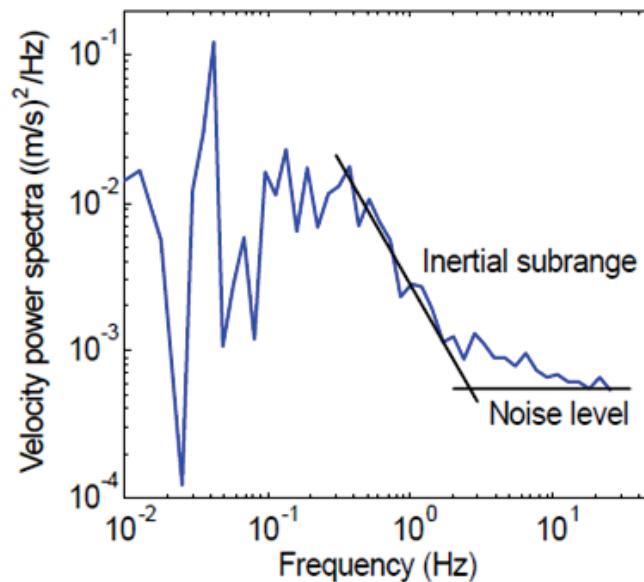
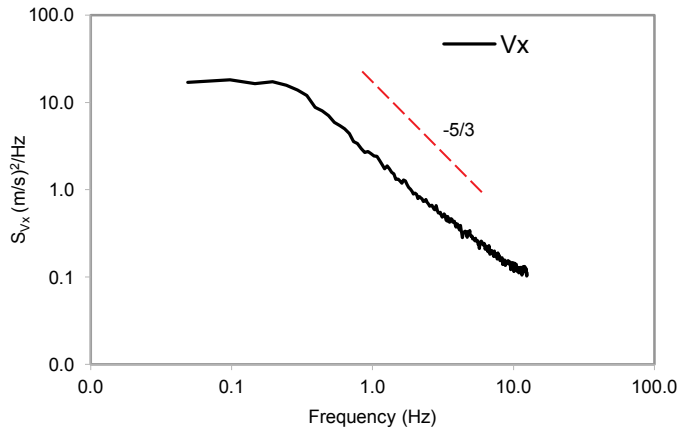
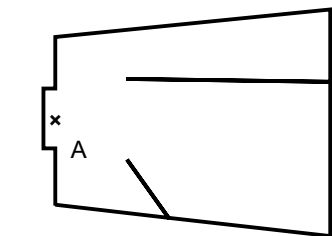


Figure C.15 Different parts of a typical velocity spectrum (Gordon et al., 2000)



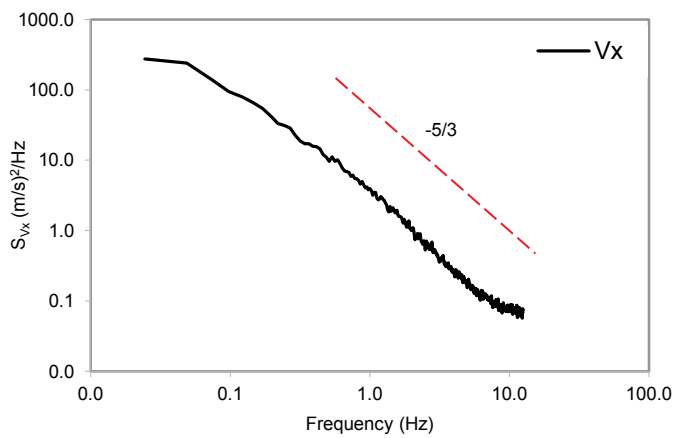
(a)



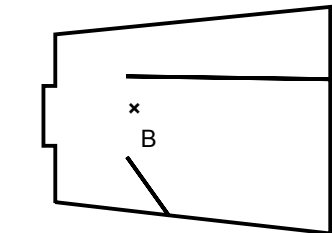
The measured velocity point A for Figure C.16 (a).

(b)

Figure C.16 The turbulent velocity spectrum for the measured point, A as shown in (b) with a Fast Fourier Transform sample block of 512.



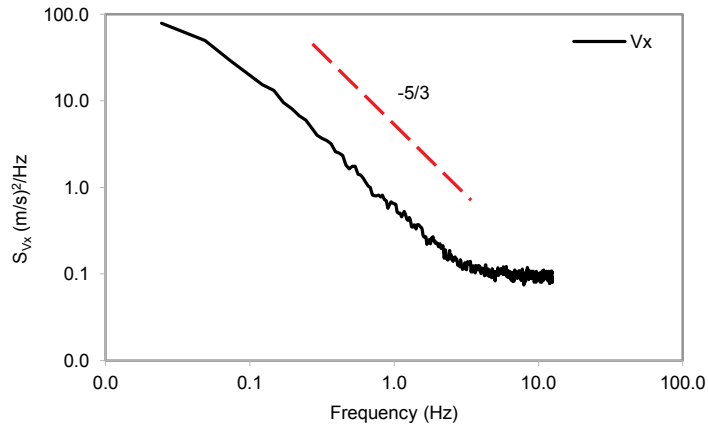
(a)



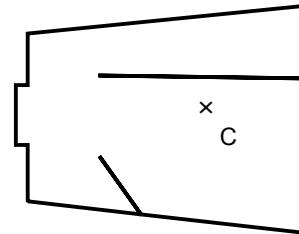
The measured velocity point B for Figure C.17 (a).

(b)

Figure C.17 The turbulent velocity spectrum for the measured point B as shown in (b) with a Fast Fourier Transform sample block of 512.



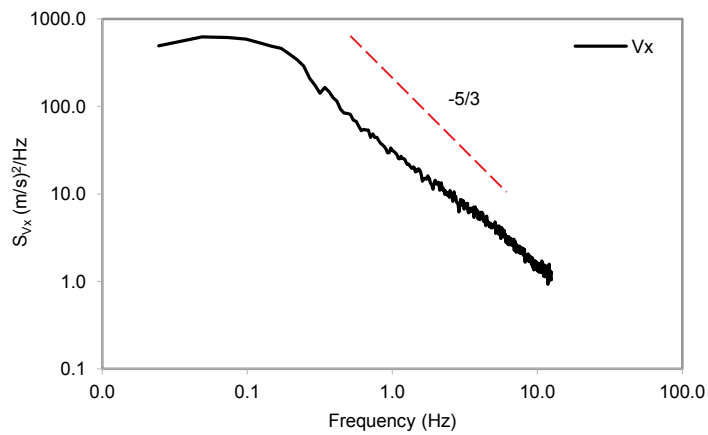
(a)



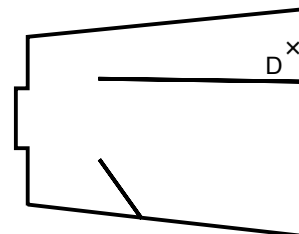
The measured velocity point C for Figure C.18 (a).

(b)

Figure C.18 The turbulent velocity spectrum for the measured point C as shown in (b) with a Fast Fourier Transform sample block of 512.



(a)



The measured velocity point D for Figure C.19 (a).

(b)

Figure C.19 The turbulent velocity spectrum for the measured point D as shown in (b) with a Fast Fourier Transform sample block of 512.

Comparison of the side and down-Looking ADV probes

Measurements of the free stream velocities in the centre of the flume were taken with the down and side-looking ADV probes for comparisons. These probes were mounted on a horizontal support on top of the flume and positioned to measure the exact location. The flow was seeded with a mixture of French chalk and water. The results are shown in Figure C.20-22 for the three directional velocity components (V_x , V_y , V_z), respectively. In these figures, comparisons with the down (A813F, 0007F) and side-looking (A843F) probes are overall within 7% and 9%.

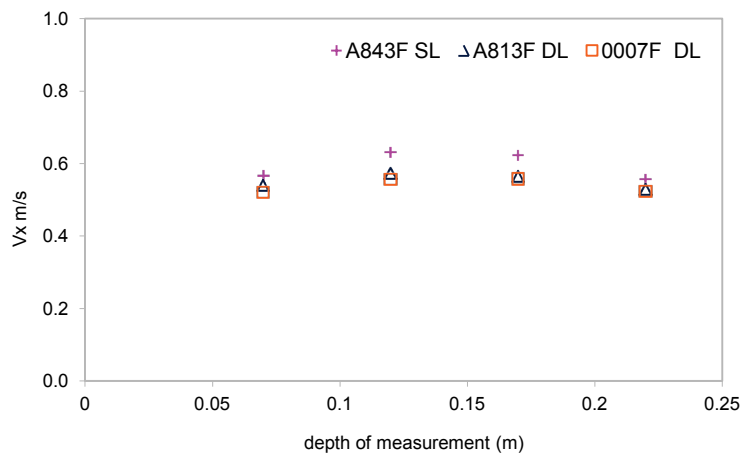


Figure C.20 Comparative measurements taken with the down (DL) and side-looking (SL) ADV probes for the downstream velocity component (V_x).

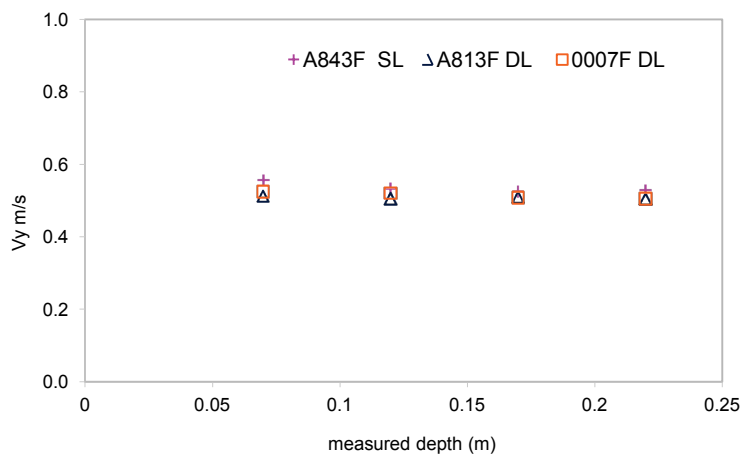


Figure C.21 Comparative measurements taken with the down (DL) and side-looking (SL) ADV probes for the downstream velocity component (V_y).

Previously, tow-tank tests of ADVs have been reported to verify the linearity of ADVs over its full dynamic range (Lohrmann et al., 1999). Strong linearity was found over this range indicating that it was possible to calibrate the ADV instrument in a single-speed tow channel. It was also found that the ADV is suitable for low flow measurements with accuracies better than 0.1 mm/s over a range of few cm/s.

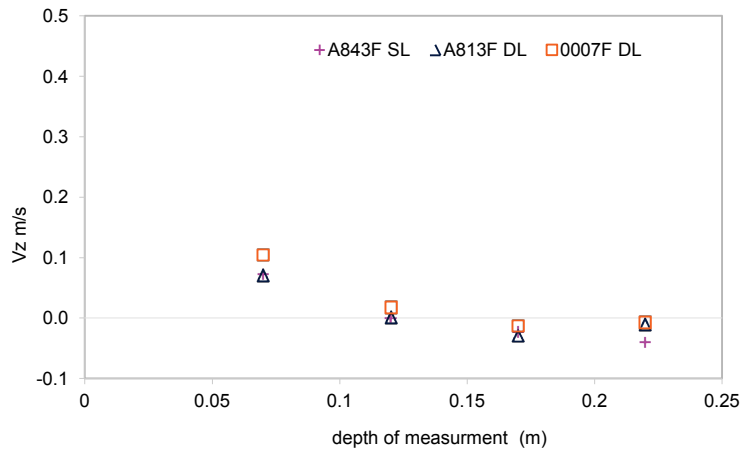


Figure C.22 Comparative measurements taken with the down (DL) and side-looking (SL) ADV probes for the downstream velocity component (V_z).

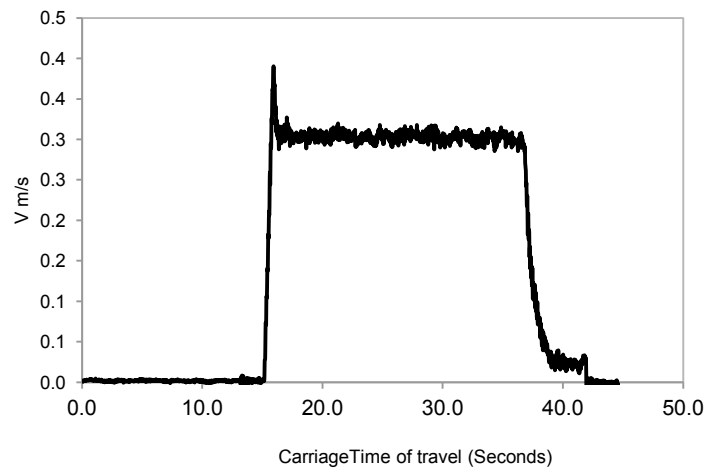


Figure C.23 Signal from the ADV probe showing the movement of carriage.

To extend the comparative ADV probe study, measurements were performed with the carriage moving at a constant velocity. Prior to commencing the measurements, the seeding material was disturbed by sweeping the floor of the flume

with a broom. When the flow in the flume was observed to be free from surface disturbances, the movement of the carriage was timed between two consecutive points as recorded in Figure C.23). In Figure C.23, a typical signal from the ADV probe is shown between starting and finishing the test.

A series of tests were performed with each of the ADV probes and the results are shown in Table C.2. In Table C.2 some abnormalities were observed with the down-looking probe (A813F) and errors of up to 15% were observed. The side-looking probe appeared to be the most accurate (0.35%). Further investigation with this probe using the beam check utility in the Horizon ADV data collecting program (SonTek/YSI) revealed distorted signals from the receiver. Beam check is typically used for examining signals near the boundaries as shown in Figure C.24. Consequently, the newly acquired probes were sent back to the manufacturer for repairs. A replacement was used to complete the measurements which had been recently tested and calibrated by the suppliers.

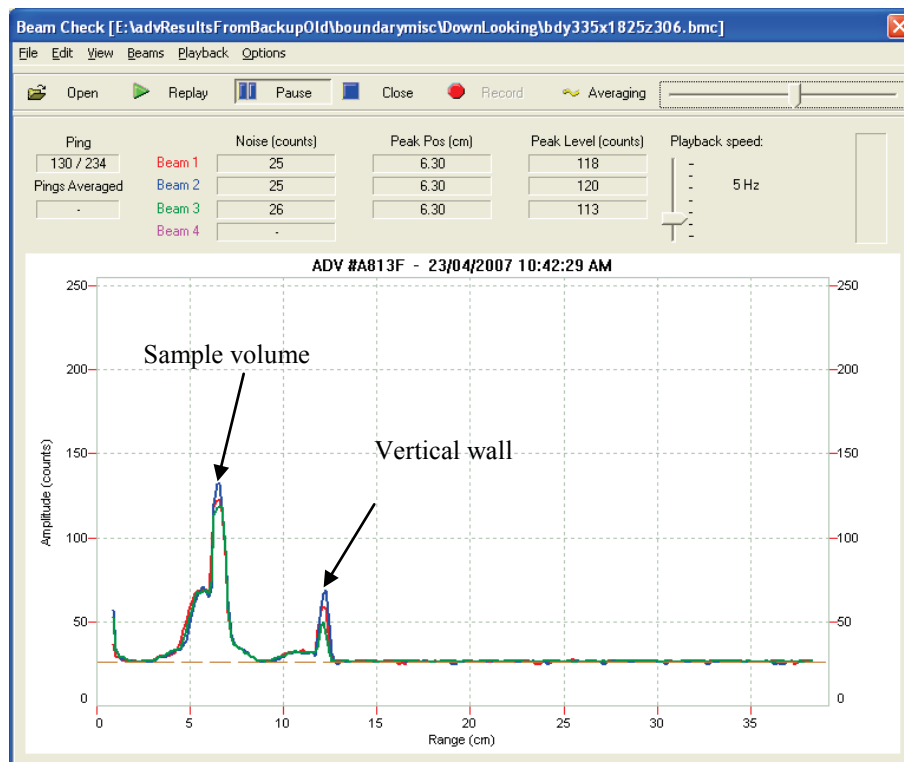


Figure C.24 Typical signals from the ADV probe using beam check utility in Horizon ADV data collecting program from SonTek/YSI.

Table C.2 Results from the tests with the ADV mounted on the carriage and moving with a constant velocity.

1	2	3	4	5	6	7
Test No.	Serial No.	Type	Orientation (X/Y/Z)	ADV velocity (m/s)	Carriage velocity (m/s)	Average error (%) [cols. (5- 6)]
1-8	A843F	side-looking	Y	0.3136	0.3138	0.35
9-11	A843F	side-looking	Z	0.3039	0.3038	2.50
12-16	A813F	down-looking	X	0.2741	0.3102	11.64
17-19	A813F	down-looking	Y	0.2668	0.3129	14.74
20-22	0007 F	down-looking	X	0.2942	0.3130	6.01
23-26	0007 F	down-looking	Y	0.2939	0.3120	5.78

REFERENCES

- Balachandar, R. and Bhuiyan, F. (2007). Higher-order moments of velocity fluctuations in an open-channel flow with large bottom roughness. *Journal of Hydraulic Engineering*, 133(1), 77-87.
- Gordon, L., Cox, J. and Oxford, M. (2000). *Acoustic Doppler Velocimeter performance in a laboratory flume report* (Vol. 24). California: NortekUSA. Retrieved 26 February 2010, from <http://williamlohrmann.com/PDF/NSL-NDV.pdf>
- Lauder, B. E. and Spalding, D. B. (1974). The numerical computation of turbulent flows. *Computational Methods Applied Mechanical Engineering*, 3, 269-289.
- Lohrmann, A., Cabrera, R. and Kraus, N. C. (1999). Acoustic-Doppler velocimeter (ADV) for laboratory use. In C. A. Pugh (Ed.), *Proceeding of Conference on Fundamentals and Advancements in Hydraulic Measurements and Experimentation* (pp. 351-365). Buffalo, New York: American Society of Civil Engineers (ASCE).

APPENDIX D: FLUME/PHYSICAL MODELLING OF THE GPT

Measurements were carried out in the 20 m flume at the QUT laboratory (Figures D.1-2). The downstream view of the flume and collection tank at the end of the raceway is shown in Figure D.2. The flow rate was measured at the collection tank with a custom made plug apparatus as depicted in Figure D.3.

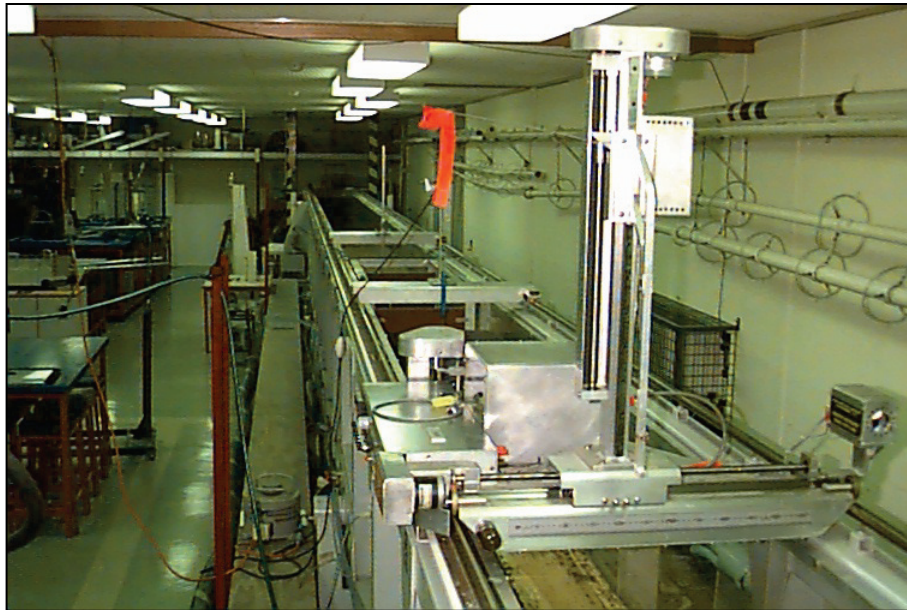


Figure D.1 The 19 m flume in the laboratory at QUT with the mounted carriage on slider rails.

The ADV measurements were performed with the instrument mounted on the front end of the carriage. The carriage is mounted on slider rails fitted on top of the flume (Figure D.4). This was used to position the ADV probe inside the 50% scale model GPT within the flume. The experimental GPT rig with a rectangular channel and a circular pipe inlet configured GPT are shown in Figures D.5-7. A GPT with a raised circular inlet pipe is also shown in Figure D.8. To model blocked internal retaining screens of the GPT, perforated and solid walls were used to represent 33%, 68% and 100% blockages as shown in Figures D.9-11.

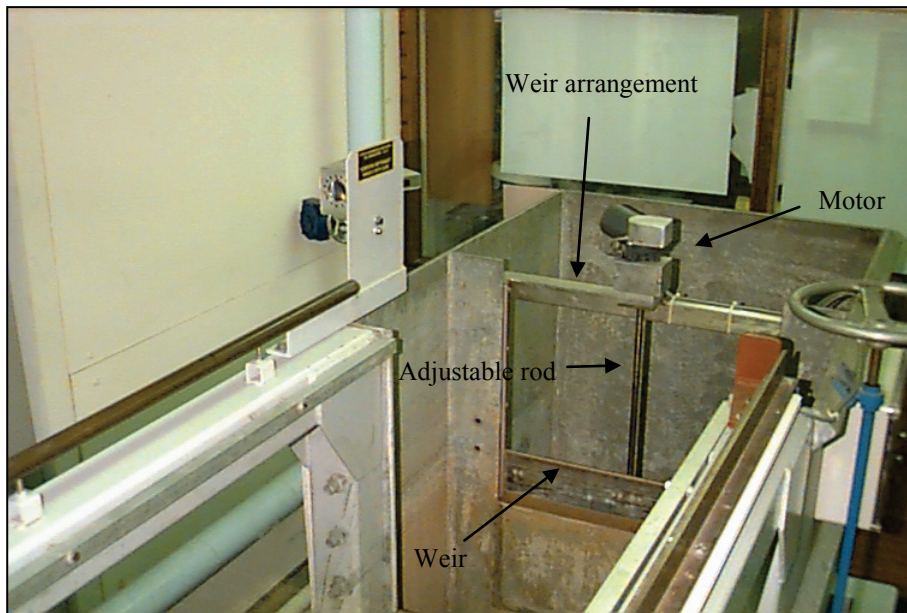


Figure D.2 Downstream end of the flume raceway, weir arrangement and collection tank.



Figure D.3 The custom built plug used in the collection tank to measure the flow rate. The flow rate was calculated by timing the amount of water collected at a marked height in the tank.

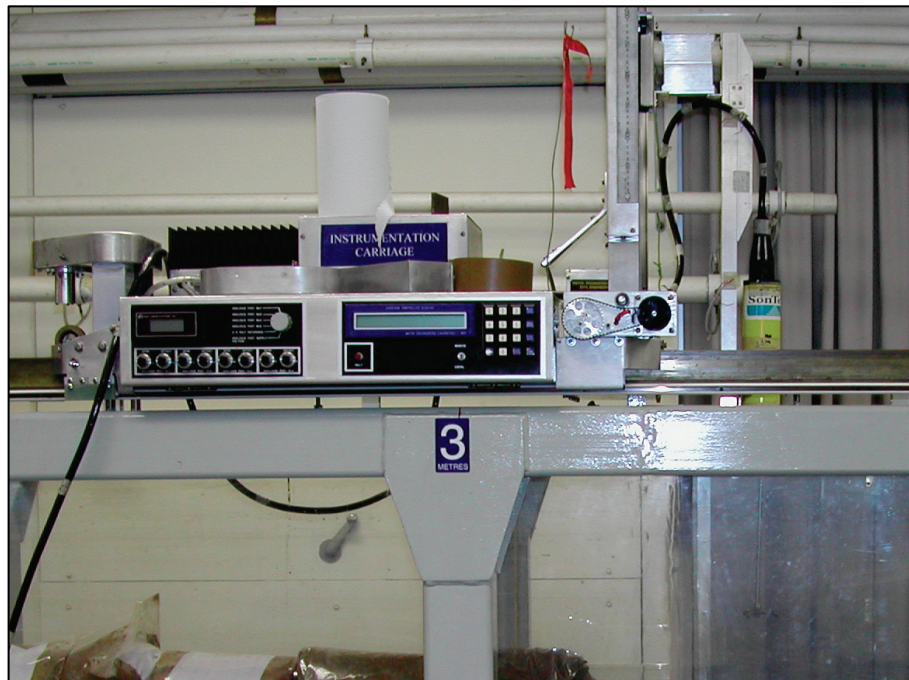


Figure D.4 A closer view of the carriage and the ADV mounted at front end.

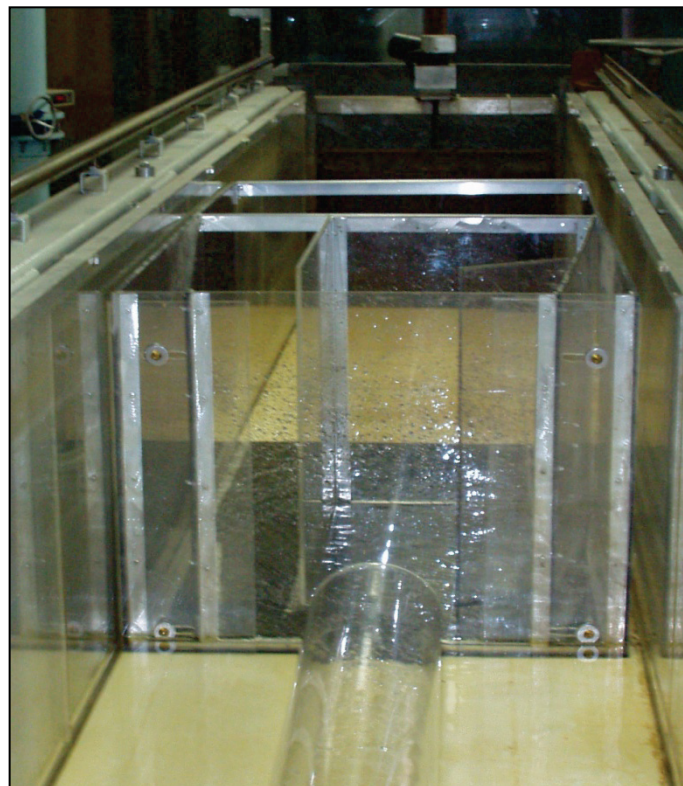


Figure D.5 The circular pipe (diameter = 144 mm) inlet GPT inside the hydraulic flume.

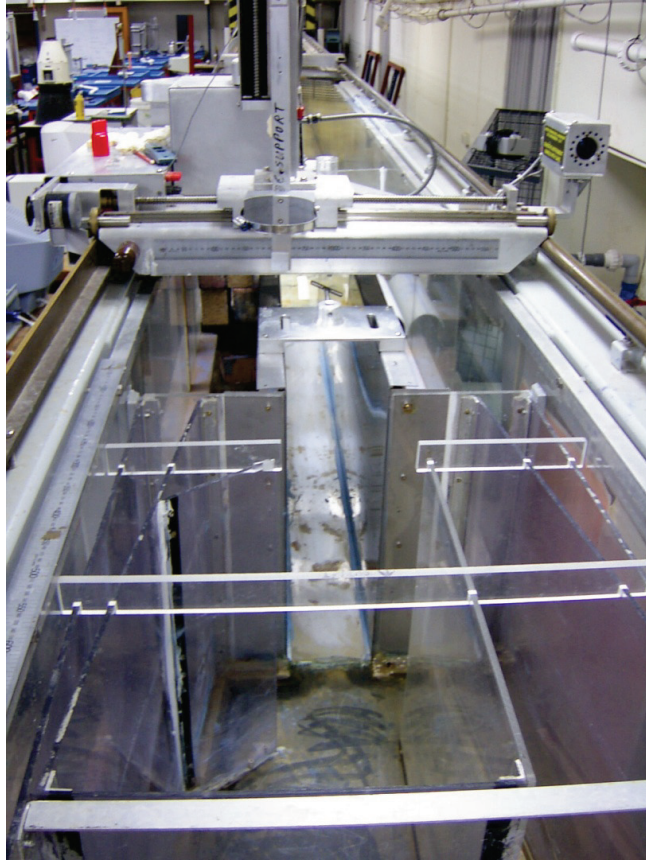


Figure D.6 The experimental GPT rig with a rectangular channel (width = 144 mm) inlet.



Figure D.7 Upstream view of the rectangular channel inlet GPT.



Figure D.8 A raised circular pipe (diameter =100 mm) inlet GPT.

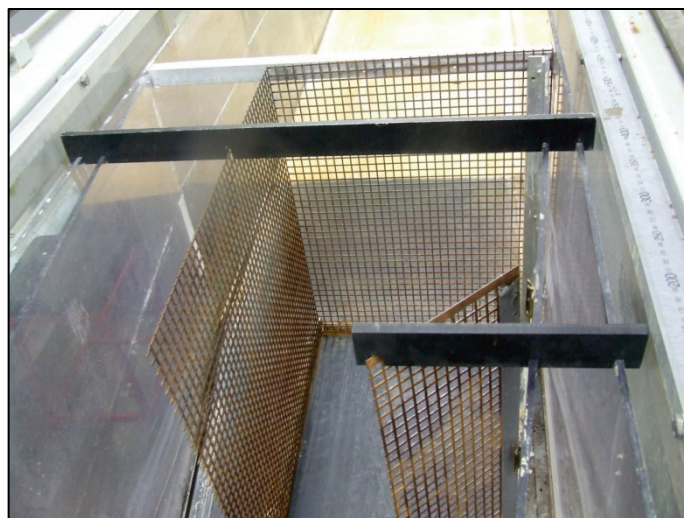


Figure D.9 Internal retaining screens representing 33% blockages.

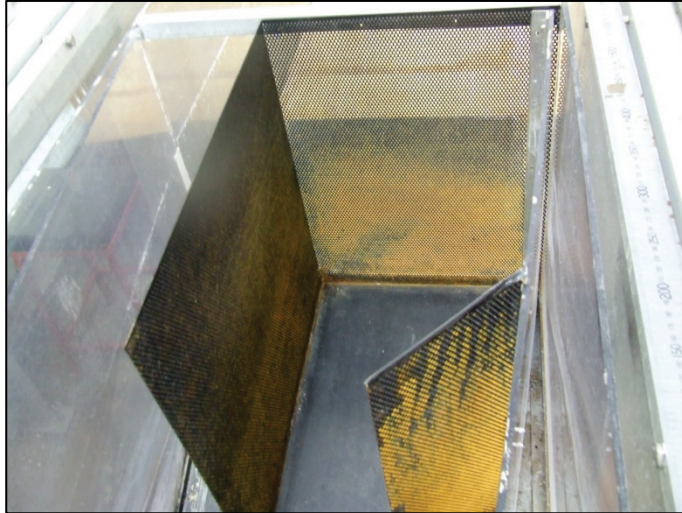


Figure D.10 Internal retaining screens representing 68% blockages.

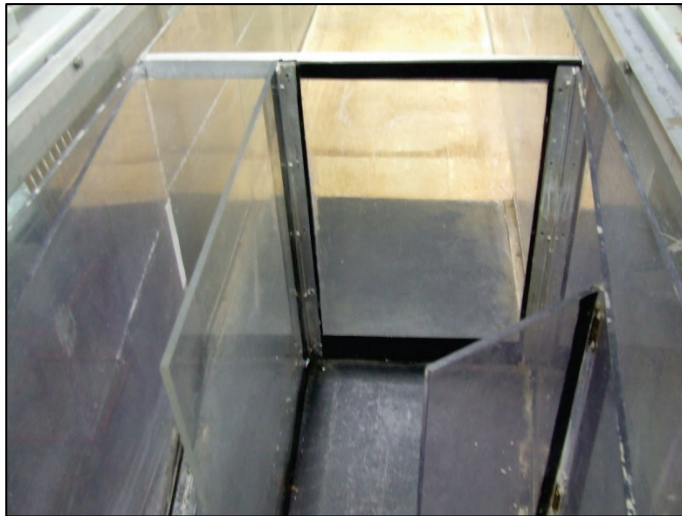


Figure D.11 Internal retaining screens representing 100% blockages.

APPENDIX E: SIGNAL PROCESSING PROGRAMS FOR THE DYE DATA

This appendix supplements Chapters 4 and 9 by providing a more detailed overview of the signal processing routines written in Matlab® (2008b, The MathWorks, Melbourne, Victoria, Australia) to address the calibration, noise and electrical drift in the data collected from the Komori instrumentation. Figure E.1 typically shows the dye concentration measurement of the Komori probe in water (0 ppm) and in the mixture containing water and dye (8 ppm). The data collected during measurement including the calibration is processed through a series of steps as shown in the flowchart Figure E.2. The processed data from the signal processing routines is typically shown in Figure E.3.

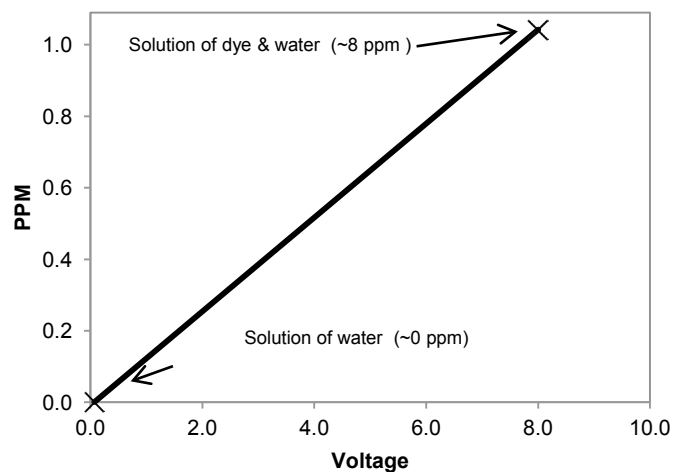


Figure E.1 A typical calibration of the Komori dye concentration probe in water and dye mixture.

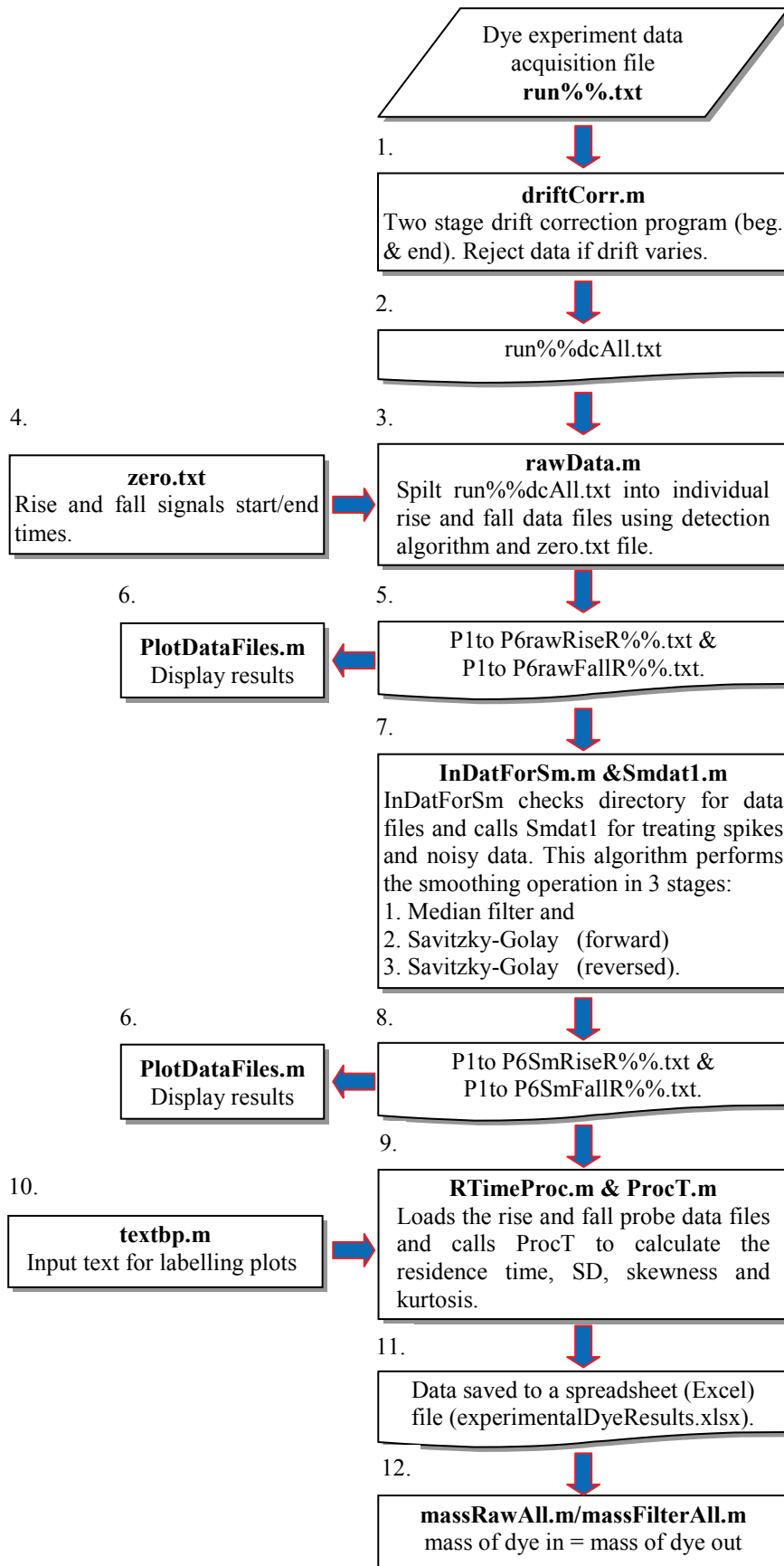
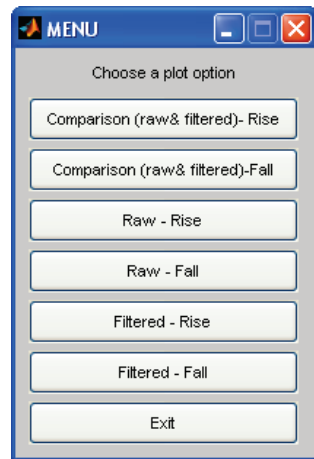


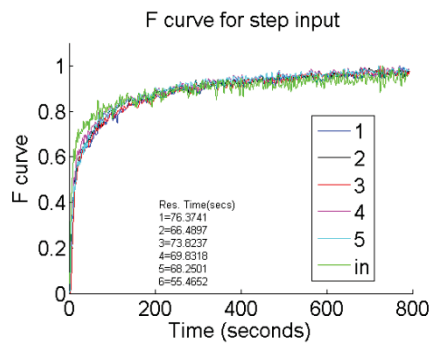
Figure E.1 A detailed flowchart of the signal processing routines used to process the data collected from the tracer dye experiments.



6.

← **PlotDataFiles.m**
Display results

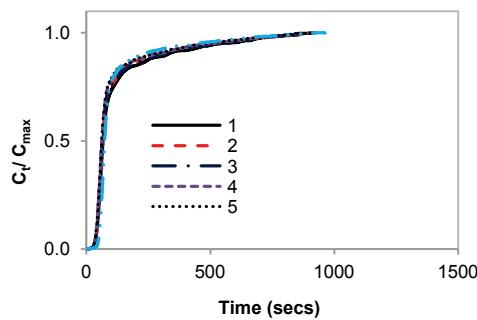
(a)



9.

← **RTimeProc.m & ProcT.m**
Loads the rise and fall probe data files and calls ProcT to calculate the residence time, SD, skewness and kurtosis.

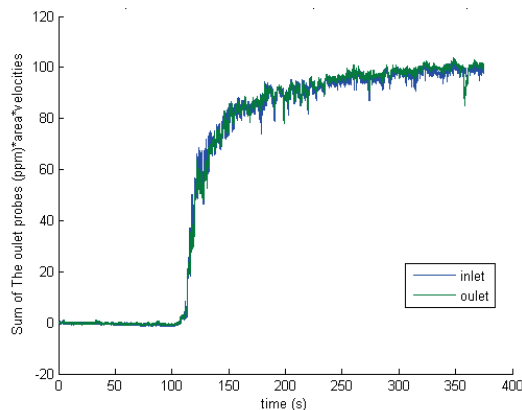
(b)



11.

← Data saved to a spreadsheet (Excel) file (experimentalDyeResults.xlsx).

(c)



12.

← **massRawAll.m/massFilterAll.m**
mass of dye in = mass of dye out

(d)

Figure E.2. A series of output from the signal process routines (a) menu options; (b) residence time F curves (c) saving the data to a spreadsheet file and (d) a mass balance check of the output and input data of the dye probes.

[This page has been left blank intentionally.]

APPENDIX F: VECTOR PLOTS FROM PIV SOFTWARE AND OPENDX

This appendix supplements Chapter 8 and contains the plots obtained from the PIV software (proVision-XSTM version 3.08.30) supplied by Integrated Design Tools (IDT) via SciTech Pty Ltd (Figure F.1-12). These plots were processed using a high resolution grid consisting of approximately 5000 nodes.

Attempts to improve the vector plots were made by importing the PIV dataset into the IBM Research Open Visualisation Data Explorer, OpenDx version 4.4.0 and the corresponding outputs are shown in Figures F.13-24. The data displayed in these figures have been reduced by one third to half its original size.

Also, included in this appendix are snapshots taken from visualisation experiments using sediments as shown in Figures F.25-F.28. The manner in which the sediments were deposited when the water was drained from the GPT appeared to be similar to the flow patterns documented in Chapter 6 and 8.

The experimental setup parameters (denoted R1-R12) referenced in these figures are tabulated in Table F.1 in terms of experimental setup conditions of weir height, inlet velocity, flow rate, water depth and screen blockages.

Table F.1 Matrix of flow regimes used in the experimental setup to reference the plots shown in F.1-28

Flow regime	Weir height (m)	Inlet velocity (m/s)	Flow rate (L/s)	Water depth (m)	Screen blockages %		
					100	68	33
Experiment numbers							
Low	0.108	0.09	1.3	0.1	R1	R3	R5
↑	0.286	0.09	3.9	0.3	R2	R4	R6
↓	0.000	0.39	6.1	0.1	R7	R9	R11
High	0.000	2.14	35.0	0.3	R8	R10	R12

F.1 Vector plots of GPT captured flow field produced by PIV software

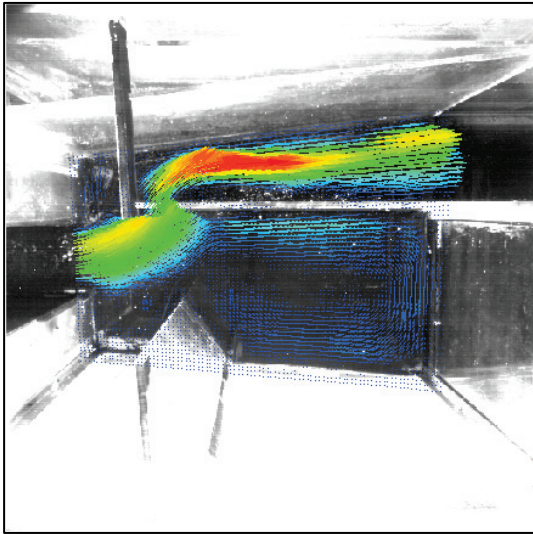


Figure F.1 R1 (Table F.1), 100% screen blocked, 1.3 L/s and 100 mm water depth.

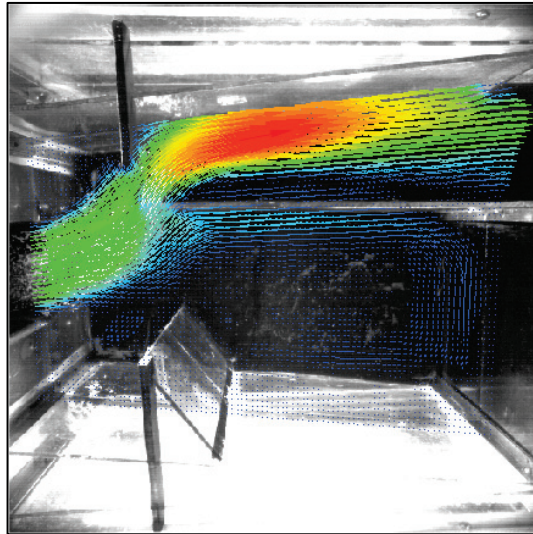


Figure F.2 R2, 100% screen blocked, 3.9 L/s and 300 mm water depth.

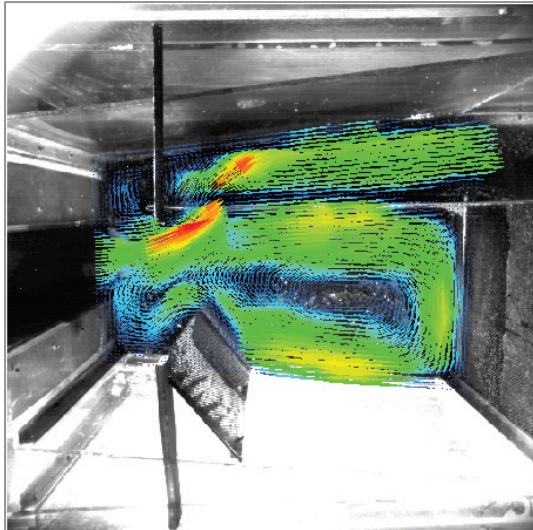


Figure F.3 R3, 68% screen blocked, 1.3 L/s and 100 mm water depth.

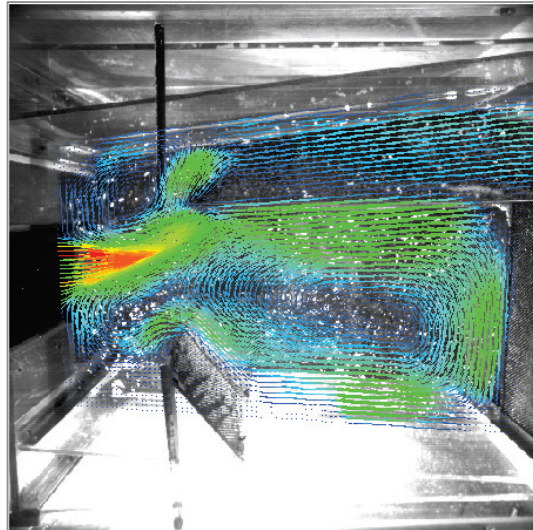


Figure F.4 R4, 68% screen blocked, 3.9 L/s and 300 mm water depth.

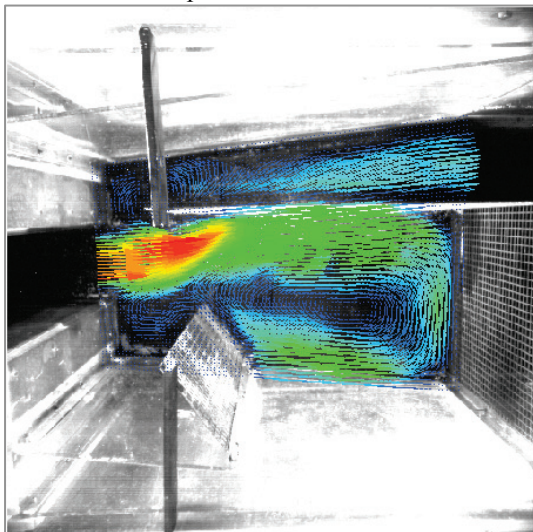


Figure F.5 R5, 33% screen blocked, 1.3 L/s and 100 mm water depth.

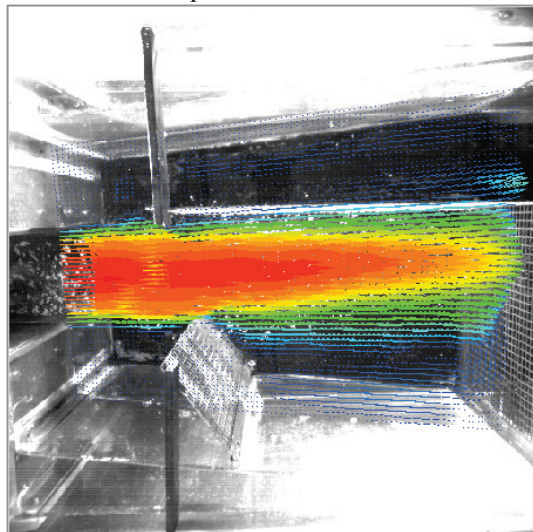


Figure F.6 R6, 33% screen blocked, 3.9 L/s and 300 mm water depth.

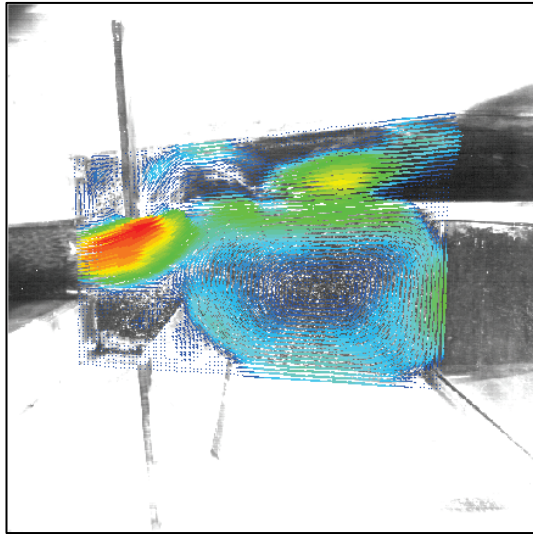


Figure F.7 R7, 100% screen blocked, 6.0 L/s and 100 mm water depth.

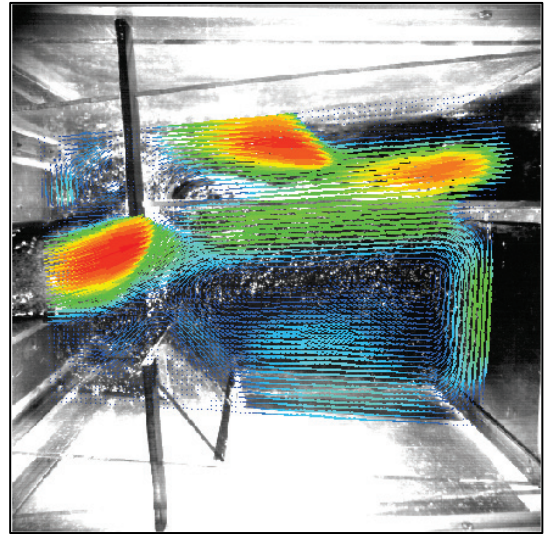


Figure F.8 R8, 100% screen blocked, 35.0 L/s and 300 mm water depth.

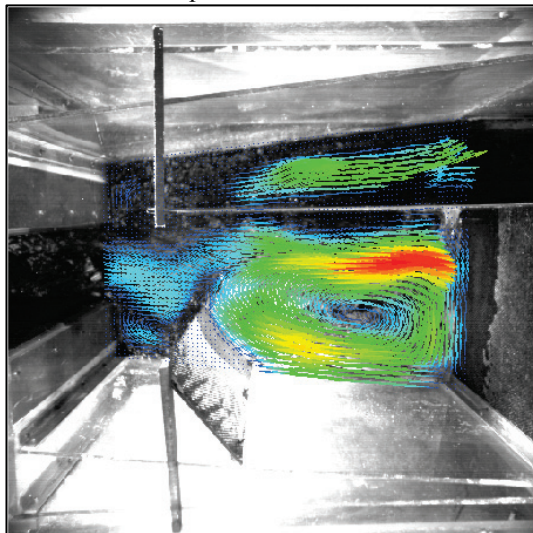


Figure F.9 R9, 68% screen blocked, 6.0 L/s and 100 mm water depth.

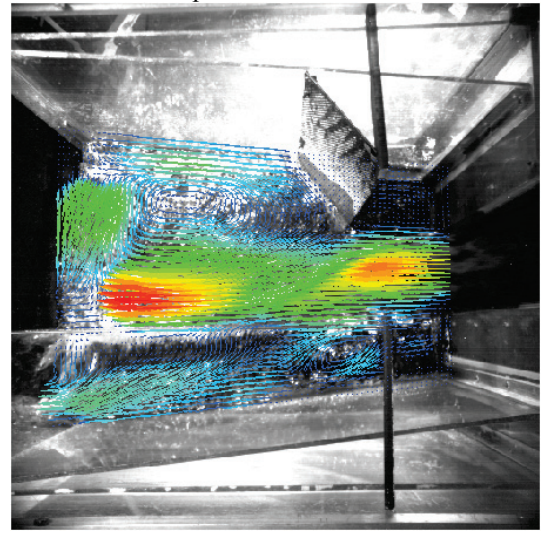


Figure F.10 Run 10, 68% screen blocked, 35.0 L/s and 300 mm water depth.

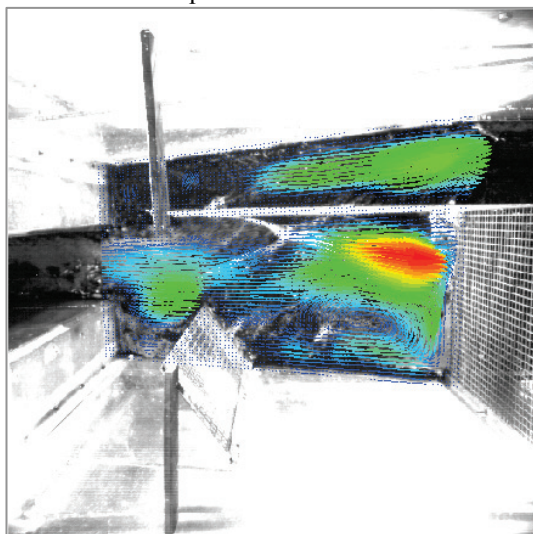


Figure F.11 R11, 33% screen blocked, 6.0 L/s and 100 mm water depth.

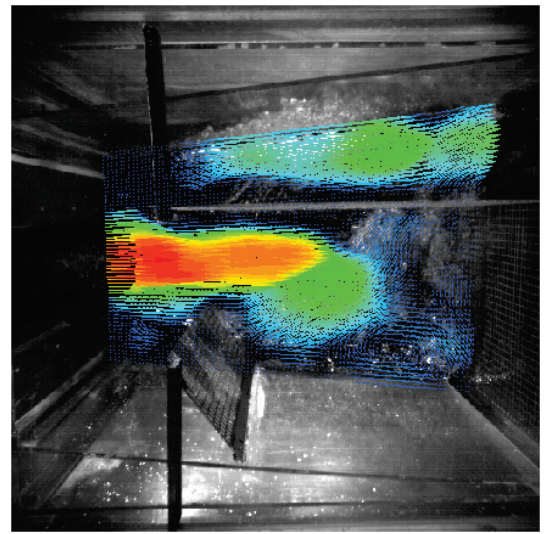


Figure F.12 R12, 33% screen blocked, 35.0 L/s and 300 mm water depth.

F.2 The PIV dataset was imported, reduced and displayed in OpenDX

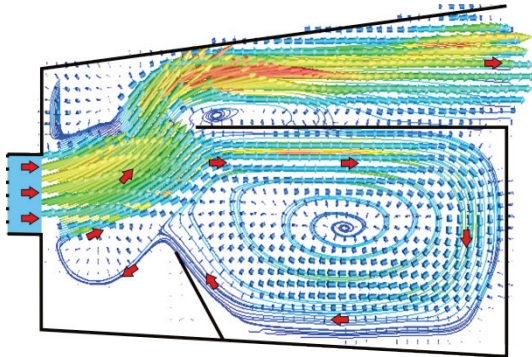


Figure F.13 R1 (Table F.1), 100% screen blocked, 1.3 L/s and 100 mm water depth.

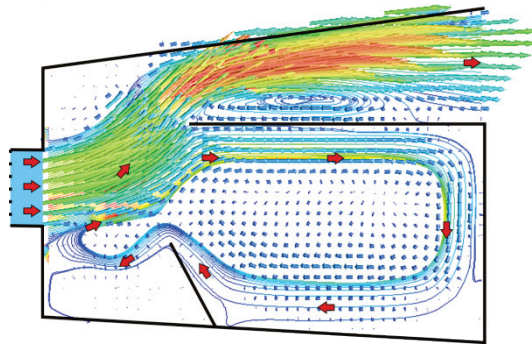


Figure F.14 R2, 100% screen blocked, 3.9 L/s and 300 mm water depth.

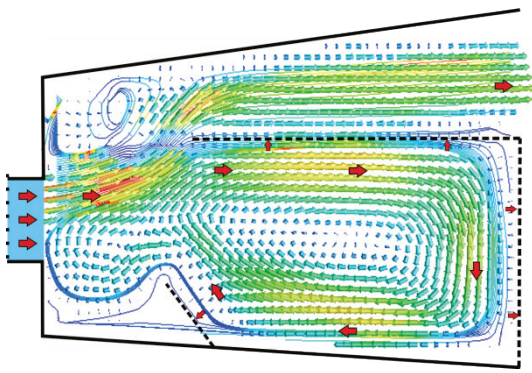


Figure F.15 R3, 68% screen blocked, 1.3 L/s and 100 mm water depth.

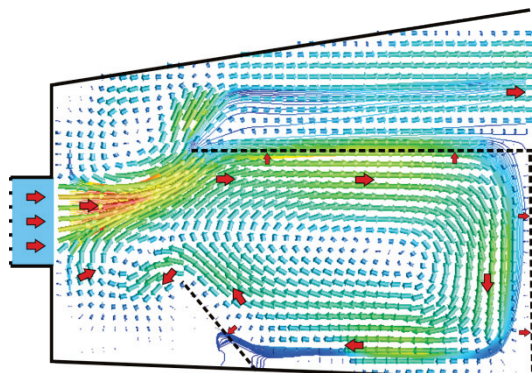


Figure F.16 R4, 68% screen blocked, 3.9 L/s and 300 mm water depth.

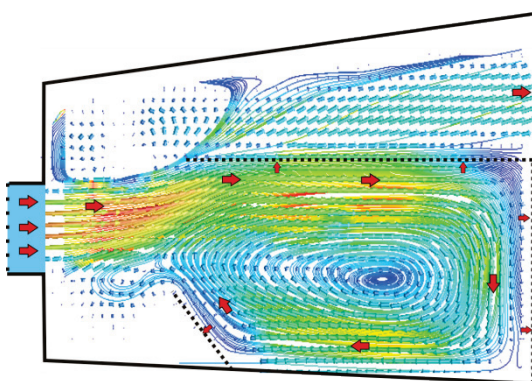


Figure F.17 R5, 33% screen blocked, 1.3 L/s and 100 mm water depth.

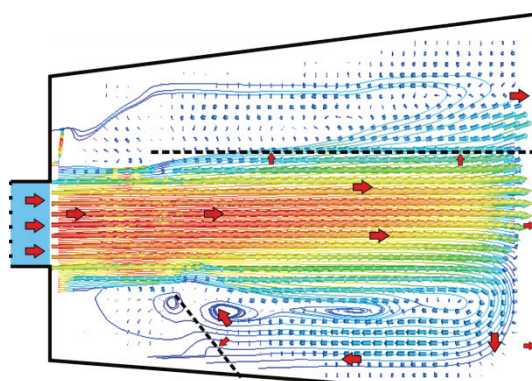


Figure F.18 R6, 33% screen blocked, 3.9 L/s and 300 mm water depth.

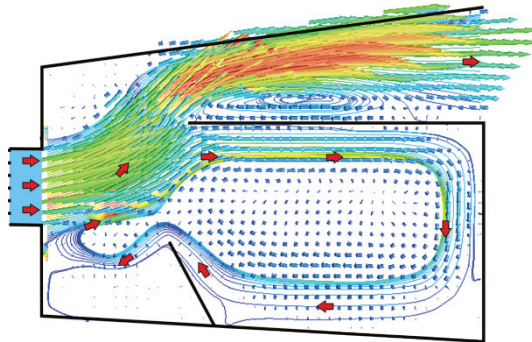


Figure F.19 R7, 100% screen blocked, 6.0 L/s and 100 mm water depth.

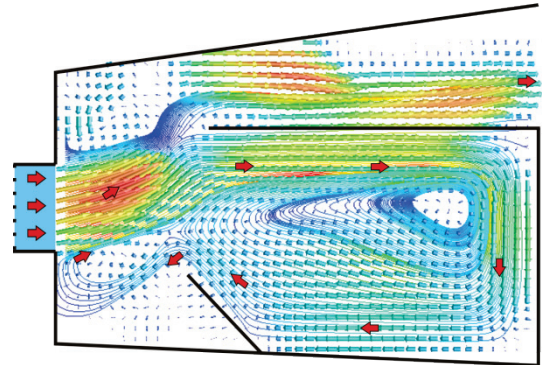


Figure F.20 R8, 100% screen blocked, 35.0 L/s and 300 mm water depth.

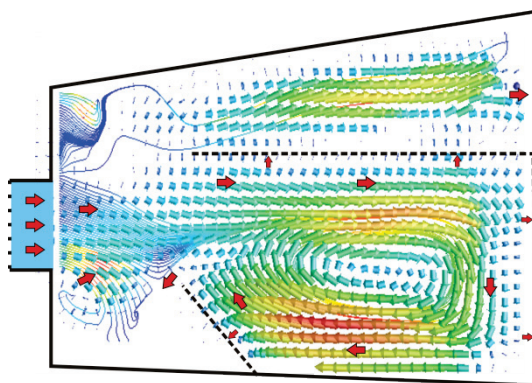


Figure F.21 R9, 68% screen blocked, 6.0 L/s and 100 mm water depth.

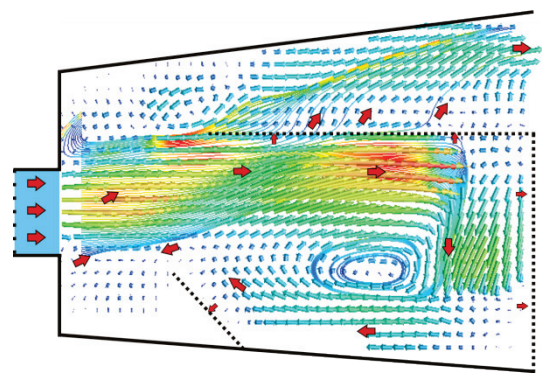


Figure F.22 R10, 68% screen blocked, 35.0 L/s and 300 mm water depth.

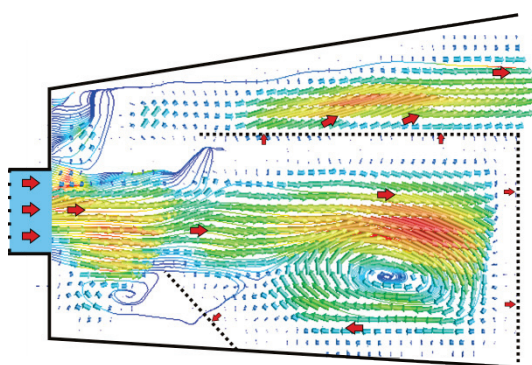


Figure F.23 R11, 33% screen blocked, 6.0 L/s and 100 mm water depth.

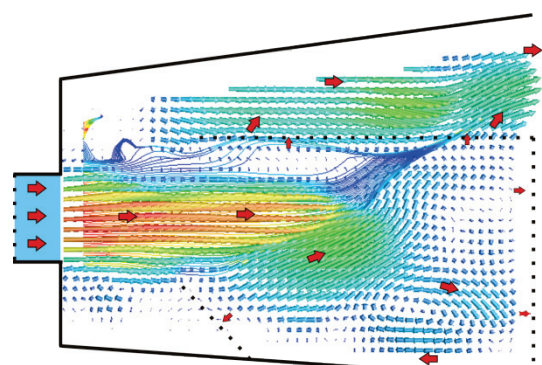


Figure F.24 R12, 33% screen blocked, 35.0 L/s and 300 mm water depth.

F.3 Visualisation of flow in the GPT using sediments

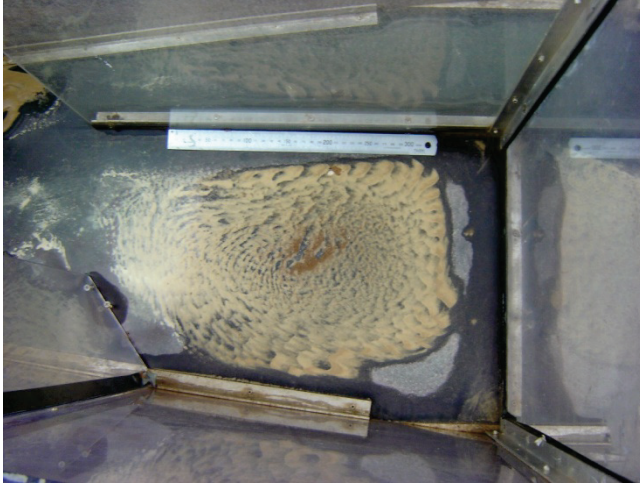


Figure F.25 The retention area of the GPT with 100% blocked screens is shown on the left. The experiment was initially conducted at R1 and the fluid was allowed to drain from the GPT. This resulted in an outlining formation of sediments similar to the large recirculation flow pattern defined in Chapter 6.

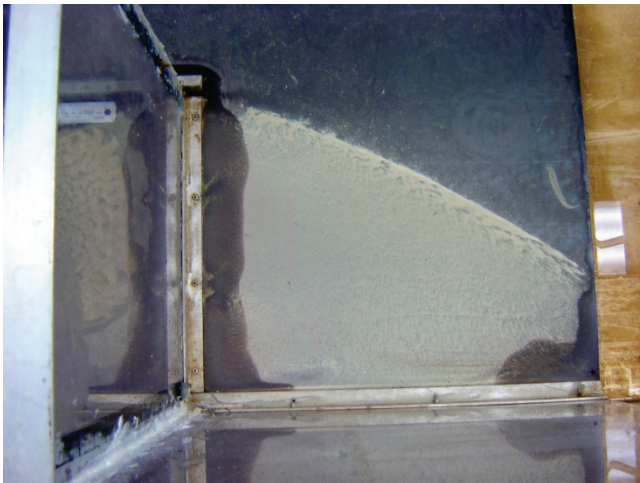


Figure F.26 The area behind the baffle of the GPT with 100% blocked screens is shown on the left (See Figure F.25 for experimental details). The outlining deposition of sediments is similar to the low recirculation zone defined in Chapter 6.



Figure F.27 A view of the area behind the baffle and the top left corner of the bypass channel in the GPT.

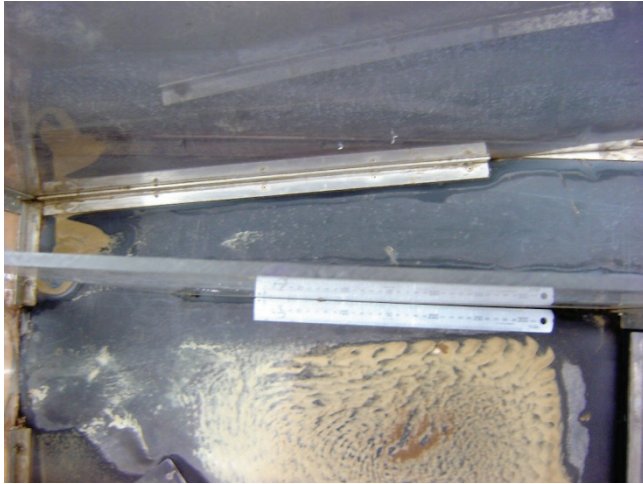


Figure F.28 A closer view of the formation of sediments in the top left corner of the GPT as shown in Figure F.27.

[This page is left blank intentionally]

APPENDIX G: GROSS POLLUTANT CAPTURE/RETENTION EXPERIMENTAL RESULTS

This appendix contains experimental graphic results from the gross pollutant capture/retention investigation as documented in Chapter 9. These results are organised under the following headings: Capture/retention experiments with artificial gross pollutants intermittently fed into the rectangular channel inlet GPT (See Figures G.1-11, Section G.1), Capture/retention experiments with artificial gross pollutants continuously fed into the rectangular channel inlet GPT (See Figures G.12-22 Section G.2), Comparing the Capture/retention experimental results of the continuously with the intermittently fed artificial gross pollutants into the rectangular channel inlet GPT (See Figures G.23-34 Section G.3), Capture/retention experiments with artificial gross pollutants intermittently fed into the circular pipe inlet GPT (See Figures G.35-43, Section G.4), Capture/retention experiments with artificial gross pollutants continuously fed into the circular pipe channel inlet GPT (See Figures G.44-52, Section G.5), and Comparing capture/retention experimental results of continuously with intermittently fed artificial gross pollutants into the circular pipe inlet GPT (See Figures G.53-64, Section G.6).

G.1 Capture/retention experiments with artificial gross pollutants intermittently fed into the rectangular channel inlet GPT

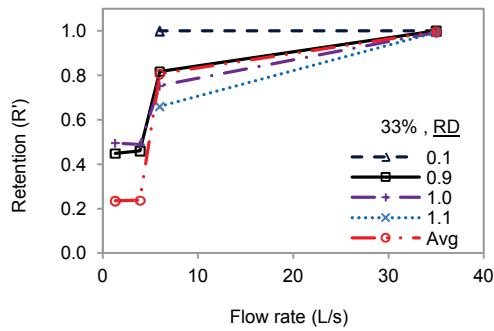


Figure G.1 Normalised capture/retention profiles R' for intermittently fed variable density spheres (RD) = 0.1, 0.9, 1.0 and 1.1. The channel inlet GPT experiment is with 33% blocked screens conducted under varying flow rates.

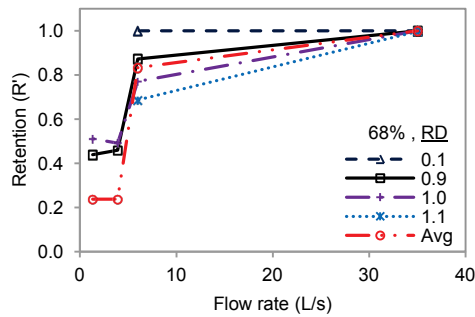


Figure G.2 Normalised capture/retention profiles R' for intermittently fed variable density spheres (RD) = 0.1, 0.9, 1.0 and 1.1. The channel inlet GPT experiment is with 68% blocked screens conducted under varying flow rates.

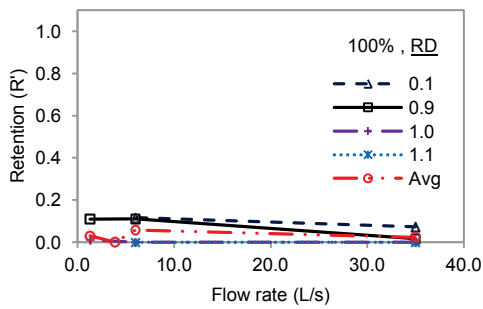


Figure G.3 Normalised capture/retention profiles R' for intermittently fed variable density spheres (RD) = 0.1, 0.9, 1.0 and 1.1. The channel inlet GPT experiment is with 100% blocked screens conducted under varying flow rates.

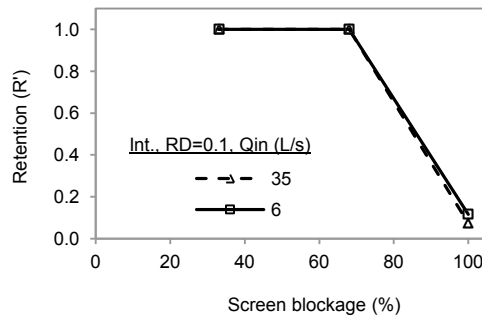


Figure G.4 Normalised capture/retention profiles R' for intermittently fed variable density spheres (RD) = 0.1. The channel inlet GPT is tested under varying screen blockages at different inlet flow rates.

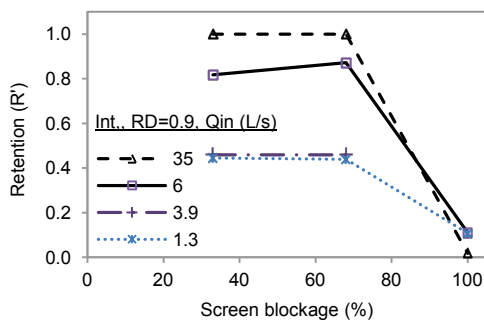


Figure G.5 Normalised capture/retention profiles R' for intermittently fed variable density spheres (RD) = 0.9. The channel inlet GPT is tested under varying screen blockages at different inlet flow rates.

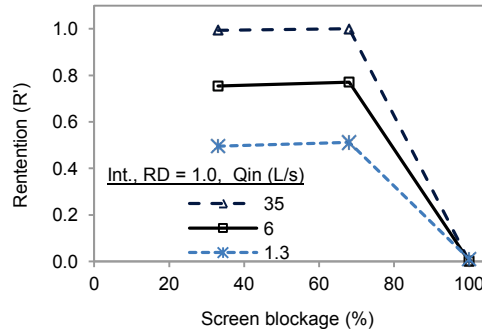


Figure G.6 Normalised capture/retention profiles R' for intermittently fed variable density spheres (RD) = 1.0. The channel inlet GPT is tested under varying screen blockages at different inlet flow rates.

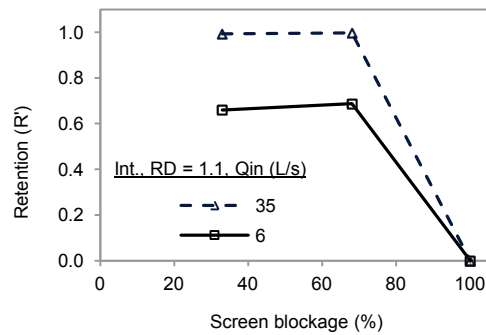


Figure G.7 Normalised capture/retention profiles R' for intermittently fed variable density spheres (RD) = 1.1. The channel inlet GPT is tested under varying screen blockages at different inlet flow rates.

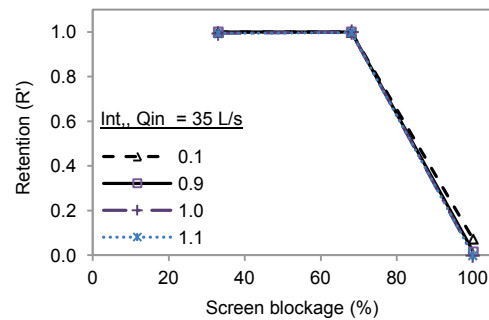


Figure G.8 Normalised capture/retention profiles R' for intermittently fed variable density spheres (RD) = 0.1, 0.9, 1.0 and 1.1. The channel inlet GPT experiment is conducted at 35.0 L/s under varying screen blockages.

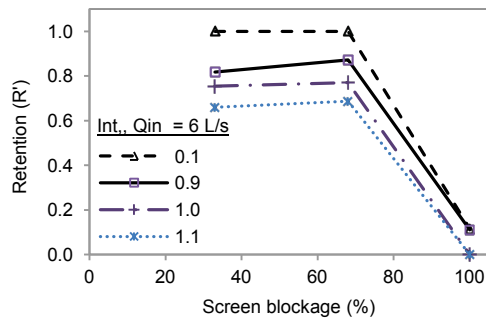


Figure G.9 Normalised capture/retention profiles R' for intermittently fed variable density spheres (RD) = 0.1, 0.9, 1.0 and 1.1. The channel inlet GPT experiment is conducted at 6.0 L/s under varying screen blockages.

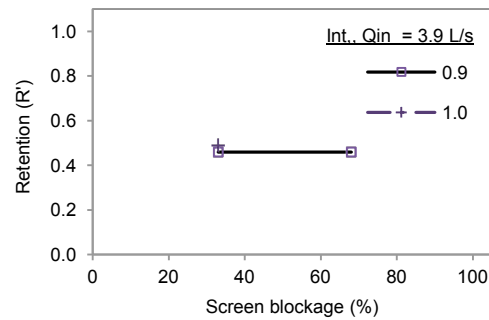


Figure G.10 Normalised capture/retention profiles R' for intermittently fed variable density spheres (RD) = 0.1, 0.9, 1.0 and 1.1. The channel inlet GPT experiment is conducted at 3.9 L/s under varying screen blockages.

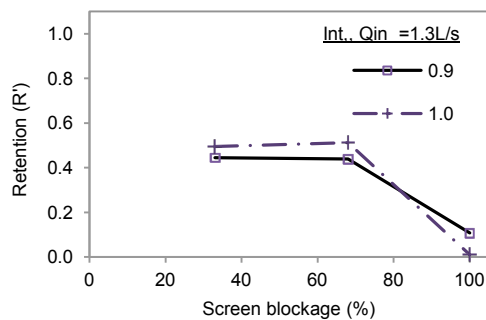


Figure G.11 Normalised capture/retention profiles R' for intermittently fed variable density spheres (RD) = 0.1, 0.9, 1.0 and 1.1. The channel inlet GPT experiment is conducted at 1.3 L/s screens a under varying screen blockages.

G.2 Capture/retention experiments with artificial gross pollutants continuously fed into the rectangular channel inlet GPT

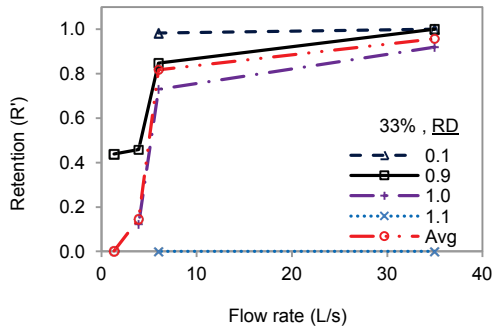


Figure G.12 Normalised capture/retention profiles R' for continuously fed variable density spheres (RD) = 0.1, 0.9, 1.0 and 1.1. The channel inlet GPT experiment is with 33% blocked screens conducted under varying flow rates.

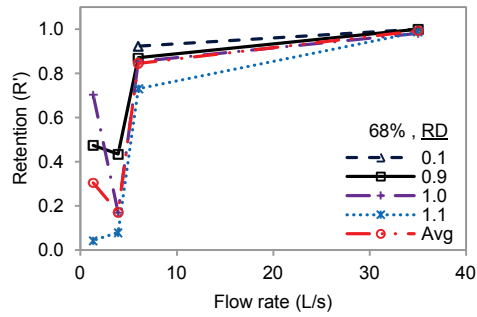


Figure G.13 Normalised capture/retention profiles R' for continuously fed variable density spheres (RD) = 0.1, 0.9, 1.0 and 1.1. The channel inlet GPT experiment is with 68% blocked screens conducted under varying flow rates.

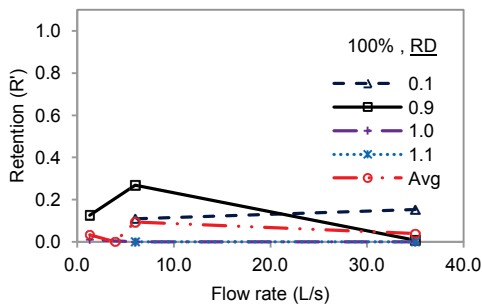


Figure G.14 Normalised capture/retention profiles R' for continuously fed variable density spheres (RD) = 0.1, 0.9, 1.0 and 1.1. The channel inlet GPT experiment is with 100% blocked screens conducted under varying flow rates.

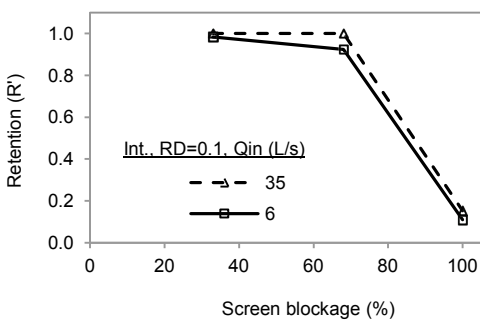


Figure G.15 Normalised capture/retention profiles R' for continuously fed variable density spheres (RD) = 0.1. The channel inlet GPT is tested under varying screen blockages at different inlet flow rates.

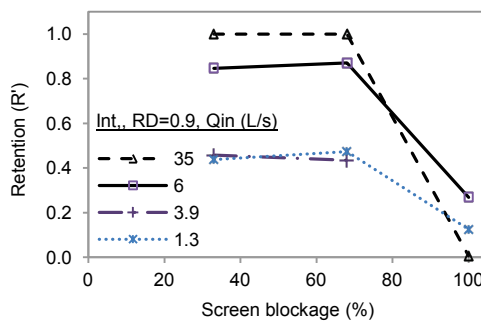


Figure G.16 Normalised capture/retention profiles R' for continuously fed variable density spheres (RD) = 0.9. The channel inlet GPT is tested under varying screen blockages at different inlet flow rates.

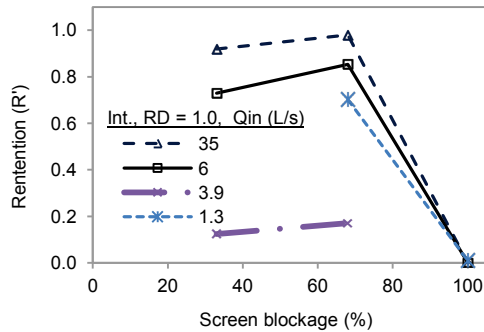


Figure G.17 Normalised capture/retention profiles R' for continuously fed variable density spheres (RD) = 1.0. The channel inlet GPT is tested under varying screen blockages at different inlet flow rates.

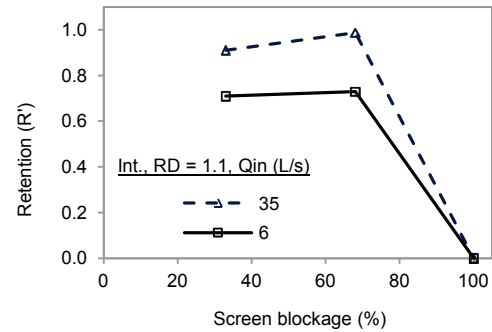


Figure G.18 Normalised capture/retention profiles R' for continuously fed variable density spheres (RD) = 1.1. The channel inlet GPT is tested under varying screen blockages at different inlet flow rates.

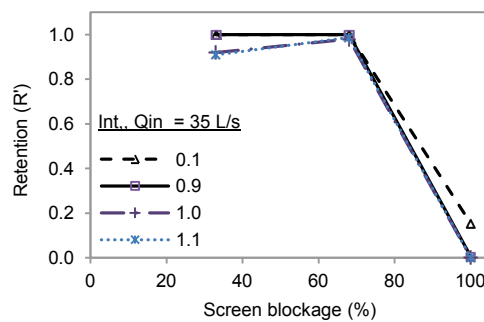


Figure G.19 Normalised capture/retention profiles R' for continuously fed variable density spheres (RD) = 0.1, 0.9, 1.0 and 1.1. The channel inlet GPT experiment is conducted at 35.0 L/s screens under varying screen blockages.

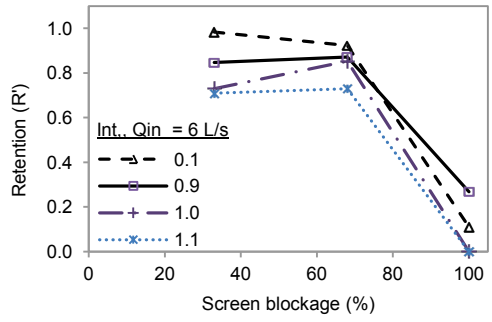


Figure G.20 Normalised capture/retention profiles R' for continuously fed variable density spheres (RD) = 0.1, 0.9, 1.0 and 1.1. The channel inlet GPT experiment is conducted at 6.0 L/s screens under varying screen blockages.

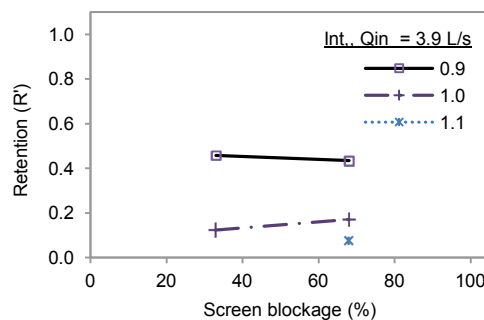


Figure G.21 Normalised capture/retention profiles R' for continuously fed variable density spheres (RD) = 0.1, 0.9, 1.0 and 1.1. The channel inlet GPT experiment is conducted at 3.9 L/s screens under varying screen blockages.

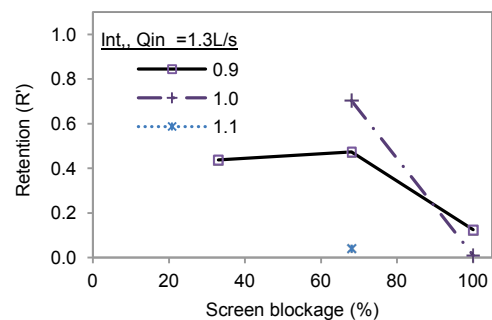


Figure G.22 Normalised capture/retention profiles R' for continuously fed variable density spheres (RD) = 0.1, 0.9, 1.0 and 1.1. The channel inlet GPT experiment is conducted at 1.3 L/s screens under varying screen blockages.

G.3 Comparing the capture/retention experimental results of continuously with intermittently fed artificial gross pollutants into the rectangular channel inlet GPT

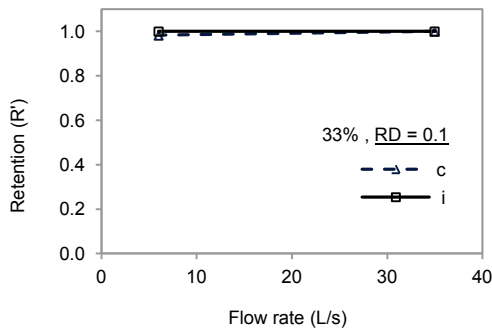


Figure G.23 Normalised capture/retention profiles R' for continuously (c)/intermittently (i) fed variable density spheres (RD) = 0.1. The channel inlet GPT experiment is with 33% blocked screens conducted under varying flow rates.

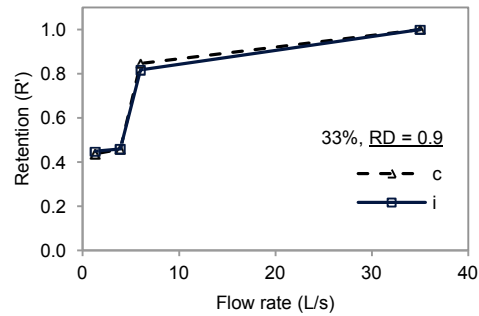


Figure G.24 Normalised capture/retention profiles R' for continuously (c)/intermittently (i) fed variable density spheres (RD) = 0.9. The channel inlet GPT experiment is with 33% blocked screens conducted under varying flow rates.

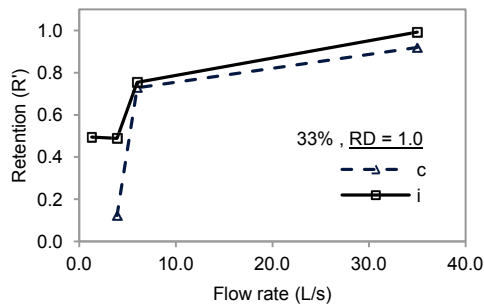


Figure G.25 Normalised capture/retention profiles R' for continuously (c)/intermittently (i) fed variable density spheres (RD) = 1.0. The channel inlet GPT experiment is with 33% blocked screens conducted under varying flow rates.

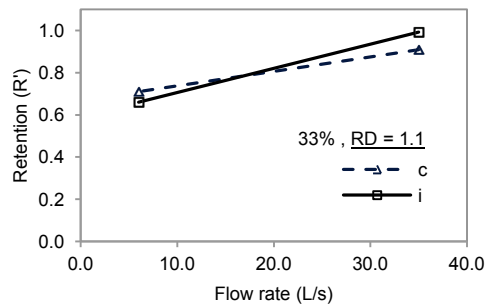


Figure G.26 Normalised capture/retention profiles R' for continuously (c)/intermittently (i) fed variable density spheres (RD) = 1.1. The channel inlet GPT experiment is with 33% blocked screens conducted under varying flow rates.

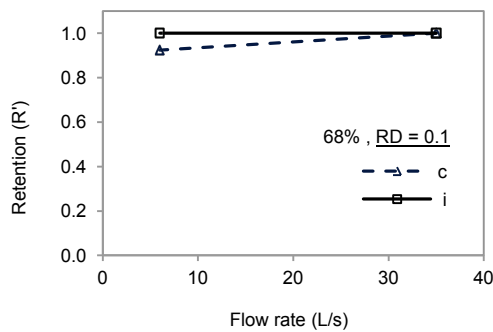


Figure G.27 Normalised capture/retention profiles R' for continuously (c)/intermittently (i) fed variable density spheres (RD) = 0.1. The channel inlet GPT experiment is with 68% blocked screens conducted under varying flow rates.

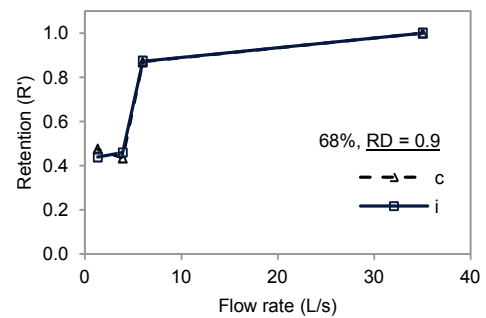


Figure G.28 Normalised capture/retention profiles R' for continuously (c)/intermittently (i) fed variable density spheres (RD) = 0.9. The channel inlet GPT experiment is with 68% blocked screens conducted under varying flow rates.

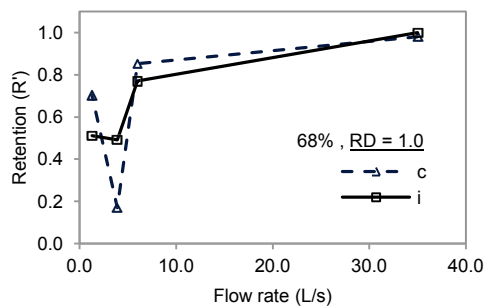


Figure G.29 Normalised capture/retention profiles R' for continuously (c)/intermittently (i) fed variable density spheres (RD) = 1.0. The channel inlet GPT experiment is with 68% blocked screens conducted under varying flow rates.

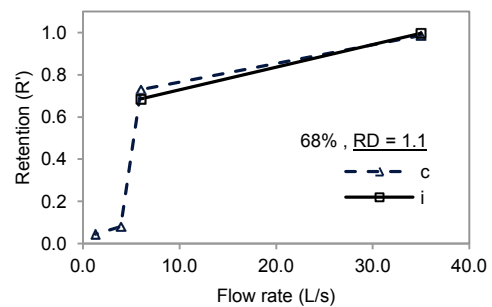


Figure G.30 Normalised capture/retention profiles R' for continuously (c)/intermittently (i) fed variable density spheres (RD) = 1.1. The channel inlet GPT experiment is with 68% blocked screens conducted under varying flow rates.

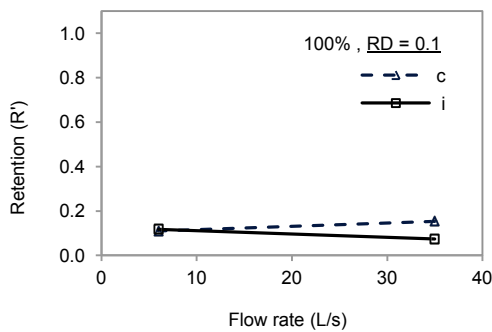


Figure G.31 Normalised capture/retention profiles R' for continuously (c)/intermittently (i) fed variable density spheres (RD) = 0.1. The channel inlet GPT experiment is with 100% blocked screens conducted under varying flow rates.

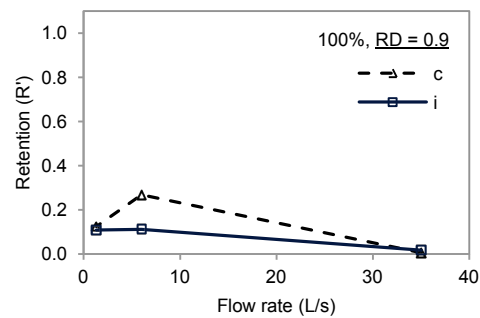


Figure G.32 Normalised capture/retention profiles R' for continuously (c)/intermittently (i) fed variable density spheres (RD) = 0.9. The channel inlet GPT experiment is with 100% blocked screens conducted under varying flow rates.

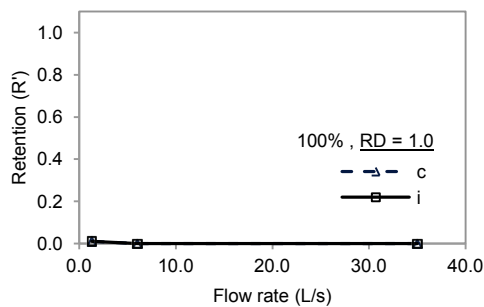


Figure G.33 Normalised capture/retention profiles R' for continuously (c)/intermittently (i) fed variable density spheres (RD) = 1.0. The channel inlet GPT experiment is with 68% blocked screens conducted under varying flow rates.

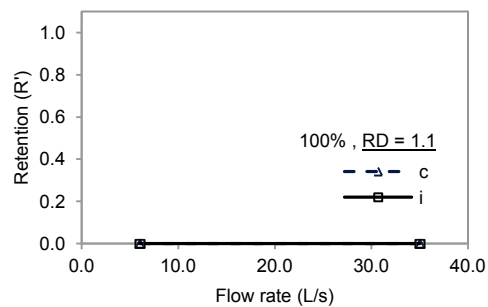


Figure G.34 Normalised capture/retention profiles R' for continuously (c)/intermittently (i) fed variable density spheres (RD) = 1.1. The channel inlet GPT experiment is with 100% blocked screens conducted under varying flow rates.

G.4 Capture/retention experiments with artificial gross pollutants intermittently fed into the raised circular pipe inlet GPT

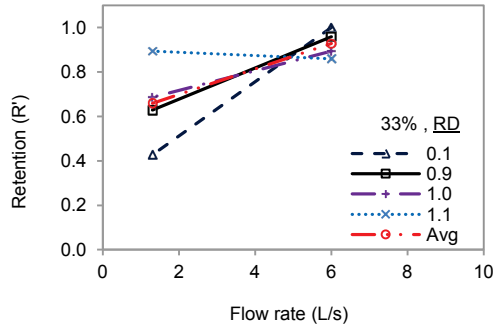


Figure G.35 Normalised capture/retention profiles R' for intermittently fed variable density spheres ($RD = 0.1, 0.9, 1.0$ and 1.1). The pipe inlet GPT experiment is with 33% blocked screens conducted under varying flow rates.

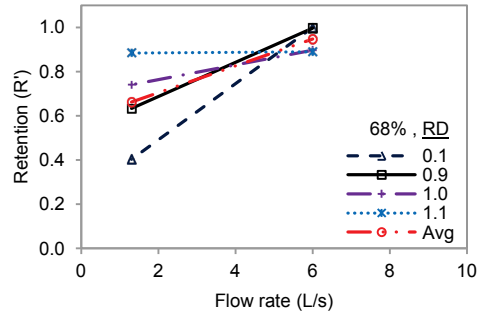


Figure G.36 Normalised capture/retention profiles R' for intermittently fed variable density spheres ($RD = 0.1, 0.9, 1.0$ and 1.1). The pipe inlet GPT experiment is with 68% blocked screens conducted under varying flow rates.

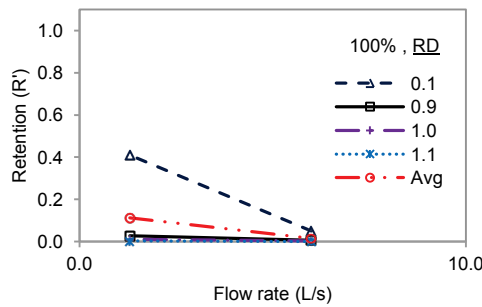


Figure G.37 Normalised capture/retention profiles R' for intermittently fed variable density spheres ($RD = 0.1, 0.9, 1.0$ and 1.1). The pipe inlet GPT experiment is with 100% blocked screens conducted under varying flow rates.

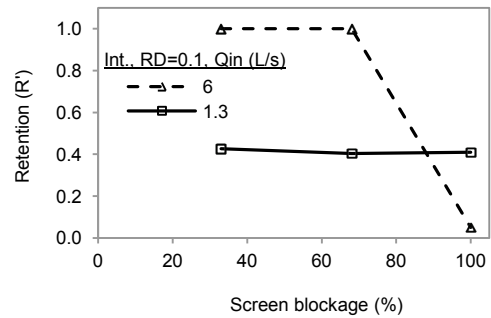


Figure G.38 Normalised capture/retention profiles R' for intermittently fed variable density spheres ($RD = 0.1$). The pipe inlet GPT experiment is conducted under varying screen blockages at different flow rates.

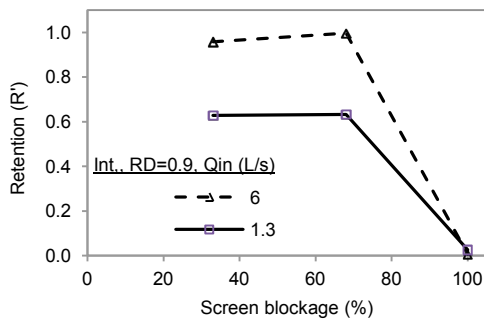


Figure G.39 Normalised capture/retention profiles R' for intermittently fed variable density spheres ($RD = 0.9$). The pipe inlet GPT experiment is conducted under varying screen blockages at different flow rates.

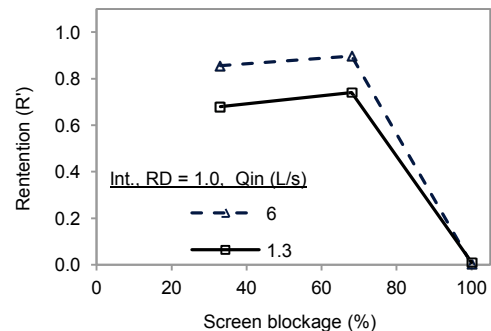


Figure G.40 Normalised capture/retention profiles R' for intermittently fed variable density spheres ($RD = 1.0$). The pipe inlet GPT experiment is conducted under varying screen blockages at different flow rates.

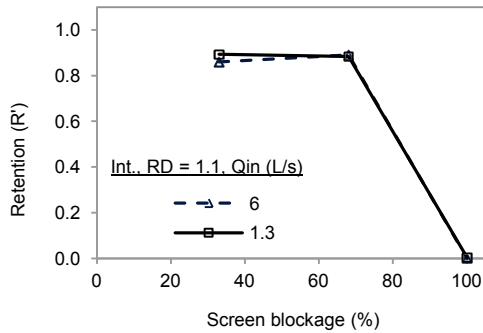


Figure G.41 Normalised capture/retention profiles R' for intermittently fed variable density spheres (RD) = 1.1. The pipe inlet GPT is tested under varying screen blockages at different inlet flow rates.

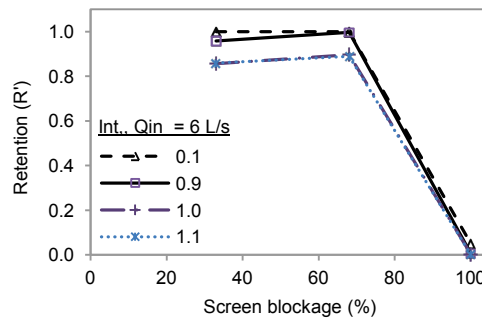


Figure G.42 Normalised capture/retention profiles R' for intermittently fed variable density spheres (RD) = 0.1, 0.9, 1.0 and 1.1. The pipe inlet GPT experiment is conducted at 6.0 L/s screens conducted under varying screen blockages.

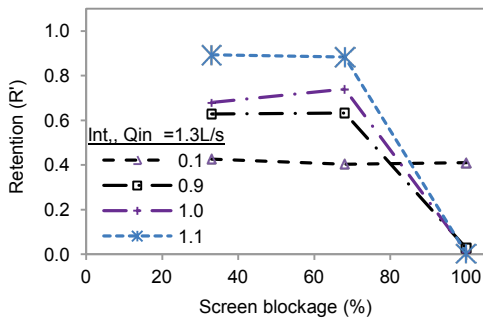


Figure G.43 Normalised capture/retention profiles R' for intermittently fed variable density spheres (RD) = 0.1, 0.9, 1.0 and 1.1. The channel inlet GPT experiment is with 1.3 L/s conducted under varying screen blockages.

G.5 Capture/retention experiments with artificial gross pollutants continuously fed into the raised circular pipe inlet GPT

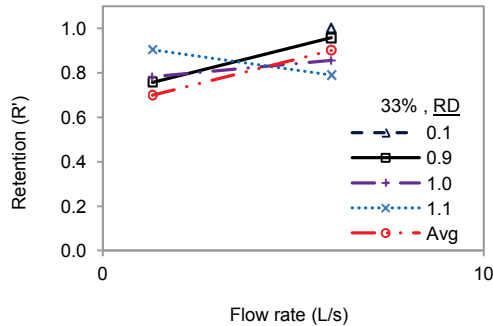


Figure G.44 Normalised capture/retention profiles R' for continuously fed variable density spheres (RD) = 0.1, 0.9, 1.0 and 1.1. The pipe inlet GPT experiment is with 33% blocked screens conducted under varying flow rates.

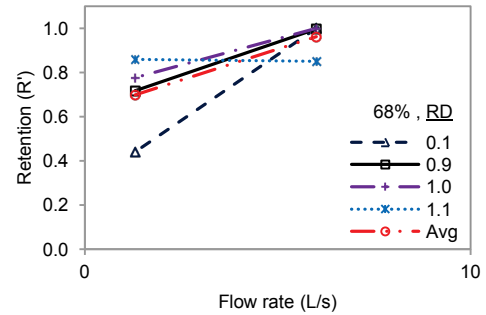


Figure G.45 Normalised capture/retention profiles R' for continuously fed variable density spheres (RD) = 0.1, 0.9, 1.0 and 1.1. The pipe inlet GPT experiment is with 68% blocked screens conducted under varying flow rates.

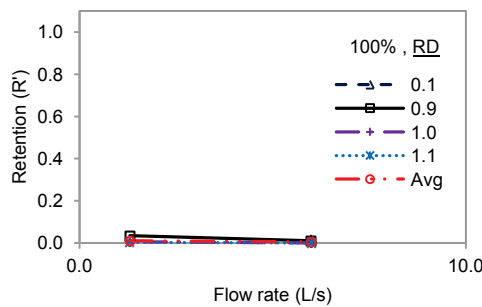


Figure G.46 Normalised capture/retention profiles R' for continuously fed variable density spheres (RD) = 0.1, 0.9, 1.0 and 1.1. The pipe inlet GPT experiment is with 100% blocked screens conducted under varying flow rates.

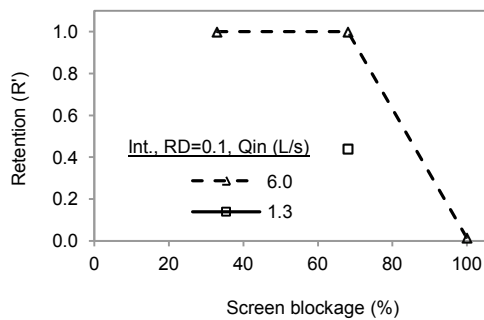


Figure G.47 Normalised capture/retention profiles R' for continuously fed variable density spheres (RD) = 0.1. The pipe inlet GPT is tested under varying screen blockages at different inlet flow rates.

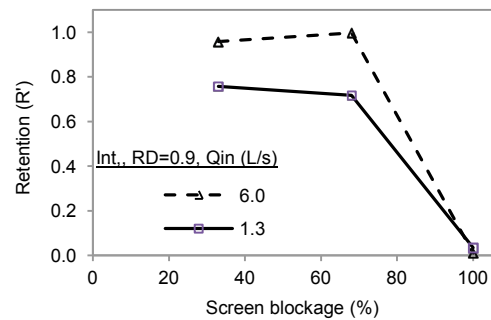


Figure G.48 Normalised capture/retention profiles R' for continuously fed variable density spheres (RD) = 0.9. The pipe inlet GPT is tested under varying screen blockages at different inlet flow rates.

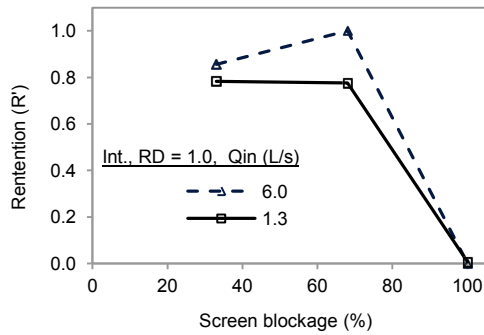


Figure G.49 Normalised capture/retention profiles R' for continuously fed variable density spheres (RD) = 1.0. The channel inlet GPT experiment is tested under varying screen blockages.

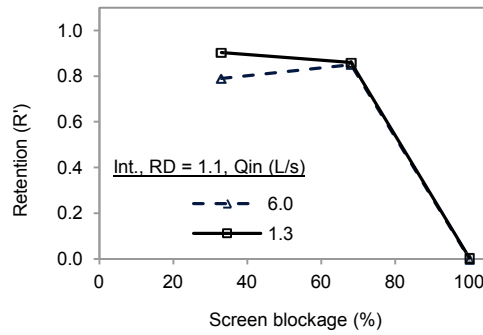


Figure G.50 Normalised capture/retention profiles R' for continuously fed variable density spheres (RD) = 1.1. The channel inlet GPT experiment is tested under varying screen blockages.

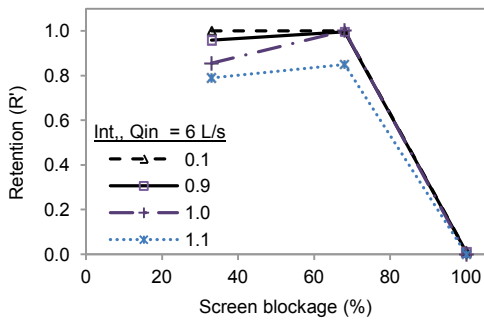


Figure G.51 Normalised capture/retention profiles R' for continuously fed variable density spheres (RD) = 0.1, 0.9, 1.0 and 1.1. The channel inlet GPT experiment is with 3.9 L/s blocked screens tested under varying screen blockages.

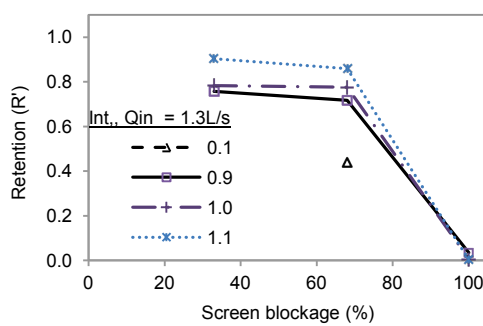


Figure G.52 Normalised capture/retention profiles R' for continuously fed variable density spheres (RD) = 0.1, 0.9, 1.0 and 1.1. The channel inlet GPT experiment is with 6.0 L/s blocked screens tested under varying screen blockages.

G.6 Comparing the capture/retention experimental results of continuously with intermittently fed artificial gross pollutants into the circular pipe inlet GPT

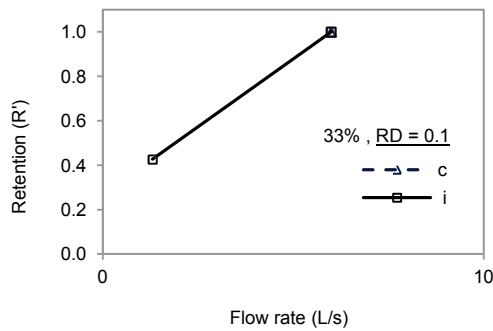


Figure G.53 Normalised capture/retention profiles R' for continuously (c)/intermittently (i) fed variable density spheres (RD) = 0.1. The pipe inlet GPT experiment is with 33% blocked screens conducted under varying flow rates.

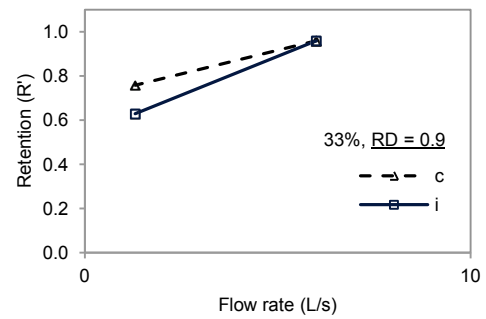


Figure G.54 Normalised capture/retention profiles R' for continuously (c)/intermittently (i) fed variable density spheres (RD) = 0.9. The pipe inlet GPT experiment is with 33% blocked screens conducted under varying flow rates.

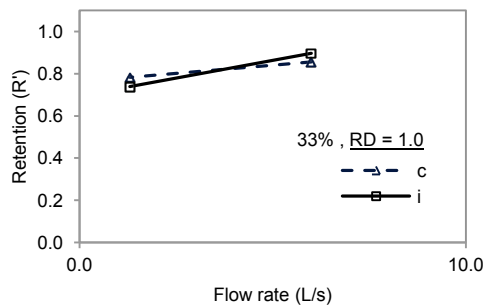


Figure G.55 Normalised capture/retention profiles R' for continuously (c)/intermittently (i) fed variable density spheres (RD) = 1.0. The pipe inlet GPT experiment is with 33% blocked screens conducted under varying flow rates.

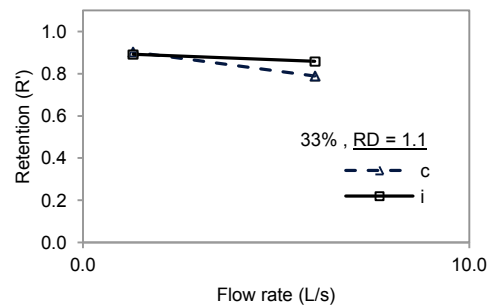


Figure G.56 Normalised capture/retention profiles R' for continuously (c)/intermittently (i) fed variable density spheres (RD) = 1.1. The pipe inlet GPT experiment is with 33% blocked screens conducted under varying flow rates.

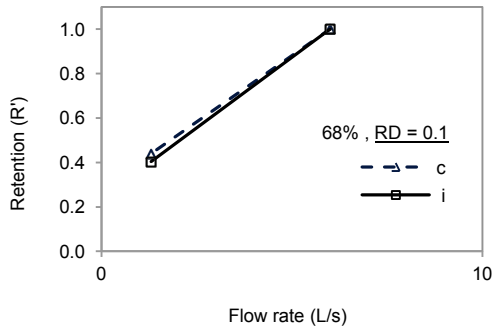


Figure G.57 Normalised capture/retention profiles R' for continuously (c)/intermittently (i) fed variable density spheres (RD) = 0.1. The pipe inlet GPT experiment is with 68% blocked screens conducted under varying flow rates.

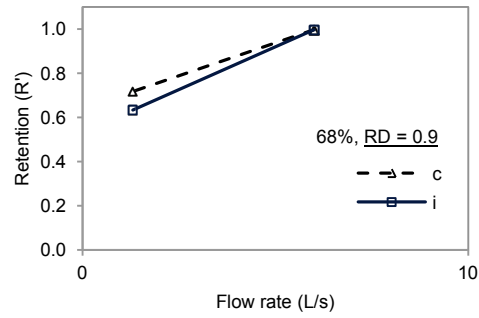


Figure G.58 Normalised capture/retention profiles R' for continuously (c)/intermittently (i) fed variable density spheres (RD) = 0.9. The channel inlet GPT experiment is with 68% blocked screens conducted under varying flow rates.

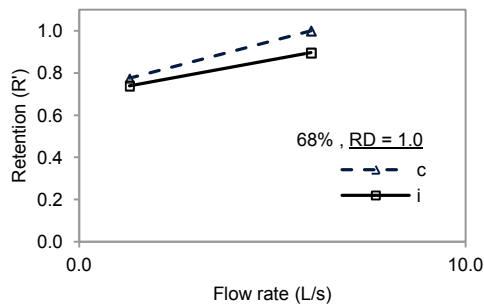


Figure G.59 Normalised capture/retention profiles R' for continuously fed variable density spheres (RD) = 1.0. The pipe inlet GPT experiment is with 68% blocked screens conducted under varying flow rates.

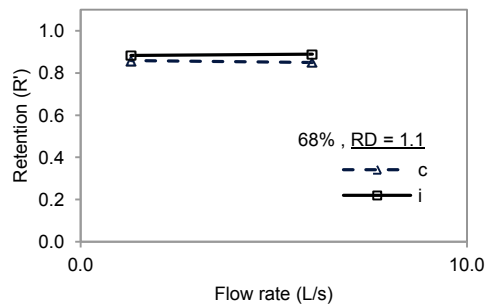


Figure G.60 Normalised capture/retention profiles R' for continuously fed variable density spheres (RD) = 1.1. The pipe inlet GPT experiment is with 68% blocked screens conducted under varying flow rates.

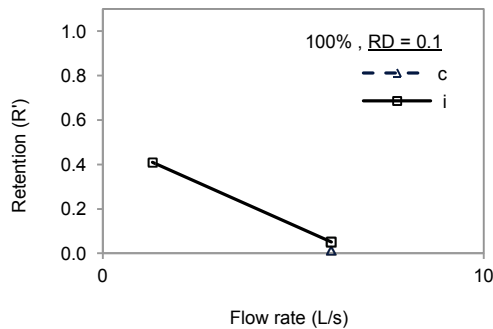


Figure G.61 Normalised capture/retention profiles R' for continuously (c)/intermittently (i) fed variable density spheres (RD) = 0.1. The pipe inlet GPT experiment is with 100% blocked screens conducted under varying flow rates.

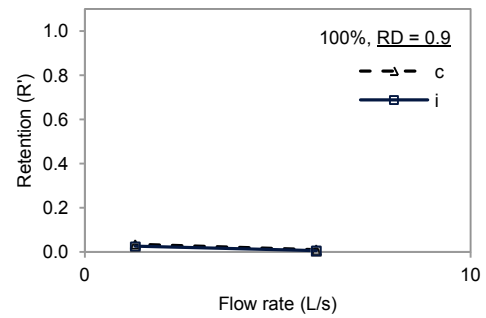


Figure G.62 Normalised capture/retention profiles R' for continuously (c)/intermittently (i) fed variable density spheres (RD) = 0.9. The pipe inlet GPT experiment is with 100% blocked screens conducted under varying flow rates.

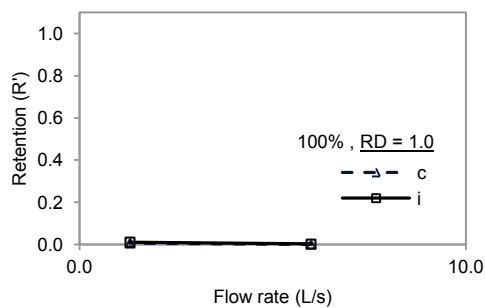


Figure G.63 Normalised capture/retention profiles R' for continuously (c)/intermittently (i) fed variable density spheres (RD) = 1.0. The pipe inlet GPT experiment is with 68% blocked screens conducted under varying flow rates.

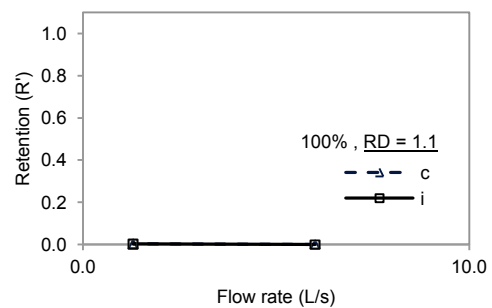


Figure G.64 Normalised capture/retention profiles R' for continuously (c)/intermittently (i) fed variable density spheres (RD) = 1.1. The pipe inlet GPT experiment is with 100% blocked screens conducted under varying flow rates.

